



**UNIVERSIDADE FEDERAL DO CEARÁ  
INSTITUTO DE CIÊNCIAS DO MAR - LABOMAR  
PROGRAMA DE PÓS- GRADUAÇÃO EM CIÊNCIAS MARINHAS  
TROPICAIS**

**QUIMIOESTRATIGRAFIA DA BACIA SEDIMENTAR DO ARARIPE  
(CRETÁCEO INFERIOR), NORDESTE DO BRASIL**

**IGOR HAMID RIBEIRO AZEVEDO**

**FORTALEZA- CE,**

**2024**

IGOR HAMID RIBEIRO AZEVEDO

**QUIMIOESTRATIGRAFIA DA BACIA SEDIMENTAR DO ARARIPE  
(CRETÁCEO INFERIOR), NORDESTE DO BRASIL**

Tese apresentada ao Programa de Pós-graduação em Ciências Marinhas Tropicais do Instituto de Ciências do Mar da Universidade Federal do Ceará como requisito para obtenção do título de Doutor em Ciências Marinhas Tropicais.

**Orientador:** Prof. Dr. Luiz Drude de Lacerda

**Co-orientador:** Prof. Dr. Antônio Alamo Feitosa Saraiva

FORTALEZA-CE,

2024

Dados Internacionais de Catalogação na Publicação  
Universidade Federal do Ceará  
Sistema de Bibliotecas

Gerada automaticamente pelo módulo Catalog, mediante os dados fornecidos pelo(a) autor(a)

---

A987q Azevedo, Igor Hamid Ribeiro.

Quimioestratigrafia da Bacia sedimentar do Araripe (Cretáceo Inferior), Nordeste do Brasil / Igor Hamid Ribeiro Azevedo. – 2024.

147 f. : il. color.

Tese (doutorado) – Universidade Federal do Ceará, Instituto de Ciências do Mar, Programa de Pós-Graduação em Ciências Marinhas Tropicais, Fortaleza, 2024.

Orientação: Prof. Dr. Luiz Drude de Lacerda.

Coorientação: Prof. Dr. Antônio Álamo Saraiva Feitosa.

1. Quimioestratigrafia. 2. Metais-traço. 3. Fator de Enriquecimento. 4. Condições paleoredox . 5. Vulcanismo. I. Título.

CDD 551.46

---

À toda minha família e amigos

## **AGRADECIMENTOS**

Primeiramente, gostaria de agradecer ao meu Orientador, **Professor Dr. Luiz Drude de Lacerda**, por todo apoio, suporte, orientação, paciência e grande conhecimento transmitido durante o desenvolvimento deste projeto. A finalização desta tese tem grande contribuição do senhor, pois a sua curiosidade e o seu apreço em aprender e ensinar é um espelho para os futuros pesquisadores deste país.

À **Professora Dra. Rozane Valente Marins** o meu muito obrigado pelo apoio, confiança e paciência para o desenvolvimento desse trabalho. Agradeço muito por suas indagações que me auxiliaram na produção desta Tese.

Gostaria de agradecer ao meu Co- Orientador, **Professor Dr. Álamo Saraiva**, e a toda equipe do Laboratório de Paleontologia (LPU) da URCA, pelo grande conhecimento compartilhado, pela lógica e atividades de campo. O meu muito obrigado ao Professor Álamo pela disponibilidade, mesmo à distância, em auxiliar no desenvolvimento desta pesquisa. A sua paixão pelo Cariri e pelo conhecimento são de grande inspiração. Agradeço também ao **Dr. Lucas Antonietto** e **Dr. Borja Holgado** pela parceria para o desenvolvimento desta pesquisa. Agradeço ao **Museu de Paleontologia Plácido Cidade Nuvens** por auxiliar no desenvolvimento desta pesquisa.

Agradeço também ao professor **Dr. Alcides Sial** e aos técnicos do Laboratório de Isótopos Estáveis (NEG- LABISE) pela parceria e contribuição para o desenvolvimento do projeto.

Meu muito obrigado aos professores **Dra. Taissa Rodrigues**, **Dr. Tristan Rousseau** e **Dr. Renan Bantim** por aceitarem participar da defesa da tese e colaborar para a melhoria do trabalho.

O meu muito obrigado aos professores **Dra. Samara Eschrique**, **Dr. Edvar Aguiar** e **Dr. Franscisco Dias (UFMA)** pelo conhecimento transmitido por vocês durante a minha formação acadêmica. Aos professores **Dra. Ana Paul Benigno (IFCE)** e **Dr. Tristan Rousseau (UFC)** pelas contribuições na qualificação deste trabalho e pelas sugestões na elaboração da Tese.

Agradeço a toda equipe do Laboratório de Biogeoquímica Costeira (LBC) da Universidade Federal do Ceará (UFC): **Andréa Consolação**, **Andréia Campos “Tubarão”**, **Cesar Barrios**, **Isabelle Caracas**, **Leticia Paulino**, **Liana Raquel**, **Marcus Vinicius**, **Maria Andreia**, **Mariana Silvestre**, **Mariany Cavalcante**, **Moises Bezerra**,

**Thays Santos, Wesleandro Vasconcelos, Victor Lacerda e Victoria Emily** pela ajuda nas análises e pelos momentos de descontração tão necessários.

Aos docentes do **Programa de Pós- Graduação em Ciências Marinhas Tropicais (PPGCMT)** pela oportunidade no desenvolvimento desse projeto; e aos funcionários do **LABOMAR** pela atenção e presteza diária.

Aos meus pais (**Stélio e Socorro**), irmã (**Susane**) e sobrinha (**Alice**) que sempre acreditaram na minha capacidade. O apoio dos meus pais foi extremamente importante para a realização deste trabalho, auxiliando nas viagens de campo. À família Azevedo: primos (**Abdul, Enéias, Guy, Hugo, Filipe e Cauê**) e tios/ tias (**Ana, Ana Lúcia, Paulo, Conceição, Eurinice, Guy Júnior, Karine e Verlene**) que sempre me ajudaram nos encontros de família. À família Ribeiro, em especial, minha segunda mãe (**Júlia Ribeiro**), meus primos (**Eduardo Chaves, Maiara Chaves, Priscila Chaves, Júnior “Neném”, Carol Portela e Felipe Toledo**) e “aos pequenos” (**Arthur, Malu, Maju, Manu e Laís**), que apesar da distância sempre me incentivaram e ajudaram nos momentos de dificuldade.

O meu muito obrigado à **Lourena Abreu Magalhães** por me acompanhar nessa jornada, por todo o apoio, companheirismo, paciência, incentivo e pelos momentos felizes proporcionados ao longo dos anos.

Aos meus grandes amigos do **Estudo Bíblico/ UFMA (Clarisso Figueiredo, Daniel Dionísio, Eduardo Kayk, Fernanda Filgueira, Jamerson Aguiar, Laiane Lima, Lucas Silva, Matheus Maia, Renan Mescouto, Rubens Marques e Samara Saraiva)**, que me auxiliaram e me aguentam desde a graduação. Aos meus amigos grandes amigos **Hugo Pereira, Jefferson Horley, Mariana Correa, Thamires Torres e Vinícius Henrique**.

Gostaria de agradecer à **FUNCAP** e ao **INCT-TMCOcean** pelo apoio financeiro para concluir o doutorado. O presente trabalho foi realizado com o apoio da Coordenação de Aperfeiçoamento de Pessoal de Nível Superior- Brasil (CAPES)- Código de Financiamento 001, através da bolsa de doutorado.

Por fim, gostaria de agradecer a **Deus** por todas as pessoas que foram colocadas em minha vida, que contribuíram de alguma forma para o meu crescimento pessoal e profissional.

**IGOR HAMID RIBEIRO AZEVEDO**

**QUIMIOESTRATIGRAFIA DA BACIA SEDIMENTAR DO ARARIPE  
(CRETÁCEO INFERIOR), NORDESTE DO BRASIL**

Tese apresentada ao Programa de Pós-graduação em Ciências Marinhas Tropicais do Instituto de Ciências do Mar da Universidade Federal do Ceará como requisito para obtenção do título de Doutor em Ciências Marinhas Tropicais.

**BANCA EXAMINADORA**

---

Prof. Dr. Luiz Drude de Lacerda (Orientador)  
**Universidade Federal do Ceará (UFC)**

---

Prof. Dr. Antônio Álamo Feitosa Saraiva (Co-orientador)  
**Universidade Regional do Cariri (URCA)**

---

Prof. Dr. Tristan Charles Clitandre Rousseau  
**Universidade Federal do Ceará (UFC)**

---

Profa. Dra. Taissa Rodrigues Marques da Silva  
**Universidade Federal do Espírito Santo (UFES)**

---

Prof. Dr. Renan Alfredo Machado Bantim  
**Universidade Regional do Cariri (URCA)**

## RESUMO

A Quimioestratigrafia é uma ferramenta essencial para compreender as características deposicionais e os processos responsáveis pelas mudanças paleoclimáticas da Terra. Através do uso dos metais-traço e isótopos estáveis pode-se entender os processos geológicos ao longo da evolução do planeta e sua interferência na evolução da vida. Os eventos de vulcanismo são responsáveis pela injeção de CO<sub>2</sub> na atmosfera causando grandes crises biológicas e oscilações paleoclimáticas globais e regionais. Deste modo, esta tese buscou compreender o comportamento dos indicadores geoquímicos durante as perturbações paleoambientais que ocorreram no Cretáceo Inferior (Aptiano-Albiano) na Bacia do Araripe (Ceará, Nordeste, Brasil). A bacia do Araripe é caracterizada por apresentar um rico acervo fossilífero (*Konservat-Lagerstätte*), em que, os processos que foram responsáveis pela preservação dos fósseis estão vinculados com as mudanças paleoambientais. Para avaliar as variações paleoambientais, determinou-se os indicadores geoquímicos do vulcanismo (Hg/COT, Hg/Al e Hg/Fe), paleosalinidade (Sr/Ba), as condições de oxirredução (V/Cr, V/V+Ni e V/Ni), oscilações isotópicas ( $\delta^{13}\text{C}_{\text{VPDB}}$  e  $\delta^{18}\text{O}_{\text{VPDB}}$ ), anomalias de paleoprodutividade (Cu<sup>FE</sup>, Zn<sup>FE</sup>, Ni<sup>FE</sup> e Ba<sup>FE</sup>) e paleoredox (V<sup>FE</sup>, Fe<sup>FE</sup>, Cr<sup>FE</sup>, Mn<sup>FE</sup> e Pb<sup>FE</sup>). Os eventos de vulcanismo foram responsáveis pelas mudanças da paleoprodutividade e condições paleoredox durante a deposição das formações Barbalha, Crato e Romualdo podendo estar associados aos vulcanismos dos platôs Ontong Java (OJP, 124 – 120 Ma) e Rajmahal-Kerguelen Sul (SKP, 119 – 110 Ma). Neste caso, o aumento do CO<sub>2</sub> atmosférico gerado pelo vulcanismo pode ter gerado o desenvolvimento da produtividade e da anoxia nos ecossistemas aquáticos. Além disso, os processos globais resultaram em mudanças locais na Bacia do Araripe, podendo estes eventos estarem vinculados com os eventos cíclicos de mortalidade em massa registrados.

**Palavras-chave:** Quimioestratigrafia. Metais-traço. Fator de Enriquecimento. Condições paleoredox. Paleoprodutividade. Vulcanismo. Isótopos Estáveis.

## ABSTRACT

Chemostratigraphy is an essential tool for the understanding of the depositional characteristics and the processes that are responsible for the paleoclimatic changes on Earth. Trace metal and stable isotopes are used to understand geologic processes during planetary evolution and how they interacted with life. Therefore, the aim of this work was to understand the behavior of geochemical indicators during the paleoenvironmental perturbations that occurred during the Lower Cretaceous (Aptian-Albian) in the Araripe Basin (Ceará, Northeast, Brazil). The Araripe Basin is characterized by a rich fossil assemblage (*Konservat -Laggerstätte*), in which the processes responsible for fossil preservation are linked to paleoenvironmental changes. To evaluate the paleoenvironmental variations, geochemical indicators of volcanism (Hg/TOC, Hg/Al, and Hg/Fe), paleosalinity (Sr/Ba), redox conditions (V/Cr, V/V+Ni and V /Ni), isotopic oscillations ( $\delta^{13}\text{C}_{\text{VPDB}}$  and  $\delta^{18}\text{O}_{\text{VPDB}}$ ), paleoproductivity ( $\text{Cu}^{\text{EF}}$ ,  $\text{Zn}^{\text{EF}}$ ,  $\text{Ni}^{\text{EF}}$ , and  $\text{Ba}^{\text{EF}}$ ), and paleoredox anomalies ( $\text{V}^{\text{EF}}$ ,  $\text{Fe}^{\text{EF}}$ ,  $\text{Cr}^{\text{EF}}$ ,  $\text{Mn}^{\text{EF}}$ , and  $\text{Pb}^{\text{EF}}$ ) were determined. Volcanic events were responsible for changes in paleoproductivity and paleoredox conditions during deposition of the Barbalha, Crato, and Romualdo formations and could be associated with the volcanism of the Ontong Java (OJP) and Rajmahal-Kerguelen South (SKP) plateaus. Increased anomalies in proxies of paleoproductivity, and paleoredox conditions were observed during volcanism events. In this case, the development of productivity and anoxia in aquatic ecosystems may have been triggered by the increase in atmospheric CO<sub>2</sub> caused by volcanism. Furthermore, the cyclic mass mortality events recorded may be related to global processes that caused local changes in the Araripe Basin.

**Keywords:** Chemostratigraphy. Trace Metals. Enrichment Factor. Paleoredox conditions. Paleoproductivity. Volcanism. Stable isotopes.

## LISTA DE FIGURAS

<b>Figura 1.</b> Localização e distribuição das litofácies da Bacia do Araripe.....	19
<b>Figura 2.</b> Carta estratigráfica da Bacia do Araripe .....	20
<b>Figura 3.</b> Esquema ilustrativo do ciclo do mercúrio (Hg), destacando o seu papel como indicador geoquímico de atividade vulcânica. ....	23
<b>Figura 4.</b> Classificação redox utilizando a razão entre metais proposta por Jones e Manning (1994). ....	26
<b>Figura 5.</b> Comportamento dos indicadores geoquímicos das condições paleoredox no ambiente aquático. ....	265
<b>Figura 6.</b> Comportamento dos indicadores geoquímicos da paleoprodutividade no ecossistemas aquáticos. ....	308
<b>Figura 7.</b> Comportamento isotópico do $\delta^{13}\text{C}_{\text{carbonato}}$ de acordo com os períodos de variações magmáticas. ....	33
<b>Figure 8.</b> A) 120 Ma paleogeographic map (modified from Scotese, 2016) showing the location of the Araripe Basin- BSA (yellow circle) and the volcanisms of Ontong Java-OJP (red star) and Southern Kerguelen Plateau- SKP (white star). B) Map of the location of the sampling points in the Araripe Basin. ....	41
<b>Figure 9.</b> Stratigraphic characterization of the Araripe Basin. A) Stratigraphic profile of the sampled sections, lithofacies, and height based on Benigno et al. (2021), Coimbra et al. (2002) e Fara et al. (2005). B) Aptian and early Albian depositional sequence of the studied interval, according to Fauth et al. (2023); Guzmán et al. (2023); Ogg et al. (2016); Varejão et al. (2021a, b). DS- Depositional system.....	47
<b>Figure 10.</b> Chemostratigraphy of the Barbalha Formation. A) Hg/TOC (Volcanism); B) Aluminum (Detrital supplay); C) Sr/Ba (Paleosalinity); D) V/Cr, E) V/V + Ni, F) V/Ni, G) Pb <sup>EF</sup> , H) Mn <sup>EF</sup> , I) V <sup>EF</sup> , J) Cr <sup>EF</sup> and K) Fe <sup>EF</sup> (paleoredox); L) $\delta^{18}\text{O}$ (Paleoclimate); M) Cu <sup>EF</sup> , N) Zn <sup>EF</sup> , O) Ni <sup>EF</sup> , P) Ba <sup>EF</sup> , Q) TOC, R) $\delta^{13}\text{C}_{\text{carbonato}}$ (Paleoproductivity). ....	51
<b>Figure 11.</b> Chemostratigraphy of the Crato Formation. A) Hg/TOC (Volcanism); B) Aluminum (Detrital supplay); C) Sr/Ba (Paleosalinity); D) V/Cr, E) V/V + Ni, F) V/Ni, G) Pb <sup>EF</sup> , H) Mn <sup>EF</sup> , I) V <sup>EF</sup> , J) Cr <sup>EF</sup> and K) Fe <sup>EF</sup> (paleoredox); L) $\delta^{18}\text{O}$ (Paleoclimate); M) Cu <sup>EF</sup> , N) Zn <sup>EF</sup> , O) Ni <sup>EF</sup> , P) Ba <sup>EF</sup> , Q) TOC, R) $\delta^{13}\text{C}_{\text{carbonato}}$ (Paleoproductivity). ....	53
<b>Figure 12.</b> Chemostratigraphy of the Romualdo Formation. A) Hg/TOC (Vulcanism); B) Aluminum (Detrital supplay); C) Sr/Ba (Paleosalinity); D) V/Cr, E) V/V + Ni, F) V/Ni,	

G) Pb <sup>EF</sup> , H) Mn <sup>EF</sup> , I) V <sup>EF</sup> , J) Cr <sup>EF</sup> and K) Fe <sup>EF</sup> (paleoredox); L) δ <sup>18</sup> O (Paleoclimate); M) Cu <sup>EF</sup> , N) Zn <sup>EF</sup> , O) Ni <sup>EF</sup> , P) Ba <sup>EF</sup> , Q) TOC, R) δ <sup>13</sup> C <sub>VPDB</sub> .....	55
<b>Figure 13.</b> Location map of the Araripe basin (ASB). A) Distribution area and location of lithofacies in the ASB (Modified from Assine, 2007 and Warren <i>et al.</i> , 2017). B) Location of the ASB at 120 Ma (Modified from Scotese, Wright, 2018). S- Stage; T- Tectonostratigraphic; Sand- Sandstone, Silt- Siltstone, Sha- Shale, Gyps- Gypsum.....	71
<b>Figure 14.</b> Profile of the controlled excavation of the Crato Formation at the Antonio Finelon mine (modified from Storari <i>et al.</i> , 2021). The samples come from the C6 layer of the Crato Formation, identifying 10 mortalities events (Dastilbe sp and Hexagenitidae) in the Crato paleolake.....	72
<b>Figure 15.</b> Chemostratigraphy of the Crato paleolake. A) Paleodetritic proxies (Al and Fe); volcanism proxies (Hg/Al and Hg/Fe ratios) and Hg concentration (ng g-1). B) Paleoclimatic proxy (Sr/Cu); paleosalinity (Sr/Ba); and variation in the depth of the lake system (Fe/Mn) and δ <sup>18</sup> O <sub>VPDB</sub> . .....	78
<b>Figure 16.</b> Enrichment factor of paleoredox proxies (Pb <sup>EF</sup> , Mn <sup>EF</sup> and Fe <sup>EF</sup> ), and paleoproductivity proxies (Cu <sup>EF</sup> , Zn <sup>EF</sup> , Ni <sup>EF</sup> , Ba <sup>EF</sup> , and δ <sup>13</sup> C <sub>VPDB</sub> ) in the Crato paleolake. A) Enrichment factor using Aluminum (Al) as a normalizer; B) Enrichment factor using Iron (Fe) as a normalizer.....	79
<b>Figure 17.</b> Principal component analysis with enrichment factor of trace metals (Ba, Cu, Zn, Pb, Fe, Mn, and Ni), volcanism (Hg/Al and Hg/Fe), paleodetritic (Al and Fe), lake lavel (Fe/Mn), paleoclimate conditions (Sr/Cu), paleosalinity (Sr/Ba) and the correlations with mortality events. A) Enrichment factor using Aluminum as a normalizer; B) Enrichment factor using Iron as a normalizer.....	80
<b>Figure 18.</b> Scheme demonstrating the paleoenvironmental variations (wet-dry) of the Konservat -Laggerstätten of the Crato paleolake. A) Arid paleoclimatic conditions and mortality of Ephemeroptera; B) Humid paleoclimatic conditions and mortality of <i>Dastilbe</i> sp.....	92
<b>Figure 19.</b> Map of the Araripe Basin, northeastern Brazil, highlighting the geographic distribution of the Santana Group (including the Romualdo Formation).....	98
<b>Figure 20.</b> Average results of (Hg)sample in fossil taxa of the Romualdo Formation analyzed in the present work .....	101
<b>Figure 21.</b> A summary of the Romualdo Formation trophic web based on litarature and present Hgsample results, including the following groups or taxa 1) Phytoplankton; 2) Zooplankton; 3) <i>Santanichthys diasii</i> ; 4) <i>Rhacolepis buccalis</i> ; 5) <i>Tharrhias araripis</i> ; 6)	

*Vinctifer comptoni*; 7) *Neoproscinetes penalvai*; 8) Batoidea indet.; 9) Benthic invertebrates; 10) *Cladocyclus gardneri*; 11) *Calamopleurus cylindricus*; 12) Ornithocheiriformes; 13) Thalassodrominae; 14) Other terrestrial Tetrapoda ..... 104

## SUMÁRIO

1. INTRODUÇÃO .....	15
2. BACIA DO ARARIPE .....	20
2.1 Contexto Histórico .....	20
2.2 Contexto Geológico .....	21
3. INDICADORES GEOQUÍMICOS PALEOAMBIENTAIS	Erro! Indicador não definido.
3.1 Indicador de vulcanismo (Hg).....	23
3.2 Indicadores das condições Paleoredox .....	25
3.3 Paleoprodutividade .....	29
3.4 Isótopo de Carbono ( $\delta^{13}\text{C}_{\text{VPDB}}$ ) .....	32
3.5 Isótopo de oxigênio ( $\delta^{18}\text{O}_{\text{VPDB}}$ ) .....	33
HIPÓTESE.....	35
4. OBJETIVOS .....	35
4.1 Objetivos Específicos .....	35
CAPÍTULO 1 .....	37
5.1 Introduction .....	40
5.2 Stratigraphic Settings .....	41
5.2.1 Barbalha Formation.....	43
5.2.2 Crato Formation.....	44
5.2.3 Romualdo Formation.....	45
5.3 Materials and methods .....	46
5.3.1 Total Organic Carbon (TOC).....	48
5.3.2 Stable isotopes (C and O).....	48
5.3.3 Metals concentrations .....	48
5.3.4 Mercury .....	49
5.3.5 Enrichment factor .....	49
5.3.6 Statistics.....	50
5.4 Results .....	51
5.4.1 Barbalha Formation.....	51
5.4.2 Crato Formation.....	54
5.4.3 Romualdo Formation.....	56
5.5 Discussion .....	58
5.5.1 Paleosalinity .....	58
5.5.2 Paleoredox conditions .....	60

<b>5.5.3 Volcanism and palaenvironmental changes .....</b>	62
<b>5.7 Conclusion .....</b>	67
<b>CAPÍTULO 2 .....</b>	69
<b>6.1 Introduction .....</b>	71
<b>6.2 Material and methods .....</b>	73
<b>6.2.1 Material studied.....</b>	73
<b>6.2.2 Metals analysis.....</b>	75
<b>6.2.3 Mercury analysis .....</b>	75
<b>6.2.4 Stable isotopes (<math>\delta^{13}\text{C}_{\text{VPDB}}</math> and <math>\delta^{18}\text{O}_{\text{VPDB}}</math>).....</b>	75
<b>6.2.5 Enrichment Factor (EF) .....</b>	76
<b>6.2.6 Statistics methodology .....</b>	77
<b>6.3 Results .....</b>	78
<b>6.3.1 Characterization of the Crato paleolake.....</b>	78
<b>6.3.2 Volcanism, paleoproductivity and paleoredox conditions in the Crato paleolake.....</b>	78
<b>6.4 Discussion .....</b>	83
<b>6.4.1 Characterization of the Crato paleolake.....</b>	83
<b>6.4.2 Paleoproductivity .....</b>	87
<b>6.4.3 Paleoredox conditions of the Crato paleolake .....</b>	88
<b>6.4.4 Volcanism .....</b>	88
<b>6.4.5 Mortality events and paleoenvironmental changes.....</b>	91
<b>6.4.6 Exceptional fossil preservation in the Crato paleolake.....</b>	95
<b>6.5 Conclusion .....</b>	96
<b>CAPÍTULO 3 .....</b>	97
<b>7.1 Introduction.....</b>	99
<b>7.2 Methodology .....</b>	100
<b>7.3 Trophic relations between fish species .....</b>	102
<b>7.4 The role of pterosaurs as mesopredators and opportunists .....</b>	104
<b>7.5 An integrative analysis of the Romualdo vertebrate assemblage .....</b>	104
<b>8. Considerações finais .....</b>	107
<b>REFERÊNCIAS .....</b>	109
<b>Material Suplementar- CAPÍTULO 1 .....</b>	136
<b>Material Suplementar- CAPÍTULO 2 .....</b>	142
<b>Material Suplementar- CAPÍTULO 3 .....</b>	148

## 1. INTRODUÇÃO

O planeta Terra passou por cinco grandes extinções em massa (*Big five*) ao longo de sua história geológica: final do Ordoviciano (~ 444 Ma), quando cerca de 85% das espécies presentes na época foram extintas; no Devoniano Superior (~ 372 Ma, 75% das espécies extintas); no final do Permiano (~ 252 Ma, 95% das espécies extintas); no final do Triássico (~ 201 Ma, 80% das espécies extintas) e no final do Cretáceo (~ 66 Ma, 75% das espécies extintas, incluindo os dinossauros não-avianos) (Racki, 2021; Raup, 1986; Raup, Sepkoski, 1982). Esses acontecimentos servem como base para compreender os processos envolvidos durante as transições geológicas. Para isso, destacamos a importância de informações essenciais para elucidar os fenômenos responsáveis pelos eventos de extinção e os processos que os desencadearam, como através da Quimioestratigrafia. A Quimioestratigrafia tem demonstrado ser uma ferramenta essencial para caracterizar as condições deposicionais nas extinções do Ordoviciano (Lu *et al.*, 2021), Devoniano (Kuwahara *et al.*, 2022; Lu *et al.*, 2021), Permiano (Shen *et al.*, 2019; Sial *et al.*, 2021), Triássico (Sun *et al.*, 2015; Thibodeau *et al.*, 2016) e Cretáceo (Abu-Ali, El-Kammar, Kuss, 2020; Alvarez *et al.*, 1980; Benigno, Sial, Lacerda, 2018; Font *et al.*, 2016; Sial *et al.*, 2013).

Através da aplicação da Quimioestratigrafia observou-se anomalias de Irídio (Ir), um elemento químico de origem sideral, associadas à extinção do Cretáceo-Paleógeno com o impacto de um bólido e como principal causa da extinção dos dinossauros não avianos (Alvarez *et al.*, 1980). Através da aplicação da quimioestratigrafia também foi possível observar anomalias do Hg, um indicador geoquímico do vulcanismo, simultâneas às extinções nas Cretáceo-Paleógeno, Permiano-Triássico, Triássico-Jurássico, Devoniano e Ordoviciano, podendo os eventos magmáticos terem desencadeado mudanças climáticas através da emissão de CO<sub>2</sub> e outros gases (e.g. SO<sub>2</sub>, HCl, HF e CH<sub>4</sub>) (e.g. Font, Bond, 2021; Racki, 2021; Sial *et al.*, 2013, 2016, 2021). Neste contexto, vários indicadores geoquímicos como os metais-traço têm demonstrado ser excelentes na identificação das variações da paleoprodutividade (Tribovillard *et al.*, 2006, 1994), paleosalinidade (Wei, Algeo, 2020), estado paleoredox (Algeo, Li, 2020; Algeo, Liu, 2020; Lewan, Maynard, 1982) e vulcanismo (Sanei, Grasby, Beauchamp, 2012; Sial *et al.*, 2010) durante os eventos mais extremos e de maiores crises biológicas da história da Terra.

Vários proxies geoquímicos têm sido usados para a reconstrução paleoambiental, possibilitando entender a origem de vários elementos químicos e, portanto, seus processos

de transporte e deposição. Aportes detriticos para bacias sedimentares são bem identificados através da variação da concentração e distribuição de elementos geogênicos como: Titânio (Ti), Silício (Si), Alumínio (Al) e Potássio (K) (Calvert, Pedersen, 1993; Soua *et al.*, 2011; Touati, Haji, 2019; Tribovillard *et al.*, 1994). As condições paleoredox no momento da deposição dos sedimentos é geralmente caracterizada pelo uso de oligoelementos sensíveis ao estado redox, como: Ferro (Fe), Cádmio (Cd), Cromo (Cr), Manganês (Mn), Molibdênio (Mo), Chumbo (Pb), Vanádio (V) e Arsênio (As) (Algeo e Li, 2020). Enquanto para avaliar a magnitude da paleoprodutividade, geralmente são usados metais-traço e suas razões de concentração, particularmente o Cobre (Cu), Zinco (Zn), Níquel (Ni) e Bário (Ba) (Tribovillard *et al.*, 2006). Além disso, macronutrientes como o carbono e o fósforo também podem ser utilizados para determinar as condições de produtividade (e.g. Steiner *et al.*, 2017; Touati, Haji, 2019; Tribovillard *et al.*, 2006). Mais recentemente, o mercúrio (Hg), em conjunto com o carbono orgânico total (COT), o Alumínio e o Ferro, tem sido utilizado para indicar contribuições vulcânicas em bacia sedimentares marinhas e continentais (e.g. Benigno *et al.*, 2018, 2021; Font *et al.*, 2016; Galloway *et al.*, 2023; Grasby *et al.*, 2019; Sial *et al.*, 2016, 2013).

A Bacia do Araripe é reconhecida internacionalmente pelo seu rico acervo fossilífero e excelente qualidade da preservação dos fósseis, sendo classificada como Konservat-Lagerstätte (Assine, 2007). Esta bacia sedimentar estende-se por 9.000 km<sup>2</sup> e abrange três estados do Nordeste brasileiro (Ceará, Pernambuco e Piauí) (Figura 1). É considerada o registro sedimentar mais completo do Cretáceo Inferior das bacias sedimentares do interior do Nordeste do Brasil (Assine, 1992, 2007; Neumann, 1999; Valença, Neumann, Mabesoone, 2003). A sua complexidade está relacionada com o registro dos processos de abertura e desenvolvimento do oceano Atlântico, apresentando informações do processo de abertura do oceano Atlântico- períodos Pré-Rifte, Rifte, Pós-Rifte I e Pós-Rifte II (Assine, 2007; Fambrini *et al.*, 2020).

A aplicação da quimioestratigrafia na Bacia do Araripe ainda é pouco explorada em comparação aos estudos fossilíferos, estratigráficos e sedimentológicos. Entre os estudos quimioestratigráficos utilizando metais-traço destacam-se: Benigno *et al.* (2021), Bom *et al.* (2021), Lúcio *et al.* (2022) e Salgado-Campos *et al.* (2021). Benigno *et al.* (2021) identificaram eventos de vulcanismo no processo deposicional do Grupo Santana e possíveis interferências paleoambientais locais. Bom *et al.* (2021), Lúcio *et al.* (2022) e Salgado-Campos *et al.* (2021) identificaram mudanças da paleosalinidade, paleoprodutividade e paleoredox nas Formações Romualdo, Ipobi e Crato,

respectivamente. Os estudos que visam a caracterização isotópica ( $\delta^{13}\text{C}$ ,  $\delta^{18}\text{O}$  e  $\delta^{34}\text{S}$ ) restringem-se a Castro *et al.* (2017), Pontes *et al.* (2021), Varejão *et al.* (2021a, 2021b). Castro *et al.* (2017) e Varejão *et al.* (2021a, 2021b) destacaram oscilações na paleoprodutividade e paleotemperatura, enquanto Pontes *et al.* (2021) identificaram condições extremamente redutoras influenciados pela sulfato-redução bacteriana. Considerando as variações paleoambientais e os períodos caracterizados nos estudos citados esses trabalhos estão focados principalmente no intervalo Aptiano-Albiano (~ 121,4 a 113 Ma) do Cretáceo Inferior.

Em relação aos eventos globais que ocorreram durante o Aptiano, e que podem ter influenciado as alterações paleoambientais já observadas na Bacia do Araripe, destacam-se os Eventos Anóxicos Oceânicos (OAE) 1a e 1b, vinculados à ativação de Grandes Províncias Ígneas (LIP's) do Ontong Java e do Platô Kerguelen Sul (e.g. Coffin *et al.*, 2006; Erba *et al.*, 2015; Keller, 2008; Walker-Trivett *et al.*, 2024). Esses eventos citados, no contexto global, foram responsáveis pelo soterramento de grande quantidade do COT, anomalias na razão Hg/COT (vulcanismo) e enriquecimento por metais-traço. O vulcanismo foi responsável pela emissão de grande quantidade de CO<sub>2</sub> para atmosfera, gerando perturbações no ciclo do carbono global (Bodin *et al.*, 2023; Grasby *et al.*, 2019). Vale destacar que Benigno *et al.* (2021) encontraram anomalias de Hg no intervalo Aptiano-Albiano na Bacia do Araripe e as associaram ao vulcanismo do Platô Kerguelen Sul.

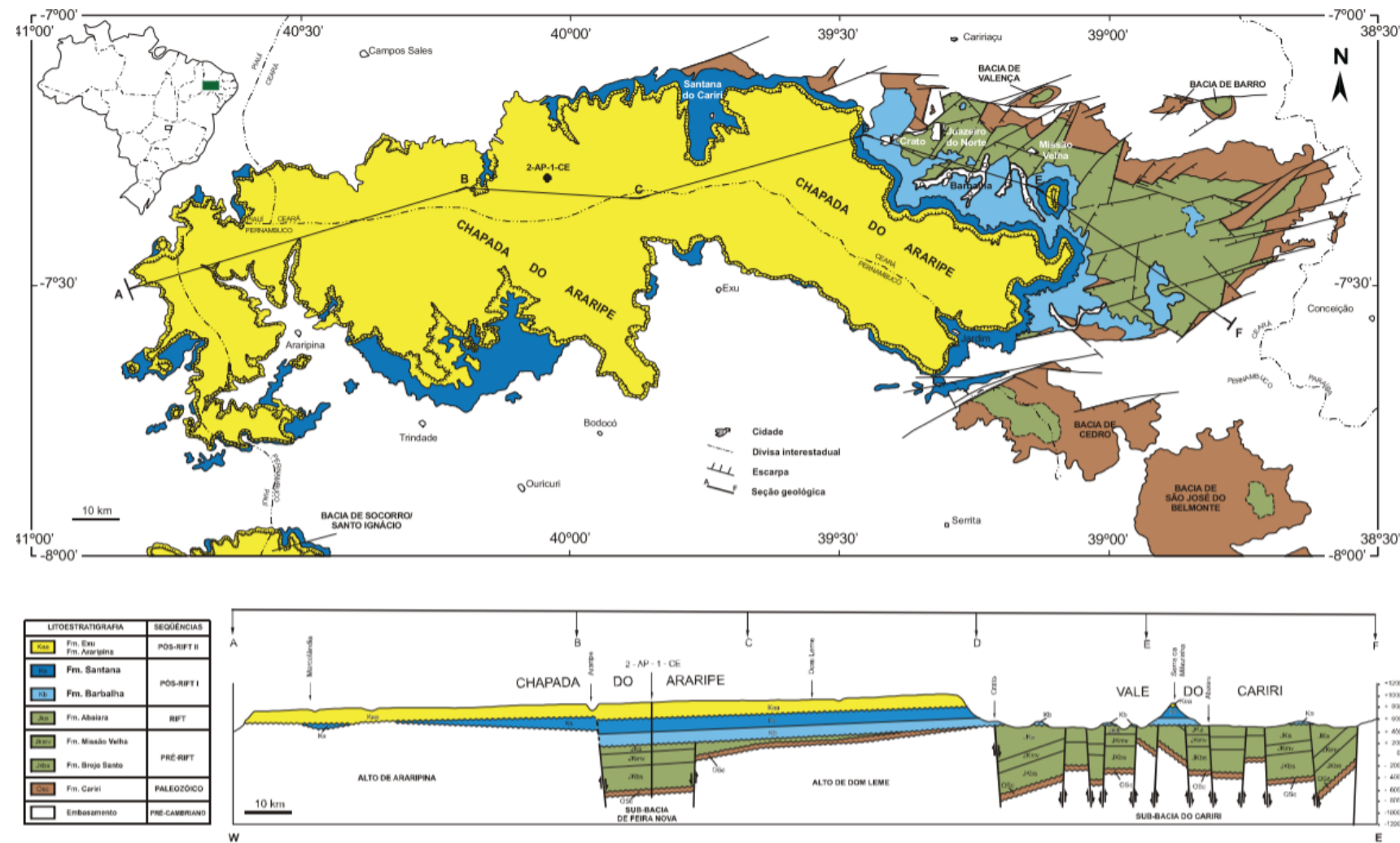
Dentro desse contexto, o presente estudo visa caracterizar a químioestratigrafia da Bacia do Araripe através da utilização de indicadores metálicos, com o intuito de determinar: os aportes paleodetríticos (Al), paleoprodutividade ( $\delta^{13}\text{C}_{\text{VPDB}}$ , COT, Cu, Ni, Ba e Zn), condições de paleoredox (Cr, Fe, Pb, V, Mn, V/Cr, V/Ni e V/V+Ni), vulcanismo (anomalias de Hg- Hg/TOC, Hg/Al e Hg/Fe), paleoclima ( $\delta^{18}\text{O}_{\text{VPDB}}$  e Sr/Cu) e suas relações com as mudanças paleoclimáticas e biológicas registradas na Bacia do Araripe durante o Cretáceo Inferior.

O presente estudo é apresentado em 3 capítulos principais, a saber:

- **CAPÍTULO 1:** Caracterizar a geoquímica paleoambiental da transição Aptiano-Albiano na Bacia do Araripe. Apresenta-se uma avaliação das condições deposicionais do Grupo Santana (formações Barbalha, Crato e Romualdo), sendo possível estabelecer uma correlação com os Eventos Anóxicos Oceânicos (OAE 1a e 1b).

- **CAPÍTULO 2:** Avaliar as correlações bioestratigráficas entre os eventos de mortalidade registrados no Konservat-Lagerstätte do paleolago Crato e a quimioestratigrafia no Cretáceo Inferior (Formação Crato) da Bacia do Araripe. Neste caso o manuscrito irá demonstrar os fatores responsáveis pelos eventos cíclicos de mortalidade registrados na Formação Crato.
- **CAPÍTULO 3:** Estudo com o objetivo de identificar o desenvolvimento da cadeia paleotrófica no Konservat -Lagerstätte da Formação Romualdo através das variações das concentrações do mercúrio (Hg). Observou-se o desenvolvimento da paleoictiofauna e o comportamento de outros organismos (pterossauros) na Formação Romualdo.

**Figura 1.** Localização e distribuição das litofácies da Bacia do Araripe.



Fonte: Assine (2007).

## **2. BACIA DO ARARIPE**

### **2.1 Contexto Histórico**

Os primeiros registros de descrição dos fósseis na Bacia do Araripe são de 1800, quando foram enviados relatórios do pesquisador português João da Silva Feijó ao governador da Capitania do Ceará sobre a ocorrência de peixes e anfíbios com tecidos moles (Silva, 2007). Posteriormente, expedições alemãs ocorreram entre 1817 – 1823, chefiadas por von Spix e von Martius na província do Siará, atual Estado do Ceará (Maisey, 1991). No século XIX, as primeiras descrições fossilíferas foram de peixes, principalmente, nas concreções calcárias da Formação Romualdo. No século XX grandes expedições da Inspetoria Federal de Obras contra as Secas, atual Departamento Nacional de Obras contra as Secas (DNOCS), desenvolveram estudos focados em fósseis de peixes (Bantim, Lima, Saraiva, 2021). Apenas em meados dos anos 60, foram realizados os primeiros estudos voltados a outros grupos fósseis na Formação Romualdo, como: o primeiro crocodiliano, moluscos e equinóides-registro da influência marinha nesta formação (Braun, 1966; Price, 1959). Além disso, o trabalho inicial de Beurlen (1962) estabeleceu os primeiros critérios estratigráfico da Bacia do Araripe, definindo as Formações Cariri, Missão Velha, Santana e Exu.

Nas décadas de 70 e 80, a expansão dos estudos gravimétricos (Rand, Manso, 1984), do mapeamento geológico de Ghignone (1986) e o início da exploração do calcário laminado da Formação Crato auxiliaram no desenvolvimento e conhecimento sobre a estratigrafia e a biodiversidade na Bacia do Araripe, como: copépodes (Cressey, Patterson, 1973), ostracodes (Bate, 1972), pólens (Lima, 1978), tartarugas (Price, 1973), pterossauros (Price, 1971) e vários grupos de insetos, como: os Blattodea (Pinto, Purper, 1986) e Lepidoptera (Martins-Neto, 2006). Para a Formação Romualdo, observou-se a presença de tubarões (Brito, Ferreira, 1989), tecido moles de peixes bem preservados (Martill, 1988), crocodilos (Kellner, 1987), pterossauros (Kellner, 1996; Kellner, Almeida Campos, 1988, 1994; Pégas, Costa, Kellner, 2021) e dinossauros (Kellner, 1996; Sayão *et al.*, 2020). Devido ao grande acervo fossilífero da Bacia do Araripe, em 1985 foi criado por Plácido Cidade Nuvens o Museu de Fósseis de Santana do Cariri, com o objetivo de proteger os exemplares fósseis encontrados na Bacia do Araripe (Bantim, Lima, Saraiva, 2021; Bétard *et al.*, 2018).

No final do século XX e início do século XXI as descobertas fossilíferas e estudos estratigráficos (Assine, 1992, 2007; Ponte, Ponte-Filho, 1996) estabeleceram as

sequências deposicionais na Bacia do Araripe associando-as com o processo de abertura do oceano Atlântico. Além disso, a descrição fossilífera dos calcários laminados da Formação Crato e dos folhelhos betuminosos da Formação Romualdo auxiliaram na classificação destas formações como Konservat-Lagerstätte, devido ao excelente estado de preservação do conteúdo fossilífero e grande quantidade de fósseis (Maisey, 1991; Martill, 1988). Como resultado de impedir o tráfico de fósseis e devido à alta qualidade de preservação dos fósseis, a parceria entre a Universidade Regional do Cariri (URCA) e o Governo do Estado do Ceará solicitou em 2005 a candidatura do Geopark Araripe para ingressar na Rede Global de Geoparques. No ano de 2006 a UNESCO (Nações Unidas para a Educação, a Ciência e a Cultura) reconheceu o Geopark Araripe incluso na Rede Global de Geoparks (Global Geoparks Network), tornando-se o primeiro geoparque da América Latina e Caribe (Bantim, Lima, Saraiva, 2021; Bétard *et al.*, 2018; Mochiutti *et al.*, 2012).

## 2.2 Contexto Geológico

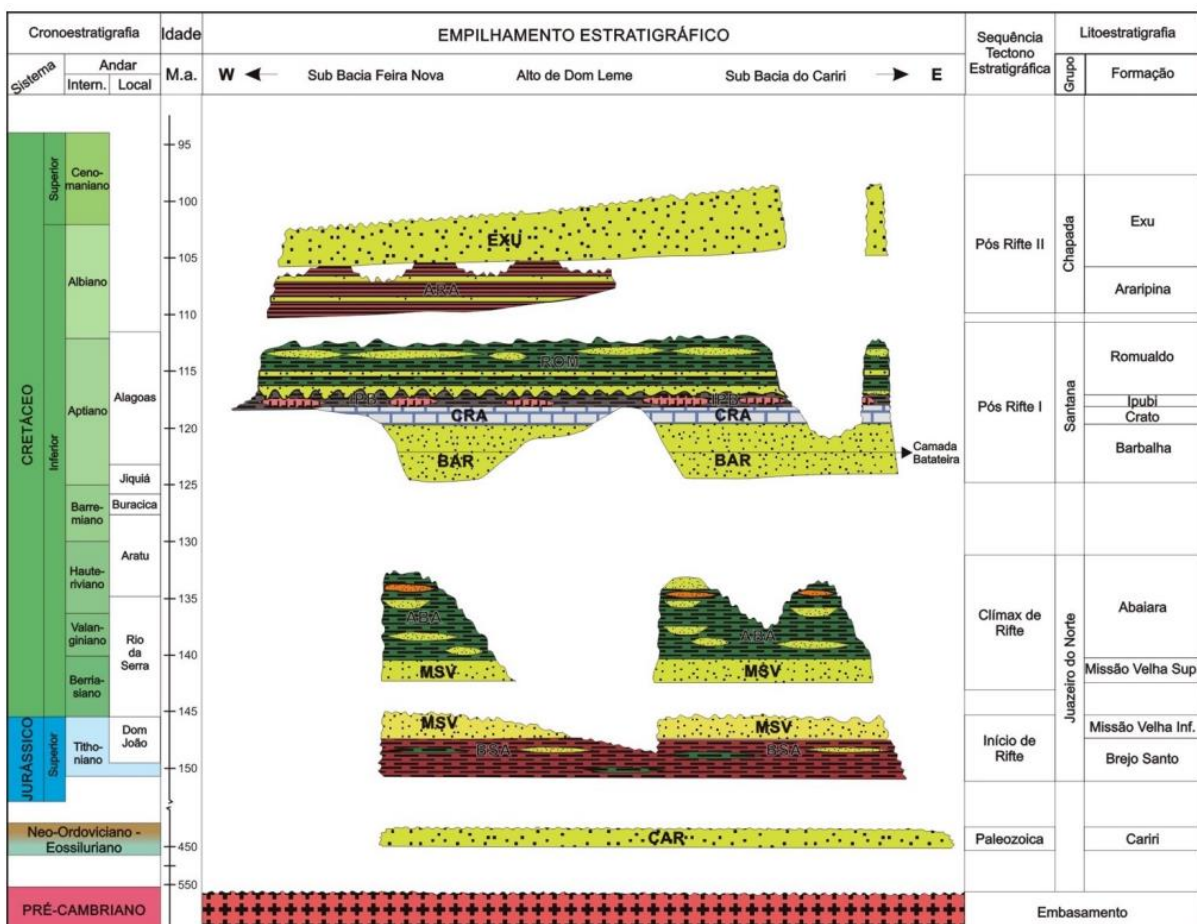
A Bacia do Araripe, com área de 9.000 km<sup>2</sup> abrange os Estados do Ceará, Piauí e Pernambuco (Nordeste do Brasil) (Assine, 1992, 2007). A Bacia do Araripe desenvolveu-se através da reativação das falhas do embasamento cristalino Pré-Cambriano da Zona Transversal da Província Borborema, formada durante a Orogênese Brasiliana-Pan-Africana. Além disso, encontra-se delimitada pelas Zonas de cisalhamento Neoproterozóicas de Pernambuco e Patos (Assine, 2007; Brito Neves; Santos; Van Schmus, 2000; Neves *et al.*, 1995). A origem e a evolução da Bacia do Araripe decorrem do processo de ruptura do supercontinente Gondwana e abertura do oceano Atlântico, sendo este evento o responsável pelo desenvolvimento das bacias marginais brasileiras e africanas (Alkmim, 2015; Godot Souza *et al.*, 2022).

A Bacia do Araripe apresenta a maior complexidade entre todas as bacias sedimentares do interior do Nordeste brasileiro, pois ocorrem 5 sequências deposicionais, além de apresentar duas feições geomorfológicas: a Chapada do Araripe e o Vale do Cariri (Assine, 2007; Peulvast e Bétard, 2015). A Chapada do Araripe apresenta orientação Leste-Oeste e abrange as sequências deposicionais Cretáceas dos eventos Pós-Rifte I e II (Aptiano-Cenomaniano) do processo de abertura do Oceano Atlântico (Figura 2). O Vale do Cariri contém os registros dos períodos mais antigos da Bacia do Araripe, englobando as sequências Paleozoicas, Pré-Rifte e Rifte do evento de ruptura do Gondwana (Fambrini *et al.*, 2020).

Como relatado anteriormente, a Bacia do Araripe apresenta sequência cinco sequências tecno-sedimentares (Assine, 2007; Fambrini *et al.*, 2019):

- **Seqüência Sinéclise:** Arenitos médios a grossos fluviais da Formação Cariri, com idade neordoviciano a eossiluriana;
  - **Seqüência Pré-Rifte:** Apresentam idade Jurássica e são compostos por pelitos vermelhos alternados com arenitos calcíferos da Formação Brejo Santo (Neojurássico) e pelos arenitos da parte basal da Fm. Missão Velha;
  - **Seqüência Rifte:** Neste estágio a idade é Cretácea Inferior, representado inicialmente pelos arenitos da parte superior da Fm. Missão Velha e pelos pelitos da Formação Abaíara;
  - **Seqüência Pós-Rifte:** Possui dois estágios, o estágio Pós-Rifte I, com idade Aptiana-Albiana é representado pelo Grupo Santana (Formações Barbalha, Crato, Ipobi e Romualdo); enquanto o estágio Pós-Rifte II, com idade Albiana-Cenomaniano, apresentam ambiente deposicional aluvial das Formações Araripeana e Exu.

**Figura 2.** Carta estratigráfica da Bacia do Araripe.



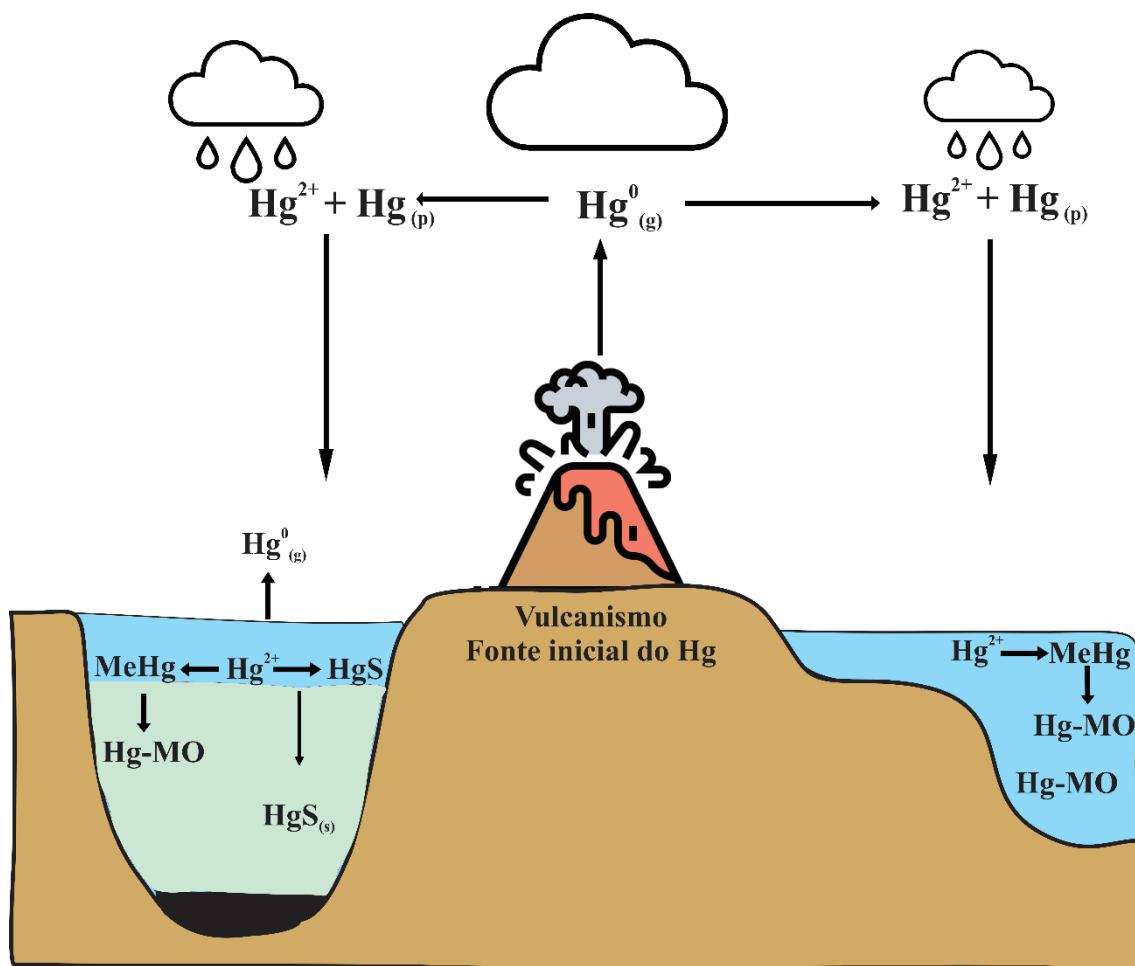
Fonte: Fambrini et al., (2020)

### 3. INDICADORES GEOQUÍMICOS PALEOAMBIENTAIS

#### 3.1 Indicador de vulcanismo (Hg)

As atividades vulcânicas têm papel importante na emissão do mercúrio (Hg), sendo a principal forma de entrada natural desse elemento para a atmosfera (Pyle e Mather, 2003). O Hg é emitido para a atmosfera na forma de vapor ( $Hg^0$ ), com grande distribuição global atingindo a estratosfera e com tempo de residência de 1 a 3 anos (Benigno, Sial, Lacerda, 2018). Na atmosfera, o mercúrio pode sofrer oxidação e formar o  $Hg^{2+}$ , forma iônica mais reativa e solúvel em água. Levando em conta essa característica, o Hg pode ser incorporado no ciclo hidrológico e sofrer deposição através da precipitação (Figura 3). Após a deposição, este elemento pode ser adsorvido aos minerais presentes no solo e na água, e fazer parte do ciclo das rochas, sendo um excelente indicador de atividades vulcânicas tanto no presente quanto em situações pretéritas (e.g. Benigno *et al.*, 2018; Grasby *et al.*, 2019; Sial *et al.*, 2016).

**Figura 6.** Esquema ilustrativo do ciclo do mercúrio (Hg), destacando o seu papel como indicador geoquímico de atividade vulcânica.



Fonte: Adaptado de Percival *et al.*, (2015).

No ambiente terrestre, o mercúrio pode sofrer a influência de diversos processos bióticos e abióticos, podendo complexar com o COT, Al e em sulfetos ( $H_2S$ ) (Erickson *et al.*, 2003). No caso da relação Hg com o COT e o sulfetos, há a formação dos complexos orgânicos estáveis e precipitados em sulfetos-Hg (Gamboa Ruiz, Tomiyasu, 2015; Pyle, Mather, 2003). A utilização do COT destaca-se devido a sua grande capacidade de formar complexos orgânicos, sequestrando o Hg ao longo do tempo geológico (Grasby *et al.*, 2019; Sial *et al.*, 2010). Estudos anteriores encontraram uma correlação estratigráfica entre as anomalias da razão Hg/COT com os eventos extinção em massa, indicando a interferência da ativação de Grandes Províncias Ígneas (LIP's) nas mudanças climáticas, resultando na deterioração das condições da vida nos ecossistemas aquáticos e terrestres (Grasby *et al.*, 2019). Entretanto, é possível utilizar correlações geoquímicas entre Hg/paleodetríticas (Al, Fe, Zr, Ti e filossilicatos), indicando a interferência dos processos detritícios no soterramento do Hg (Font *et al.*, 2016; Sabatino *et al.*, 2018; Sanei, Grasby, Beauchamp, 2012; Sial *et al.*, 2013)

Anomalias do Hg foram encontradas na transição Cretáceo-Paleógeno (vulcanismo do Deccan) (Font *et al.*, 2016; Sial *et al.*, 2013, 2016, 2018), Triássico-Jurássico (Província Magmática do Atlântico Central - CAMP) (Thibodeau *et al.*, 2016), Permiano-Triássico (Siberian Trap) (Sanei, Grasby, Beauchamp, 2012; Sial *et al.*, 2021), Devoniano (Viluy Trap) (Lu *et al.*, 2021) e Ordoviciano-siluriano (Lu *et al.*, 2021). Além disso, perturbações de menor impacto também estão associadas com ativação das grandes LIP's, denominadas de Eventos de Anoxia Oceânica (OAE's). Ao longo do tempo geológico, foram identificadas as seguintes anomalias na razão Hg/COT associadas a eventos de OAE: OAE Toarciano (~ 183 Ma) (Gambacorta *et al.*, 2023; Liu *et al.*, 2020), OAE 1a (~ 120 Ma) (Erba *et al.*, 2015; Fan, *et al.*, 2021; Núñez-Useche *et al.*, 2020), OAE 1b (~ 113 Ma) (Galloway *et al.*, 2023; Sabatino *et al.*, 2015, 2018) e OAE 1d (~ 103 Ma) (Rodríguez-Cuicas, Montero-Serrano, Garbán, 2019).

As ativações das LIP's foram responsáveis pelo enriquecimento dos oceanos por metais-traço, aumento da produtividade, anoxia oceânica, mudanças da comunidade planctônica, crises dos organismos calcificadores, mudanças climáticas e pequenas extinções (e.g. Bodin *et al.*, 2023; Bond, Grasby, 2017; Davies *et al.*, 2020; Davis, 2023; Keller, 2008). De acordo com Robock, (2000), a ativação das LIP's ocasiona aumento no teor de dióxido de carbono ( $CO_2$ ) na atmosfera, podendo causar acidificação dos oceanos; maior incidência de chuva ácida; danos à camada de ozônio ( $O_3$ ) atmosférico; aumento da radiação UV-B; aumento na concentração de metais tóxicos; resfriamento da

superfície; aquecimento da estratosfera; aumento da poeira atmosférica, causando bloqueio da luz solar e diminuição da temperatura.

### 3.2 Indicadores das condições Paleoredox

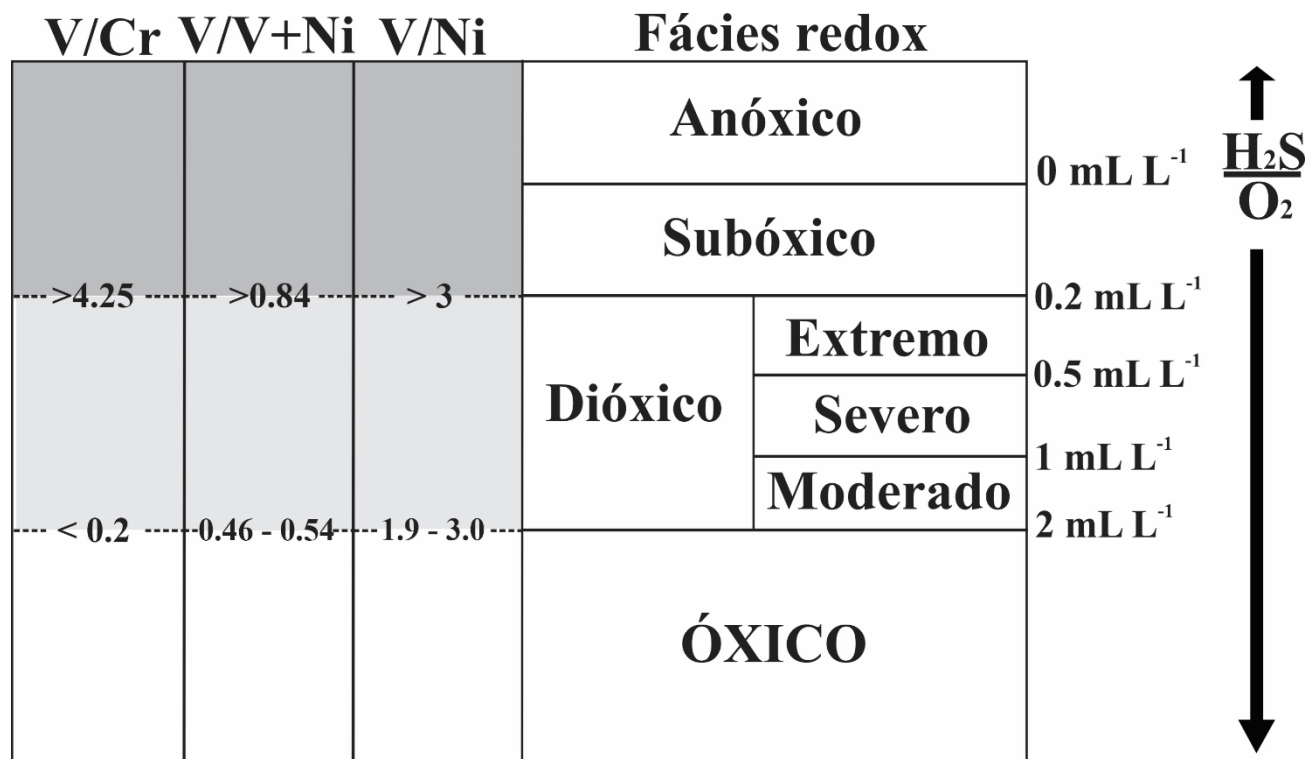
Os metais-traço são sensíveis às mudanças do estado redox, sendo removidos do ambiente aquoso e transferidos para o sedimento quando submetidos a alterações do potencial redox do meio. Esta transferência pode ocorrer por adsorção com os oxihidróxidos (Fe, Al e Mn), soterramento com a matéria orgânica (formação de compostos organometálicos), e co-precipitação com minerais (Tribovillard *et al.*, 2006). As condições deposicionais são influenciadas diretamente pela disponibilidade de oxigênio e enxofre no ambiente, o que pode gerar o aumento ou a diminuição das concentrações desses elementos no sedimento (Algeo, Li, 2020; Tribovillard *et al.*, 2006). Estudos anteriores demonstraram a eficácia na aplicação de V, Cr, Fe, Mn, Ni e Pb para identificar as alterações do estado paleoredox em diversos períodos, ambientes deposicionais e distintas estratigráfias: Criogeniano, Cambriano (evento SPICE) (Mackey, Stewart, 2019), Edicarano-Cambriano (Guo *et al.*, 2007), Devoniano (Kuwahara *et al.*, 2022), Aptiano-Albiano (Hamid *et al.*, 2024; Sabatino *et al.*, 2015; Saucedo-Samaniego *et al.*, 2021), Cenomaniano-Turoniano (Bentum *et al.*, 2009) e grandes eventos de extinção em massa (Permiano-Triássico e Cretáceo-Paleógeno) (Abu-Ali; El-Kammar; Kuss, 2020; Benigno; Sial; Lacerda, 2018; Sial *et al.*, 2018, 2021).

Além disso, com o intuito de determinar a característica geral dos ambientes deposicionais, nós seguimos a classificação proposta por Jones, Manning (1994) e Tyson, Pearson (1991) (Figura 4). Nesta condição o ambiente é categorizado de acordo com a concentração de oxigênio e a presença dos sulfetos oriundos da sulfato-redução bacteriana no ambiente deposicional. Neste contexto, os ambientes são classificados em óxico ( $> 2\text{mL O}_2\text{L}^{-1}$ ), dióxico (2 a 0 mL  $\text{O}_2\text{L}^{-1}$ ), subóxico (0 mL  $\text{O}_2\text{L}^{-1}$ ,  $\text{Fe}^{2+} > 0$ ,  $\text{H}_2\text{S} = 0$ ) e anóxico-euxínico (0 mL  $\text{O}_2\text{L}^{-1}$ ,  $\text{Fe}^{2+} = 0$ ,  $\text{H}_2\text{S} > 0$ ) (Algeo, Li, 2020; Algeo, Maynard, 2004; Tribovillard *et al.*, 2006).

Jones e Manning (1994) classificaram as condições paleoambientais (óxido, dióxico e anóxico) através das razões: V/Cr (Vanádio/Cromo) e V/V+Ni (Vanádio/Vanádio + Níquel). Galarraga *et al.*, (2008) utilizaram a razão bimetal V/Ni também para classificar as condições óxicas deposicionais. A razão  $\text{V}/\text{Cr} < 2,0$  indica que o ambiente é óxico; condições dióxicas ocorrem entre 2,0 – 4,25; e subóxicas a anóxicas quando a razão  $\text{V}/\text{Cr} > 4,25$ . Para a razão V/Ni, os valores entre 1,9 - 3 indicam ambiente

subóxico, enquanto valores de  $V/Ni > 3,0$  são típicos de ambiente anóxicos. Utilizando-se a razão  $V/V+Ni$ , os valores  $> 0,84$  indicam condições euxínicas, entre  $0,54 - 0,83$  ambiente anóxico, enquanto valores entre  $0,46$  a  $0,54$  dióxico (Galarraga *et al.*, 2008; Jones, Manning, 1994; Rivera *et al.*, 2018).

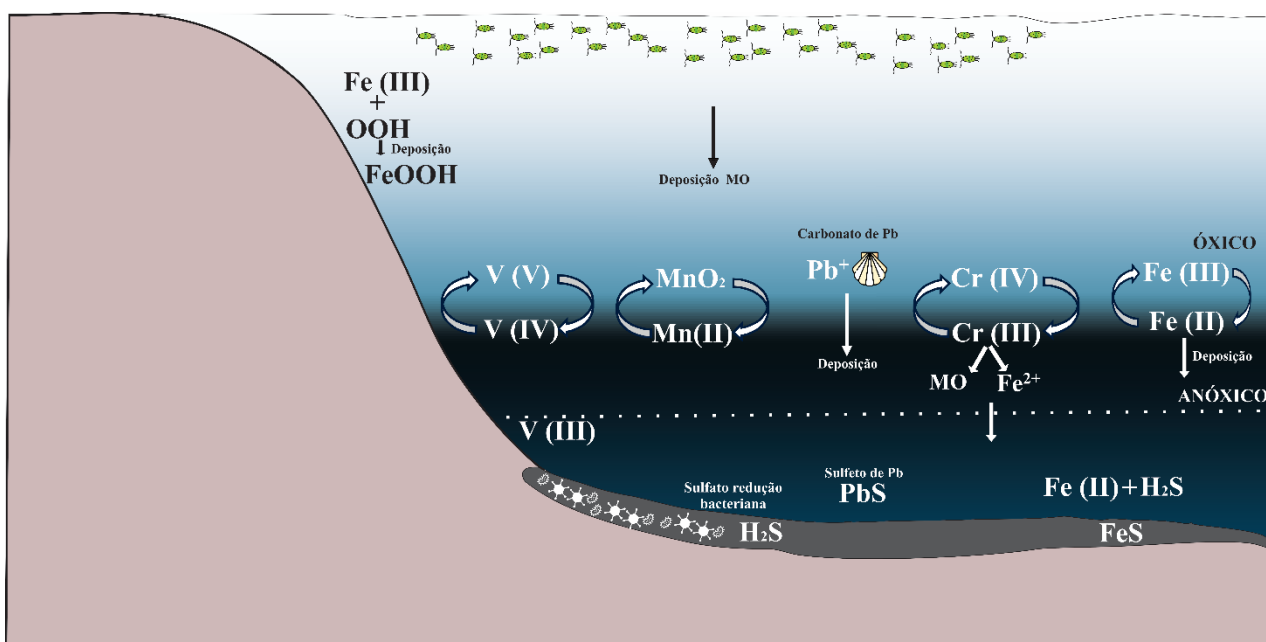
**Figura 9.** Classificação redox utilizando a razão entre metais proposta por Jones e Manning (1994).



Fonte: Adaptado de Jones; Manning (1994) e Algeo; Liu (2020).

Para determinar as alterações relevantes das mudanças paleoredox pode ser utilizado o fator de enriquecimento (EF) dos metais:  $Pb^{EF}$ ,  $V^{EF}$ ,  $Cr^{EF}$ ,  $Mn^{EF}$  e  $Fe^{EF}$ . A aplicação desses metais leva em consideração o seu comportamento em ambiente redutor e ambiente óxico (Algeo, Liu, 2020; Algeo, Maynard, 2004). Em ambientes óxicos a tendência dos metais-traço é adsorver aos oxi-hidróxidos de Al, Fe e Mn, além de coprecipitar com a matéria orgânica formando complexos orgânicos. Para ambiente anóxicos e submetidos à sulfato-redução bacteriana, os metais-traço adsorvem com o sulfeto de hidrogênio ( $H_2S$ ) e são transferidos para o compartimento sedimentar. A figura 5 demonstra o comportamento dos metais-traço indicadores de paleoredox no ambiente aquático.

**Figura 5.** Comportamento geoquímico dos indicadores geoquímicos das condições paleoredox no ambiente aquático.



Fonte: Autor.

A seguir, serão descritos os comportamentos dos metais-traço utilizados como indicadores das condições paleoredox em ambientes aquáticos quando submetidos a ambiente óxicos e anóxicos:

**Vanádio (V):** apresenta três espécies iônicas (penta-, tetra- e tri- valente), sendo a sua espécie predominante modificada de acordo com o estado redox do ambiente deposicional influenciado diretamente pelas perturbações climáticas do ambiente (Fan *et al.*, 2021; Wu *et al.*, 2020). A forma pentavalente do V é comum em condições óxicas e normalmente encontra-se adsorvida aos oxi-hidróxidos de Fe-Mn (Wu *et al.*, 2019). Em ambientes redutores, há a redução da forma oxidada para a forma V(IV), e co-precipitação com minerais e, principalmente, com a matéria orgânica, conforme observado durante o evento OAE 2- Cenomaniano-Turoniano (94 Ma) (Ostrander, Owens, Nielsen, 2017). Ambientes extremamente redutores, onde há a presença de H<sub>2</sub>S livre devido à sulfato-redução bacteriana, favorecem a redução para a forma trivalente predominante nem condições anóxicas (Gustafsson, 2019; Lewanand, Maynard, 1982; Tribouillard *et al.*, 2006; Wu *et al.*, 2020, 2019).

**Cromo (Cr):** O Cr (VI) é predominante em ambientes oxigenados ( $\text{CrO}_4^{2-}$ ), enquanto sua forma reduzida, Cr (III), principal espécie encontrada no sedimento, é predominante em ambientes subóxicos na forma de  $\text{Cr}(\text{OH})_3$  (Calvert, Pedersen, 1993;

Nasemann *et al.*, 2020). O processo de sedimentação do Cr inicia-se no processo de adsorção às partículas de matéria orgânica, sendo depositados em condições com pouco oxigênio disponível (Reinhard *et al.*, 2014). A redução do cromo em ambientes óxicos pode ser catalisada pela presença de agentes redutores, como: matéria orgânica, H<sub>2</sub>O<sub>2</sub> e Fe (II) (Saad *et al.*, 2017). Além disso, há indícios da mediação microbiana na zona de mínimo de oxigênio marinho (OMZ), favorecendo a predominância do Cr trivalente (Huang *et al.*, 2021). Estudos anteriores identificaram que há períodos da história da Terra que a forma Cr (III) foi predominante, devido à desoxigenação marinha e expansão da OMZ (Nana Yobo *et al.*, 2022).

**Chumbo (Pb):** o Pb em condições óxicas encontra-se na forma de cátion livre (Pb<sup>+</sup>), podendo ser adsorvido com o carbonato (PbCO<sub>3</sub>). Em condições anóxicas, a tendência é haver precipitação com espécies de sulfeto (Algeo, Maynard, 2004; Morse, Luther, 1999). A assimilação do Pb com os sulfetos ocorre também em condições euxínicas (2 a 0 mL O<sub>2</sub> L<sup>-1</sup>) demonstrando alta capacidade desse elemento em precipitar quando submetido à redução do oxigênio (Gregory *et al.*, 2015). O processo de deposição do Pb em ambientes anóxicos está associado com a presença de piritas diagenéticas em xisto preto e outras litofácies (Tribovillard *et al.*, 2006). Os estudos de Algeo, Liu (2020) e Milot *et al.* (2021) demonstraram o enriquecimento de Pb em rochas do Fanerozóico durante grandes eventos de anoxia (Criogeniano- 613 Ma, Devoniano Superior- 395 Ma, OAE Toarciano- 186 Ma, e nos eventos OAE 1a- 120 Ma, OAE 1b -114 Ma, OAE 2- 93 Ma), indicando a influência direta na formação dos minerais de sulfetos (pirita) no processo deposicional do Pb devido à baixa concentração de oxigênio do ambiente.

**Manganês (Mn):** o Mn é encontrado na natureza nas formas Mn<sup>2+</sup> e MnCl<sup>+</sup>, sendo comum a forma Mn (II) em ambientes anóxicos. Nos ambientes sedimentares com altas concentrações de oxigênio é comum suas formas insolúveis Mn (III) e Mn (IV) (Algeo, Maynard, 2004; Tribovillard *et al.*, 2006). As formas oxigenadas do Mn são responsáveis pela transferência de metais-traço do compartimento aquoso para o sedimento através da formação de oxihidróxidos (MnO<sub>2</sub>) (Gambacorta *et al.*, 2023). Estudos anteriores demonstraram que durante o Grande Evento de Oxidação (GOE, entre 2.501 e 2.220 Ga) o Mn teve grande capacidade de precipitar de metais-traço (As, Cu, Zn, Pb, Co, Ni, Cr e U), transferindo-os do ambiente aquático para o sedimento (Hashempour *et al.*, 2023; Konovalov *et al.*, 2004). Na interface água-sedimento, em contato com o ambiente redutor, pode ocorrer a dissolução do manganês para a forma Mn (II) (Robbins *et al.*, 2023). Neste caso, retorna para a coluna de água por difusão ascendente podendo

precipitar novamente através da adsorção com o carbonato de cálcio formando o mineral rodocrosita ( $\text{MnCO}_3$ ) e/ou precipitar com a pirita (Santos *et al.*, 2022).

**Ferro (Fe):** o ferro é encontrado na natureza em duas formas principais, nas quais o seu comportamento está associado com as concentrações de oxigênio do ambiente. O Fe (II) é comum em ambientes anóxicos, enquanto o Fe (III) está associado com os oxi-hidróxido (Tribovillard *et al.*, 2006). A forma oxi-hidróxido de Fe possui grande capacidade de transporte e transferência de outros metais-traço para o compartimento sedimentar (Ramírez-Pérez, Blas, 2017). Este elemento atua como limitante no desenvolvimento da cadeia trófica dos ambientes aquáticos e forma complexos com a matéria orgânica (Weber, Allard, Benedetti, 2006). Sob condições redutoras e ricas em matéria orgânica, ocorre a formação de piritas ( $\text{FeS}_2$ ) mediada pela sulfato-redução bacteriana. Quando há o aumento do oxigênio, o Fe (II) é liberado na interface-água sedimento e retorna para sua fase Fe (III) (Chen *et al.*, 2022; Tribovillard *et al.*, 2006). Como exemplo de mudanças do estado redox no passado geológico, pode-se destacar o evento OAE-Toarciano, a ativação da LIP Karoo -Ferrar foi responsável panoxia oceânica e formação de piritas frambooidais, que também foi capaz de adsorver metais-traço e transferir esses elementos para o compartimento sedimentar (Chen *et al.*, 2023).

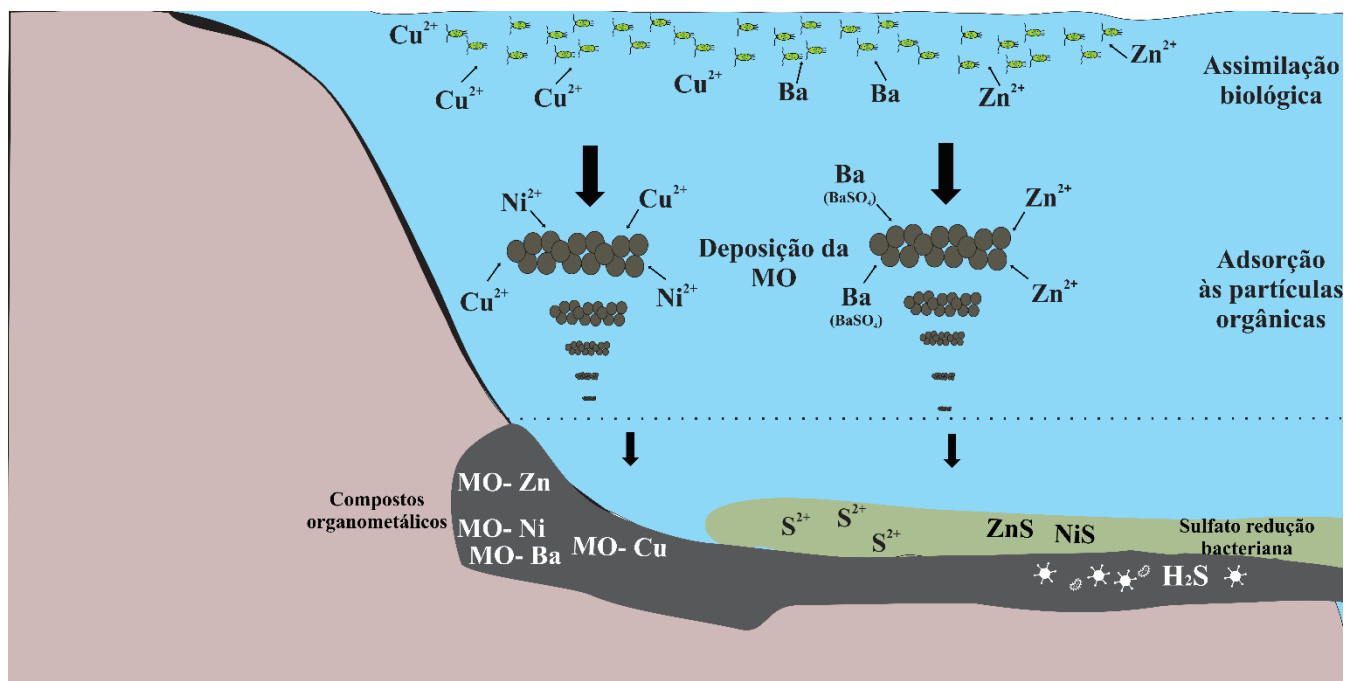
### 3.3 Paleoprodutividade

Para determinar a variação da paleoprodutividade em eventos de perturbações no ciclo do carbono (OAE e extinções em massa), normalmente utilizam-se o carbono orgânico total (COT) e os isótopos de carbono ( $\delta^{13}\text{C}_{\text{Carbonato}}$  e  $\delta^{13}\text{C}_{\text{Orgânico}}$ ). Estes eventos normalmente são marcados pela deposição de folhelhos ricos em COT e/ou mudanças isotópicas no comportamento do carbono (Davis, 2023; Grasby *et al.*, 2019). Entretanto, a adição de outros indicadores geoquímicos, como os metais-traço, auxilia a determinar as mudanças da paleoprodutividade durante os eventos onde há a perturbações no ciclo do carbono (Galloway *et al.*, 2023; Sabatino *et al.*, 2015). Neste contexto, o uso de metais-traço essenciais e/ou que tem forte correlação com a matéria orgânica (Bário, Cobre, Zinco e Níquel) têm demonstrado ser uma importante ferramenta para determinar alterações na paleoprodutividade durante as mudanças climáticas globais (Lu *et al.*, 2021).

Para determinar as alterações da paleoprodutividade foi aplicado o Fator de Enriquecimento (FE) para o  $\text{Cu}^{\text{EF}}$ ,  $\text{Zn}^{\text{EF}}$ ,  $\text{Ni}^{\text{EF}}$  e  $\text{Ba}^{\text{EF}}$ . O uso desses elementos está vinculado a suas capacidades de adsorção com o COT e por serem elementos essenciais

no desenvolvimento da cadeia trófica, indicando oscilações e condições anômalas da paleoprodutividade (Steiner *et al.*, 2017; Tribovillard *et al.*, 2006). A figura 6 demonstra o comportamento dos metais-traço de paleoprodutividade no ambiente.

**Figura 6.** Comportamento dos indicadores geoquímicos da paleoprodutividade no ecossistema aquático.



Fonte: Autor.

A seguir serão descritos o comportamento dos metais-traço utilizados como indicadores geoquímicos da paleoprodutividade em ambientes aquáticos e os processos deposicionais que influenciam em sua deposição:

**Cobre (Cu):** o cobre apresenta uma correlação positiva com a produção primária funcionando como um micronutriente para o desenvolvimento da cadeia trófica (Pinedo-González *et al.*, 2015). Além disso, forma complexos organometálicos estáveis acelerando o processo de deposição e enriquecimento do sedimento, sendo assim um importante indicador geoquímico das variações dos fluxos deposicionais da matéria orgânica. Esta aplicabilidade foi usada nos estudos de Sabatino *et al.* (2015) e Núñez-Useche *et al.* (2020), durante os eventos de anoxia oceânica (OAE 1a e 1b), os autores observaram que durante a ativação dos vulcanismos do Ontong Java e do Planalto Kerguelen, respectivamente, foram registrados o aumento do Cu devido ao aumento da paleoprodutividade. No sedimento, o Cu (II) é complexado com a matéria orgânica em condições anóxicas, pode ser reduzido via sulfato-redução bacteriana, tendo como

resultado dessa mineralização o Cu(I). Posteriormente, pode precipitar na forma de sulfeto de cobre (CuS) (Ai *et al.*, 2023; Steiner *et al.*, 2017).

**Zinco (Zn):** em condições óxicas o Zn encontra-se em sua forma solúvel ( $Zn^{2+}$  ou  $ZnCl^+$ ), podendo complexar com a matéria orgânica e adsorver aos oxi-hidróxidos de Fe e Mn (Tribovillard *et al.*, 2006). O Zn em sua forma oxidada é um micronutriente essencial e limitante para o desenvolvimento da produtividade primária nos ambientes aquáticos (Gueguen, Rouxel, Fouquet, 2022). A correlação existente do Zn com o COT ao longo do tempo geológico demonstra a importância do Zn na base da cadeia trófica e, portanto, capaz de identificar períodos com maiores contribuições orgânicas (Benamara *et al.*, 2020). Além disso, quando submetidos a condições anóxicas (principalmente quando influenciado pela sulfato-redução), esse elemento pode precipitar com os sulfetos livres, adsorvendo às piritas frambooidais, formando a esfarelita (Ai *et al.*, 2023).

**Níquel (Ni):** é encontrado em duas formas principais nos ambientes óxicos ( $Ni^{+2}$  e  $NiCl^+$ ), sendo frequentemente encontrado na natureza complexado com carbonatos ( $NiCO_3$ ) (Algeo, Liu, 2020; Algeo, Maynard, 2004; Calvert, Pedersen, 1993). Em altas concentrações podem estar vinculados com condições deposicionais anóxicas, sendo comum estar associado com os folhelhos ricos em matéria orgânica e em ambientes ricos em sulfetos (Galarraga *et al.*, 2008). O processo deposicional do Ni em condições anóxicas ocorre com a sedimentação e complexação com a matéria orgânica, formando compostos organometálicos (Rinklebe, Shaheen, 2017). Este processo foi demonstrado por Sabatino *et al.* (2015) durante o OAE 1b, onde há o aumento da concentração do Ni em conjunto com o soterramento do COT devido ao aumento da anoxia. Quando submetido a ambiente onde ocorre sulfato redução bacteriana, o Ni liga-se aos sulfetos formando sulfeto insolúvel (NiS) que pode ser adsorvido por solução sólida das piritas autigênicas (Lewan, Maynard, 1982; Lúcio *et al.*, 2022).

**Bário (Ba):** Nos ambientes aquáticos o Ba associa-se com os sulfatos formando a barita ( $BaSO_4$ ), onde este mineral pode associar-se aos carbonatos, matéria orgânica e sílica biogênica (Robin *et al.*, 2003). Este elemento é adsorvido pelo sulfato ( $SO_4$ ) oriundo da degradação da matéria orgânica, formando este mineral e precipitando no compartimento sedimentar (House, Norris, 2020; Tribovillard *et al.*, 2006). Neste caso, os cristais de barita têm a capacidade de registrar as oscilações da paleoprodutividade devido a correlação com a matéria orgânica (Liguori, Almeida, Rezende, 2016; Shen *et al.*, 2015).

### **3.4 Isótopo de Carbono ( $\delta^{13}\text{C}_{\text{VPDB}}$ )**

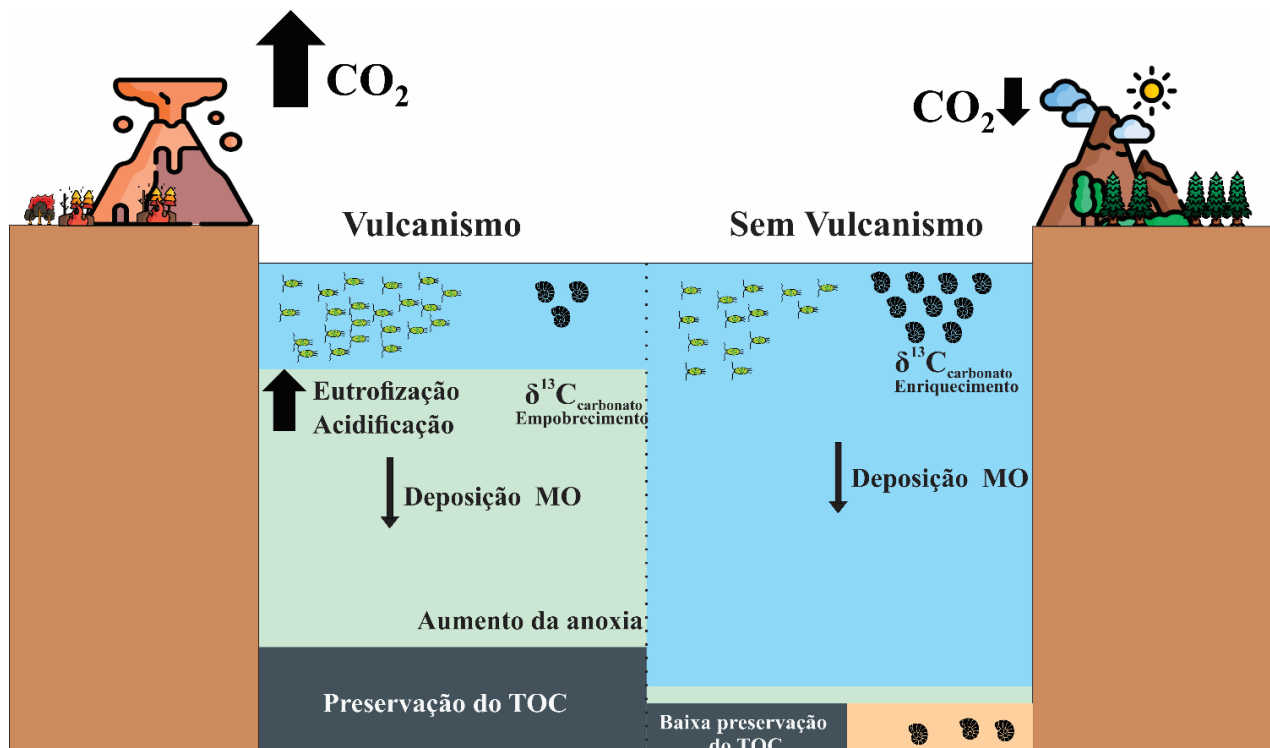
Os isótopos de carbono estão nos ambientes aquáticos em duas formas estáveis:  $^{12}\text{C}$  (99% do carbono) e  $^{13}\text{C}$  (1% do carbono). As suas proporções variam na natureza mediadas por processos químicos, físicos e biológicos variando as suas concentrações de acordo com os eventos a que são submetidos no espaço e no tempo (Pessenda *et al.*, 2005). Para determinar os desvios das proporções entre  $^{12}\text{C}$  e  $^{13}\text{C}$  utiliza-se a notação  $\delta^{13}\text{C}_{\text{VPDB}}$  (Vienna Pee Dee Belemnite) (Hoefs, 2009). Na atmosfera, os valores do  $\delta^{13}\text{CO}_2$  atmosférico apresentam valores negativos (-6,6 ‰), sendo sua concentração alterada quando por processos bioquímicos e físicos nos reservatórios marinhos e continentais (Graven, Keeling, Rogelj, 2020).

No ambiente terrestre os isótopos de  $\delta^{13}\text{CO}_2$  são fracionados durante a fotossíntese (~ 8‰). É importante destacar que dependendo do tipo de planta, C<sub>3</sub> (árvores) e C<sub>4</sub> (gramíneas), também há discriminação isotópica (Swart, 2015). No ambiente aquático, o CO<sub>2</sub> entra por difusão, carregando a assinatura isotópica do  $\delta^{13}\text{CO}_2$  atmosférico. Em seguida, os processos físico-químicos (bomba de solubilidade) e biológicos (bomba biológica) modificam a assinatura isotópica do  $\delta^{13}\text{CCO}_2$  atmosférico (Eide *et al.*, 2017). No caso da bomba de solubilidade, há a reação química do CO<sub>2</sub> com a água formando o Carbono Inorgânico Dissolvido (DIC), formando outros compostos: H<sub>2</sub>CO<sub>3</sub>, HCO<sup>-</sup><sub>3</sub> e CO<sub>2</sub><sup>-3</sup> (Millero, 2007). No caso da bomba biológica, os processos que mediam a assinatura isotópica do  $\delta^{13}\text{C}$  são a fotossíntese (~ -24 a -20‰) e a degradação bacteriana (McCormack, Kwiecien, 2021). Quando o fitoplâncton incorpora o  $^{12}\text{C}$ , fração mais leve, ocorre o enriquecimento do  $^{13}\text{C}$  nas águas superficiais. Neste caso, a matéria orgânica particulada formada assimila a assinatura e registra as condições da paleoprodutividade (Swart, 2015).

As oscilações do  $\delta^{13}\text{C}_{\text{Carbonato}}$  são controladas pela variação do pH, pois controlam a relação entre a precipitação ou dissolução dos minerais de aragonita e calcita nos ecossistemas aquáticos (Weissert *et al.*, 1998; Weissert, Erba, 2004). Dentro desse contexto, incursões positivas do  $\delta^{13}\text{C}_{\text{Carbonato}}$  são indícios de um período com maior preservação e produção dos organismos calcificadores, enquanto incursões negativas do  $\delta^{13}\text{C}_{\text{Carbonato}}$  assinalam uma crise biológica dos calcificadores, diminuindo o enriquecimento deste elemento e aumentando o soterramento do carbono orgânico (Eide *et al.*, 2017; O'Leary, 1981).

Exemplo da oscilação do  $\delta^{13}\text{C}_{\text{Carbonato}}$  pode ser destacado durante as transições Cretáceo-Paleógeno (~ 66 Ma) e Permiano-Triássico (~ 251 Ma), foram constatadas crises biológicas do plâncton marinho (Shen *et al.*, 2019; Sial *et al.*, 2013). As incursões negativas do  $\delta^{13}\text{C}_{\text{Carbonato}}$  e as anomalias de Hg demonstram que as ativações das grandes LIP's (Deccan e Siberian Trap) foram responsáveis por injetar grandes quantidades de CO<sub>2</sub> na atmosfera, tendo como resultado acidificação oceânica e crises biológicas, principalmente sobre os organismos calcificadores (Figura 7) (Font *et al.*, 2016; Sanei, Grasby, Beauchamp, 2012; Sial *et al.*, 2018, 2021). Nos eventos de extinções do PTE e KPg as perturbações do plâncton marinho resultaram na supressão das plataformas continentais carbonáticas e expansão das plataformas siliciclásticas (Beauchamp; Grasby, 2012; Grasby *et al.*, 2015).

**Figura 7.** Comportamento isotópico do  $\delta^{13}\text{C}_{\text{Carbonato}}$  de acordo com os períodos de variações magmáticas.



Fonte: Autor.

### 3.5 Isótopo de oxigênio ( $\delta^{18}\text{O}_{\text{VPDB}}$ )

Os isótopos de oxigênio ( $\delta^{18}\text{O}$ ) são encontrados na natureza nas fases sólidas, líquidas e gasosas. As três formas isotópicas principais existentes na natureza são <sup>16</sup>O (99,757%), <sup>17</sup>O (0,038%) e <sup>18</sup>O (0,205%) (Gradstein, Ogg *et al.*, 2020). Por conta de sua abundância isotópica, utiliza-se a razão <sup>18</sup>O/ <sup>16</sup>O para determinar as alterações

paleoclimáticas (Hoefs, 2009). O  $\delta^{18}\text{O}_{\text{VPDB}}$  é utilizado para carbonatos de baixa temperatura, enquanto o  $\delta^{18}\text{O}_{\text{SMOW}}$  são usuais em outras matrizes (água, silicatos, fosfatos, sulfatos e carbonatos de altas temperaturas) (Gradstein, Ogg *et al.*, 2020; Pearson, 2012). Durante a sua deposição, os registros do  $\delta^{18}\text{O}$  em carbonatos são influenciados pela temperatura, fluido precipitante, mineralogia e pH da solução (Swart, 2015). Existem duas escalas na determinação do isótopo de oxigênio:  $\delta^{18}\text{O}_{\text{VPDB}}$  (*Vienna Pee Dee Belemnite*) e  $\delta^{18}\text{O}_{\text{SMOW}}$  (*Standard Mean Ocean Water*), sendo suas aplicabilidades distintas.

Portanto, a aplicação do  $\delta^{18}\text{O}_{\text{VPDB}}$  visa determinar períodos de glaciação e interglaciais em escalas de tempo curta. O empobrecimento desse isótopo assinala períodos interglaciais, enquanto o enriquecimento demonstra estágios glaciais (Ruddiman, 2008). Também é possível determinar as oscilações da pluviosidade, onde os valores negativos do  $\delta^{18}\text{O}_{\text{VPDB}}$  assinalam períodos com maior evaporação, enquanto o enriquecimento deste elemento assinala períodos com aumento da pluviosidade (Pearson, 2012). Além disso, o  $\delta^{18}\text{O}_{\text{VPDB}}$  também é utilizado para determinar as variações da paleotemperatura através das proporções existentes nos registros de  $^{16}\text{O}$  e  $^{18}\text{O}$ . No caso, o enriquecimento do  $\delta^{18}\text{O}_{\text{VPDB}}$  caracteriza um ambiente com diminuição da paleotemperatura, enquanto períodos com empobrecimento do  $\delta^{18}\text{O}_{\text{VPDB}}$  indica o aumento (Gradstein, Ogg *et al.*, 2020; Scotese *et al.*, 2021).

## HIPÓTESE

A Bacia do Araripe é caracterizada por apresentar grandes variações litológicas e paleoambientais, rico acervo fossilífero e o registro de crises biológicas. O uso da Quimioestratigrafia pode colaborar na compreensão das relações entre as mudanças paleoambientais climáticas e as crises biológicas que ocorreram na Bacia do Araripe. Dentro desse contexto, a ativação das Grandes Províncias Ígneas (LIP's) do intervalo Aptiano-Albiano foram responsáveis mudanças nos processos deposicionais, gerando o aumento da produtividade, paleoredox, paleosalinidade, oscilações paleoclimáticas (períodos úmidos-secos) e eventos de mortalidade na Bacia do Araripe.

## 4. OBJETIVOS

O presente estudo tem o objetivo de caracterizar através da Quimioestratigrafia as mudanças paleoambientais que ocorreram na Bacia do Araripe durante o Cretáceo Inferior (Formações Barbalha, Crato e Romualdo). Além disso, correlacionar e identificar prováveis interferência dos eventos vulcânicos que foram responsáveis por mudanças paleoambientais na Bacia do Araripe e, consequentemente, associá-las com as crises biológicas registradas no ambiente deposicional.

### 4.1 Objetivos Específicos

- Apresentar os processos paleoambientais que ocorreram na Bacia do Araripe no Grupo Santana (formações Barbalha, Crato e Romualdo), identificando as alterações da paleoprodutividade, paleoredox e paleoclima durante Cretáceo Inferior (Aptiano-Albiano) na Bacia do Araripe;
- Correlacionar as anomalias de mercúrio (Hg) oriundas do vulcanismo e seus impactos locais na Bacia do Araripe através das anomalias de metais-traços. A interferência dos eventos de vulcanismo foi avaliada através das análises das razões (Hg/COT, Hg/Al e Hg/Fe). Para identificar as anomalias dos metais-traço foi determinado os fatores de enriquecimento da paleoprodutividade ( $Cu^{EF}$ ,  $Zn^{EF}$ ,  $Ni^{EF}$ ,  $Ba^{EF}$ ) e do estado paleoredox ( $Pb^{EF}$ ,  $V^{EF}$ ,  $Cr^{EF}$ ,  $Mn^{EF}$ ,  $Fe^{EF}$ ). Além disso, aplicou-se a razões elementares dos metais-traço para determinar as oscilações paleoredox ( $V/Cr$ ,  $V/Ni$  e  $V/V+Ni$ ), paleosalinidade ( $Sr/Ba$ ), paleoclimatologia ( $Sr/Cu$ ) e aportes detriticos ( $Al$  e  $Fe$ );
- Determinar as condições deposicionais através dos isótopos estáveis de carbono ( $\delta^{13}C_{VPDB}$ ) e oxigênio ( $\delta^{18}O_{VPDB}$ ), sendo possível estabelecer as oscilações da paleoprodutividade e o paleoclimáticas, respectivamente;

- Determinar através dos métodos geoestatísticos e oscilações dos metais-traço os mecanismos responsáveis pelas mudanças paleoambientais que resultaram nos eventos de mortalidade registrados na Formação Crato;
- Identificar o desenvolvimento da cadeia trófica da paleoictiofauna e outros organismos através das concentrações do Hg nos registros fossilíferos da Formação Romualdo.

## CAPÍTULO 1

### Aptian-Albian Paleoenvironmental Geochemistry: Araripe Basin, Northeastern Brazil

O primeiro manuscrito, em síntese, trata-se da caracterização geoquímica do intervalo Aptiano e transição com o Albiano na Bacia do Araripe. O objetivo principal é caracterizar as mudanças paleoambientais influenciadas pelos eventos de vulcanismo que ocorreram no Cretáceo Inferior. Este trabalho possibilitou observar mudanças paleoclimáticas influenciadas, provavelmente, pelo vulcanismo do Ontong Java (OJP) e platô Kerguelen Sul (SKP). Ambos foram responsáveis pelos eventos de anoxia oceânica 1a e 1b (OAE) e podem ter desencadeados grandes modificações do estado paleoredox, paleoprodutividade e paleoclimáticas na Bacia do Araripe. Autorias de Igor Hamid Ribeiro Azevedo, Luiz Drude Lacerda, Antônio Álamo Feitosa Saraiva, Alcides Nóbrega Sial, Ana Paula Aquino Benigno e José Edvar Aguiar, intitulado “*Aptian-Albian Paleoenvironmental Geochemistry: Araripe Basin, Northeastern Brazil*”.

---

<sup>1</sup>Hamid, I. R. A.; Lacerda, L. D.; Saraiva, A. A. F.; Sial, A. N.; Benigno, A. P.; Aguiar, J. E. Aptian-Albian paleoenvironmental geochemistry: Araripe Basin, Northeastern Brazil. **Journal of South American Earth Sciences**. <https://doi.org/10.1016/j.jsames.2024.104856>.



## Aptian-Albian paleoenvironmental geochemistry: Araripe Basin, Northeastern Brazil

Igor Hamid Ribeiro Azevedo <sup>a,\*</sup>, Luiz Drude Lacerda <sup>a</sup>, Antônio Álamo Feitosa Saraiva <sup>c</sup>, Alcides Nóbrega Sial <sup>b</sup>, Ana Paula Aquino Benigno <sup>d</sup>, José Edvar Aguiar <sup>e</sup>

<sup>a</sup> LABOMAR, Institute of Marine Sciences, Federal University of Ceará, Fortaleza, CE, 60165-081, Brazil

<sup>b</sup> NEG-LABISE, Dept. of Geology, Federal University of Pernambuco, Recife, PE, 50740-530, Brazil

<sup>c</sup> Department of Physical and Biological Sciences, Regional University of Cariri, Crato, CE, Brazil

<sup>d</sup> IFCE, Federal Institute of Ceará, Campus of Umirim, Umirim, CE, 62660-000, Brazil

<sup>e</sup> Department of Engineering, Federal University of Maranhão, Campus do Bacanga, São Luís, MA, 65080-805, Brazil

### ARTICLE INFO

#### Keywords:

Metals  
Anoxic environment  
Ocean anoxic events  
Paleosalinity  
Isotopic carbon and oxygen  
Volcanism

### ABSTRACT

The geochemical record of the early Aptian and the transition to the Albian exposes the presence of Hg/TOC anomalies, revealing the interference of LIPs in paleoenvironmental changes in the Araripe basin. Redox-sensitive ( $V^{EF}$ ,  $Fe^{EF}$ ,  $Cr^{EF}$ ,  $Mn^{EF}$ ,  $Pb^{EF}$ ,  $V/Cr$ ,  $V/V + Ni$  and  $V/Ni$ ) and paleoproductivity ( $Cu^{EF}$ ,  $Zn^{EF}$ ,  $Ni^{EF}$  and  $Ba^{EF}$ ) proxies in the Santana Group (Barbalha, Crato and Romualdo formations) indicate conditions ranging from oxic to anoxic, and increased paleoproductivity and of trace elements concentrations during LIPs activation. Statistical analyses demonstrated that volcanism was associated with oscillations in paleosalinity ( $Sr/Ba$ ) and detrital supply ( $Al$ ). LIPs activity was responsible for the emission of  $CO_2$  into the atmosphere, generating paleoclimatic changes in temperature ( $\delta^{18}O$ ), a crisis in the productivity of calcifying organisms ( $\delta^{13}C_{carbonate}$ ), and an increase in the load of organic matter (TOC). We suggest that trace elements anomalies found in the early Aptian (Barbalha Formation) are associated with Ontong Java Plateau (OJP), responsible for OAE 1a, while the volcanism's proxies found in the Romualdo Formation occurred due to the Kerguelan South Plateau (SKP) volcanism, triggering the OAE 1 b.

## Highlights

- Changes in paleoproductivity, paleoredox state, paleosalinity and paleoclimate occurred in Aptian- Albian (Araripe Basin).
- Activation of LIPs and oceanic anoxia events (OAE).
- Stable isotopes ( $\delta^{13}C$  and  $\delta^{18}O$ ) and trace metal enrichment were consistent proxies of paleoenvironmental changes.

## Abstract

The geochemical record of the early Aptian and the transition to the Albian exposes the presence of Hg/TOC anomalies, revealing the interference of LIPs in paleoenvironmental changes in the Araripe basin. Redox-sensitive ( $V^{EF}$ ,  $Fe^{EF}$ ,  $Cr^{EF}$ ,  $Mn^{EF}$ ,  $Pb^{EF}$ ,  $V/Cr$ ,  $V/V+Ni$  and  $V/Ni$ ) and paleoproductivity ( $Cu^{EF}$ ,  $Zn^{EF}$ ,  $Ni^{EF}$  and  $Ba^{EF}$ ) proxies in the Santana Group (Barbalha, Crato and Romualdo formations) indicate conditions ranging from oxic to anoxic, and increased paleoproductivity and of trace elements concentrations during LIPs activation. Statistical analyses demonstrated that volcanism was associated with oscillations in paleosalinity ( $Sr/Ba$ ) and detrital supply ( $Al$ ). LIPs activity was responsible for the emission of  $CO_2$  into the atmosphere, generating paleoclimatic changes in temperature ( $\delta^{18}O$ ), a crisis in the productivity of calcifying organisms ( $\delta^{13}C_{carbonate}$ ), and an increase in the load of organic matter (TOC). We suggest that trace elements anomalies found in the early Aptian (Barbalha Formation) are associated with Ontong Java Plateau (OJP), responsible for OAE 1a, while the volcanism's proxies found in the Romualdo Formation occurred due to the Kerguelen South Plateau (SKP) volcanism, triggering the OAE 1b.

## 5.1 Introduction

The Aptian and the Aptian-Albian transition (121.4 to 113 Ma), Early Cretaceous, are marked by great transformations on Earth, including sea-level rise, volcanism, global warming, oceanic anoxia events (OAE) and marine and terrestrial biotic changes (Ogg *et al.*, 2016). Extreme events in the Aptian-Albian transition are associated with the activation of Large Igneous Provinces (LIPs), generating an increase in atmospheric carbon dioxide and other gases (HS, HCl, and HF), intensifying greenhouse effect (Sabatino *et al.*, 2018; Xu *et al.*, 2022). The rapid injection of CO<sub>2</sub> and methane into the atmosphere is responsible for drastic changes in the hydrological cycle; global warming; ocean acidification; acid rain; depletion of the ozone layer; trace metals and organic matter enrichment of sediment; primary productivity and terrestrial and marine biological global crises (Davis, 2023; Font, Bond, 2021; Grasby *et al.*, 2019; Racki, 2021).

The application of geochemical proxies such as trace metals and isotopes of  $\delta^{13}\text{C}_{\text{carbonate}}$  and  $\delta^{18}\text{O}$  are essential tools for determining variations in seawater chemistry, correlating global stratigraphic changes, and understanding impact of the LIPs on sedimentary basins. (Madhavaraju *et al.*, 2021; Saucedo-Samaniego *et al.*, 2021; Tribouillard *et al.*, 2006). Mercury anomalies are associated with emissions from volcanisms of LIPs during that period, the Ontong Java (OJP) and South Kerguelen Plateau (SKP). These LIPs were also responsible for Ocean Anoxic Events (OAE) (Charbonnier, Föllmi, 2017; Sabatino *et al.*, 2018). OAEs promoted changes in the carbon cycle, suggested by  $\delta^{13}\text{C}_{\text{carbonate}}$  oscillations (reduction of planktonic calcification) and increase in the organic carbon deposition (Tedeschi *et al.*, 2020; Weissert, Erba, 2004). OAEs also caused variations in paleotemperature ( $\delta^{18}\text{O}$ ), increased chemical weathering (Ti, Si, Al, and K) (Calvert, Pedersen, 1993; Touati, Haji, 2019), enrichment of geochemical proxies of paleoproductivity (Cu, Zn, Ni, and Ba), and redox-sensitive trace elements (Fe, Cd, Mn, Mo, Ni, V, and As) (Algeo, Li, 2020; Algeo, Liu, 2020; Tribouillard *et al.*, 2006).

The OJP volcanism occurred in the early Aptian (~120 Ma), with higher CO<sub>2</sub> emissions indicating perturbations on the global climate and holding it directly responsible for the OAE 1a (Mehay *et al.*, 2009). It has been estimated that approximately 9,600 Gt of CO<sub>2</sub> were emitted by OJP into the atmosphere, resulting in the high carbon deposition, changes in  $\delta^{13}\text{C}_{\text{carbonate}}$ , global changes in paleoproductivity and paleoredox state (Adloff *et al.*, 2020; Erba *et al.*, 2015; Fan *et al.*, 2021; Naafs *et al.*, 2016; Weissert,

Erba, 2004). The SKP (~118 – 110 Ma) was responsible for the OAE 1b, which caused enrichment of trace metals, increased TOC burial in sediments, biological crises of calcifying marine organisms, and oceanic anoxia (Erba *et al.*, 2015; Sabatino *et al.*, 2015). Most affected calcifying organisms in OAE 1b, were planktonic organisms with biogenic silica, as suggested by the decrease of ornamented calcifying species and the predominance of small-sized calcium carbonate species (Huber, Leckie, 2011; Leckie *et al.*, 2002; Petrizzo *et al.*, 2012). The OAE 1b as a longer perturbation (~ 3,8 Ma) presented four sub-events (Jacob, Kilian, Paquier, and Leenhardt) based on different disturbance strength of the carbon cycle (Coccioni *et al.*, 2014; Leckie *et al.*, 2002; Sabatino *et al.*, 2015).

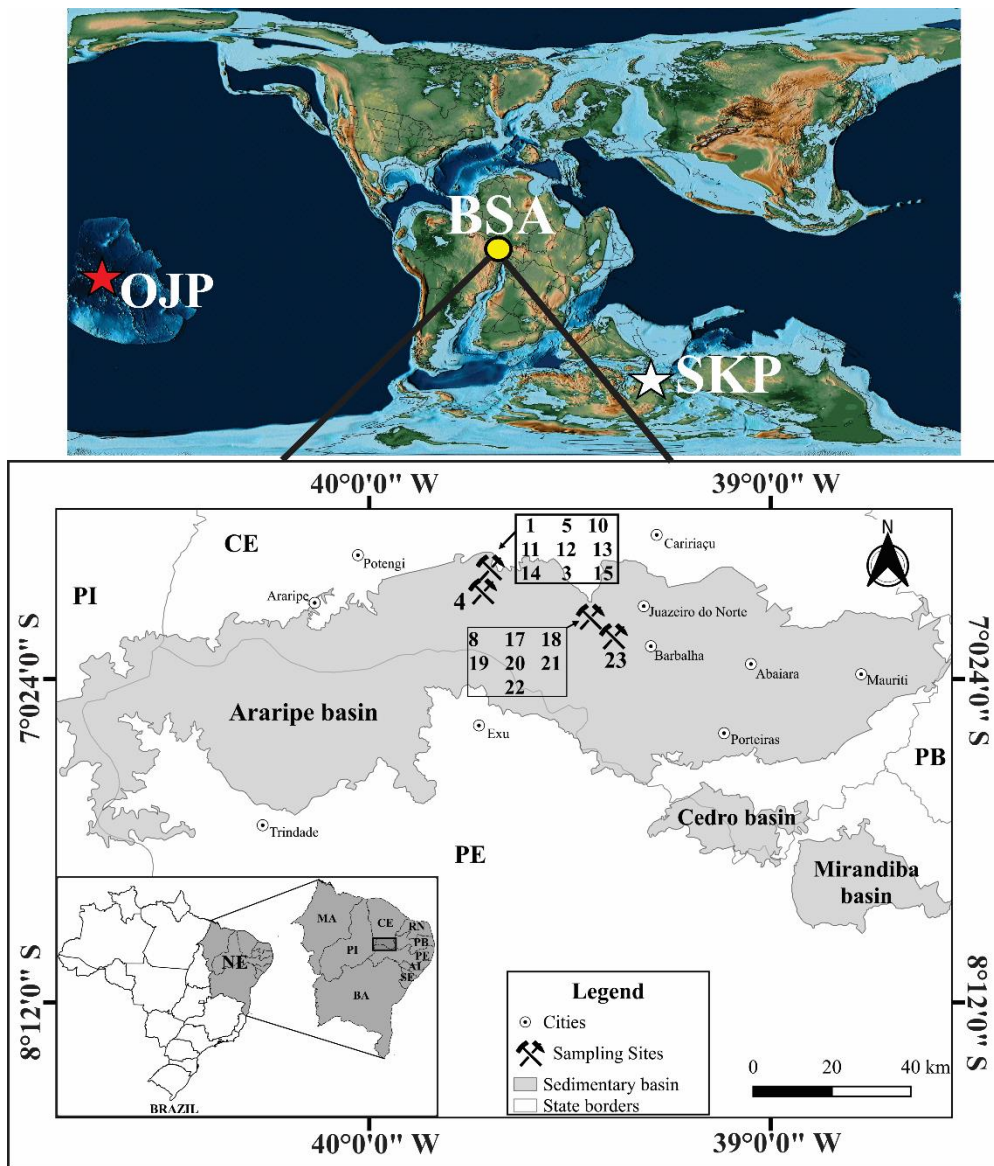
The Araripe Basin in Northeastern Brazil has been the subject of numerous sedimentological, paleontological, and stratigraphic studies (Assine *et al.*, 2014; Fara *et al.*, 2005; Martill, 1988; Rios-Netto *et al.*, 2012; Silvestre *et al.*, 2020; Valença *et al.*, 2003). However, geochemical investigations capable of revealing the paleoenvironmental conditions of this basin are still scarce, although a general description Hg chemostratigraphy and some other proxies can be found in Benigno *et al.* (2021). The Early Aptian to Aptian-Albian transition (Early Cretaceous) in this basin witnessed a global variation in the carbon cycle, causing several climate changes and biological crises. Thus, this study focuses on geochemical proxies to interpret the paleoenvironmental consequences of LIPs activation eventually registered in the Araripe Basin. The application of geochemical multi-proxies (trace metals) helps interpreting the environmental evolution of the events that occurred during the deposition of the Santana Group (Barbalha, Crato, and Romualdo formations), making it possible to interpret and reconstruct the paleo redox, paleoproductivity and paleodetrital changes in the Araripe sedimentary basin.

## 5.2 Stratigraphic Settings

The Araripe Sedimentary Basin extends over 9,000 km<sup>2</sup> included in three states in the Brazilian Northeast (Figure 8) (Ceará, Pernambuco and Piauí). It is considered the most complete sedimentary record from the Cretaceous of the sedimentary basins in Northeastern Brazil (Assine, 1992, 2007; Neumann, 1999; Valença *et al.*, 2003). The geological history of this intrachronic basin is associated with the break-up of Gondwana and the opening of the South Atlantic, dating back to 150 Ma. The basin comprises four

technostratigraphic stages: synecesis, pre-rift, rift, and post-rift (I and II) (Assine *et al.*, 2014; Fambrini *et al.*, 2011; Martill *et al.*, 2007; Paula Freitas, Borghi, 2011; Silvestre *et al.*, 2020). This study followed the dates proposed by Assine (2007), Fauth *et al.* (2023), Guzmán *et al.* (2023), Melo *et al.* (2020), and Silvestre *et al.* (2020), who used biostratigraphic and lithostratigraphic correlations. Therefore, it is restricted to the post-rift I Aptian sequence (Figure 8), which includes a fluvio-lacustrine system, the Barbalha, Crato and Ipobi formations and a heterogeneous system with marine incursions, the Romualdo Formation (Assine, 2007; Melo *et al.*, 2020; Silvestre *et al.*, 2020).

**Figure 8.** A) 120 Ma paleogeographic map (modified from Scotese, 2016) showing the location of the Araripe Basin- BSA (yellow circle) and the volcanisms of Ontong Java- OJP (red star) and Southern Kerguelen Plateau- SKP (white star). B) Map of the location of the sampling points in the Araripe Basin.



### 5.2.1 Barbalha Formation

The Barbalha Formation, from the base of the Aptian, has a stratigraphic profile marked by fluvial-lacustrine cycles (Figure 8B) (Assine, 2007; Coimbra *et al.*, 2002; Rios-Netto *et al.*, 2012; Vallejo *et al.*, 2023). The 60 meters-thick base of this formation, is an intertwined fluvial environment with multi channels and characterized by upward fining, composed of coarse to medium sandstones, conglomerate levels, cross-bedding, and interspersed with red mudstones (Assine, 2007; Scherer *et al.*, 2015; Silvestre *et al.*,

2020). Following the deposition of the basal part, depositional conditions changed, and sedimentation was characterized by the predominance of mudstones, green shales, and black pyrobitumen, rich in carbonate algae, ostracods and fish remains, known as the Batateira beds (Figure 8B) (Assine, 2007, 1992; Fambrini *et al.*, 2019). These suggest an anoxic continental lacustrine system, rich in pyrite and a high load of organic matter (>30% TOC) (Claes *et al.*, 2021). However, biological multiproxies (especially microfossils) have shown increased salinity in the Batateira beds, which may be influenced by saline water intrusion associated with depositional characteristics of a deltaic system (Varejão *et al.*, 2021). Subsequently, fluvial conditions in the Barbalha Formation return, presenting medium to fine sandstones with the presence of shales, being typical of river systems anastomosed with extensive floodplains (Assine, 2007; Fambrini *et al.*, 2019; Silvestre *et al.*, 2020).

### 5.2.2 Crato Formation

The Crato Formation of Aptian age is the second lacustrine phase of the post-rift event of the opening of the Atlantic Ocean (Figure 8B) (Coimbra *et al.*, 2002). It is 90 meters thick, and rich fossil content and displaying six carbonate layers (C1 to C6) formed by calcitic limestones, a micritic matrix with micro to nanometric rhombohedral crystals (Assine, 2007; Catto *et al.*, 2016; Neumann, 1999). The origin of these limestones associates with authigenic chemical precipitation and biologically induced precipitation by calcifying organisms (Cabral *et al.*, 2019; Catto *et al.*, 2016; Heimhofer *et al.*, 2010). Due to its rich fossil content and excellent preservation, this formation is classified as Konservat-Lagerstätte (CKL), presenting a rich diversity of fossils: vertebrates (dinosaurs, pterosaurs, and fishes) and invertebrates (shrimp, insects, plants, and spiders). As for environmental conditions, limestone laminations, the presence of halite and pyrite crystals indicate a lacustrine environment (Crato paleolake), under saline to hypersaline and anoxic conditions (Barling *et al.*, 2015; Martill *et al.*, 2005; Osés *et al.*, 2016; Varejão *et al.*, 2019; Fambrini *et al.*, 2020; Storari *et al.*, 2021). Overlying the CKL is the Caldas bed, characterized by lithofacies alternating between silty and clayey sandstones, with the fossiliferous presence of mollusks (bivalves and gastropods) and fragments of carbonized plants (Varejão *et al.*, 2021). The upper part of the Crato Formation suggests marine incursions or restricted contact with the sea, as per its composition of sandstone, black to green shales, and limestone (Salgado-Campos *et al.*, 2021; Varejão *et al.*, 2021).

### **5.2.3 Romualdo Formation**

The Romualdo Formation, an Aptian-Albian 120 meters-thick layer, is also recognized as *Konservat-Lagerstätte* for its rich fossil content and preservation of fossil soft tissues (dinosaurs, pterosaurs, turtles, and fishes) (Figure 8B) (Duque, Barreto, 2018; Fambrini *et al.*, 2020; Oliveira, Kellner, 2007; Sayão *et al.*, 2020). A palaeoichthyological fauna typical of a marine environment (Fara *et al.*, 2005) and the composition of microfossils corroborates the characteristics of a marine depositional system (Custódio *et al.*, 2017; Melo *et al.*, 2020).

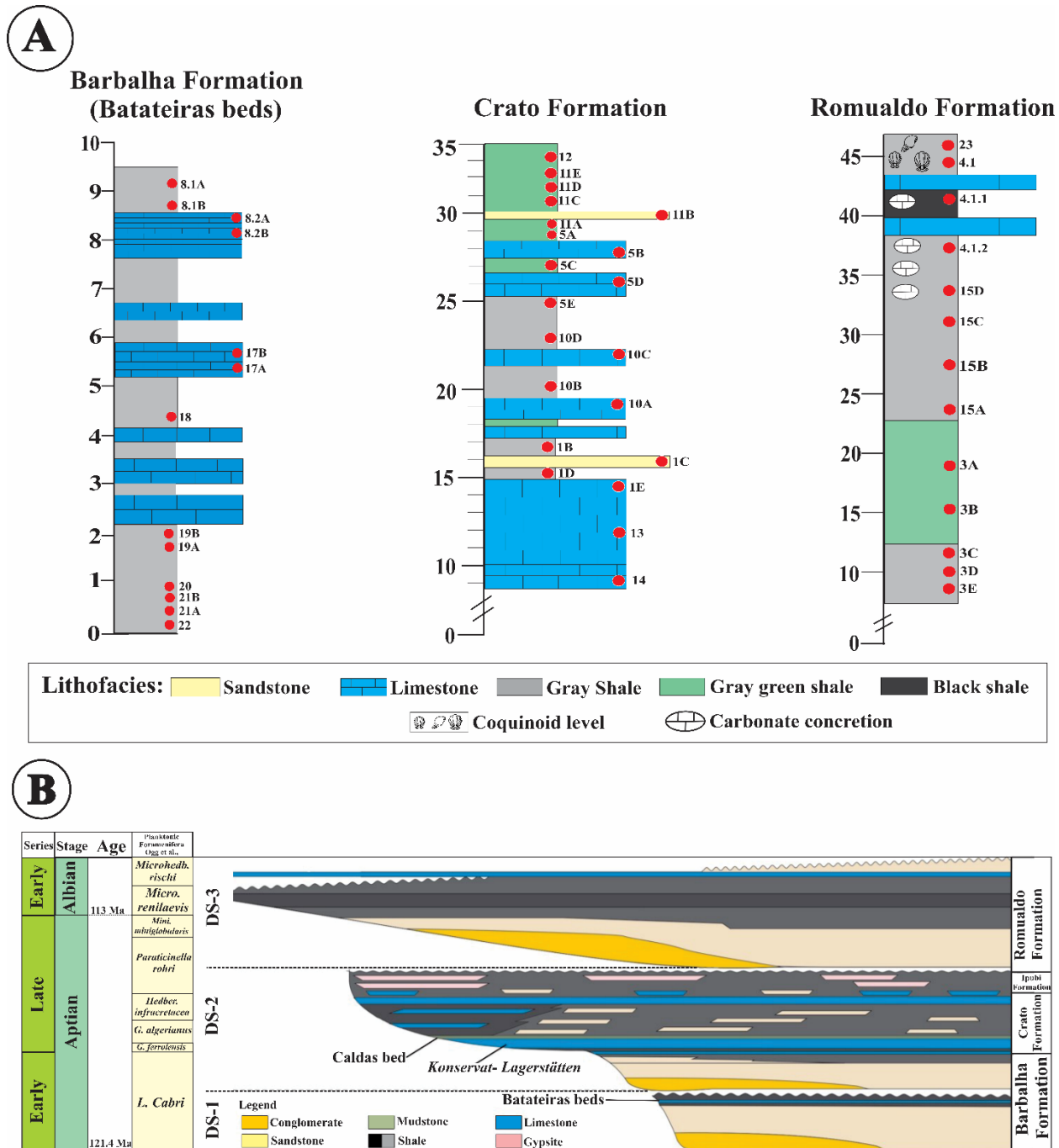
The lithofacies of the Romualdo Formation exhibits large variability, being composed of stratified conglomerates, fine to coarse sandstones, laminated limestones, marls, dark gray and greenish shales, being rich in organic matter and calcareous levels (Assine, 2007; Custódio *et al.*, 2017; Fambrini *et al.*, 2020). The variety of lithofacies suggests large variation in sea-level, with the occurrence of shales common in marine transgression events, and the predominance of sandstones in regression events (Assine *et al.*, 2014; Custódio *et al.*, 2017). This condition was observed in other studies using microfossils (foraminifera and ostracods), through the composition of organic matter and geochemical studies, demonstrates periods of greater coastal influence and marine transgression events (Araripe *et al.*, 2019, 2021; Bom *et al.*, 2021; Pontes *et al.*, 2021; Teixeira *et al.*, 2018). The presence of *Classopollis* and *Araucariacites* pollens indicates a strong influence of a marine regression event in a typical coastal system (Arai and Assine, 2020). According to Araripe *et al.* (2021), the Center-South part of the Araripe basin presented marine conditions, while in the Southwest of the basin, deposition occurred under coastal conditions.

The Romualdo Formation is also marked by fish mortality events (Martill *et al.*, 2008), which may be associated with major paleoenvironmental changes. Effects of distal volcanism were recorded in the Araripe basin in the Romualdo Formation and could impact and alter paleoclimate processes and, consequently, leading to biological crises (Benigno *et al.*, 2021; Sabatino *et al.*, 2018). The paleoenvironmental conditions in this environment were of great stress to organisms, presenting dyoxic to anoxic conditions, with little oxygen and great saline variability (Bom *et al.*, 2021; Fürsich *et al.*, 2019; Pontes *et al.*, 2021). These conditions directly interfered with the distribution of microfossils along the stratigraphic column (Araripe *et al.*, 2021).

### **5.3 Materials and methods**

The present study analyzed 47 samples collected by the transversal excavation of the outcrops, using only the non-weathered surfaces. Samples were collected from the post-rift I period of the Santana Group (Barbalha, Crato, and Romualdo formations), stranding from the base of the Aptian to the base of the Albian. Thirteen samples were collected from the Barbalha Formation (Batateira beds), 21 from the Crato Formation, and 13 from the Romualdo Formation. Samples collected in the Crato Formation have varied layers, including the laminated limestones of the *Konservat-Lagerstätten* layer (14, 13, and 1E) and sandstones and shales of the Caldas bed (1B, 1C, and 1D). At the top of the Crato Formation, there is an alternation between sandstones, shales, and limestones (5 A – E, 10 A – E, and 12). In the case of the samples from the Romualdo Formation, there is intercalation of sandstones, limestones, and black to green shales. The location of the samples in the stratigraphic profile of the Santana Group is shown in Figure 9. Samples were grounded, homogenized and dried (60°C for 12 hours), and preserved in hermetically closed flasks until analysis. Previous results of Total Organic Carbon (TOC), mercury (Hg), and isotopes ( $\delta^{13}\text{C}_{\text{carbonate}}$  and  $\delta^{18}\text{O}$ ) are available in Benigno *et al.*, (2021).

**Figure 9** Stratigraphic characterization of the Araripe Basin. A) Stratigraphic profile of the sampled sections, lithofacies, and height based on Benigno *et al.* (2021), Coimbra *et al.* (2002) and Fara *et al.* (2005). B) Aptian and early Albian depositional sequence of the studied interval, according to Fauth *et al.* (2023); Guzmán *et al.* (2023); Ogg *et al.* (2016); Varejão *et al.* (2021a, b). DS- Depositional system.



### **5.3.1 Total Organic Carbon (TOC)**

Total organic carbon (TOC) was quantified according to Yeomans, Bremner, (1988) in 0.5 g subsamples, digested with 5 mL K<sub>2</sub>Cr<sub>2</sub>O<sub>7</sub> 0.167 M solution and 7.5 mL of concentrated H<sub>2</sub>SO<sub>4</sub> at 170° C for 30 min. After cooling in room temperature, 3 to 5 drops of ferroin (1.485 g o-fenatrolin, plus 0.695 g Fe<sub>2</sub>SO<sub>4</sub>) were added to 80 mL of the extract and followed by titration with (Fe(NH<sub>4</sub>)<sub>2</sub>(SO<sub>4</sub>)<sub>2</sub>) 0.2 M).

### **5.3.2 Stable isotopes (C and O)**

Stable isotopes of Carbon ( $\delta^{13}\text{C}$ ) and Oxygen ( $\delta^{18}\text{O}$ ) were quantified in the CO<sub>2</sub> extracted from samples by digestion with orthophosphoric acid at 25°C, in a Thermofinnigan Delta V Advantage mass spectrometer. Results are expressed in the  $\delta$  notation (‰) with accuracy above  $\pm 0.1\text{\textperthousand}$ ; Vienna Pee Dee Belemnite international standards calibrated the isotopic data. Eventual C or O-signals showing post-depositional change of their isotope values were identified by Mn/Sr ratio; values lower than 10 suggest near primary isotopic abundances (Kaufman, Knoll, 1995; Kaufman *et al.*, 1993). See Benigno *et al.*, (2021) for details of procedures adopted to verify pos-depositional changes of stable isotopes of Carbon ( $\delta^{13}\text{C}_{\text{VPDB}}$ ) and Oxygen ( $\delta^{18}\text{O}_{\text{VPDB}}$ ).

### **5.3.3 Metals concentrations**

The concentrations of Al, Fe, Mn, Sr, Cu, Pb, Ni, V, Ba, Cr and Zn were quantified using subsamples of approximately 0.5 g mixed in teflon tubes with 20 mL Aqua Regia (50% v/v) and digested in a microwave (at 1,600 W and 175 °C, for 20 min). Extracts were taken in volumetric flasks to 25 mL with HNO<sub>3</sub> 0.2% v/v. All glassware were previously washed with deionized water in a 10% v/v (10% v/v) solution bath for 24 hours and then in an HCl bath (Sigma-Aldrich) 10% v/v for 24 hours. The reliability of the analytical results was monitored by means of the simultaneous analysis of certified sediment standard (NIST 1646A) and duplicate analyses of all samples. Standard recovery varied from 79% to 95%, whereas the detection limit of the procedure varied from 0.01 µg g<sup>-1</sup> to 0.03 µg g<sup>-1</sup>, depending on the metal. Quantification of the metals used Flame Atomic Absorption Spectrometry - AAS (AA 6200, SHIMADZU), with calibration curves of each metal constructed from MERCK standard solutions (1,000 µg g<sup>-1</sup>).

### **5.3.4 Mercury**

Mercury (Hg) concentrations were quantified in duplicates after digestion of 0.5 g of the samples in 125 mL Erlenmeyer flasks, containing 20 mL of aqua regia (50% v/v), in a water bath at a temperature between 70 and 80° C for two hours. Erlenmeyer flasks were closed using thermokinetic reactors (cold fingers). The resulting extracts were quantitatively transferred to volumetric flasks (50 mL) and calibrated with deionized water (Aguiar *et al.*, 2007). All glassware were previously washed with deionized water in an Extran® solution bath (10% v/v) for 24 hours and then in an acid bath of HCl (Sigma-Aldrich) 10% v/v also for 24 hours. Quantification used a Cold Vapor Generation Atomic Absorption Spectrometry (CVAAS), in a NIC RA-3 (NIPPON®) spectrophotometer. Analyses of reference material (NIST-1646A) were performed simultaneously with the samples, and mean recovery was  $78.4 \pm 6.6\%$ ; the limit of detection of the procedure was 0.02 ng g<sup>-1</sup> and the limit of quantification was 0.06 ng g<sup>-1</sup>.

### **5.3.5 Enrichment factor**

Aluminum (Al) was used to identify the contributions and paleodetrital processes, as it is a constituent element of the siliciclastic group that is associated with silt and clay particles and is part of the composition of the main detrital minerals (phyllosilicates, quartz, plagioclase, and K-feldspar). In addition, Al presents high stability and low mobility in the environment (Barbieri, 2016; Merli *et al.*, 2020; Montero-Serrano *et al.*, 2015; Rodríguez-Cuicas *et al.*, 2019; Montero-Serrano and Garbán, 2019).

Trace metals are especially enriched in shales and claystone compared to the upper crust, thus to remove interference from proximal sediment sources and decrease the potential dilution effects of biogenic components (carbonates, silica, and phosphorites), the present study used Al as a normalizer to determine the sudden changes in paleoproductivity ( $\text{Ni}^{\text{EF}}$ ,  $\text{Cu}^{\text{EF}}$ ,  $\text{Zn}^{\text{EF}}$  e  $\text{Ba}^{\text{EF}}$ ) and the paleoredox proxies ( $\text{Pb}^{\text{EF}}$ ,  $\text{V}^{\text{EF}}$ ,  $\text{Mn}^{\text{EF}}$ ,  $\text{Cr}^{\text{EF}}$ ,  $\text{Fe}^{\text{EF}}$ ) (Sabatino *et al.*, 2015; Soua *et al.*, 2011; Touati, Haji, 2019; Tribovillard *et al.*, 2006). The EF allows a general assessment regarding the enrichment/impoverishment of metals, evidencing relevant paleoenvironmental changes in the formations under study, deeming its applicability in chemostatigraphy extremely important (Algeo, Liu, 2020). The application of these metals considers their behavior in a reducing environment, to which organic matter adsorbs and co-precipitates with sulfur when subjected to bacterial sulfate reduction (Algeo, Liu, 2020; Algeo, Maynard, 2004; Herndon *et al.*, 2018; Tribovillard *et al.*, 2006).

The calculation of the enrichment factor (EF) consists of the ratio between the concentration of the element in shales or claystone and the corresponding average concentration of the element in the upper middle crust (Cao *et al.*, 2012). The EF is determined using the equation:  $EF_{Element} = [(X/Al)_{Sample} / (X/Al)_{Average\ shale}]$ , where  $(X/Al)_{(Sample)}$  represents the concentrations of elements X and Al measured in the samples, while  $(X/Al)_{(Average\ shale)}$  corresponds to the concentrations of elements in the "average shale" of the crust according to the values proposed by Turekian, Wedepohl (1961), and Wedepohl (1995).

### **5.3.6 Statistics**

The statistical analysis used the RStudio software (version 4.3.1 – © 2009 – 2023 RStudio, Inc.) after performing homogeneity and normality tests to the data which suggested Spearman's correlation coefficient ( $p < 0.05$ ,  $n= 47$ ) (Correlation Index from -1 to +1) (Miller, 2010) to be used.

## 5.4 Results

Variability of geochemical proxies of paleoproductivity, paleoredox, and volcanism are shown in Figures 10, 11, and 12. There is a clear association between Hg/TOC peaks (volcanism events) and trace metal enrichment in all studied Formations. Volcanism may have been responsible for global paleoenvironmental changes with local impacts in the Araripe Basin during the Aptian and Albian (Cretaceous). It is worth noting that volcanism events during the Cretaceous marked main global climate changes, being responsible for marine plankton shifts and oceanic anoxia events (OAE 1a and 1b) (Adloff *et al.*, 2020; Benigno *et al.*, 2021; Erba *et al.*, 2015; Li *et al.*, 2023; Sabatino *et al.*, 2015). Proxies of other drivers of environmental changes in the Araripe Basin are presented separately according to the specific Formation.

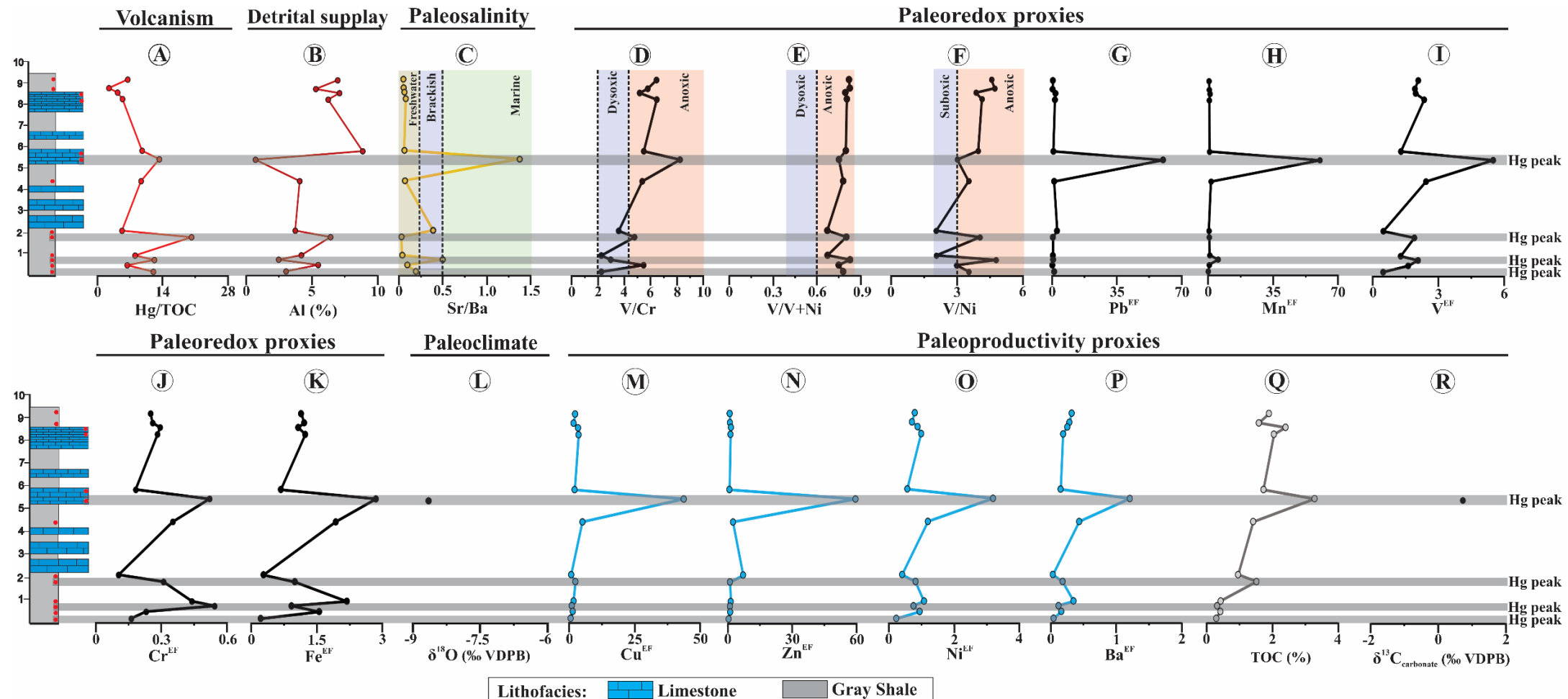
### 5.4.1 Barbalha Formation

In the Batateira beds, Al ranged from 0.72% to 8.86% in superposed limestone beds (Figure 9B). A probable paleodetrital source is indicated by a direct correlation between Al and Fe ( $p < 0.05$ ;  $n = 13$ , Spearman) ( $r = 0.62$ ), Ni ( $r = 0.76$ ), Cr ( $r = 0.81$ ) and V ( $r = 0.79$ ) (Figure 10 B), and a negative correlation between Al and Hg/TOC ( $r = -0.58$ ) and Sr/Ba ( $r = -0.74$ ). The Sr/Ba ratio (a paleosalinity proxy) observed in the Batateira beds varied from 0.03 to 1.37 (Figure 10 C), with the highest ratio found in sample 17A (1.37) and the lowest in 21B (0.04), indicating paleosalinity ranging from freshwater to marine. Metals concentrations ratios proxies of paleoredox conditions (V/Cr, V/Ni, and V/V+Ni) indicate depositional conditions ranging from anoxic to suboxic, 2.24 to 8.24, 0.67 to 0.84, and 2.05 to 5.09, respectively (Figures 10 D, E, and F).

Spearman analysis ( $p < 0.05$ ;  $n = 13$ ) showed significant correlation between paleoredox proxies and TOC ( $Pb = 0.65$ ,  $V = 0.72$ ,  $Fe = 0.54$ , and  $Mn = 0.62$ ). Enrichment factors for  $Pb^{EF}$  ranged from 0.3 to 60.0, for  $V^{EF}$  from 0.4 to 5.5, for  $Cr^{EF}$  from 0.1 to 0.5, for  $Mn^{EF}$  from 0.03 to 34.39 and for  $Fe^{EF}$  from 0.2 to 2.85 (Figure 10 G – K). Significant Spearman's correlations of the paleoproductivity proxies with TOC ( $Zn = 0.65$ ,  $Cu = 0.91$ ,  $Ni = 0.66$ , and  $Ba = 0.70$ ). The Batateira beds showed  $Cu^{EF}$  ranging from 0.6 to 43.6,  $Zn^{EF}$  from 0.4 to 59.5,  $Ni^{EF}$  from 0.2 to 3.1, and  $Ba^{EF}$  from 0.04 to 1.2, whereas TOC ranged from 0.3 to 3.2% (Figure 10 M - Q). Hg concentrations ranged from 2.7 to 43.6 ng g<sup>-1</sup>, and the Hg/TOC ratio varied from 2.5 to 20.2 showing 4 sharp peaks (Figure 10A).  $\delta^{13}C_{carb}$  and  $\delta^{18}O$ , were, unfortunately, only quantified in sample 17A, and showed values

of +0.72‰ and -8.65‰, respectively (Figures 10 L, and R). Sample 17A of the Batateira beds recorded anomalies of all paleoproductivity ( $\text{Cu}^{\text{EF}}$ ,  $\text{Zn}^{\text{EF}}$ ,  $\text{Ni}^{\text{EF}}$ ,  $\text{Ba}^{\text{EF}}$ , and TOC), and paleoredox ( $\text{Pb}^{\text{EF}}$ ,  $\text{V}^{\text{EF}}$ ,  $\text{Cr}^{\text{EF}}$ ,  $\text{Mn}^{\text{EF}}$ , and  $\text{Fe}^{\text{EF}}$ ) proxies. This enrichment of trace metals and a positive incursion of the Hg/TOC ratio suggest strong a paleoenvironmental disturbance.

**Figure 10.** Chemostratigraphy of the Barbalha Formation. A) Hg/TOC (Volcanism); B) Aluminum (Detrital supply); C) Sr/Ba (Paleosalinity); D) V/Cr, E) V/V + Ni, F) V/Ni, G) Pb<sup>EF</sup>, H) Mn<sup>EF</sup>, I) V<sup>EF</sup>, J) Cr<sup>EF</sup> and K) Fe<sup>EF</sup> (paleoredox); L) δ<sup>18</sup>O (Paleoclimate); M) Cu<sup>EF</sup>, N) Zn<sup>EF</sup>, O) Ni<sup>EF</sup>, P) Ba<sup>EF</sup>, Q) TOC, R) δ<sup>13</sup>Ccarbonate (Paleoproductivity).

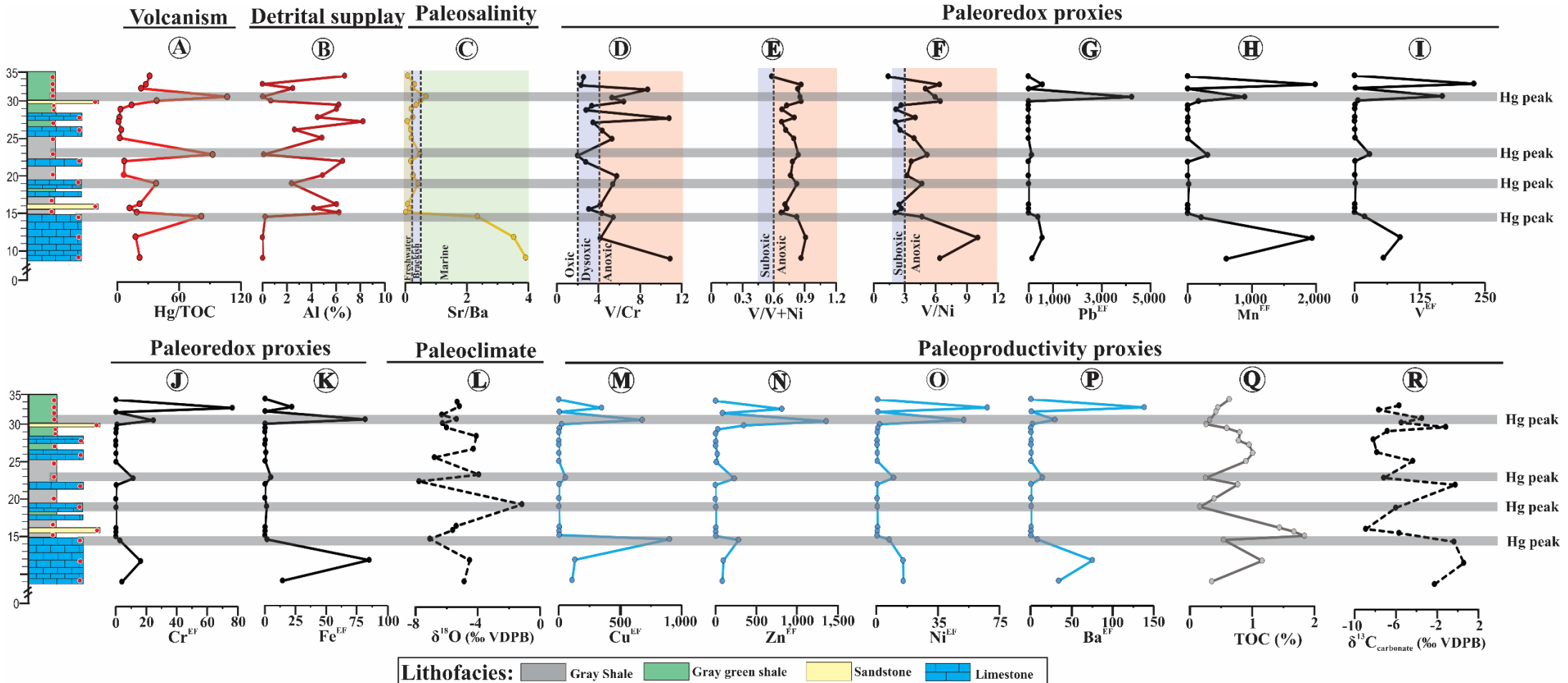


## 5.4.2 Crato Formation

The Crato Formation presented Al values ranging from 0.02 to 8.25%, with lower concentrations in the laminated limestone (point 13) and higher concentrations in the black shale (point 5C) (Figure 10B). Significant positive Spearman correlations ( $p < 0.05$ ;  $n = 21$ ) between Al (detrital supply) and Cr ( $r = 0.50$ ), Ni ( $r = 0.90$ ), V ( $r = 0.50$ ), and TOC ( $r = 0.47$ ), suggest possible paleodetrital contributions of these elements to the depositional environment. Furthermore, negative correlations were observed between Al and Zn ( $r = -0.32$ ), Mn ( $r = -0.59$ ), Pb ( $r = -0.31$ ), Sr/Ba ( $r = -0.59$ ), and Hg/TOC ( $r = -0.62$ ). The Sr/Ba ratio in the Crato Formation ranged from 0.02 – 3.93 (Figure 10C), with highest values found in samples 14, 13, 1E, 11B and 11C, suggesting a marine environment ( $\text{Sr}/\text{Ba} > 0.5$ ). Followed by intermediate values, suggesting brackish waters ( $\text{Sr} > \text{Ba}$  between 0.2 to 0.5) in samples 10A, 10B, 10D, 5E, 5B, 5A, 11A, 11D and 11E. Freshwaters depositional conditions ( $\text{Sr}/\text{Ba} > 0.2$ ) were observed in samples 1D, 1C, 1B, 10C, 5D, 5C and 12. Paleoredox proxies suggest a predominantly reducing paleoenvironment. Metals ratios (V/Cr, V/Ni, and V/V+Ni) varied from 2.0 to 10.9 (oxic to suboxic), 0.58 to 0.91 (dyoxic to euxinic), and 1.4 to 10.1 (oxic to anoxic), respectively (Figures 10D, E, and F).

Significant positive Spearman's correlation ( $p < 0.05$ ;  $n = 21$ ) in the Crato Formation were observed between paleoredox proxies with Hg/TOC ratios ( $\text{Pb} = 0.66$ ,  $\text{V} = 0.43$ ,  $\text{Mn} = 0.32$ , and  $\text{Fe} = 0.77$ ). Enrichment factors for  $\text{Pb}^{\text{EF}}$  varied from 0.5 to 4.246; for  $\text{V}^{\text{EF}}$  from 0.5 to 229; for  $\text{Cr}^{\text{EF}}$  from 0.08 to 76; for  $\text{Mn}^{\text{EF}}$  from 0.3 to 1.99; and for  $\text{Fe}^{\text{EF}}$  from 0.5 to 171 (Figure 10G – K). Paleoproductivity proxies varied from 0.7 to 901 for  $\text{Cu}^{\text{EF}}$ , from 1.8 to 1.36 for  $\text{Zn}^{\text{EF}}$ , from 0.5 to 63 for  $\text{Ni}^{\text{EF}}$ , 0.1 to 138 for  $\text{Ba}^{\text{EF}}$ , and from 0.1 to 1.84% for TOC (Figure 10M – Q). There were significant positive correlations between Ni and Ba with TOC ( $r = 0.30$  and  $r = 0.38$ , respectively). Hg concentrations varied from 1.2 to 44 ng g<sup>-1</sup>, and the Hg/TOC ratio showed 5 peaks with values ranging from 1.2 to 106 (Figure 10A).  $\delta^{13}\text{C}_{\text{carbonate}}$  varied from -8.90‰ to +0.61‰ (Figure 10R), with significant peaks in samples 13 (+0.61‰) and 10C (-0.22‰).  $\delta^{18}\text{O}$  values ranged between -7.77‰ and -1.77‰ (Figure 10L), with sharp peaks observed in stations 10A (-1.17‰) and 10D (-3.94‰).

**Figure 11.** Chemostratigraphy of the Crato Formation. A) Hg/TOC (Volcanism); B) Aluminum (Detrital supply); C) Sr/Ba (Paleosalinity); D) V/Cr, E) V/V + Ni, F) V/Ni, G) Pb<sup>EF</sup>, H) Mn<sup>EF</sup>, I) V<sup>EF</sup>, J) Cr<sup>EF</sup> and K) Fe<sup>EF</sup> (paleoredox); L) δ<sup>18</sup>O (Paleoclimate); M) Cu<sup>EF</sup>, N) Zn<sup>EF</sup>, O) Ni<sup>EF</sup>, P) Ba<sup>EF</sup>, Q) TOC, R) δ<sup>13</sup>Ccarbonate (Paleoproductivity).

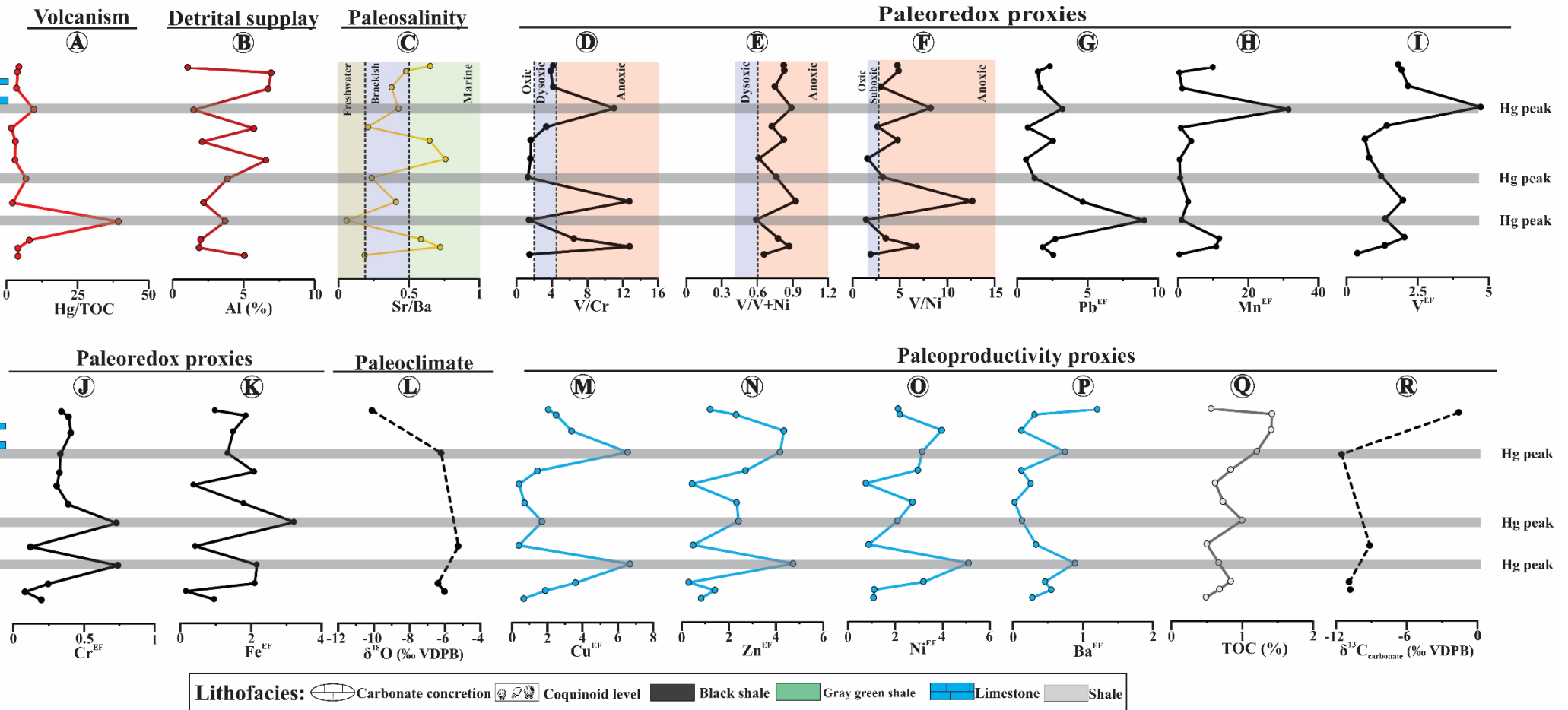


### 5.4.3 Romualdo Formation

Aluminum concentrations (paleodetrital contributions) in the Romualdo Formation varied from 1.02 to 6.72%, with higher values in sample 4.1.1 (black shale) and lower in 23 (green shale) (Figure 12 B). Significant positive Spearman correlation ( $p < 0.05$ ,  $n = 13$ ) was found between Al and Fe ( $r = 0.83$ ), Zn ( $r = 0.84$ ), Ni ( $r = 0.84$ ), Cr ( $r = 0.84$ ), V ( $r = 0.68$ ) and TOC ( $r = 0.46$ ). Furthermore, significant negative correlations were found between Al and the Sr/Ba ratio ( $r = -0.53$ ). The Sr/Ba ratio varied from 0.05 – 0.76 (Figure 12 C), where the highest concentrations (marine environment) were at points 3D, 3C, 15B, 15C, 4.1 and 23. Samples 3A, 15A, 15D, 4.2.1 and 4.1.1 showed characteristics of brackish water, while samples 3E and 3B suggest a freshwater environment. The paleoredox proxies in Romualdo Formation varied from: V/Cr: 1.3 to 12.8 (oxic to anoxic), V/V+Ni: 0.53 to 0.93 and V/Ni 1.5 to 12.7 (anoxic- euxinic) (Figures 12 D, E, and F).

Positive, significant ( $p < 0.05$ ,  $n = 13$ ) Spearman's correlation were observed between TOC and the concentrations of V ( $r = 0.89$ ), Cr ( $r = 0.55$ ) and Fe ( $r = 0.54$ ), while Pb concentrations correlated only with the Hg/TOC ratio. Enrichment factors varied from 0.6 to 9.0 for  $Pb^{EF}$ , 0.4 to 4.7 for  $V^{EF}$ , the 0.1 to 0.7 for  $Cr^{EF}$ , 0.3 to 31.4 for  $Mn^{EF}$  and 0.2 to 3.2 for  $Fe^{EF}$  (Figure 12 G – K). Paleoproductivity proxies,  $Cu^{EF}$  varied from 0.4 to 6.7,  $Zn^{EF}$  from 0.3 to 4.7,  $Ni^{EF}$  from 0.7 to 5.1,  $Ba^{EF}$  from 0.03 to 1.2 and TOC from 0.5 to 1.4% (Figure 12 M – Q). Significant positive correlations were found for TOC with Cu ( $r = 0.70$ ), Zn ( $r = 0.73$ ), Ni ( $r = 0.57$ ), and Ba ( $r = 0.72$ ). Hg concentrations varied from 1.1 to 26.3 ng g<sup>-1</sup>, and the Hg/TOC ratio from 1.8 to 39.3, with peaks recorded in 3 samples (Figure 12 A).  $\delta^{13}C_{carbonate}$  and  $\delta^{18}O$  varied from -11.5 to -1.61‰ (Figure 12 R) and from -10.1 to -5.3‰ (Figure 12 L), respectively.

**Figure 12.** Chemostratigraphy of the Romualdo Formation. A) Hg/TOC (Vulcanism); B) Aluminum (Detrital supply); C) Sr/Ba (Paleosalinity); D) V/Cr, E) V/V + Ni, F) V/Ni, G) Pb<sup>EF</sup>, H) Mn<sup>EF</sup>, I) V<sup>EF</sup>, J) Cr<sup>EF</sup> and K) Fe<sup>EF</sup> (paleoredox); L) δ<sup>18</sup>O (Paleoclimate); M) Cu<sup>EF</sup>, N) Zn<sup>EF</sup>, O) Ni<sup>EF</sup>, P) Ba<sup>EF</sup>, Q) TOC, R) δ<sup>13</sup>Ccarbonate.



## 5.5 Discussion

### 5.5.1 Paleosalinity

To determine the paleosalinity of depositional environments, we used the classification proposed by Wei, Algeo (2020), which divides the saline conditions of the environment according to ranges of the Sr/Ba ratio: < 0.2, freshwater environment; between 0.2 – 0.5, brackish water; and Sr/Ba ratios > 0.5, typical of marine environments.

#### 5.5.1.1 Barbalha Formation

Previous studies characterize the Batateira beds as a freshwater, low-energy lacustrine environment (Assine *et al.*, 2014; Fambrini *et al.*, 2020; Scherer *et al.*, 2015). However, the present study demonstrated saline characteristics ranging from freshwaters to marine waters along lithofacies composed of black shales and limestones. The Sr/Ba ratios of black shales suggest a typical freshwater to brackish environment (Sr/Ba < 0.2 and between 0.2- 0.5), whereas those of the limestones a marine deposition (Sr/Ba > 0.5), indicating a marine environment in the Araripe Basin by the early Aptian. The paleoenvironment of the Batateira beds has characteristics of a coastal transgressive system (fluvial-deltaic) (Varejão *et al.*, 2021) toward a marine environment (Fauth *et al.*, 2023). Marine transgressions in Batateira beds are supported by typical marine microfossils (foraminifera, dinocysts, and calcareous nannofossils; *Leupoldina cabri* and *Subtilisphaera*) (Fauth *et al.*, 2023; Vallejo *et al.*, 2023). The increase in salinity in Batateira beds caused a local biological crisis, as evidenced by the observed local mortality of non-marine adult ostracods, situated in the same layer as the foraminifera, and marine calcareous nannofossils, indicating that the increase in salinity generated a stressful environment for the development of ostracods (Fauth *et al.*, 2023).

It is worth noting that the early Aptian is marked by marine transgression events and increased salinity in continental environments, with these changes in paleosalinity being associated with major global climate changes (Fan *et al.*, 2021; Peropadre, Liesa e Meléndez, 2013; Tedeschi *et al.*, 2020). Global events associated with sea-level rise and higher aridity events during the Ontong Java volcanism have been suggested to have triggered changes in paleosalinity in different sedimentary basins (Sergipe-Alagoas, Brazil; Hongmiaozi, China; Hailar, Mongolia; and Liaoning Province, China) (Min-Na *et al.*, 2013; Fan *et al.*, 2021; Li *et al.*, 2023; Tedeschi *et al.*, 2020).

### 6.5.1.2 Crato Formation

The base of the Crato Formation is composed by a laminated siliciclastic-limestone layer, internationally recognized as Konservat-Lagerstätte (CKL). These carbonates are authigenic, originating from biochemical processes, with microbial mats and cyanobacteria responsible for the precipitation of calcium carbonate (Catto *et al.*, 2016). Values of Sr/Ba ratio  $> 0.5$  in this layer may be related to the high concentrations of calcium carbonate and/or the hypersaline environmental conditions of the Crato paleolake (Barling *et al.*, 2015; Barling, Martill, Heads, 2020; Heimhofer *et al.*, 2010). Sr can replace  $\text{Ca}^{2+}$  in the mineral structure of the rock, including dolomite and calcite, which can lead to increased concentrations of this element in limestone layers and strontianite ( $\text{SrCO}_3$ ) precipitation resulting in high Sr concentrations in laminated limestones (Roden, Leonardo, Ferris, 2002; Wei, Algeo, 2020). Another factor that might be related to the high Sr/Ba ratios is the hypersalinity found in the Crato paleolake. Halite crystals were found in the CKL, indicating dry periods, influenced by high evaporation and low rainfall (Martill, Loveridge, Heimhofer, 2007; Storari *et al.*, 2021). For example, the depositional conditions and fossil content (fauna and flora) of the Crato paleolake were associated with modern African hypersaline and alkaline lakes (Ribeiro *et al.*, 2021). Similarly, for the carbonate paleolake of the Serra do Tonã Formation (Tucano Basin, Northeast Brazil), stratigraphically correlated with the CKL, indicating variation in lake level with rainwater (Silveira *et al.*, 2014).

The Caldas bed has Sr/Ba ratio values  $< 0.2$ , suggesting a freshwater environment, in agreement with a reduction in paleosalinity as observed in the Caldas bed when compared to the hypersalinity of the Crato paleolake (CKL level). This scenario corroborates earlier studies (Silva *et al.*, 2020; Vallejo *et al.*, 2023; Varejão *et al.*, 2021) characterizing the Caldas bed as a closed freshwater lacustrine system with an abundance of non-marine fossils and peaks of freshwater microphytoplankton.

The upper Crato Formation is a succession of layers classified as a heterolithic succession of facies (Assine *et al.*, 2014; Varejão *et al.*, 2021). There, Sr/Ba ratios indicate a transition from freshwater to marine paleoenvironments, suggesting an increase in salinity (Sr/Ba between 0.25 to 0.68) towards the upper Crato Formation. Studies on microfossils showing a reduction of terrigenous phytoclasts, growth of clustered marine foraminifera, and *Classopolis* pollens, common in warm, and dry coastal systems, also demonstrate a variation in the transition of the Ipobi and Crato formations, from a predominantly freshwater paleoenvironment to a transgressive system influenced by

brackish waters (tidal-dominated bays and confined bays, coastal lakes, and sabkha) (Goldberg *et al.*, 2019; Guzmán *et al.*, 2023; Vallejo *et al.*, 2023; Varejão *et al.*, 2021).

### 6.5.1.3 Romualdo Formation

Paleosalinity varied in the Romualdo Formation with periods of marine and continental contributions. The observed Sr/Ba ratios < 0.2 and between 0.2 – 0.5 points to an environment with great saline variations, with periods of highest continental fluvial contributions, also with strong positive correlation between Al and TOC. Periods with Sr/Ba > 0.5 indicate the lowest fluvial contributions and the dominance of a paleosalinity typical of a marine environment. This agrees with the scenario proposed by Custódio *et al.* (2017) and Melo *et al.* (2020), the Romualdo Formation is characterized by being a transgressive-regressive system, with the presence of coastal alluvium, tidal-dominated facies, and marine shales rich in fish and marine microfossils.

Previous geochemical studies have demonstrated a variation of paleosalinity in the Romualdo Formation, ranging from an estuarine to a marine system (Bom *et al.*, 2021; Pontes *et al.*, 2021). Saline oscillation in the Romualdo Formation has been associated with the interference of OAE 1b in the regional hydrological cycle, with alternating periods of greater freshwater contribution and greater marine influence (Bom *et al.*, 2023). Periods of greater continental contributions are demonstrated by the pollen enrichment (*Araucariacites* and *Classopolis*) (Arai, Assine, 2020; Fürsich *et al.*, 2019; Teixeira *et al.*, 2018), whereas influences from a marine environment are supported by the occurrence of fossiliferous crustaceans, fish, mollusks, and microfossils (planktonic foraminifera and ostracods (Arai, 2014; Fara *et al.*, 2005; Guzmán *et al.*, 2023; Martill *et al.*, 2008; Prado *et al.*, 2019; 2018).

### 5.5.2 Paleoredox conditions

Trace metals are sensitive to redox state changes being removed from the aqueous environment and transferred to the sediment when subjected to changing reducing conditions. This transfer can occur by adsorption with oxyhydroxides (Fe, Al, and Mn), burial with organic matter, generating organometallic compounds, and co-precipitation with minerals (Tribovillard *et al.*, 2006). Redox classification of environments followed Algeo, Li (2020); Algeo, Liu (2020); Algeo, Maynard (2004) and Tribovillard *et al.* (2006), being are classified as oxic ( $> 2\text{ mL O}_2\text{ L}^{-1}$ ), dyoxic (2 a 0  $\text{mL O}_2\text{ L}^{-1}$ ), suboxic (0  $\text{mL O}_2\text{ L}^{-1}$ ,  $\text{Fe}^{2+} > 0$ ,  $\text{H}_2\text{S} = 0$ ), and anoxic-euxinic (0  $\text{mL O}_2\text{ L}^{-1}$ ,  $\text{Fe}^{2+} = 0$ ,  $\text{H}_2\text{S} > 0$ ). The

paleoredox proxies V/Cr < 2.0 indicates an oxic environment; V/Cr between 2.0 - 4.25 a dyoxic environment and V/Cr > 4.25 suggests suboxic to anoxic conditions (Jones, Manning, 1994). For the V/Ni ratio, values between 1.9 - 3 indicate a suboxic environment, while V/Ni values > 3.0 are typical of anoxic environments (Galarraga *et al.*, 2008). Using the V/V+Ni ratio, values > 0.84 indicate euxinic conditions; an anoxic environment between 0.54 - 0.83; while values between 0.46 to 0.6 indicate dyoxic conditions (Rivera *et al.*, 2018).

### 6.5.2.1 Barbalha Formation

The depositional conditions of the Batateira beds presented a depositional environment ranging from suboxic to anoxic characterized by the presence of lithofacies composed by black bituminous shales, mineralized pelagic limestone rich in sulfide, pyrite-rich minerals, fragments of charred vegetation, and a high TOC (Assine, 2007; Claes *et al.*, 2021; Paula Freitas, Borghi, 2011; Silvestre, Fambrini, Costa, 2020). The exclusive presence of *Ammobaculites* (benthic foraminifera) and agglutinated foraminifera are indicative of a marine paleoenvironment with restricted circulation, eutrophic and anoxic (Guzmán *et al.*, 2023). Sulfur isotopic analysis ( $\delta^{34}\text{S}$ ) in the Batateira beds demonstrates negative values, typical of bacterial origin produced by bacterial sulfate reduction under anaerobic conditions (Pontes *et al.*, 2021). Under anoxic conditions, bacteria promote sulfate reduction with  $\text{H}_2\text{S}$  as a product, producing sedimentary pyrite (Jørgensen, 1982; Liu *et al.*, 2021).

### 6.5.2.2 Crato Formation

The CKL levels were deposited under dyoxic to anoxic conditions and were characterized by siliciclastic-calcareous lithofacies. Excellent fossil preservation is directly related to the reducing conditions of the Crato paleolake. The presence of microbial mats, the absence of bioturbation, as well as the formation of microframbooidal pyrites in the fossils indicate a reducing environment, with low oxygenation, allowing the preservation of the soft tissues of the fossils (Heimhofer *et al.*, 2010; Osés *et al.*, 2016). The formation of pyrite is attributed to bacterial sulfate reduction, an event that occurs with the degradation of organic matter under reducing conditions (Jørgensen, 1982).

The Caldas bed and the upper Crato Formation showed decreasing oxygenation, resulting in predominantly reducing conditions from dyoxic to anoxic. The Caldas bed

and the upper Crato showed an increase in organic matter contents supporting a paleoenvironment with low oxygen and preservation of organic matter. In addition, metals ratios also characterize environmental conditions varying from oxic to anoxic (Salgado-Campos *et al.*, 2021; Tyson, 1995; Vallejo *et al.*, 2023; Varejão *et al.*, 2021).

### 6.5.2.3 Romualdo Formation

The metal ratios identified conditions that ranged from oxic to anoxic, indicating that the environment of the Romualdo Formation presented oscillation in oxygen concentrations and, consequently, extremely stressful conditions for organisms. It is possible to observe that during periods of lower salinity and high detrital input, the conditions range from oxic to dyoxic, while when there is an increase in salinity, anoxic conditions predominate and the detrital supply input decreases. Bom *et al.* (2023, 2021) suggested the Kilian event (OAE 1b) as responsible for the input of phosphorus allowing for excellent fossil preservation in the Romualdo Formation, associating high sediment deposition of continental detrital input and a eutrophic environment favoring anoxic conditions.

The enrichment in sulfur isotopes ( $\delta^{34}\text{S}$ ), the production of frambooidal pyrite and preservation of labile materials were observed, indicating a paleoredox dyoxic-anoxic condition, with a strong influence of bacterial sulfate reduction (Custódio *et al.*, 2017; Fürsich *et al.*, 2019; Heimhofer *et al.*, 2008; Pontes *et al.*, 2021; Varejão *et al.*, 2019). These depositional conditions played a role in the excellent preservation of the fossils (three-dimensional fish, muscles, and blood vessels of pterosaurs). The 20 meters interval composed of dark gray to black shales, with a high load of organic matter is an indication of the strong reducing conditions that dominated the Romualdo Formation (Assine, 2007; Custódio *et al.*, 2017; Kellner, 1996).

### 5.5.3 Volcanism and palaenvironmental changes

Hg/TOC peaks indicate activation of LIPs, and the use of TOC as a normalizer is due to its affinity for Hg, acting as the main mechanism capable of retaining Hg over the geological time (Grasby *et al.*, 2019). Volcanism is responsible for releasing Hg in its elemental form ( $\text{Hg}^0$ ) to the stratosphere causing a global distribution. Gaseous elemental  $\text{Hg}^0$  is oxidized in the atmosphere forming the reactive form  $\text{Hg}^{2+}$ . Subsequently, the

reactive Hg<sup>2+</sup> associates with the water present in the atmosphere, precipitating with rainwater (Bond, Grasby, 2017; Font, Bond, 2021; Sial *et al.*, 2016).

Considering the activation of LIPs during the Early Cretaceous, we highlight the Paraná-Etendeka (~132 Ma), Ontong Java (~124 to 120 Ma), Southern Kerguelen Plateau and Rajmahal (~119 to 110 Ma), Elan Bank (~110 Ma) and Central Kerguelen Plateau (~105 Ma) volcanisms (Coffin *et al.*, 2006; Erba *et al.*, 2015; Keller, 2008; Li *et al.*, 2023). Among these LIPs, the OJP and the SKP stand out, as they were responsible for the oceanic anoxia events OAE 1a and OAE 1b, respectively (Erba *et al.*, 2015; Li *et al.*, 2023; Sabatino *et al.*, 2018).

### 6.5.3.1 Barbalha Formation

Biostratigraphically the Batateira beds was associated with the global foraminifera biozones *Leupoldina cabri* and *Globigerinelloides algerianus*, indicating an early Aptian deposition (Fauth *et al.*, 2023; Ogg *et al.*, 2016; Weissert, Erba, 2004). The Batateira beds showed four Hg/TOC peaks, indicating the activation of volcanism at the Early Aptian, with sample 17A (limestone) standing out due to the simultaneous enrichment of all proxies of paleoproductivity and paleoredox. Regarding the activation period of the LIPs and their association with the Araripe sedimentary basin, we can suppose that the principal mechanism responsible for the paleoenvironmental disturbances in the Batateira beds was the Ontong Java Plateau. The activation age of Ontong Java ranges from 124 Ma to 120 Ma and this volcanism was responsible for the oceanic anoxia event (OAE 1a), which had a large impact on marine plankton, responsible for the burial of a large TOC load and enrichment of trace metals (Erba *et al.*, 2015; Ogg, Ogg, Gradstein, 2016; Stein *et al.*, 2011; Weissert, Erba, 2004).

Disturbances events in the carbon cycle were related in the Araripe basin: one associated with the Batateira beds; and the other with the Romualdo Formation (Heimhofer, Hochuli, 2010). The activation of OJP is responsible for the TOC and metals enrichment during early Aptian (Bottini, Mutterlose, 2012; Erba *et al.*, 2015). The same process was observed for the extinction events of the Ordovician-Silurian and Permian-Triassic, in which the increase of the CO<sub>2</sub> emission by volcanic activities was able to modify the global carbon cycle (Lu *et al.*, 2021; Sial *et al.*, 2021; Tang *et al.*, 2020). Thus, we can infer that trace metal anomalies found in the Batateira beds were influenced by the volcanic emissions of OJP, resulting in increased CO<sub>2</sub> in the atmosphere, intensifying the biological pump and the supply of nutrients to the aquatic environment. Consequently,

the increase in primary production generates a higher TOC and higher deposition of paleoproductivity anomalies metals ( $\text{Cu}^{\text{EF}}$ ,  $\text{Zn}^{\text{EF}}$ ,  $\text{Ba}^{\text{EF}}$ ,  $\text{Ni}^{\text{EF}}$ ,  $\delta^{13}\text{C}_{\text{carb.}}$  and TOC) due to the intensification of the degradation process of organic matter, which results in an anoxic environment, as seen by the anomalies of the paleoredox proxies ( $\text{Pb}^{\text{EF}}$ ,  $\text{Cr}^{\text{EF}}$ ,  $\text{Fe}^{\text{EF}}$ ,  $\text{Mn}^{\text{EF}}$  e  $\text{V}^{\text{EF}}$ ) in the Araripe Basin.

### 6.5.3.2 Crato Formation

The Crato Formation is from late Aptian, corresponding to the Alagoas level (Assine, 2007; Fambrini *et al.*, 2020; Guzmán *et al.*, 2023) and with the presence of the foraminifera groups *P. blakenensis*, *H. gorbachikae*, and *M. miniglobularis* (Guzmán *et al.*, 2023) demonstrating the location between the foraminifera zones *Hedbergella infracretacea* (~ 118 Ma) and *P. rohri* (~ 114 Ma) (Ogg *et al.*, 2016). Considering the volcanism events that occurred in this period, we highlight the activation of the Southern Kerguelen plateau (~ 119 to 110 Ma) and of the Rajmahal (118 – 113 Ma) (Coffin *et al.*, 2002, 2006).

The CKL levels (Crato paleolake), presented the enrichment of paleoproductivity and paleoredox proxies and changes in the  $\delta^{13}\text{C}_{\text{carbonate}}$  and  $\delta^{18}\text{O}$  isotopes values. The peaks found in CKL of Crato Formation showed enrichment of all paleoproductivity and paleoredox proxies. This enrichment may be related to the anoxic condition characteristic of this layer and/or to the high paleoproductivity. The high primary productivity and low oxygen concentration at the bottom of the Crato paleolake generated excellent conditions for the reduction of bacterial sulfate reduction, which is responsible for the formation of hydrogen sulfide ( $\text{H}_2\text{S}$ ) (Osés *et al.*, 2016). In an anoxic environment rich in sulfides, the tendency is for trace metals to adsorb with sulfur and enrich the sediment (Tribovillard *et al.*, 2006). Galene and sphalerite minerals were recorded in the limestone layers of the Crato Formation, confirming reducing conditions by bacterial sulfate-reduction (Martill, Loveridge, Heimhofer, 2007; Osés *et al.*, 2016).

The enrichment of trace metals in samples 1E, 11C, 10A, and 10D, together with Hg/TOC peaks signals the action of volcanisms and their record in the Araripe Basin. Spearman's correlation demonstrated the relationship between Hg/TOC (vulcanism) and trace metals (Pb, V, Mn, Fe, Cu, and Zn), indicating the interference of volcanism in the trace metals deposition, following increasing biological productivity, changes in redox state, and paleoclimatic conditions.

During volcanic degassing, trace metals are emitted into the atmosphere (associated with dust, volcanic ash, and sulfides) (Mason *et al.*, 2021), increasing deposition, further favored by increased paleoproductivity and anoxic conditions (Fan *et al.*, 2021; Galloway *et al.*, 2023). Furthermore, low correlation between Al with Pb, Mn, Fe, Cu, and Zn indicates little contribution of detrital elements (Tribouillard *et al.*, 2006). Only Ni, V, and Cr concentrations were correlated with those of Al, demonstrating the influence of external detrital input on the deposition of these metals.

$\delta^{18}\text{O}$  and  $\delta^{13}\text{C}_{\text{carbonate}}$  in samples 1E, 11C, 10A, and 10D mark sudden changes when there are peaks of Hg/TOC, indicating the interference of volcanism in paleotemperature and paleoproductivity in the Araripe basin. During the Aptian, variations of  $\delta^{18}\text{O}$  and  $\delta^{13}\text{C}_{\text{carb.}}$  were recorded, indicating oscillations in carbon cycle as well as in paleotemperatures (Bottini, Erba, 2018; Li *et al.*, 2014). Occurrence of evaporites, the absence of coal seams, and the xerophytic vegetation resistant to drought demonstrate that the depositional conditions of the Crato Formation are in the Tropical Equatorial Hot belt (Chumakov *et al.*, 1995; Ribeiro *et al.*, 2021).

When there is an injection of  $\text{CO}_2$  originating from the terrestrial mantle, the imbalance in the carbonate system occurs, directly influencing the mixture of calcifying organisms (Bond, Grasby, 2017). In this context,  $\delta^{13}\text{C}_{\text{carb.}}$  and  $\delta^{18}\text{O}$  oscillations in the Crato Formation occurs because the disturbances in the carbon cycle, in which the  $\text{CO}_2$  (intensifying the greenhouse effect), sulfur dioxide and atmospheric dust (decreasing the temperature) emitted by volcanism were able to generate changes in paleotemperature and changes in paleoproductivity.

### 6.5.3.3 Romualdo Formation

The Romualdo Formation dates between the Aptian-Albian transition ( $\sim 113.1$  Ma), based on the presence of benthic foraminifera *Paraticinella rohri* (middle Aptian), *Microhedbergella miniglobularis* (late Aptian - 113.1 Ma), and the nannofossil *Hayesites albiensis* (early Albian) (Araripe *et al.*, 2021, 2022; Assine, 2007; Assine *et al.*, 2014; Fambrini *et al.*, 2020; Melo *et al.*, 2020). Among the volcanism events that occurred during the late Aptian and early Albian are the Southern Kerguelen and Raajmahal plateaus (118 – 110 Ma) (Coffin *et al.*, 2002; 2006). Sabatino *et al.* (2018, 2015) and (Galloway *et al.*, 2023) found Hg/TOC anomalies in the foraminifera zones *P. rohri*, *M. miniglobularis*, and *Hayesites albiensis* and associated these anomalies to the event ocean anoxia 1b (OAE 1b) resulting from the Southern Kerguelen (SKP) plateau volcanism,

which also caused the enrichment of trace metals, biological crises of calcifying marine organisms, the burial of TOC, and oceanic anoxia (Erba *et al.*, 2015; Sabatino *et al.*, 2015).

The Hg/TOC anomalies found in the present study in the Romualdo Formation, in addition to the burial of TOC and trace metals enrichment, are indicative of changes in paleoproductivity and paleoredox, which may be associated with the OAE 1b event, influenced by the SKP. This is consistent with a scenario of distal effects of the OAE 1b in the Araripe basin, biostratigraphic correlations (Guzmán *et al.*, 2023), and accumulation of organic matter (Heimhofer *et al.*, 2008). More recently, metal enrichment and  $\delta^{13}\text{C}_{\text{organic}}$  isotopic signatures were also related to the activation of volcanism on the SKP- Kilian subevent (Benigno *et al.*, 2021; Bom *et al.*, 2023).

Metals anomalies found of paleoproductivity ( $\text{Cu}^{\text{EF}}$ ,  $\text{Zn}^{\text{EF}}$ ,  $\text{Ba}^{\text{EF}}$ ,  $\text{Ni}^{\text{EF}}$  and TOC) and paleoredox ( $\text{Pb}^{\text{EF}}$ ,  $\text{Cr}^{\text{EF}}$ ,  $\text{Mn}^{\text{EF}}$ ,  $\text{V}^{\text{EF}}$  and  $\text{Fe}^{\text{EF}}$ ) proxies in the Romualdo Formation were linked to the influence of SKP volcanism in the Araripe basin, as observed by the Hg/TOC peaks in the same layers. Li *et al.* (2014) found increasing  $\text{CO}_2$  emissions during the activation of the Southern Kerguelen plateau. The injection of  $\text{CO}_2$  and other gases ( $\text{HCl}$  and  $\text{SO}_4^-$ ) led to the development of the biological pump, resulting in greater productivity, metals enrichment, ocean acidification, as well as increased weathering due to the acidity of the atmosphere (Bodin *et al.*, 2023; Coffin *et al.*, 2006; Grasby *et al.*, 2019). Spearman correlation coefficients were significantly positive between TOC and detrital supply (Al), paleoproductivity and paleoredox proxies. Whereas a negative correlation was observed with paleosalinity. These suggest the impact of the SKP volcanism in the paleoenvironmental depositions of the Araripe Basin. The increase in atmospheric  $\text{CO}_2$  from SKP generates continuous consequences to the paleoenvironment, such as: intensified continental input, more nutrients to the coastal environment, increased primary production, the greater deposition of organic matter, and the immobilization of metals in environment with low oxygenation, and these are reflected in the variability of proxies observed in the Romualdo Formation.

The changes in  $\delta^{13}\text{C}_{\text{carbonate}}$  marked variations in paleoproductivity, and depletion of  $\delta^{13}\text{C}_{\text{carb.}}$  occurs due to changes in the carbon cycle, directly impacting calcifying organisms, while enrichment indicates a stable environment with the re-establishment of those organisms (Weissert *et al.*, 1998).  $\delta^{13}\text{C}_{\text{carbonate}}$  showed impoverishment in the basal samples of the Romualdo Formation, while towards the upper samples there is an enrichment of  $\delta^{13}\text{C}_{\text{carbonate}}$ . This behavior demonstrates that during Hg/TOC anomalies

there is a reduction in  $\delta^{13}\text{C}_{\text{carb}}$ , and an increase in the TOC, while after volcanic anomalies an increase in  $\delta^{13}\text{C}_{\text{carb}}$  is observed, indicating the recovery of calcifying organisms. Heimhofer *et al.* (2008) identified that the organic matter in the Romualdo Formation comes mainly from autochthonous material (primary production) and continental contributions. During different OAE events, where there is a decrease in planktonic calcifying organisms, there is growth of siliciclastic planktonic organisms and cyanobacteria, and consequently, an increase in organic matter deposition (Coccioni *et al.*, 2014; Kuypers *et al.*, 2004; Petrizzo *et al.*, 2012).

The  $\delta^{18}\text{O}$  showed enrichment at the base of the Romualdo Formation, while towards the upper part there is a decrease. The activation of LIPs was responsible for  $\text{CO}_2$  and  $\text{SO}_2$  emissions, impacting the hydrological cycle and global paleoclimatic conditions (Bond, Grasby, 2017). Weissert, Erba (2004) observed paleotemperature variations during OAE 1b associated with volcanism on the Kerguelen plateau.  $\delta^{18}\text{O}$  in the Romualdo Formation demonstrated probable oscillation in the hydrological cycle, with hot humid and hot dry cycles. Paleoclimatic changes were previously reported in this environment, demonstrating that interference in the hydrological regime may had been influenced by  $\text{CO}_2$  oscillations due to volcanism and, consequently, fluvial discharge (Araripe *et al.*, 2019; Bom *et al.*, 2021, 2023; Teixeira *et al.*, 2018).

Therefore, the Hg/TOC peaks found in the Romualdo Formation influenced by the volcanism of the Kerguelen plateau and the biostratigraphic dynamics with the OAE 1b event. The increase of  $\text{CO}_2$  in the atmosphere generated global climate changes and had a direct impact on the Araripe Basin, causing an increase in biological production, the burial of large amounts of TOC, enrichment of trace metals, anoxia events, and climate variations. These processes may have generated biological crises in the Romualdo Formation, as there are reports of mass fish mortality events, low diversity of organisms, and forest fires, demonstrating extremely challenging conditions for the survival of local organisms (Custódio *et al.*, 2017; Martill, 1988; Martill, Brito, Washington-Evans, 2008).

## 5.7 Conclusion

The results showed the influence of the volcanism events of Ontong Java, Southern Kerguelen Plateau, and Raajmahal in the Araripe Sedimentary Basin. Trace metal enrichments found in the Barbalha, Crato, and Romualdo formations characterize the increase in paleoproductivity and changes in the redox state during Hg/TOC peaks. Variations of these proxies may be related to the emission of  $\text{CO}_2$  and other gases into the

atmosphere, which directly affect the development of the biological pump and anoxic conditions.

The Batateira beds (Barbalha Formation) characterized by paleosalinity changes indicating that the first marine intrusions in the Araripe Basin occurred in the early Aptian, anticipating the intrusions previously recorded. Paleoredox conditions indicate that the environment was predominantly anoxic. In addition, the Hg/TOC ratio anomalies and metal enrichments indicate interference signals from the Ontong Java volcanism, which was responsible for the oceanic anoxia event 1a. Biostratigraphic correlations point to a possible depositional system influenced by OAE 1a.

In the Crato Formation, a very heterogeneous environment was identified, with large variations in salinity, redox state, paleoproductivity, and paleoclimate. In this unit, the influence of volcanism was also observed, through the enrichment of the paleoproductivity and paleoredox proxies, being correlated with the Hg/TOC anomalies. Furthermore, the correlation found between volcanism and trace metal proxies demonstrates their volcanic source.

The Romualdo Formation, Aptian-Albian transition, was characterized by presenting a brackish to marine transition environment. Anoxic conditions were observed, corroborating previous studies. Furthermore, Hg anomalies show the influence of the Southern Kerguelen Plateau on paleoenvironmental processes, through the enrichment of paleoproductivity and paleoredox trace metals. Mercury peaks may be related to ocean anoxia 1b events, responsible for major biological crises.

## Acknowledgments

The authors are deeply indebted to the many students at the Regional University of Cariri, who have helped in the intensive field campaigns in the Araripe Basin. Technicians from the Marine Biogeochemistry Laboratory (LBC-UFC) helped preparing samples for chemical analyses. Technicians from the NABISE-UFPE, for isotopes analysis.

## CAPÍTULO 2

### Geochemistry approach to mortality events of autochthonous fauna in Konservatt-Lagerstätte Crato paleolake (Crato Formation, Araripe basin, Brazil)

O segundo manuscrito, aborda uma caracterização geoquímica do Konservat - Lagerstätten do paleolago Crato (Bacia do Araripe). O objetivo principal é caracterizar as mudanças paleoambientais que podem ter resultado nos eventos de mortalidade (*Dastilbe* sp. e epheméropteras) registrados no sistema lacustre. Este trabalho possibilitou observar que as mudanças paleoclimáticas no sistema lacustre eram comuns, onde as variações da profundidade, paleredox e paleoprodutividade do ambiente deposicional podem ter interferido nos eventos de mortalidade registrados. Além disso, observou-se uma interferência dos vulcanismos dos platôs Rajmahal- Kerguelen na paleoclimatologia, podendo ter intensificado a mortandade no Konservat -Lagerstätte do paleolago Crato. Autorias de Igor Hamid Ribeiro Azevedo \*; Luiz Drude de Lacerda, Antônio Álamo Feitosa Saraiva, Alcides Nobrega Sial, Ana Paula Aquino Benigno, Flaviana Jorge de Lima, Renan Alfredo Machado Bantim, Mariana Silvestre Martins, Maria Andrea Ferreira, José Edvar Aguiar.

**Keywords:** Water level, Volcanism, Paleoclimatic changes, Metals, Enrichment factor

#### Highlights

- Changes in paleoproduction, paleoredox state, paleosalinity and paleoclimate in the Konservat- Lagerstätte of the Crato paleolake (Araripe Basin- AB).
- Stable isotopes ( $\delta^{13}\text{C}_{\text{VPDB}}$  and  $\delta^{18}\text{O}_{\text{VPDB}}$ ) and trace metal enrichment were consistent proxies of paleoenvironmental changes.
- Paleoenvironmental changes in the Crato paleolake resulting in cyclical mass mortality events.

---

Hamid, I. R. A.; Martins, M. S.; Saraiva, A. A. F.; Benigno, A. P. A.; De Lima, F. J.; Bantim, R. A. M.; Sial, A. N.; Aguiar, J. E.; Lacerda, L. D. Geochemistry approach and mortality events of autochthonous fauna in Konservatt-Lagerstätten Crato paleolake (Crato Formation, Araripe Basin, Brazil). Submitted to Palaeogeography, Palaeoclimatology, Palaeoecology.

## ABSTRACT

Geochemical records from the Konservat-Lagerstätte of the Crato paleolake (Aptian, Lower Cretaceous) revealed the influence of paleoclimatic variations (wet-dry) on the lake system. Paleoredox ( $\text{Pb}^{\text{EF}}$ ,  $\text{Mn}^{\text{EF}}$ , and  $\text{Fe}^{\text{EF}}$ ) and paleoproductivity ( $\text{Cu}^{\text{EF}}$ ,  $\text{Zn}^{\text{EF}}$ ,  $\text{Ni}^{\text{EF}}$ ,  $\text{Ba}^{\text{EF}}$ , and  $\delta^{13}\text{C}_{\text{VPDB}}$ ) indexes recorded oscillations in the Crato paleolake, including the influence of paleodetrital transport (Al and Fe), paleoclimatic conditions (Sr/Cu), volcanism (Hg/Al and Hg/Fe) and lake level (Fe/Mn and  $\delta^{18}\text{O}_{\text{VPDB}}$ ). The survival the mass mortality of organisms present in the Crato paleolake were related to the paleoclimatic variations experienced by the environment. The Hg anomalies in the Aptian reveal that volcanism of the Rajmahal-Kerguelen plateaus interfered with the climatic and depositional processes of the Crato palaeolake, which led to changes in redox conditions and palaeoproductivity, aridity intensification in the interior of the continent and local mortality events. Furthermore, wet periods show redox conditions and palaeoproductivity that can indicate hypoxia in the aquatic system and the mass mortality events recorded in the Konservat-Lagerstätte of the Crato paleolake.

## 6.1 Introduction

The Araripe Basin (AB), with an area of 9,000 km<sup>2</sup> and 950 m of thickness (Figure 13), near the borders of the states of Ceará, Piauí and Pernambuco (Northeast Brazil) (Assine, 1992, 2007). Its origin and evolution are related to the reactivation of faults in the crystalline basement during fragmentation of the Gondwana supercontinent and the opening of the Atlantic Ocean (Brito Neves *et al.*, 2000; Neves *et al.*, 1995). As a result, the Brazilian and African marginal basins were developed due to the mechanical subsidence during the fragmentation of Africa and South America (Alkmim *et al.*, 2015; Godot Souza *et al.*, 2022). The Araripe Basin is bounded by the Neoproterozoic Pernambuco and Patos shear zones, which are associated with the Brazilian-Pan-African orogeny (Assine, 2007; Brito Neves *et al.*, 2000; Neves *et al.*, 1995).

The ASB shows the highest complexity among all the sedimentary basins in the Brazilian Northeast, as it presents 5 depositional sequences which are furrowed in two geomorphological features: the Araripe plateau surface and the Cariri Valley (Assine, 2007; Peulvast, Bétard, 2015). The Araripe plateau has an East-West orientation and encompasses the Cretaceous (Aptian-Cenomanian) depositional sequences of the post-rift I (Barbalha, Crato, Ipobi and Romualdo formations) and II (Araripina and Exu formations) stages of the Atlantic Ocean opening process (Assine, 2007). The Cariri Valley contains records of the oldest periods of the ASB, including the Paleozoic (Cariri Formation), the Jurassic pre-rift (Brejo Santo and base of Missão Velha formations) and the Cretaceous rift (Upper of the Missão Velha and Abaiara formations) sequences from Gondwana rift event (Fambrini *et al.*, 2020).

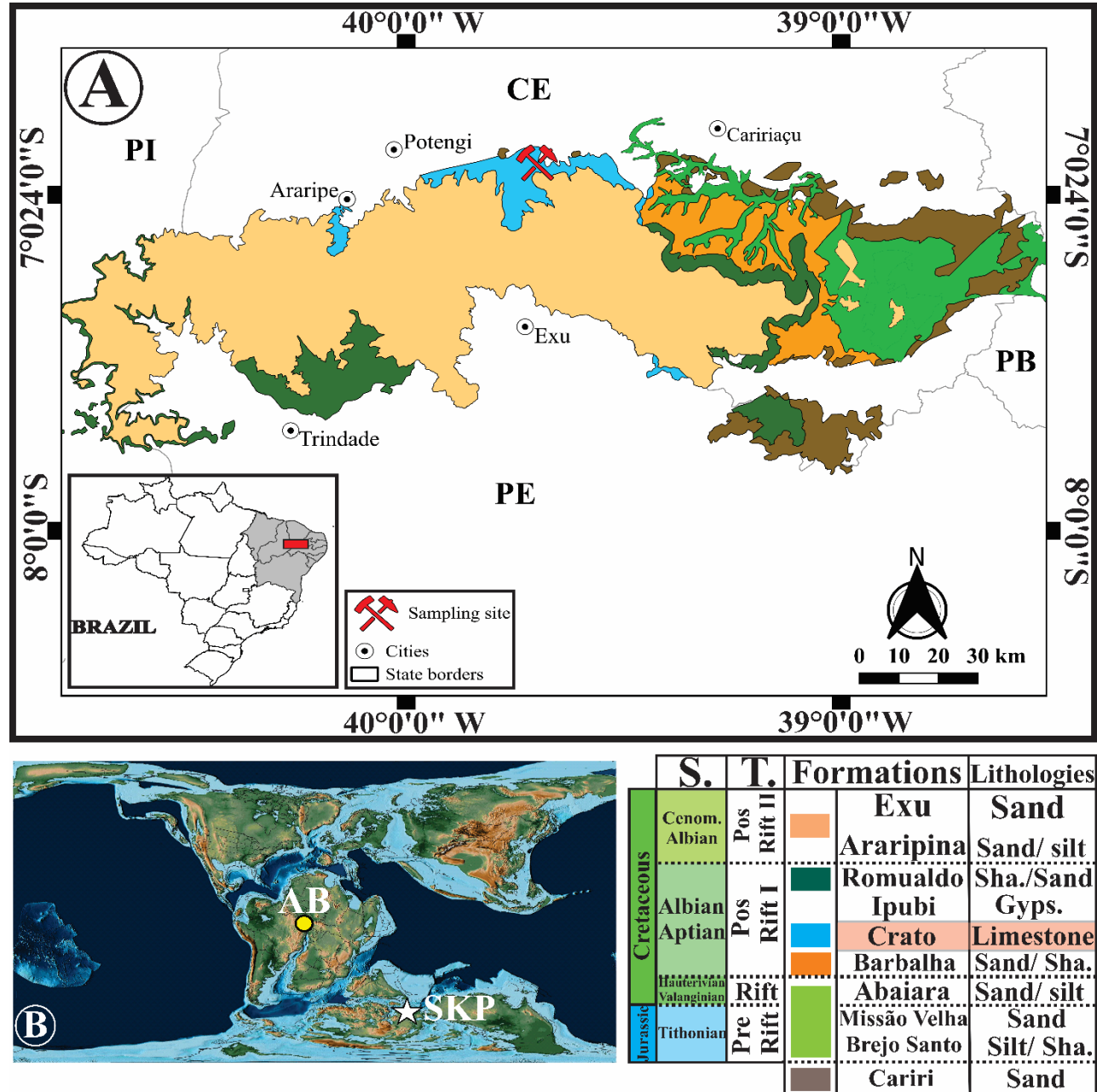
The Crato Formation (Aptian, Lower Cretaceous) represents the second lacustrine phase (Crato paleolake) of the Araripe Basin. It is described as 60 m thick and a lithostratigraphy composed of six calciferous carbonate layers (C1 to C6) intercalated with green shales and fine sandstones (Assine *et al.*, 2014; Coimbra, Arai, Carreño, 2002; Neumann, 1999). The presence of calcified coccoid and biofilms of calciferous filamentous bacteria indicates that the laminated limestones of the Crato Formation are products of biological mineralization (Catto *et al.*, 2016). The exceptional paleontological assemblage of the Crato Formation in the carbonate levels has classified such paleoenvironment as Konservat-Lagerstätte (CKL), due to the remarkable quality of fauna (pterosaurs, insects, crocodyliforms and fish) and flora (gymnosperms and angiosperms) (Assine, 2007; Ribeiro *et al.*, 2021; Varejão *et al.*, 2021).

The location of the Crato paleolake, in the Warm Equatorial Tropical belt (Chumakov *et al.*, 1995), in conjunction with the xerophytic vegetation (Ribeiro *et al.*, 2021), provides evidence of a depositional paleoenvironment characterized by arid to semi-arid conditions. Nevertheless, it is important to distinguish the oscillation between wet and dry periods in the lake system. Such behavior has been observed and documented through fossil record (do Nascimento *et al.*, 2023; Martill *et al.*, 2005; Mendes *et al.*, 2020) and geochemistry (Benigno *et al.*, 2018; Hamid *et al.*, 2024; Salgado-Campos *et al.*, 2021). Previous research has identified that the Crato paleolake exhibits distinct humidity zones, analogous to modern hypersaline lakes of the Andes (Warren *et al.*, 2017) or Lake Chad in Sub-Saharan Africa (Ribeiro *et al.*, 2021).

The Crato paleolake exhibited depositional conditions that suggest an anoxic/dysoxic lacustrine paleoenvironment (Osés *et al.*, 2016), characterized by extremely arid periods, highlighted by the presence of halite crystals (Martill, Loveridge, Heimhofer, 2007), and paleo-wildfires (Lima *et al.*, 2019). In this context, cyclical changes in humidity may have resulted in unfavorable conditions for the survival of organisms in the Crato paleolake, as the lake system experienced significant fluctuations in depth, salinity, productivity, and redox state. These oscillations have resulted in the occurrence of periodical mortality events (Martins-Neto, 2006; Storari *et al.*, 2021).

The present study aims to elucidate the cyclical factors involved in mortality events recorded by Storari *et al.* (2021), and other authors in the Crato Formation. To achieve such goal, the study aims to determine the relationships between the paleoenvironmental changes of the Crato paleolake, and the consequences that led to the mass mortality events. The application of multi-proxies (trace metals and ratios between them and isotopes) will facilitate the interpretation of the evolution and development of the Konservat -Lagerstätte Crato paleolake, enabling the reconstruction of paleoredox conditions, paleoproductivity, and paleodetritic inputs variations in the Araripe basin.

**Figure 13.** Location map of the Araripe basin (AB). A) Distribution area and location of lithofacies in the ASB (Modified from Assine, 2007 and Warren *et al.*, 2017). B) Location of the AB at 120 Ma (Modified from Scotese, Wright, 2018). S- Stage; T- Tectonostratigraphic; Sand- Sandstone, Silt- Siltstone, Sha- Shale, Gyps- Gypsum.



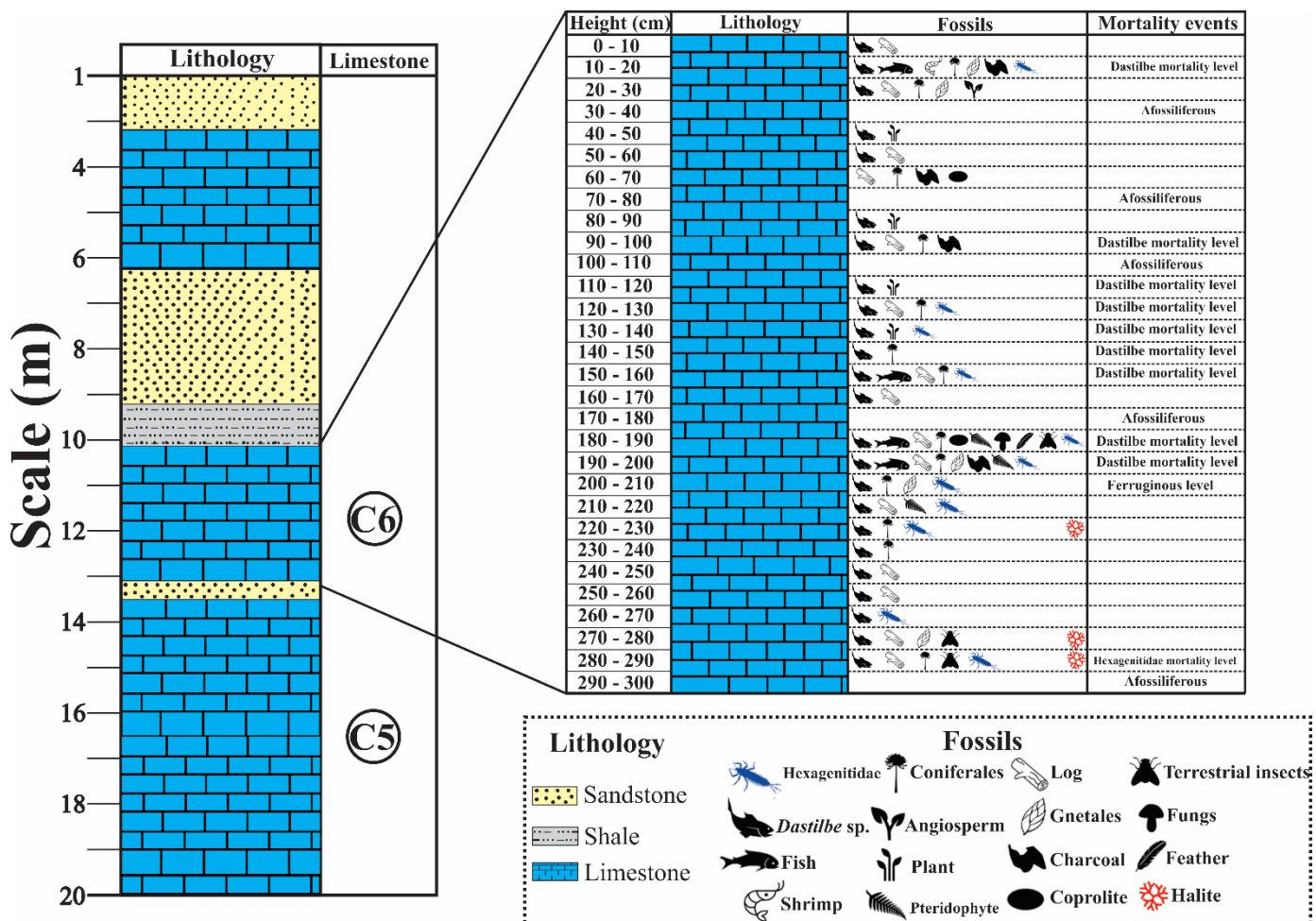
## 6.2 Material and methods

### 6.2.1 Material studied

Samples were collected in the fine-scale profiles of the post-rift I period of the outcrop of the Crato Formation at the Antônio Finelon Mine ( $S\ 7^{\circ}07'22.5''$  and  $W\ 39^{\circ}42'01''$ ) in the Nova Olinda municipality, Ceará State, Brazil (Figure 14). The samples were collected from a layer of the C6 Konservat-Lagerstätten Crato paleolake, more

specifically from the top of the Crato Formation. The controlled excavations were collected in the quarry's surface, divided into  $5\text{ m}^2 \times 5\text{ m}^2$ , and happened from the base to the upper part of the outcrop, totaling 3.20 meters in depth (Figure 14). About 84 samples were collected in the laminated limestones of the Konservat-Lagerstätte, layer and samples were ground, homogenized and dried ( $60^\circ\text{C}$  for 12 hours), then preserved in hermetically closed flasks until analysis. The fossil records indicate the existence of 10 levels of mortality (9 events with *Dastilbe* sp. and with Ephemeroptera larvae) in the Crato paleolake. For more information about the fossil content (integrity of the fossils, type of preservation, length, width, and orientation) of the Crato paleolake consult Storari *et al.* (2021).

**Figure 14.** Profile of the controlled excavation of the Crato Formation at the Antonio Finelon mine (modified from Storari *et al.*, 2021). The samples come from the C6 layer of the Crato Formation, identifying 10 mortality events (*Dastilbe* sp. and Hexagenitidae) in the Crato paleolake.



### **6.2.2 Metals analysis**

The concentrations of Al, Fe, Mn, Sr, Cu, Pb, Ni, Ba, and Zn were measured in 84 samples by Flame Atomic Absorption Spectrometry - FAAS (AA 7000, SHIMADZU). About 0.7 g of the samples were placed in Teflon tubes closed pressure vessels with 15 mL Aqua Regia 100% v/v (3 HCl:1 HNO<sub>3</sub>) and were digested in microwaves (1,600 W and 175 °C, for 20 min). The extracts were taken in volumetric flasks to 30 mL with HNO<sub>3</sub> 0.2% v/v. All glassware was previously washed with deionized water in a 10% v/v Extran detergent solution (10% v/v) for 24 hours, and then in an HCl bath (Sigma-Aldrich) 10% v/v for 24 hours. Reference standard materials (NIST 1646A), reagent blanks and duplicated samples were prepared and measured to assess the accuracy (between 84% - 97%), whereas the detection limit of the procedure varied from 0.02 (Ni) to 0.37 µg g<sup>-1</sup> (Al). Quantification of the metals used Flame Atomic Absorption Spectrometry - AAS (AA 6200, SHIMADZU), with calibration curves of each metal constructed from MERCK standard solutions (1,000 µg mL<sup>-1</sup>).

### **6.2.3 Mercury analysis**

The quantification of mercury (Hg) was performed in duplicates after digestion of 1 g of the samples were placed in Teflon tubes closed pressure vessels with a 10 mL of concentrated nitric acid (HNO<sub>3</sub> 65%) for 1 h pre-digestion. Total samples digestion was carried out in a microwave digestion (at 1,600 W and 175 °C, for 30 min). The final extract was quantitatively transferred and diluted in volumetric flasks (100 mL). All glassware was previously washed with deionized water in an Extran® solution bath (10% v/v) for 24 hours and then in an acid bath of HCl (Sigma-Aldrich) 10% v/v also for 24 hours. The quantification of Hg was performed using Cold Vapor Generation Atomic Absorption Spectrometry (CV-AAS), in a NIC-RA-3 (NIPPON®). Furthermore, analyses with reference material (NIST-1646A) were performed simultaneously with the samples, in which the mean recovery was 93 ± 6%; the limit of detection of the procedure was 0.04 ng g<sup>-1</sup>, and the limit of quantification was 0.13 ng g<sup>-1</sup>.

### **6.2.4 Stable isotopes ( $\delta^{13}\text{C}$ and $\delta^{18}\text{O}_{\text{VPDB}}$ )**

Seventeen samples were selected from the CKL layer of the Crato Formation for Carbon ( $\delta^{13}\text{C}$ ) and Oxygen ( $\delta^{18}\text{O}$ ) stable isotopes analysis. Stable isotope analysis was quantified in the CO<sub>2</sub> extracted from the samples by digestion with orthophosphoric acid

at 25°C, using a Thermofinnigan Delta V Advantage mass spectrometer. Results are expressed in the  $\delta$  notation (‰) with an accuracy better than  $\pm 0.1\text{‰}$ ; Carbon and Oxygen isotopic data were calibrated to international standards (Vienna Pee Dee Belemnite).

### 6.2.5 Enrichment Factor (EF)

In order to eliminate the potential impact of sediment sources in the surrounding area and to mitigate the effects of biogenic components (carbonates, silica and phosphorites) upon the results, the present study has used Al and Fe as normalizers, with the objective of discerning abrupt shifts in paleoproductivity ( $\text{Ni}^{\text{EF}}$ ,  $\text{Cu}^{\text{EF}}$ ,  $\text{Zn}^{\text{EF}}$ , and  $\text{Ba}^{\text{EF}}$ ) and the paleoredox state ( $\text{Pb}^{\text{EF}}$ ,  $\text{Mn}^{\text{EF}}$ , and  $\text{Fe}^{\text{EF}}$ ) (Sabatino *et al.*, 2015; Soua *et al.*, 2011; Touati, Haji, 2019; Tribouillard *et al.*, 2006). The application of EF allows for the general assessment of the enrichment/impoverishment of metals, pertinent paleoenvironmental alterations, and their essential role in chemostratigraphy (Algeo e Liu, 2020). The utilization of such metals considers their behavior in a reducing environment, in which they can adsorb with organic matter, carbonates, and co-precipitate with sulphur (Algeo, Liu, 2020; Algeo, Maynard, 2004; Herndon *et al.*, 2018).

Al and Fe are constituents of siliciclastic groups and are associated with silt and clay particles. Furthermore, they are constituents of the major detrital minerals, which include phyllosilicates, quartz, plagioclase, and k-feldspar. These minerals are characterized by high stability and low mobility in the environment (Merli *et al.*, 2020; Montero-Serrano *et al.*, (2015); Rodríguez-Cuicas; Montero-Serrano *et al.*, (2019)). Although the geochemical indicator is for paleoredox conditions (Tribouillard *et al.*, 2006), the present study has used Fe as an indicator of palaeodetritic input and the identification of EF anomalies in the calcite limestones of the Crato Formation. The application of this element is based on a proposal by Heimhofer *et al.* (2010) for the Crato palaeolake that indicates that Fe was used as the geochemical standard, which suggests that the element could originate from rock and soil weathering processes.

The calculation of the enrichment factor (EF) consists of the ratio between the concentration of the element in limestones and the corresponding average concentration of the element in the upper middle crust (Cao *et al.*, 2012). However, the present study uses the concentrations of specific elements found in limestone, as proposed by Salomons, Förstner (1984). The EF is determined using the equation:  $\text{EF}_{\text{Element}} = [(X/\text{Al}, \text{Fe})_{\text{Sample}} / (X/\text{Al}, \text{Fe})_{\text{Limestones}}]$ , in which  $(X/\text{Al})_{(\text{Sample})}$  represents the concentrations of elements X and Al, Fe measured in the samples, while  $(X/\text{Al}, \text{Fe})_{(\text{Limestones})}$  corresponds to

the concentrations of elements in the "average limestones" of the crust according to the values proposed by Salomons, Forstner, (1984).

### **6.2.6 Statistics methodology**

The statistical analysis of this study was performed using RStudio software (version 4.3.1 - © 2009 - 2023 RStudio, Inc.). Homogeneity and normality tests were carried out for the assessment of the normality of the samples. As a result, it was possible to determine a non-normal projection of the variables. In this case, Spearman's correlation coefficient was used ( $p < 0.05$ ,  $n=84$ ). The data provided, known as the correlation index, varies from -1 to +1 and assesses whether there is a relationship of dependence or independence between the parameters evaluated (Miller, 2010).

Additionally, Principal Component Analysis (PCA), a multivariate evaluation method was utilized to investigate the correlation between trace metal concentrations and observed mortality events in the depositional environment. To apply this method, it was necessary to classify the mortality events according to the presence or absence of these events along the stratigraphic column.

## 6.3 Results

### 6.3.1 Characterization of the Crato paleolake

The aluminum concentration in the Crato paleolake exhibited a range from 0.03% to 0.69%, with the highest concentration observed at a depth of 160 cm, as illustrated in Figure 15A. A significant direct correlation ( $p < 0.05$ ;  $n = 84$ ) between Al was observed with Zn ( $r = 0.61$ ), Fe ( $r = 0.34$ ), Cu ( $r = 0.42$ ), Ni ( $r = 0.40$ ), Pb ( $r = 0.28$ ), and Hg ( $r = 0.33$ ). For Iron, concentrations ranged from 0.08 to 1.90% (Figure 15A), were positively correlated ( $p < 0.05$ ;  $n = 84$ ) with Cu ( $r = 0.55$ ), Zn ( $r = 0.61$ ), Ni ( $r = 0.48$ ), Pb ( $r = 0.39$ ), Ba ( $r = 0.32$ ), and Hg ( $r = 0.34$ ). The highest iron concentrations were observed at depths of 16 cm (1.69%) and 180 cm (1.90%).

The Sr/Cu ratio, a proxy to paleoclimatic conditions, varied from 0.08 to 13.8 (Figure 15B), while the Sr/Ba ratio, a proxy to paleosalinity, varied from 0.13 to 20 (Figure 15B). Spearman's test ( $p < 0.05$ ;  $n = 84$ ) showed significant correlations between Sr/Cu and Sr/Ba ( $r = 0.47$ ), and negative with Al ( $r = -0.32$ ), Fe ( $r = -0.27$ ), Cu ( $r = -0.46$ ) and Zn ( $r = -0.31$ ). The Sr/Ba ratio was negatively correlated with Al ( $r = -0.32$ ), Ni ( $r = -0.33$ ) and Ba ( $r = -0.39$ ).

The  $\delta^{13}\text{C}_{\text{VPDB}}$  varied from  $-2.2\text{\textperthousand}$  to  $+0.3\text{\textperthousand}$  (Figure 16A), with the highest values at depths of 151.4cm ( $+0.28\text{\textperthousand}$ ) and 179.1cm ( $+0.24\text{\textperthousand}$ ).  $\delta^{18}\text{O}_{\text{VPDB}}$  values varied from  $-7.6\text{\textperthousand}$  to  $-4.9\text{\textperthousand}$  (Figure 15B), being highest at 150 cm and 179.1 cm ( $-6.25\text{\textperthousand}$ ). The  $\delta^{13}\text{C}_{\text{carb.}}$  and  $\delta^{18}\text{O}$  were positively correlated ( $r = 0.44$ ;  $p < 0.05$ ).

### 6.3.2 Volcanism, paleoproductivity and paleoredox conditions in the Crato paleolake

Mercury (Hg) concentrations exhibited a range from 12 to 355 ng g<sup>-1</sup> (Figure 15A), whereas Hg/Al and Hg/Fe ratios, a proxy of volcanic activity, exhibited sharp positive incursions of 42 to 3,050 and 19 to 882, respectively, as depicted in Figure 15A. Seven Hg concentrations anomalies were identified in the study, with the highest concentrations observed at the same depths where mortality events were recorded at the Crato paleolake. This suggests a potential correlation between Hg concentration and mortality events. Hg/Al ratio demonstrated a significant, positive correlation with Hg ( $r = 0.62$ ;  $p < 0.05$ ;  $n = 84$ ) and Sr/Cu ( $r = 0.37$ ), while Hg/Fe correlated with Hg ( $r = 0.51$ ), Sr/Cu ( $r = 0.42$ ) and Hg/Al ( $r = 0.54$ ).

The Fe/Mn ratio, a proxy of lake level changes of the Crato paleolake, varied from 0.7 to 13 (Figure 15B). Spearman's test ( $p < 0.05$ ;  $n = 84$ ) indicated a direct correlation between the Fe/Mn ratio and Al ( $r = 0.35$ ), Fe ( $r = 0.96$ ), and negative associations between Hg/Al ( $r = -0.31$ ), and Hg/Fe ( $r = -0.40$ ).

Spearman's analysis ( $p < 0.05$ ;  $n = 84$ ) revealed a statistically significant negative correlation between paleoproductivity proxies and Hg/Al ( $\text{Cu} = -0.30$ , and  $\text{Zn} = -0.30$ ), and Hg/Fe ( $\text{Cu} = -0.33$ , and  $\text{Zn} = -0.42$ ). The Fe/Mn ratio was found to be significantly correlated with Cu ( $r = 0.51$ ), Zn ( $r = 0.59$ ) and Ni ( $r = 0.35$ ). The paleoproductivity proxies in the Crato Formation were normalized using Al and Fe, respectively, as EF normalizing elements. It was observed that  $\text{Cu}^{\text{EF}}$  values ranged from 15 to 2,545 and 6 to 579; while  $\text{Zn}^{\text{EF}}$  from 39 to 451 and 13 to 331.  $\text{Ni}^{\text{EF}}$  varied from 0.2 to 32 and 0.2 to 9, while those of  $\text{Ba}^{\text{EF}}$  from 1 to 24 and 0.5 to 14 (Figure 16).

Spearman's analysis ( $p < 0.05$ ;  $n = 84$ ) showed the highest correlations between the paleoredox proxies and the Fe/Mn ratio ( $\text{Mn} = -0.31$  and  $\text{Pb} = 0.38$ ). The EF values were calculated using normalization with Al and Fe, respectively. In the limestones of the Crato Formation, the  $\text{Pb}^{\text{EF}}$  values ranged from 42 to 937 and 21 to 1,393, while the  $\text{Mn}^{\text{EF}}$  varied from 3 to 59 and 2 to 40; while the  $\text{Fe}^{\text{EF}}$  values ranged from 0.3 to 8 (normalized only for Al) (Figure 16).

A correlation analysis between EF and the volcanism proxies (Hg/Al and Hg/Fe) showed positive correlations with  $\text{Ni}^{\text{EF}}$ ,  $\text{Ba}^{\text{EF}}$ ,  $\text{Mn}^{\text{EF}}$ , and  $\text{Fe}^{\text{EF}}$ . For more detailed information on the correlations between the volcanism proxies (e.g., paleosalinity [ $\text{Sr}/\text{Ba}$ ], paleoclimate [ $\text{Sr}/\text{Cu}$ ] and depth [ $\text{Fe}/\text{Mn}$ ]), the enrichment factors of the paleoproductivity (Cu, Zn, Ba and Ni) and paleoredox (Pb, Mn and Fe) proxies see the Supplementary Material.

PCA was applied to evaluate the interference of trace metal enrichment factors and geochemical ratios (Hg/Al, Hg/Fe, Sr/Cu, Sr/Ba and Fe/Mn) in mortality events recorded in the Crato paleolake. Note that EF using Al as a normalizer accounted for 69.2% of the total variance, with PC1 and PC2 explaining 35.1% and 34.1% of this variance, respectively (Figure 17A). For EF using Fe as a normalizer (Figure 17B), we observed that 52% of the total variance of the data was accounted for, with PC1 and PC2 explaining 31.8% and 20.2% of the total variance, respectively. The PCA suggests that the mortalities recorded in the Crato Paleolake may be the result of changes in paleoproductivity and paleoredox in the lacustrine system, which may affect the survival of organisms.

**Figure 15.** Chemostratigraphy of the Crato paleolake. A) Paleodetritic proxies (Al and Fe); volcanism proxies (Hg/Al and Hg/Fe ratios) and Hg concentration ( $\text{ng g}^{-1}$ ). B) Paleoclimatic proxy (Sr/Cu); paleosalinity (Sr/Ba); and variation in the depth of the lake system (Fe/Mn) and  $\delta^{18}\text{O}_{\text{VPDB}}$ .

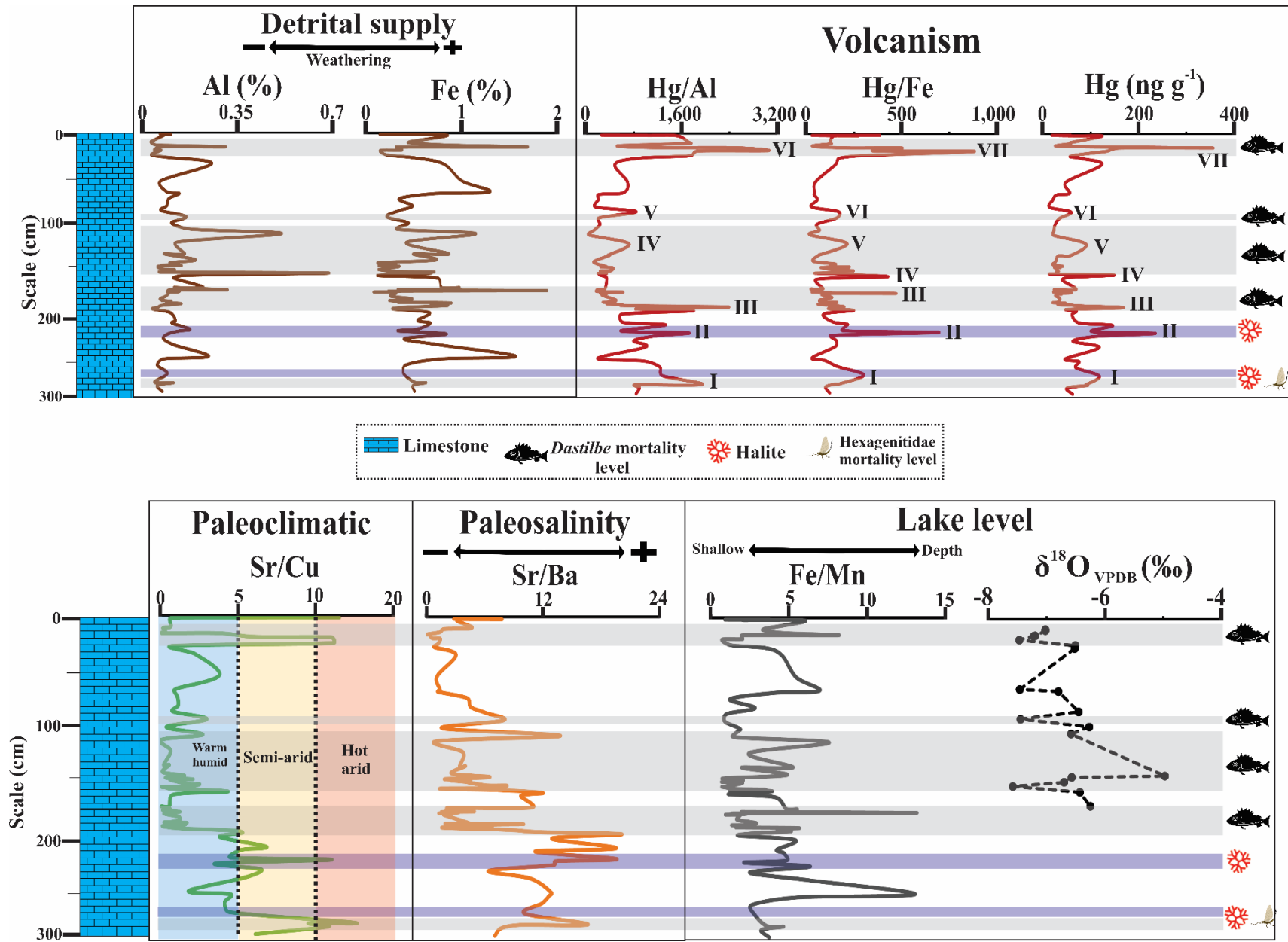


**Figure 16.** Enrichment factor of paleoredox proxies ( $\text{Pb}^{\text{EF}}$ ,  $\text{Mn}^{\text{EF}}$  and  $\text{Fe}^{\text{EF}}$ ), and paleoproductivity proxies ( $\text{Cu}^{\text{EF}}$ ,  $\text{Zn}^{\text{EF}}$ ,  $\text{Ni}^{\text{EF}}$ ,  $\text{Ba}^{\text{EF}}$ , and  $\delta^{13}\text{C}_{\text{carb}, \text{VPDB}} (\text{\textperthousand})$ ) in the Crato paleolake. A) Enrichment factor using Aluminum (Al) as a normalizer; B) Enrichment factor using Iron (Fe) as a normalizer.

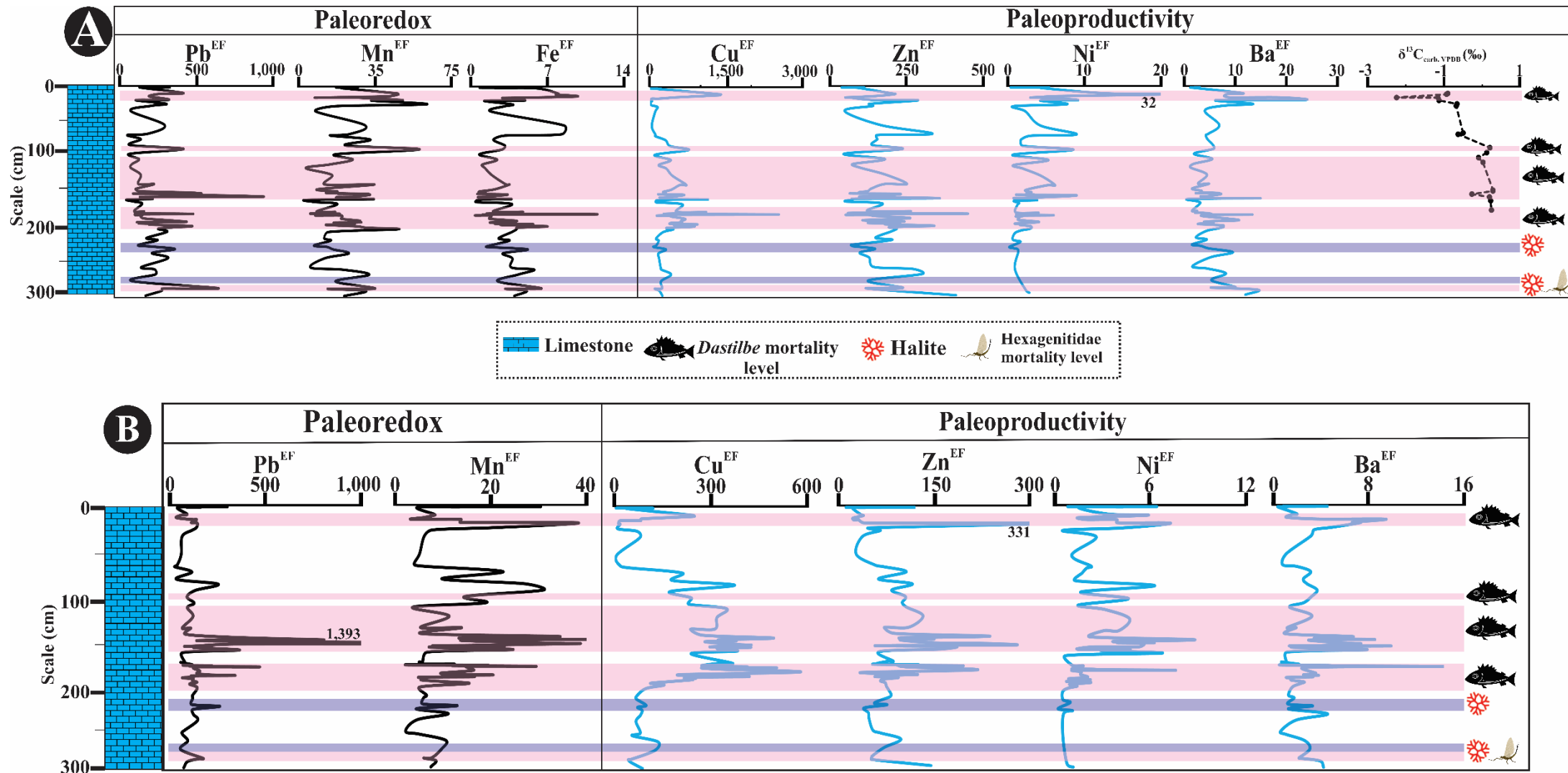
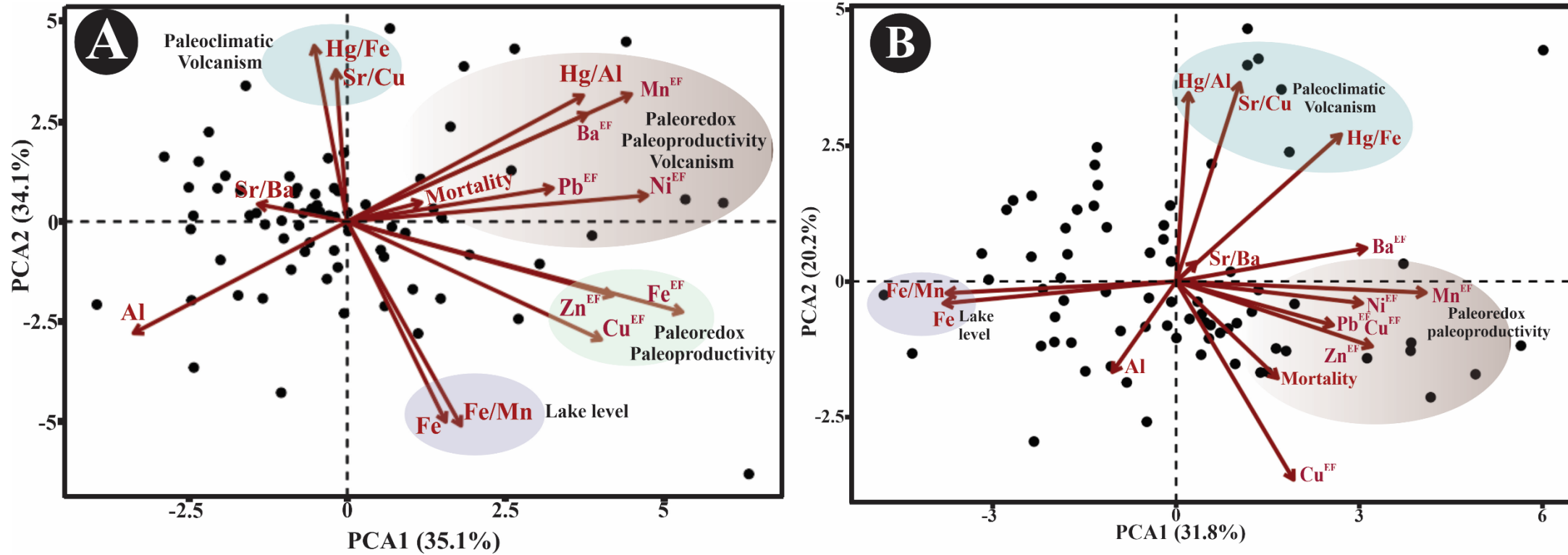


**Figure 17.** Principal component analysis with enrichment factor of trace metals (Ba, Cu, Zn, Pb, Fe, Mn, and Ni), volcanism (Hg/Al and Hg/Fe), paleodetritic (Al and Fe), lake level (Fe/Mn), paleoclimate conditions (Sr/Cu), paleosalinity (Sr/Ba) and the correlations with mortality events. A) Enrichment factor using Aluminum as a normalizer; B) Enrichment factor using Iron as a normalizer.



## **6.4 Discussion**

### **6.4.1 Characterization of the Crato paleolake**

#### **6.4.1.1 Paleosalinity**

The Sr/Ba ratio was used to determine the paleosalinity of the Crato Formation. Values of the Sr/Ba lower than 0.2 indicate a freshwater environment, whereas from 0.2 to 0.5 indicate brackish waters. Higher values ( $> 0.5$ ) indicate marine characteristics (Wei, Algeo, 2020). The Sr/Ba ratio concentrations observed in this study indicate that the Crato Formation showed characteristics of a marine depositional environment ( $\text{Sr/Ba} > 0.5$ ). The samples collected for this study were obtained from the C6 layer of the Crato Formation, situated in proximity to the upper portion of the Crato Formation, which is characterized by short events of marine input (Goldberg *et al.*, 2019; Salgado-Campos *et al.*, 2021). In the present context, it is hypothesized that the elevated Sr/Ba ratio observed in the studied samples may be attributed to two potential factors: *i)* the geochemical behavior of Strontium (Sr) in carbonates must be considered; Sr can replace calcium ( $\text{Ca}^{2+}$ ) in calcite and is a product of the chemical weathering of minerals rich in Sr-plagioclase, gypsum, calcite and strontianite (Roden *et al.*, 2002; Wei, Algeo, 2020). *ii)* the intensification of aridity in conjunction with marine intrusions and/ or stratified water column in the lacustrine system may have contributed the observed increase in salinity in the Crato paleolake.

Previous studies indicated that the Crato paleolake exhibited stratification in the water column. The upper surface waters were characterized as freshwater and oxic, while the bottom waters were classified as brackish to hypersaline and anoxic (Heimhofer *et al.*, 2010; Nascimento, Silva Filho, Erthal, 2023). The presence of a stratified water column influenced by climatic oscillations has been previously reported for other Aptian carbonate lake systems (Codó Formation - Parnaíba basin, Serra do Toná Formation - Tucano basin, and Serra Negra Formation - Jatobá basin) (Gratzer *et al.*, 2013; Heimhofer, Martill, 2007; Silveira *et al.*, 2014).

Furthermore, the presence of palynomorphs (Chagas, 2017), microforaminifera (Goldberg *et al.*, 2019), marine dinocysts, and tidal geological structures (Varejão *et al.*, 2019, 2021) suggest the occurrence of short pulses of marine intrusion in the upper layers of the Crato paleolake. In this scenario, the entry of marine waters into the lake system, brought about by arid conditions, is thought to have resulted in hypersalinity in the Crato paleolake and the precipitation of halite crystals.

Geochemical proxies (Hamid *et al.*, 2024; Salgado-Campos *et al.*, 2021), the presence of halite crystals (Martill, Loveridge, Heimhofer, 2007; Storari *et al.*, 2021), the absence of bioturbation (Warren *et al.*, 2017), along with the development of microbial mats (Catto *et al.*, 2016) corroborate the occurrence of hypersaline periods in the bottom of the Crato paleolake. Nevertheless, the oscillations in the Sr/Ba ratio indicate that, despite the hypersalinity, the Crato paleolake exhibited fluctuations in salinity. Previous reports have documented episodes of high humidity (Neumann *et al.*, 2003; Santos *et al.*, 2020; Varejão *et al.*, 2019) in the Konservat-Lagerstätten Crato paleolake, which may have contributed to a decrease in salinity in the lake system. This behavior is corroborated by the positive correlation between Sr/Cu (paleoclimatic proxy) and Sr/Ba, which indicates that salinity variations in the Crato paleolake are linked to the paleoclimatic oscillations that occurred during the Aptian. During arid periods, salinity increased, while during humid events, salinity decreased.

#### **6.4.1.2 Palaeoclimatology conditions**

Paleoclimatic variations were established by means of the Sr/Cu ratio, whose application relies on the capacity of these elements to reflect hydrological alterations in the environment. In general, the ratio classifies the environment as humid/semi-humid when values are lower than 5; semi-arid conditions (5 to 10); and arid/hot conditions when the values are higher than 10 (Cao *et al.*, 2023; Fan *et al.*, 2021).

The CKL level of the Crato Formation is composed of evaporites (Assine, 2007), paleo-wildfire records (Lima *et al.*, 2019), and xerophytic vegetation (drought-resistant) (Ribeiro *et al.*, 2021), indicating that the Crato paleolake was in a dry environment. In more precise terms, this environment can be identified as the Arid Hot Tropical Equatorial Belt (Chumakov *et al.*, 1995). However, the Sr/Cu ratio values recorded at the CKL level of the Crato Formation are not consistent with a predominantly arid paleoenvironment, as would be suggested by the occurrence of a humid episode.

The correlation observed between Sr/Cu and Sr/Ba (paleosalinity) indicates alternating periods of wet and dry environments. This suggests that the Crato paleolake experienced fluctuations in salinity, in agreement with paleoclimatic oscillations. Furthermore, the presence of wetlands in the Crato paleolake indicates periods of higher precipitation levels, greater freshwater inputs, and lower salinity levels in the lake system (Heimhofer *et al.*, 2010; Ribeiro *et al.*, 2021).

Paleontological, sedimentological, and geochemical records also indicate the alternation of wet and dry cycles at the CKL level (Guerra-Sommer *et al.*, 2021; Neumann *et al.*, 2003; Ribeiro *et al.*, 2021). This is evidenced by the analysis of plant biodiversity (Souza-Lima e Silva, 2018), their growth rings (irregular and/or absent) (Guerra-Sommer *et al.*, 2021; Santos *et al.*, 2021), and fungus-plant interaction (Santos *et al.*, 2020). Furthermore, previous geochemical evidence registered high kaolinite values in the Crato Formation, which suggests the occurrence of wet periods (Salgado-Campos *et al.*, 2021).

#### **6.4.1.3 Paleodetrital input and depth oscillation**

Al, Fe, Ti, and K are used to assess the contributions of paleodetrital inputs to aquatic systems, as they are constituents of siliciclastic minerals and are products of weathering of soils and rocks adjacent to waterbodies (Calvert, Pedersen, 1993; Tribouillard *et al.*, 2006). The present study has indicated that the contribution of paleodetritus in the Crato Formation relatively small. This suggests a reduced input of allochthonous material from the surrounding environment, particularly in terms of iron and aluminum. These observations can be linked to the paleoclimatic conditions in the region, which have been described as arid or semi-arid with low precipitation (less than 250 mm) (Heimhofer *et al.*, 2010; Salgado-Campos *et al.*, 2021). Furthermore, the low abundance of these elements to the size of the detrital material found in the laminated limestones, which is composed of subangular silty quartz and insignificant amounts of k-feldspar grains (Heimhofer *et al.*, 2010).

The positive correlation observed between paleodetrital proxies and Fe/Mn (lake level) and the negative correlation with Sr/Cu (paleoclimate) suggest that detrital inputs to the Crato paleolake are influenced by wet-arid cycles. At the CKL level of the Crato Formation, oscillations in precipitation were recorded (Neumann *et al.*, 2003), resulting in variations in paleodetrital inputs (Heimhofer *et al.*, 2010). Wet periods are characterized by the input of continental material to the lake system, which, through weathering, results in the formation of  $\text{Fe}^{3+}$  oxyhydroxides and the availability of nutrients for the biotic development of the Crato paleolake (Heimhofer, Martill, 2007; Osés *et al.*, 2017).

The oscillation levels of the Crato paleolake were determined by measuring the Fe/Mn ratio, which has been shown to be sensitive to changes in the redox state and the paleodetrital contributions (Tribouillard *et al.*, 2006). Fe is an element susceptible to redox state fluctuations, which vary according to the conditions of oxidation and

reduction. Under these conditions,  $\text{Fe}^{2+}$  adsorbs to  $\text{H}_2\text{S}$  (hydrogen sulfide) and precipitates in the sediment (Algeo, Li, 2020). In the case of Mn, when exposed to aerobic conditions, Mn oxides are formed and precipitate, whereas dissolution of Mn occurs under anoxic conditions (Robbins *et al.*, 2023). Therefore, the increase in the Fe/Mn ratio is conditioned by a decrease in the oxygenation of the environment and an increase in the depth of the lake system (Evans *et al.*, 2021; Zou *et al.*, 2022).

The positive correlations between Fe/Mn and Al and Fe indicate an increase in water depth during wet periods, while in the dry periods, it is observed a decrease in water level of the Crato paleolake. Weathering is sensitive to climatic conditions, in warm periods, there is an increase in paleodetritic contributions, whereas dry-cold climates are characterized by a reduction in weathering (Nesbitt, Young, 1982). Consequently, the humid episodes of the Crato paleolake are characterized by an increase in the contributions of terrigenous materials (increased rainfall and depth), while the reductions in paleodetrital transport indicate the predominance of an arid environment.

#### **6.4.1.4 Stable isotopes ( $\delta^{13}\text{C}_{\text{VPDB}}$ and $\delta^{18}\text{O}_{\text{VPDB}}$ )**

The isotopic variations of  $\delta^{13}\text{C}_{\text{VPDB}}$  and  $\delta^{18}\text{O}_{\text{VPDB}}$  observed in the limestones of the Crato Formation can be attributed to the balance between precipitation and evaporation, which directly influences paleoclimatic oscillations. The positive correlation between  $\delta^{13}\text{C}_{\text{VPDB}}$  and  $\delta^{18}\text{O}_{\text{VPDB}}$  indicates that the level of the Crato paleolake experienced periods in which the lake environment was closed (Heimhofer *et al.*, 2010), under conditions of a hot and dry paleoclimate with elevated evaporation (Neumann, 1999). The  $\delta^{13}\text{C}$  isotope data reveals a similar pattern of change, indicating enrichment of  $\delta^{13}\text{C}_{\text{VPDB}}$  isotope when the lake system was isolated from external fresh-water sources. Negative values of  $\delta^{13}\text{C}_{\text{VPDB}}$  indicate the input of fresh water from outside the system, which resulted in the dilution of paleoproductivity signals (Nascimento *et al.*, 2023).

The Codó (Parnaíba Basin) and Serra do Toná (Tucano Basin) formations (also located in the northeastern Brazil) are stratigraphically correlated with the Crato Formation (Araripe Basin) (Lima Barros *et al.*, 2022; Varejão *et al.*, 2016, 2021). These formations are characterized by laminated limestones typical of a lacustrine system with depth oscillation (Lindoso, Maisey, Carvalho, 2016; Pradel *et al.*, 2021; Silveira *et al.*, 2014; Varejão *et al.*, 2021). The isotopic signals for carbon and oxygen of these sedimentary basins, located in the Northeast region of Brazil, exhibited values like those reported for the Crato paleolake. The oscillations observed in these isotopic signals are

associated with changes in the hydrological cycle (precipitation-evaporation) (Bobco *et al.*, 2023; Silveira *et al.*, 2014). Consequently, the fluctuations observed in the depletion/enrichment of  $\delta^{13}\text{C}_{\text{VPDB}}$  and  $\delta^{18}\text{O}_{\text{VPDB}}$  in the Crato paleolake are similar from those observed in trace metals. This indicates that the variations in the lake system may have influenced not only the redox state and paleoproductivity but also the mortality events in the lake system.

#### 6.4.2 Paleoproductivity

The application of Cu, Zn, Ni, and Ba as proxies for paleoproductivity is based on their capacity to form organometallic complexes with organic matter and to act as micronutrients for the development of trophic webs (Tribouillard *et al.*, 2006). The presence of diagenetic barite ( $\text{BaSO}_4$ ) at the CKL level (Osés *et al.*, 2017) demonstrates that paleoproductivity in the lake system was high. This mineral is known to show a correlation with the carbon flow in aquatic ecosystems (House, Norris, 2020; Liguori, Almeida, Rezende, 2016).

The Spearman analysis and anomalies of the paleoproductivity proxies suggest that proximal sources, such as detrital inputs and distal processes, including volcanism, influenced the Crato paleolake. The paleoproductivity proxies exhibited a positive correlation with detrital inputs and lake level, indicating that during humid periods there was an increase in freshwater input and nutrient, which led to an increase in primary productivity in the lacustrine system. Previous studies in the Crato paleolake have demonstrated a correlation between the increase in productivity in the algal horizons of Crato Formation and the rise in nutrient load during humid periods. This phenomenon has been shown to facilitate the proliferation of phytoplankton activity (Heimhofer *et al.*, 2010; Martins-Neto, 2006; Osés *et al.*, 2017).

The stratification of the water column in the Crato paleolake suggests the presence of surface waters with high primary productivity and anoxic conditions at the bottom of the lake (Heimhofer, Martill, 2007). In environments with high salinity, drought, and elevated pH levels, cyanobacteria tend to prevail (Brehm *et al.*, 2002; Kifumbi *et al.*, 2022). The record of *Spirulina*, filamentous cells, well-preserved coccoid, extracellular polymers (Catto *et al.*, 2016), 14 species of algae (abundant chlorophyte *Botryococcus* sp.) (Martine, 2013), and the development of stromatolites (Warren *et al.*, 2017) attest to a productive lake paleoenvironment.

#### **6.4.3 Paleoredox conditions of the Crato paleolake**

The application of Pb, Mn and Fe as paleoredox proxies is related to their precipitation with oxyhydroxides of Al, Fe and Mn (oxic conditions) and hydrogen sulfides- H<sub>2</sub>S (anoxic conditions) (Algeo, Li, 2020; Algeo, Liu, 2020). Despite the high paleoproductivity of the lacustrine system, the occurrence of frambooidal pyrites in the fossil records of the Crato Formation indicates the possibility that these elements were also enriched through bacterial sulfate reduction. The pyritization of soft tissues in the fossils, the absence of bioturbation and the presence of microbial mats indicate anoxic depositional conditions at the CKL level of the Crato Formation (Barling *et al.*, 2020; Hamid *et al.*, 2024; Heimhofer, Martill, 2007).

The precipitation of pyrite (FeS<sub>2</sub>) in anaerobic environments can be attributed to the reduction of iron (Fe<sup>2+</sup>) in the presence of sulfide (H<sub>2</sub>S) and mediated by sulfate-reducing bacteria influence (Wilkin, Barnes, Brantley, 1996). Negative values of δ<sup>13</sup>C<sub>VPDB</sub> and high values of amorphous organic matter (AOM) are indicative of an anoxic paleoenvironment, likely influenced by sulfate bacterial reduction in the lacustrine system (Catto *et al.*, 2016; Swart, 2015; Varejão *et al.*, 2021). The presence of galena and sphalerite in the fossil record (Barling *et al.*, 2015; Martill *et al.*, 2007), in conjunction with frambooidal pyrite and marcasite (FeS<sub>2</sub>) (Cabral *et al.*, 2019), provides evidence that Zn, Cu and Pb may have co-precipitated with the reduced forms of iron (Heimhofer, Martill, 2007). Consequently, the positive correlations observed between Cu<sup>EF</sup>, Pb<sup>EF</sup>, and Zn<sup>EF</sup> and Fe<sup>EF</sup> suggest that anoxic conditions and elevated productivity were conducive to bacterial sulfate reduction. This process made the reduced forms of iron available in the Crato paleolake and in the enrichment of these elements.

#### **6.4.4 Volcanism**

Mercury (Hg) of natural origin is emitted into the atmosphere in the elemental form (Hg<sup>0</sup>), through processes such as volcanism and wildfires (Percival *et al.*, 2015). Subsequently, Hg is oxidized in the atmosphere to the ionized form (Hg<sup>2+</sup>) and transferred to terrestrial and aquatic compartments through precipitation (Benigno *et al.*, 2018; Font; Bond, 2021). In the sediment, Hg is preferentially stored over geologic time complexed with total organic carbon (TOC) (Grasby *et al.*, 2019), clay minerals (aluminum and iron), and Hg sulfides in anoxic environments (Krupp, 1988). Due to the low concentration of TOC observed in the calcitic limestone layers of the Crato Formation, the present study utilized the Hg/Al and Hg/Fe ratios as volcanism proxies. Previous studies have

demonstrated that the application of Hg/paleodetritic proxy's ratios (Al, Fe, Zr, Ti and phyllosilicates) enables the identification of the activation periods of large LIPs throughout geological time (Font *et al.*, 2016; Sabatino *et al.*, 2018; Sanei, Grasby, Beauchamp, 2012; Sial *et al.*, 2013). The role of clay minerals as geochemical carriers of Hg was validated by observing a positive correlation between paleodetritic proxies (Al and Fe) and Hg, indicating a mineral influence on the Hg burial process.

Considering the depositional age of the Crato paleolake, the presence of non-marine ostracods (*Pattersonocypris micropapillosa*), OST-11 biozone (Guzmán *et al.*, 2023) suggests a deposition period at the Alagoas level (Assine, 2007), specifically during the transition between the Upper Aptian and the end of the Aptian. The record observed in OST 11 biozone was also documented in other sedimentary basins in Brazil (Campos, Parnaíba, Sergipe-Alagoas) and Africa (Gabon, Congo, Kwanza) (Guzmán *et al.*, 2023; Lima Barros *et al.*, 2022; Poropat, Colin, 2012). Despite the limited biostratigraphic resolution at the CKL level of the Crato Formation, the Hg anomalies identified in the present study suggest the presence of volcanic episodes originating from the Rajmahal-Kerguelen plateaus (~118-110 Ma) (Coffin *et al.*, 2006, 2002; Hamid *et al.*, 2024).

#### **6.4.4.1 Volcanism as a driver of the environmental changes**

During periods of volcanism, the injection of CO<sub>2</sub> and other gases into the atmosphere (including HS, HCl, and HF) induces a series of alterations of the hydrological cycles in aquatic and terrestrial ecosystems (Bom *et al.*, 2023; Grasby, Bond, 2023). In addition, the injection of gases has been linked to ocean acidification, acid rain, elevated primary productivity, and sediments enrichment of organic matter, and trace metals (Davis, 2023; Wang *et al.*, 2022). The Hg peaks found in the Crato paleolake demonstrated a positive correlation with Sr/Cu ratio (paleoclimate), indicating that volcanic processes may have modified the hydrological cycle (increasing and/or decreasing the precipitation).

The negative correlations observed between Hg anomalies with the detrital inputs, and Fe/Mn ratio (lake level), provide further evidence that volcanic events may have limited precipitation, resulting in a decrease in the transport of terrigenous material and the depth of the lagoon system. The intensification of arid conditions in the Crato paleolake can be observed through the presence of paleo-wildfires (Lima *et al.*, 2019) and halite crystals (Martill *et al.*, 2007; Storari *et al.*, 2021). The correlation between Hg anomalies and an increased frequency of paleo-wildfires and salinity in terrestrial

ecosystems has been recorded during the activation of LIPs, indicating that climate change is caused by perturbations in the carbon cycle (Fan *et al.*, 2021; Xu *et al.*, 2022; Xu *et al.*, 2022).

Although there are records indicating that volcanism can result in increased precipitation, the present study has found a different behavior. In this case, the intensification of arid conditions in the Crato paleolake may be attributed to the location of the lacustrine system (the interior of the supercontinent Gondwana). These circumstances were attributable to the limited impact of the proto-Atlantic Ocean and the Intertropical Convergence Zone (ITCZ), which were still in a state of development (Araripe *et al.*, 2022; Burgener *et al.*, 2023; Santos *et al.*, 2022; Heimhofer, Hochuli, 2010; Varejão *et al.*, 2021). It is crucial to emphasize that, despite the presence of humid windows in the Crato Formation, arid conditions were the prevailing environmental setting in the sedimentary basins of the equatorial margin. However, there was a notable increase in humidity during the Aptian-Albian transition (Bobco *et al.*, 2023; Carvalho *et al.*, 2019; Giannerini *et al.*, 2023; Souza-Lima, Silva, 2018).

Enrichment factors of the paleoproductivity (Ni and Ba) and paleoredox (Mn and Fe) proxies exhibited a positive correlation with the anomalies from volcanism. These results suggest that the activation of LIPs may have affected the depositional processes of the Crato paleolake. This could have resulted in an increase in primary productivity and a change in redox conditions. Trace metal anomalies and isotopic changes were reported during the activation of the Rajmahal-Kerguelen plateaus, which demonstrated the interference of these events in aquatic ecosystems (Cai *et al.*, 2023; Erba *et al.*, 2015; Hamid *et al.*, 2024; Leandro *et al.*, 2022). Although the aridity is intensified during the occurrence of magmatic pulses, the increasing of productivity proxies may be linked to the increase in the atmospheric concentration of CO<sub>2</sub>, which, in turn, contributes to the enhancement of the autochthonous productivity of the lake system (phytoplankton and cyanobacteria).

Moreover, increasing productivity in aquatic ecosystems can be achieved through the deposition of pyroclastic material emitted into the atmosphere (including dust, volcanic ash, and sulfides) derived from volcanic events (Mason *et al.*, 2021). In this scenario, the dispersal of a plume from LIPs to the stratosphere results in the global distribution of aerosols and other compounds, which can generate the fertilization of aquatic environments (Robock, 2000; Wu *et al.*, 2023). An example of this fertilization process associated with explosive volcanism can be observed during the activation of

Krakatau (1883), El Chicón (1982), and Pinatubo (1991), when an increase in productivity was observed, thereby establishing a correlation between the global distribution of aerosol clouds and the deposition of the essential elements necessary for primary productivity (phosphorus and iron) (Glasspool *et al.*, 2015; Manfroi *et al.*, 2015).

#### 6.4.5 Mortality events and paleoenvironmental changes

The limestones of the Crato Formation are classified as Konservat-Lagerstätten, due to their rich collection of fossils, including insects, pterosaurs, dinosaurs, fish, plants, birds, crocodyliforms, and arachnids (Assine, 2007; Fambrini *et al.*, 2020; Ribeiro *et al.*, 2021). The exceptional condition of preservation of the fossils in the Crato paleolake can be attributed to anoxic conditions, the absence of bioturbation, and the development of microbial mats (Osés *et al.*, 2016; Varejão *et al.*, 2019). The composition of the fossils in the Crato Formation is the result of biogeochemical mediation of the preservation process, which is composed of frambooidal micopyrites and hydroxyapatite (Barling, Martill, Heads, 2020; Osés *et al.*, 2016; Varejão *et al.*, 2019).

The geochemical records presented in this study indicate that the depositional conditions of siliciclastic limestones were characterized by large shifts in wet-dry periods, accompanied by changes in paleoproductivity and redox conditions. The substantial fluctuations observed in the Crato paleolake may have created an environment that was highly stressful for the development of organisms, resulting in mortality events (Martill, Loveridge, Heimhofer, 2007; Menon, Martill, 2007; Salgado, Carvalho, 2023). Martins-Neto, (2006) identified that cyclical mortality events of Ephemeroptera species were the result of an intensification in arid conditions, which resulted in a significant reduction in the depth of the lake. The earliest record of mortality we observed occurring between 280 and 290 cm, was observed to be accompanied by the occurrence of halite crystals and anomalies in geochemical proxies (paleosalinity and paleoclimate). In this case, the intensification of aridity concomitant with the reduction in the depth of the lake system evinces that this taxon was susceptible to paleoenvironmental alterations (reduction in organism size and failure to reach larval maturity), which resulted in the mortality of these organisms in the Crato paleolake (Bezerra, Mendes, 2024; Chadwick *et al.*, 2002; Martins-Neto, 2006; Storari *et al.*, 2021). *Dastilbe* distribution did not suggest mass mortality; instead, it exhibited the presence of smaller fish—up to 5 cm in length—when compared to *Dastilbe* in the upper layer, which reached up to 21 cm in length (Storari *et al.*, 2021). This suggests that *Dastilbe* can tolerate the harsh conditions of the

paleoenvironment despite the hypersalinity of the lacustrine system (Davis, Martill, 1999).

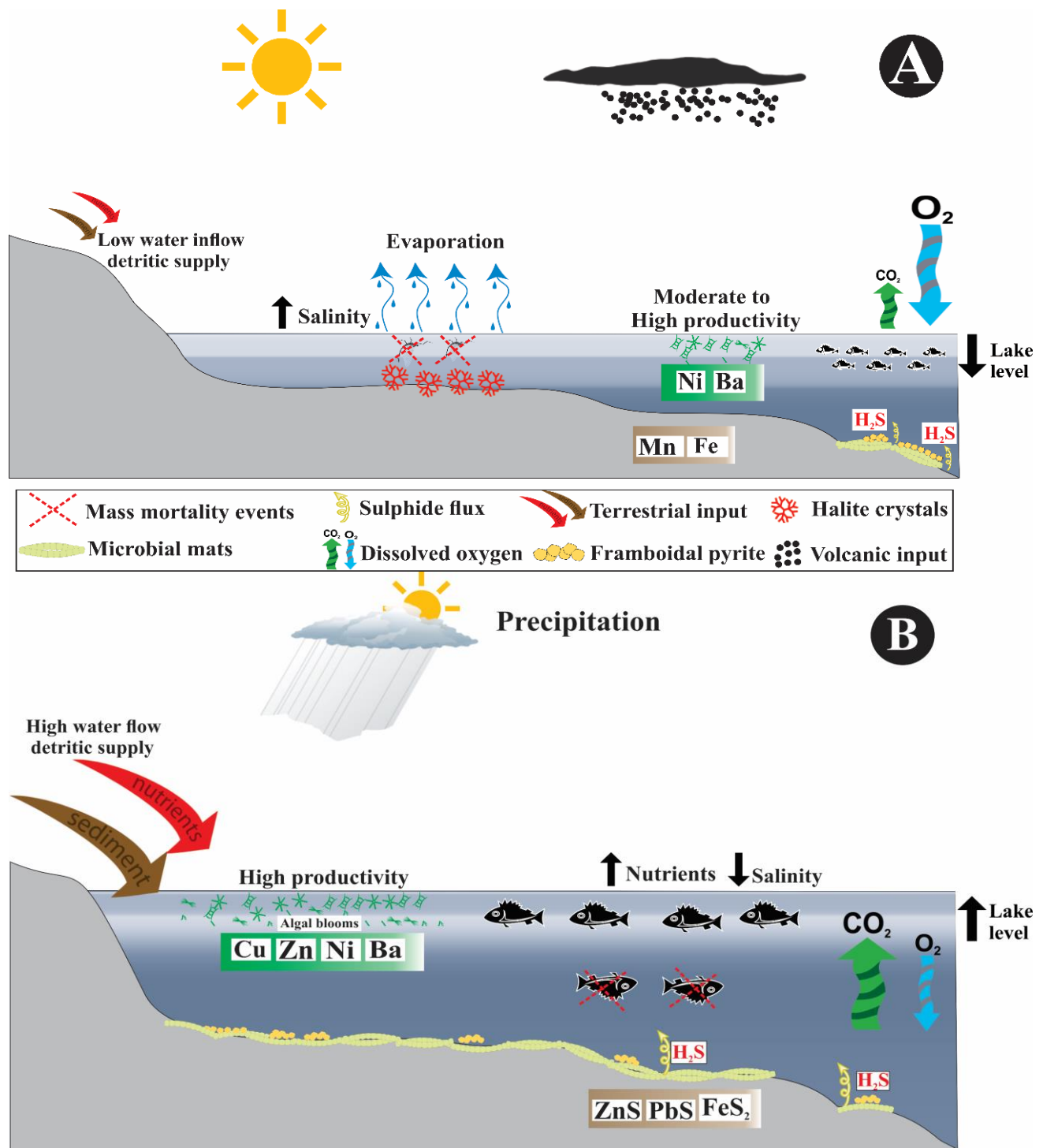
The occurrence of Hg anomalies in the 285 cm and the geochemical correlations previously characterized for the Crato paleolake the observation of a possible interference of magmatic pulses in the mass mortality of Ephemeroptera. Volcanism is an important driver of climate change and major biological crises, the increase in greenhouse gas emissions into the atmosphere modifies the hydrological cycle (Font, Bond, 2021; Zhou *et al.*, 2024). The elevation in pCO<sub>2</sub> brought about by volcanism gives rise to a chain of events in the interior of the continent. These events include an increased rate of evapotranspiration, a decline in soil moisture, and the occurrence of convective transpiration, frequent paleo-wildfires, an elevated salinity, and, consequently, a widespread aridity (Bos *et al.*, 2023; Liu *et al.*, 2024; Peyser, Poulsen, 2008; Zhang *et al.*, 2023). Consequently, the volcanism of the Rajmahal-Kerguelen plateau may have indirectly caused the mass mortality of the Ephemeroptera in the Crato paleolake through the intensification of aridity, the reduction in depth and the salinization of the lacustrine system (Figure 18A).

Towards the top of the CKL level, nine mass mortality events of *Dastilbe* were recorded, suggesting the existence of greater cyclical mortality events of these fish. The characterization of the ontogenetic stages of *Dastilbe* permitted the establishment that adults were more mobile than juveniles (Storari *et al.*, 2021). Juveniles, in contrast, feed on plankton and inhabit lake systems, being more susceptible to mortality events (Davis, Martill, 1999; Ribeiro *et al.*, 2020). Storari *et al.* (2021) observed that the *Dastilbe* identified were primarily juveniles. This evidence indicates that these organisms were susceptible to the paleoenvironmental fluctuations that occurred within the Crato paleolake.

An increase in the enrichment factor of the geochemical proxies for paleoproductivity, paleoredox, and a decrease of paleoclimatic proxy (Sr/Cu) has been observed in the layers where mass mortality events of *Dastilbe* have been identified. Previous studies reported that the *Dastilbe* mortality horizons were highly productive (Davis, Martill, 1999; Martins-Neto, 2006). Considering the mechanisms responsible for the high productivity in the Crato paleolake, it can be suggested that inputs derived from proximal (detrital inputs) and distal (volcanism) sources may have contributed to the supply of nutrients and other chemical compounds for the lacustrine system.

During periods of elevated precipitation and volcanic activity at the Rajmahal-Kerguelen plateaus, there was an influx of nutrients into the Crato paleolake, which led to an intensification of primary productivity. Consequently, eutrophication of the lake ecosystem occurred, resulting in an increase in organic matter at the lake system. Consequently, bacterial decomposition of organic matter resulted in the depletion of oxygen in the water column (hypoxia), and in the cyclic mortality events of the *Dastilbe* fish population in the lake system (Figure 18B). The presence of cyanobacteria and green sulfur bacteria (Chlorobiaceae) in the Crato paleolake corroborates the hypothesis that it as a stratified productive lacustrine system, with the bottom waters saturated with little hydrogen sulfide and low oxygen (Catto *et al.*, 2016; Heimhofer, Martill, 2007).

**Figure 18.** Scheme demonstrating the paleoenvironmental variations (wet-dry) of the Konservat -Laggerstätte of the Crato paleolake. A) Arid paleoclimatic conditions and mortality of Ephemeroptera; B) Humid paleoclimatic conditions and mortality of *Dastilbe* sp.



#### **6.4.6 Exceptional fossil preservation in the Crato paleolake**

The evolution of Konservat-Lagerstätten is contingent on the exceptional condition of their fossils (presence of soft tissues and articulated organisms) (Allison, 1988; Parry *et al.*, 2018). The condition of fossils preservation is influenced by the type of mineralization (silicification, phosphatization, pyritization, aluminosilification, carbonate preservation) and the depositional conditions of the paleoenvironment (anaerobic, euxinic conditions, rapid burial, microbial activity, minerals precipitation, and early diagenesis) (Grice *et al.*, 2019).

The Konservat-Lagerstätte of the Crato paleolake generated by favorable depositional conditions conducive to preserving the lacustrine system. The high concentrations of microframbooidal pyrites and phosphorus in the fossils indicate that mineralization of soft tissues occurred during early diagenesis, through sulfate-mediated bacterial reduction (Barling *et al.*, 2015; Barling, Martill, Heads, 2020).

The production of frambooidal pyrites requires high concentrations of iron, organic carbon, and sulfate, which allows sulfides to be fixed during the mineralization of the organisms (Allison, 1988). Nevertheless, the Crato Formation is predominantly composed of limestone sediments, which implies low concentrations of iron, thus limiting the formation of frambooidal pyrite (Berner, 1984; Osés *et al.*, 2017). In this context, it is essential to acknowledge the potential contribution of allochthonous sources, including proximal and distal sources, to the increase in iron and other element concentrations in the Konservat- Lagerstätte of the Crato paleolake. Then, periods of elevated humidity may have facilitated enhanced iron transport to the lacustrine system. This, in turn, has led to the development of bacterial reduction of sulfate and, subsequently, the generation of frambooidal pyrites (Osés *et al.*, 2016, 2017).

Moreover, the Hg anomalies recorded in the Crato paleolake indicate that distal (volcanic) contributions may have assisted in the preservation and formation of the Konservat-Lagerstätten of the Crato paleolake. Additionally, other Konservat-Lagerstätten- Romualdo Formation (Araripe basin, Brazil, early Cretaceous), and Fernie and Jehol Formation (Chaoyan basin, early Cretaceous, China); Fernie Formation (Canada), Posidonia shale (Germany), and Strawberry bank (United Kingdom), all in the Lower Jurassic - demonstrated the potential of volcanism to generate fossil preservation (Bom *et al.*, 2023; Cai *et al.*, 2023; Muscente *et al.*, 2019; Sinha *et al.*, 2021).

## **6.5 Conclusion**

The Konservat-Lagerstätte Crato paleolake exhibited considerable fluctuations in the water cycle, which resulted in pronounced alterations in paleodetritic input, salinity, depth, oxygenation, and productivity. The Hg anomalies observed in the lake system indicated a potential interference of the volcanic pulses from the Rajmahal-Kerguelen plateaus on the paleoclimate conditions of the lake ecosystem. The increase in CO<sub>2</sub> emissions into the atmosphere may have intensified aridity in the Araripe basin, thereby generating changes in the depositional process in the Crato paleolake.

Paleoclimatic alternations (wet-dry cycles) had a hostile impact on the resilience capacity of organisms, resulting in cyclical mortality events that have been recorded in the Crato paleolake. The mortality of Ephemeroptera was influenced by the aridity of the lake system, which became hypersaline, and the lake system became saline and alkaline, which impeded larval development and the maturation of the larvae of these organisms. Nevertheless, it has been demonstrated that *Dastilbe* displays tolerances to elevated salinity levels. The enrichment of paleoproductivity and redox proxies observed in *Dastilbe* mortality levels indicates that intensification of the biological pump in the lake system generates conducive conditions for bacterial activity. In this case, the occurrence of hypoxia in the Konservat-Lagerstätten of the Crato paleolake was found to be responsible for the observed mortality events in *Dastilbe*.

## **Acknowledgments**

The authors are deeply indebted to the many students at the Regional University of Cariri, who have helped in the intensive field campaigns in the Araripe Basin. Technicians from the Marine Biogeochemistry Laboratory (LBC-UFC) helped preparing samples for chemical analyses. Technicians from the NABISE-UFPE, for isotopes analysis.

## **Funding**

This study was funded by the Fundação Cearense de Apoio ao Desenvolvimento Científico e Tecnológico (FUNCAP), Proc. No. INT-0159-00009.01.00/19, and by grants to L.D. Lacerda from the Brazilian Council for Scientific and Technological Development (CNPq), Proc. No. 405.765/2022-3 (INCTTMC-Ocean). This study was financed in part by the Coordenação de Aperfeiçoamento de Pessoal de Nível Superior- Brasil (CAPES)-Finance code 001.

## CAPÍTULO 3

### **Insights into the palaeo-trophic food web of the Brazilian Romualdo Formation (Cretaceous, Aptian–Albian) based on fossil mercury bioaccumulation**

O terceiro manuscrito é uma participação no artigo intitulado “*Insights into the palaeo-trophic food web of the Brazilian Romualdo Formation (Cretaceous, Aptian–Albian) based on fossil mercury bioaccumulation*”, com autorias de Lucas Silveira Antonietto, Igor Hamid Ribeiro Azevedo, Borja Holgado, Antonio Leite Rocha, Maria A. Ferreira, Antônio Álamo Feitosa Saraiva, Luiz Drude de Lacerda.

Este manuscrito tem o objetivo de caracterizar a cadeia paleotrófica do *Konservatt Lagerstätte* da Formação Romualdo através da aplicação do Hg. Este trabalho possibilitou demonstrar o desenvolvimento da cadeia paleotrófica da paleoictiofauna da Formação Romualdo, sendo possível estabelecer os organismos representantes da base- *Rhacolepis buccalis*- até os maiores níveis tróficos- *Calamopleurus cylindricus*. Além disso, pode-se inferir sobre o comportamento alimentar dos pterossauros (Ornithocheiriformes and Thalassodrominae), organismos de grande debate na comunidade científica a respeito da sua capacidade de predação.

---

Antonietto, L. C.; Azevedo, I. H. R.; Borja, H.; Rocha, A. L.; Ferreira, M. A.; Saraiva, A. A. F.; Lacerda, L. D. Insights into the palaeo-trophic food web of the Brazilian Romualdo Formation (Cretaceous, Aptian–Albian) based on fossil mercury bioaccumulation. In revision to Nature Communications.

## ABSTRACT

In aquatic environments, mercury (Hg) bioaccumulation rates tend to reflect the organism's position in the food web – the larger the rate, the higher their position. Here we present the first attempt to reconstruct such web for the Romualdo Formation of the Araripe Basin (Northeastern Brazil), based on Hg bioaccumulation of its fossil record; the aim is to understand possible trophic relationships between vertebrate/invertebrate species inhabiting its paleoenvironments. Observed ratios between Hg concentrations [Hg] in fossils and their surrounding concretions ([Hg]<sub>sample</sub>) suggest bioaccumulation increases with the change in feeding habits and size of the fish taxa analysed, being lowest in *Rhacolepis* to a maximum peak in the large predator genera *Cladocyclus* and *Calamopleurus*. Feeding habits of *Vinctifer* were also reviewed, and the genus was reinterpreted from filter feeder to mesopredator; durophage bottom-feeding taxa recorded values compatible with their predicted feeding habits. Low [Hg]<sub>sample</sub> ratios were observed in ornithocheiriform pterosaurs, suggesting mesopredators specialized in the smaller fish species, while Thalassodrominae presented intermediate to high [Hg]<sub>sample</sub>, pointing out to a unique trophic role as a terrestrial opportunistic generalist, ranging from predator to scavenger.

## 7.1 Introduction

Mercury (Hg) is a chemical element widely distributed through different compartments of the biosphere, because of major emission being to the atmosphere through volcanism and forest fires (Beckers, Rinklebe, 2017). Volcanism emits Hg in its elementary form ( $\text{Hg}^0$ ), which undergoes oxidation in the atmosphere generating  $\text{Hg}^{2+}$  (reactive ionic form, soluble in water). Subsequently,  $\text{Hg}^{2+}$  is incorporated into aquatic ecosystems, forming stable organic complexes, and/or precipitating into sulphides in bottom sediments (Beckers, Rinklebe, 2017; Gamboa Ruiz, Tomiyasu, 2015). The Hg can undergo methylation mediated by sulphate-reducing bacteria, generating monomethyl- ( $[\text{CH}_3\text{Hg}]^+$ ) and dimethylmercury ( $[\text{CH}_3]_2\text{Hg}$ ) – both bioavailable forms of Hg (Outridge *et al.*, 2002). High bioaccumulation and biomagnification rates of Hg increase Hg concentrations ([Hg]) in organisms, amplified through the trophic web highest levels concentrations in top carnivores.

Bioaccumulated Hg can be preserved in mineralized tissues (hydroxyapatite, calcite, and aragonite) of fossil and subfossil specimens from different geological periods. That allows for a wide range of ecological and paleoecological studies-based [Hg], ranging from the relation between mammal teeth Hg increase and the onset of the Industrial Revolution, or [Hg] peaks in Pacific Cod (*Gadus microcephalus*) and Holocene glaciations (Murray *et al.*, 2015), to the ontogeny of Late Cretaceous baurusuchid crocodyliforms from Brazil (Cardia *et al.*, 2018). Therefore, Hg can become an excellent tool to assess trophic relations in both recent and fossil assemblages.

The assessment of [Hg] is also favored by exceptional fossil preservation, as observed in the Konservat-Lagerstätte of the Romualdo Formation of Brazil. This unit is the result of a regional-scale late Aptian-early Albian (Araripe *et al.*, 2022) transgression set during the earliest stages of the opening of the South Atlantic Ocean; it then reached many interior regions of northeastern Brazil including areas where the Araripe Basin is presently recorded (Figure 19) (Custódio *et al.*, 2017). The 120 m-thick succession (Assine, 2007) comprises organic-rich black shales deposited under great saline variation (Fürsich *et al.*, 2019), and anoxic to dysoxic conditions related to the Oceanic Anoxia Event (OAE) 1b (Bom *et al.*, 2023; Hamid *et al.*, 2024). Such conditions resulted in the deposition throughout the unit of stratigraphic horizons abundant in carbonate concretions, some of them yielding finely preserved plant, vertebrate (mostly fish), ostracod (Fara *et al.*, 2005) and insect fossils (Freitas, Moura, Saraiva, 2016).

Romualdo concretions preserve not only hard parts but also soft ones (Maldanis *et al.*, 2016), while at the same time protecting these records from composition-altering effects from diagenesis (Heimhofer *et al.*, 2017). This excellent fossil preservation, especially of the ichthyofauna, has already resulted in studies of trophic relations of the Romualdo assemblage, either through dietary analysis of stomach contents (Maisey, 1994) and/or tooth morphology assessment (Lopes, Barreto, 2021). They are also abundant: numerous specimens are available for research at scientific collections of Brazilian institutions such as the *Museu de Paleontologia Plácido Cidade Nuvens* (MPPCN), the *Laboratório de Paleontologia da URCA* (LPU) and the *Museu de Ciências Naturais e História de Barra do Jardim* (MCNHB) (Coutinho *et al.*, 2021). The present study is an attempt to contribute, through [Hg] analyses, to the reconstruction of the trophic relations between part of the highly diverse fossil assemblage of the Romualdo Formation; we emphasize analyses of its paleoichthyofauna, due to the amount and variability of taxa preserved, while results on pterosaur taxa are considered preliminary, although relevant for its relations with fish species that might have been (or not) part of their diet.

**Figure 19.** Map of the Araripe Basin, northeastern Brazil, highlighting the geographic distribution of the Santana Group (including the Romualdo Formation).



## 7.2 Methodology

Romualdo fossils utilized in the present work came from the scientific collections of the *Museu de Paleontologia Plácido Cidade Nuvens* (MPPCN) at the municipality of

Santana do Cariri, as well as the *Laboratório de Paleontologia da URCA* (LPU) at Crato and the *Museu de Ciências Naturais e História de Barra do Jardim* (MCNHB) at Jardim; all these cities are in the Cariri Valley, southernmost region of the State of Ceará, Brazil. Specimens belonging to the MPPCN and housed either at the MPPCN or the LPU were done so under codes “MPPCN P” (for fish) and “MPPCN R” (for reptiles) and respective numeration; materials from the MCNHB are coded with “MCNHB”, followed by their number (Coutinho *et al.*, 2021). Taxa evaluated herein were chosen based on both their large availability and presumed role in the Romualdo paleo-trophic web, considering 25 organisms (Lopes, Barreto, 2021): *Rhacolepis buccalis* (n= 5), *Vinctifer comptoni* (n= 5), *Cladocyclus gardneri* (n= 3), *Calamopleurus cylindricus* (n= 3), *Tharrhias araripis* (n= 2) and *Neoproscinetes penalvai* (Actinopterygii) (n= 2) and unidentified species of Batoidea (Chondrichthyes, n= 2), Ornithocheiriformes and Thalassodrominae (Pterosauria, n= 3), along with an unidentified ornithocheiroïd specimen, were included.

Museum specimens were first processed in the LPU, where parts of them, approximately 7 cm<sup>3</sup>, in volume were sawed off with a Makita M0400B circular saw. Resulting slabs were sent as separate samples to the Marine Science Institute (Labomar) of the Federal University of Ceará at Fortaleza, Brazil, for analysis of mercury (Hg) content. The following steps present some modifications in relation to previously published Hg concentration ([Hg]) analyses (Benigno *et al.*, 2021; Hamid *et al.*, 2024); after separating the fossil from its carbonate concretion, either were slowly ground into powder with mortar and pistil, homogenized and sealed in hermetically closed flasks. Further digestion was carried out by initially placing 1 g of each sample fraction (concretion and fossil) in polytetrafluoroethylene (Teflon<sup>TM</sup>) tubes containing 10 mL of concentrated (65%) nitric acid (HNO<sub>3</sub>) for 1 h. These were then placed in a CEM MARSXpress vessel and heated at 175 °C for 20 min in a 1,600 W MARS 240/50 synthesis microwave oven. Once heated, we transferred the resulting extracts to volumetric flasks (previously bathed in Extran® 300 [Merck] detergent at 10%, for 24 h, then latter in hydrochloric acid at 10% for another 24 h), and the volume of each extract was adjusted to 100 mL volume with Milli-Q® water. Four additional blank tubes were prepared specifically to evaluate Hg contamination in the HNO<sub>3</sub> reagent used during digestion.

Quantification was carried out in a NIC RA-3 (Nippon®) cold vapor generation atomic absorption spectrometer (CVV-AAS), coupled with an RD-3 dispenser. Each sample was quantified twice, showing reproducibility within 4.6%. The precision and

accuracy of fossil results was controlled by simultaneous quantification of a reference material (NIST-1646A Estuarine Sediments), to which the average recovery was  $98 \pm 8\%$  ( $n = 12$ ). The linearity coefficient of the calibration of curves ( $R^2$ ) was  $0.9998 \pm 0.0001$ ; limits of quantification and detection (calculated as three times the standard deviation of the reagent blank, divided by the slope of the calibration curve) were, respectively,  $0.02 \pm 0.02 \text{ ng} \times \text{g}^{-1}$  and  $0.08 \pm 0.07 \text{ ng g}^{-1}$ . Measurements were taken both in fossils and the calcite matrix of their surrounding concretions; because environmental factors can dramatically enhance [Hg] in living individuals, we used [Hg] in concretions ( $[\text{Hg}]_{\text{Rock}}$ ) as a normalizer for environmental effect over [Hg] in fossils ( $[\text{Hg}]_{\text{Fossil}}$ ), applying the following ratio (Fang *et al.*, 2017) to quantify bioaccumulation ( $[\text{Hg}]_{\text{Sample}}$ ):

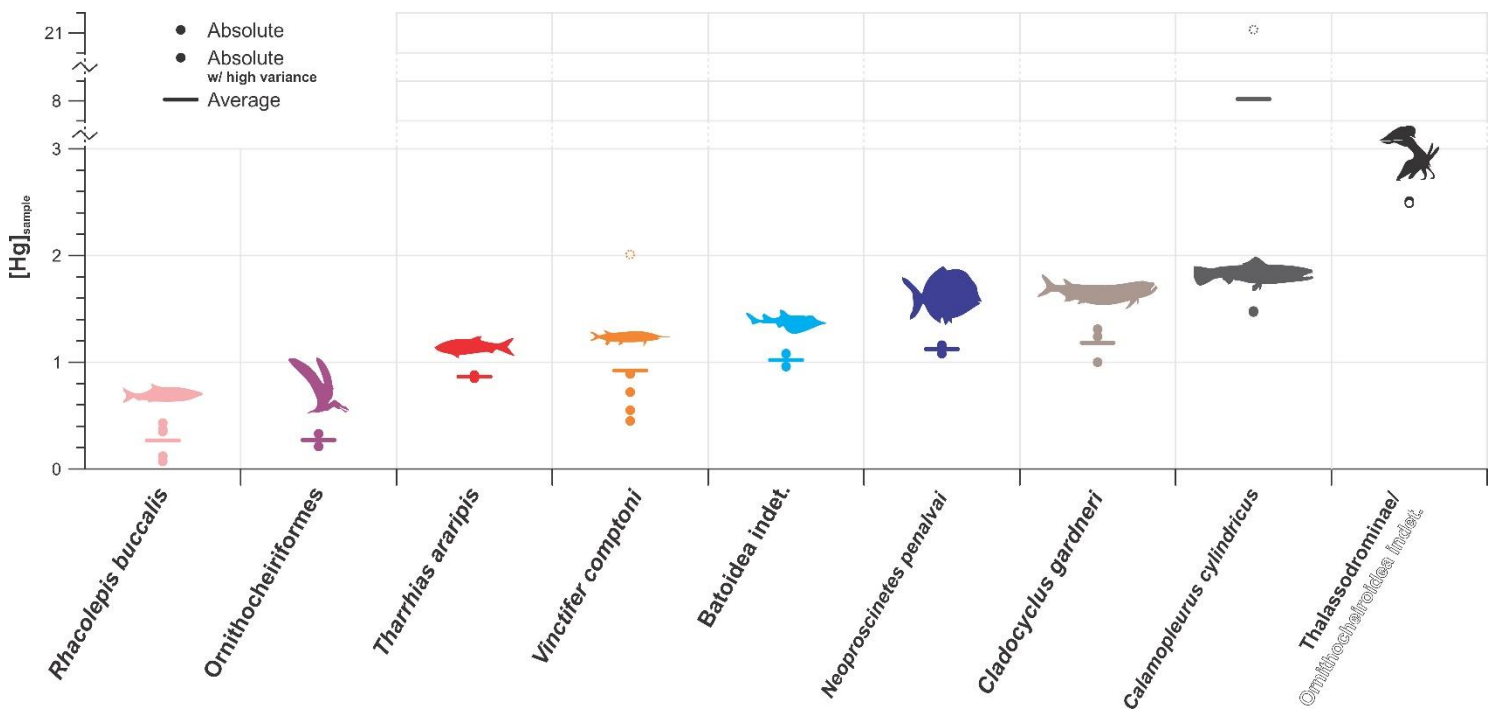
$$[\text{Hg}]_{\text{Sample}} = [\text{Hg}]_{\text{Fossil}} / [\text{Hg}]_{\text{Rock}}$$

This procedure removes interference from nearby sources of sedimentation, while also compensating for the potential diagenetic effect over biochemical compounds (carbonates, silica, phosphorite and organic matter in general) (Soua *et al.*, 2011; Touati, Haji, 2019).

### 7.3 Trophic relations between fish species

Absolute  $[\text{Hg}]_{\text{Fossil}}$  and  $[\text{Hg}]_{\text{Rock}}$ , as well as  $[\text{Hg}]_{\text{Sample}}$  values, are presented in Table 1, while  $[\text{Hg}]_{\text{Sample}}$  averages are summarized in Figure 20. The lower the trophic level of Romualdo taxa (represented by smaller species with villiform dentition) (Lopes e Barreto, 2021), presented the lower ( $< 1.00$ )  $[\text{Hg}]_{\text{sample}}$ , respectively: *R. buccalis* (0.27); *T. araripis* (0.87) and *V. comptoni* (0.92). The position of *V. comptoni* in the Romualdo food web is still dubious. It was inferred as a predatory species that fed on small fish, based on stomach content analysis of some specimens (Coutinho *et al.*, 2021; Wilby e Martill, 1992) –although there are no published images detailing this record. Similar studies (Maisey, 1994), on the other hand, found no small fish fragments while performing stomach content analysis, and linked *V. comptoni*'s reduced dentition and well-developed gill apparatus to morphologies observed in recent filter-feeding taxa, such as paddlefishes (genus *Polyodon*).

**Figure 20.** Average results of (Hg)sample in fossil taxa of the Romualdo Formation analyzed in the present work.



The observed average  $[Hg]_{sample}$  in *V. comptoni* is higher than those observed in the lower trophic levels represented by *R. buccalis* and *T. araripis*, indicating piscivore feeding habits based in consumption of the latter taxa – and possibly even smaller ones, such as *Santanichthys diasii* (Santos, 1995). However, it is important to note that these ratios show large variability per specimen (0.45–2.01), compared to other fish species currently analysed – possible evidence of foraging variation that could either be tied to geographical (Azad *et al.*, 2019) and/or ontogenetic factors (Beneditto *et al.*, 2013). Thus, this broad range of  $[Hg]_{sample}$  values in *V. comptoni* might be caused either by occupying different ecological niches through life, or simply presenting less Hg accumulation at a different ontogenetic stage at time of death.

With the increase in trophic level (transition from villiform to molariform dentition, and from the latter to conical teeth, accompanied by increase in overall size of species),  $[Hg]_{sample}$  becomes higher, indicating shifts to higher levels of the trophic web. Molariform, mid-tying level species interpreted as durophagous taxa, which fed on larger, opportunistic invertebrates (Lopes, Barreto, 2021), presented  $[Hg]_{sample}$  of ~1.00, as in *Batoidea indet.* (1.02) and *N. penalvai* (1.12). Values of  $[Hg]_{sample}$  around 1.00 were also found in individuals of *Cl. gardneri*, along with others up to 1.31, which is expected for upper ties of the trophic web, occupied by the largest fish taxa, with conical dentition, of

the Araripe. The highest  $[Hg]_{sample}$  (1.52–21.08) are observed in specimens of *Ca. cylindricus*; these might have acted as apex predators in the aquatic environments of the Romualdo, being able to feed on whatever fit into their mouths – including delving into cannibalism (Mulder, 2013).

## 7.4 The role of pterosaurs as mesopredators and opportunists

As in *V. comptoni* and *C. cylindricus*,  $[Hg]_{samples}$  in pterosaurs varied greatly between specimens. Specimens attributed to the Ornithocheiriformes showed very low  $[Hg]_{sample}$  (0.27 and 0.30), but slightly higher, in average, than those observed for *R. buccalis*. Representatives of this clade were commonly interpreted as highly capable piscivores, based on dental morphology and geochemistry, as well as digestive tract content (Bestwick *et al.*, 2018). However, the low bioaccumulation ratios observed in the present specimens suggest a foraging habit typical of mesopredators specialized in small epipelagic species of the Romualdo fish fauna, such as *R. buccalis* and *S. diasii*, or even in smaller, plankton-feeding invertebrates (Lopes, Barreto, 2021; Maisey, 1994). The presence of an air-sac system inferred from an extremely extended skeletal pneumaticity in ornithocheiriforms also indicates they used to plunge after their prey like modern pelicans (Shoop, Tilson, 2022).

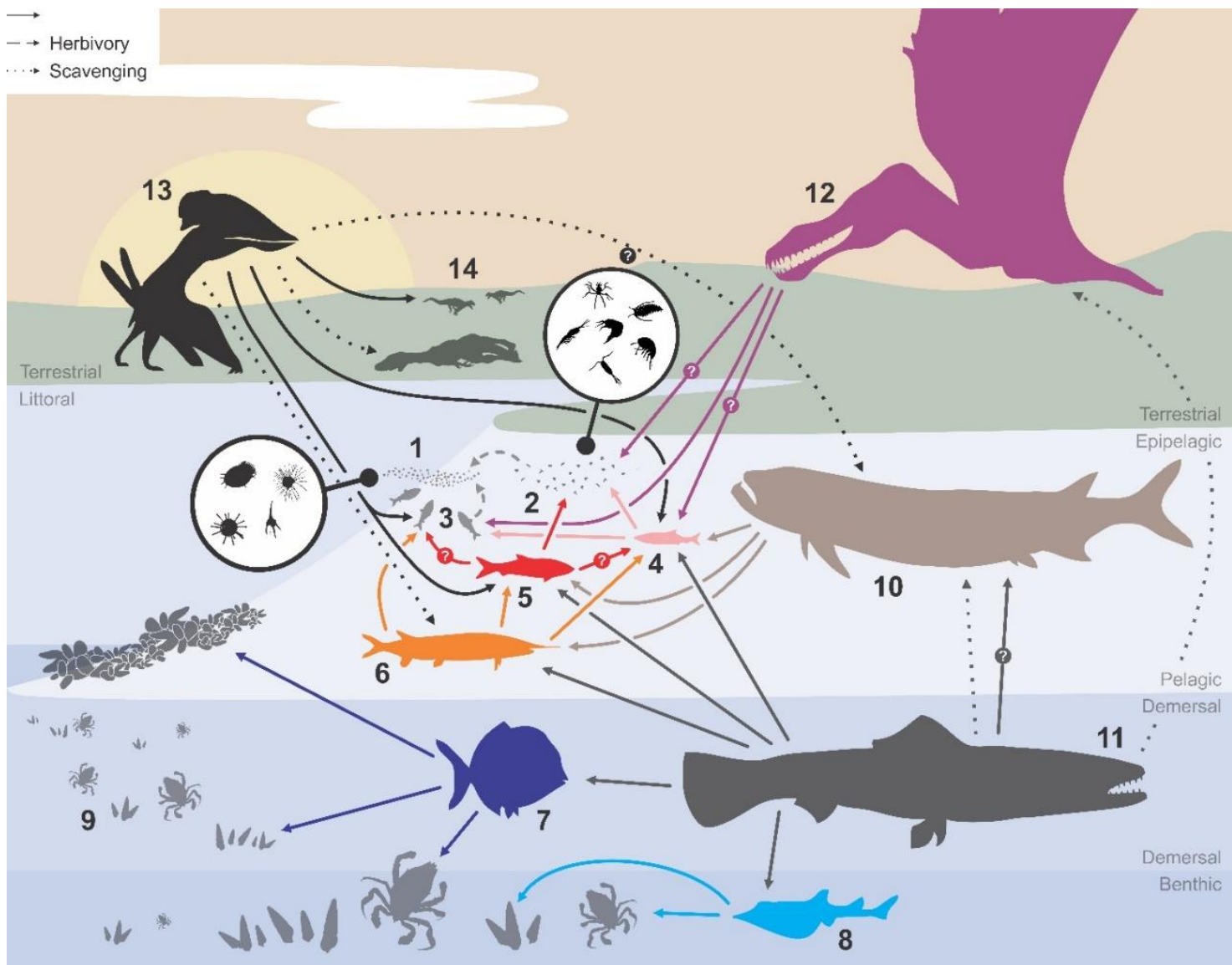
Regarding the only examined specimen of Thalassodrominae, the  $[Hg]_{sample}$  of the specimen is significantly higher (2.6) than in ornithocheiriforms. It is important, however, to highlight the possible role of vital effect in the present results, as the number of sampled specimens is very small (the observed value, nonetheless, is identical to that found in the indeterminate ornithocheiroïd). Thalassodromines were first suggested as piscivores with skim-feeding habits, but posterior studies proposed they were terrestrially foraging opportunists, because of the robust hind limbs observed in some thalassodromine specimens (Pêgas, Costa, Kellner, 2021; Witton, Witton, 2013). Present  $[Hg]_{sample}$  results strengthen the opportunistic diet hypothesis, since higher ratios would be attainable only by a combination of varied predatory (small to mid-size prey) and scavenging behaviours, as already suggested for all known thalassodromine taxa so far (Pêgas, Costa, Kellner, 2021).

## 7.5 An integrative analysis of the Romualdo vertebrate assemblage

Present inferences based on  $[Hg]$  quantified in vertebrate species of the Aptian–

Albian Romualdo Formation help reconstruct trophic relationships occurring in paleoenvironments of the Brazilian Romualdo Formation (Figure 21). Bioaccumulation ratios increased along specific chains of the Romualdo food web based on taxon size and diet, as observed from small, filiform-toothed fish specialized in smaller prey, to, large, conical-toothed fish which fed on the former. In such a scenario, bioaccumulation ratios of *V. comptoni* favour an interpretation of its feeding habits as of a predatory species, despite the absence of conical teeth. Low bioaccumulation ratios observed in ornithocheiriform pterosaurs indicate they were also part of the studied trophic web, acting as mesopredators specialized in the smaller fish species observed in the Romualdo. Molariform fish taxa fell slightly apart in the food web, as they probably tended to consume typically filtering bottom invertebrates, but at the same time might have been consumed by *C. cylindricus* – the apex predator of Romualdo aquatic paleoenvironments (and probably a scavenger as well). Meanwhile, the Thalassodrominae presented intermediate to high [Hg] samples that put them in a more separate trophic role compared to aquatic and water-dependent species, as a terrestrial generalist that not only predated small terrestrial taxa but could also have engaged in scavenging of both terrestrial and aquatic taxa inhabiting the Romualdo paleoenvironments. However, further investigation is required to comprehend the behavioural characteristics of the Thalassodrominae. The availability of a larger number of specimens would facilitate the elucidation of both the ontogenetic behaviour of these organisms as well as their feeding habits.

**Figure 21.** A summary of the Romualdo Formation trophic web based on literature and present Hg<sub>sample</sub> results, including the following groups or taxa: 1) Phytoplankton; 2) Zooplankton; 3) *Santanichthys diasii*; 4) *Rhacolepis buccalis*; 5) *Tharrhias araripis*; 6) *Vinctifer comptoni*; 7) *Neoproscoptenes penalvai*; 8) Batoidea indet.; 9) Benthic invertebrates; 10) *Cladocyclus gardneri*; 11) *Calamopleurus cylindricus*; 12) Ornithocheiriformes; and 13) Thalassodrominae; and 14) Other terrestrial Tetrapoda.



## Funding

The authors acknowledge FUNCAP (PV1-0187-00042.01.00/21 to LSA; PV1-0187-00054.01.00/21 to BH; BP5-0197-00172.01.02/23 to ALR). This study was financed in part by the Coordenação de Aperfeiçoamento de Pessoal de Nível Superior- Brasil (CAPES)- Finance code 001. We are also indebted to the MCNHBJ staff (DLC Coutinho, JA Coutinho Júnior and CC Coutinho) for all the support providing fossil specimens for analyses in the present work.

## 8. Considerações finais

Compreender o processo de formação, incluindo as diversas crises biológicas envolvidas da Bacia do Araripe, oportuniza conhecer as condições pretéritas do planeta, sendo possível estabelecer relações com o comportamento atual da vida e das transformações dos ambientes naturais. Estudos anteriores demonstraram uma grande variedade dos registros fossilíferos (fauna e flora) e estratigráficos na Bacia do Araripe, demonstrando grande heterogeneidade dos paleoambientes durante o seu desenvolvimento. Essas mudanças também foram refletidas no Quimioestratigrafia da Bacia do Araripe, sendo possível estabelecer mudanças climáticas, na paleoprodutividade, estado redox, salinidade e eventos cíclicos de mortalidade.

A Quimioestratigrafia da Bacia do Araripe demonstrou a presença de anomalias de Hg, indicando a influência das Grandes Províncias Ígneas (LIPs) na deposição desta bacia sedimentar. Considerando a idade bioestratigráfica, foi possível estabelecer uma correlação com os vulcanismos dos platôs Ontong- Java (OJP, ~120 Ma) e o Rajmahal-Kerguelen Sul (SKP, ~113 Ma). Como resultado do magmatismo dessas LIPs observou-se a intensificação da produtividade primária, o maior soterramento do carbono e metais-traço e o desenvolvimento da anoxia nos ecossistemas aquáticos. Dentro desse contexto, foi possível estabelecer o impacto dos Eventos Anóxicos Oceânicos (OAE 1a e 1b) nas formações Barbalha e Romualdo, respectivamente. Além disso, constatou-se que os eventos magmáticos foram responsáveis por mudanças paleoambientais no sistema deposicional, influenciado pelas mudanças da salinidade, umidade, paleoprodutividade e estado paleoredox.

Como resultado das grandes mudanças paleoclimáticas globais, houve um impacto direto nas condições paleoambientais, podendo ter sido este o fator principal para os eventos de mortalidade cíclicos encontrados no *Konservat-Lagerstätte* do paleolago Crato. A partir da química das rochas foi possível estabelecer que a alternância dos períodos úmidos-secos e da baixa oxigenação das águas desse sistema lacustre ocasionaram a mortandade dos *Dastilbe sp.* e Ephemeropteras. Entretanto, são necessários mais estudos voltados para a entender as variações de salinidade e clima no sistema lacustre. Além disso, será importante estabelecer uma correlação quimioestratigráfica com outras bacias sedimentares para entender o desenvolvimento dos sistemas lacustres carbonáticos do Aptiano. Vale destacar que o estabelecimento da geoquímica isotópica forense ( $\delta^{13}\text{C}_{\text{VPDB}}$  e  $\delta^{18}\text{O}_{\text{VPDB}}$ ) dessas bacias sedimentares podem

auxiliar a entender as diferenças deposicionais entre dos sistemas lacustres carbonáticos, vir a reduzir impacto do tráfico de fósseis, proteger a geodiversidade e o patrimônio paleontológico do Brasil.

Considerando o desenvolvimento da pesquisa a respeito da química dos fósseis da Bacia do Araripe, observou-se que através da determinação das concentrações do Hg nos fósseis e nas concreções calcárias possível estabelecer o desenvolvimento da cadeia trófica no *Konservat-Lagerstätte* da Formação Romualdo. Este ambiente é caracterizado por apresentar grande biodiversidade da paleoictiofauna e pterossauros. Neste caso, observou-se a evolução dos níveis tróficos de acordo com o aumento dos valores das razões do Hg (fóssil/rocha), demonstrando que o Hg possui uma grande aplicabilidade. Futuros estudos voltados para a uma integração entre as análises de morfometria, osteohistológicos e geoquímicos ( $\delta^{13}\text{C}_{\text{VPDB}}$ ,  $\delta^{18}\text{O}_{\text{VPDB}}$  e Hg) podem auxiliar no estabelecimento da cadeia trófica dos *Konservat-Lagerstätten* globais e na compreensão do comportamento dos vertebrados do passado.

## REFERÊNCIAS

- ABU-ALI, R.; EL-KAMMAR, A.; KUSS, J. Chemostratigraphy of the Upper Cretaceous-Paleogene organic-rich succession on the southern Tethys margin in Egypt. **Journal of African Earth Sciences**, v. 164, 2020.
- ADLOFF, M.; GREENE, S. E.; PARKINSON, I. J.; NAAFS, B. D. A.; PRESTON, W.; RIDGWELL, A.; LUNT, D. J.; CASTRO JIMÉNEZ, J. M.; MONTEIRO, F. M. Unravelling the sources of carbon emissions at the onset of Oceanic Anoxic Event (OAE) 1a. **Earth and Planetary Science Letters**, v. 530, p. 115947, 2020.
- AI, Y.; ZHU, G.; LI, T.; ZHU, Z. Copper and Zinc isotopes trace the evolution of the Ediacara-Early Cambrian paleo-ocean redox condition in the Tarim Basin, China. **Applied Geochemistry**, v. 150, 2023.
- ALGEO, T. J.; LI, C. Redox classification, and calibration of redox thresholds in sedimentary systems. **Geochimica et Cosmochimica Acta**, v. 287, p. 8–26, 2020.
- ALGEO, T. J.; LIU, J. A re-assessment of elemental proxies for paleoredox analysis. **Chemical Geology**, v. 540, 2020.
- ALGEO, T. J.; MAYNARD, J. B. Trace-element behavior, and redox facies in core shales of Upper Pennsylvanian Kansas-type cyclothsems. **Chemical Geology**, v. 206, n. 3–4, p. 289–318, 2004.
- ALKMIM, F. F. Geological Background: A Tectonic Panorama of Brazil. *Em: World Geomorphological Landscapes*, p. 9–17, Springer, 2015.
- ALLISON, P. A. Konservat-Lagerstätten: cause and classification. **Paleobiology**, v. 14, n. 4, p. 331–344, 1988.
- ALVAREZ, L. W.; ALVAREZ, W.; ASARO, F.; MICHEL, H. V. Extraterrestrial Cause for the Cretaceous-Tertiary Extinction. **Science**, v. 208, n. 4448, p. 1095–1108, 1980.
- ARAI, M. Aptian/Albian (Early Cretaceous) paleogeography of the South Atlantic: a paleontological perspective. **Brazilian Journal of Geology**, v. 44, n. 2, p. 339–350, 2014.
- ARAI, M.; ASSINE, M. L. Chronostratigraphic constraints and paleoenvironmental interpretation of the Romualdo Formation (Santana Group, Araripe Basin, Northeastern Brazil) based on palynology. **Cretaceous Research**, v. 116, p. 104610, 2020.
- ARARIPE, R. C.; OLIVEIRA, D. H.; TOMÉ, M. E.; MOURA DE MELLO, R.; BARRETO, A. M. F. Foraminifera and Ostracoda from the Lower Cretaceous (Aptian–lower Albian) Romualdo formation, Araripe basin, northeast Brazil: Paleoenvironmental inferences. **Cretaceous Research**, v. 122, p. 104766, 2021.
- ARARIPE, R. C.; PEDROSA LEMOS, F. A.; PRADO, L. A. C. DO; TOMÉ, M. E. T. R.; OLIVEIRA, D. H. D.; PEREIRA, P. A.; NASCIMENTO, L. R. S. L.; ASAOKURA, Y.; NG, C.; VIVIERS, M. C.; BARRETO, A. F. Upper Aptian–lower Albian of the southern-central Araripe Basin, Brazil: Microbiostratigraphic and paleoecological inferences. **Journal of South American Earth Sciences**, v. 116, p. 103814, 2022.

- ARARIPE, R.; OLIVEIRA, D.; TOMÉ, M. E.; MELLO, R.; BARRETO, A.; SIAL, A. Análise isotópica de oxigênio e carbono em microfósseis da Formação Romualdo, cretáceo inferior, bacia do Araripe, Pernambuco, nordeste do Brasil. **Geochimica Brasiliensis**, v. 33, n. 2, p. 133–142, 2019.
- ASSINE, M. L. Análise estratigráfica da Bacia do Araripe, Nordeste do Brasil. **Revista Brasileira de Geociências**, v. 22, n. 3, p. 289–300, 1992.
- ASSINE, M. L. Bacia do Araripe. **Boletim de Geociencias da Petrobras**, v. 15, n. 2, p. 371–389, 2007.
- ASSINE, M. L. Sequências deposicionais do Andar Alagoas da Bacia do Araripe, Nordeste do Brasil. **Boletim de Geociencias da Petrobras**, v. 22, p. 3–28, 2014.
- AZAD, A. M.; FRANTZEN, S.; BANK, M. S.; NILSEN, B. M.; DUINKER, A.; MADSEN, L.; MAAGE, A. Effects of geography and species variation on selenium and mercury molar ratios in Northeast Atlantic marine fish communities. **Science of The Total Environment**, v. 652, p. 1482–1496, 2019.
- BANTIM, R. A. M.; LIMA, F. J. DE; SARAIVA, A. Á. F. *Em:* SARAIVA, A. Á. F.; LIMA, F. J. DE; BARROS, O. A.; BANTIM, R. A. M. (Eds.). **Guia de Fósseis da Bacia do Araripe**. 1. ed. Crato. p. 31–44.
- BARBIERI, M. The Importance of Enrichment Factor (EF) and Geoaccumulation Index (Igeo) to Evaluate the Soil Contamination. **Journal of Geology & Geophysics**, v. 5, n. 1, 2016.
- BARLING, N.; MARTILL, D. M.; HEADS, S. W. A geochemical model for the preservation of insects in the Crato Formation (Lower Cretaceous) of Brazil. **Cretaceous Research**, v. 116, p. 104608, 2020.
- BARLING, N.; MARTILL, D. M.; HEADS, S. W.; GALLIEN, F. High fidelity preservation of fossil insects from the Crato Formation (Lower Cretaceous) of Brazil. **Cretaceous Research**, v. 52, n. PB, p. 605–622, 2015.
- BATE, R. H. Phosphatized ostracods with appendages from the Lower Cretaceous of Brazil. **Palaeontology**, v. 15, n. 3, p. 379–393, 1972.
- BEAUCHAMP, B.; GRASBY, S. E. Permian lysocline shoaling and ocean acidification along NW Pangea led to carbonate eradication and chert expansion. **Palaeogeography, Palaeoclimatology, Palaeoecology**, v. 350–352, p. 73–90, 2012.
- BECKERS, F.; RINKLEBE, J. Cycling of mercury in the environment: Sources, fate, and human health implications: A review. **Critical Reviews in Environmental Science and Technology**, v. 47, n. 9, p. 693–794, 2017.
- BENAMARA, A.; CHARBONNIER, G.; ADATTE, T.; SPANGENBERG, J. E.; FÖLLMI, K. B. Precession-driven monsoonal activity controlled the development of the early Albian Paquier oceanic anoxic event (OAE1b): Evidence from the Vocontian Basin, SE France. **Palaeogeography, Palaeoclimatology, Palaeoecology**, v. 537, p. 109406, 2020.

- BENEDITTO, A. P. M. DI; BITTAR, V. T.; REZENDE, C. E.; CAMARGO, P. B.; KEHRIG, H. A. Mercury, and stable isotopes ( $\delta^{15}\text{N}$  and  $\delta^{13}\text{C}$ ) as tracers during the ontogeny of *Trichiurus lepturus*. **Neotropical Ichthyology**, v. 11, n. 1, p. 211–216, 2013.
- BENIGNO, A. P. A.; N. SIAL, A.; D. DE LACERDA, L. D. Hg Stratigraphy as a Tracer of Volcanism and Biological Crises in the Cretaceous–Paleogene Transition. **Revista Virtual de Química**, v. 10, n. 3, p. 655–671, 2018.
- BENIGNO, A. P. A.; SARAIVA, A. Á. F.; SIAL, A. N.; LACERDA, L. D. Mercury chemostratigraphy as a proxy of volcanic-driven environmental changes in the Aptian-Albian transition, Araripe Basin, northeastern Brazil. **Journal of South American Earth Sciences**, v. 107, p. 103020, 2021.
- BENTUM, E. C. VAN; HETZEL, A.; BRUMSACK, H.-J.; FORSTER, A.; REICHART, G. J.; SINNINGHE DAMSTÉ, J. S. Reconstruction of water column anoxia in the equatorial Atlantic during the Cenomanian–Turonian oceanic anoxic event using biomarker and trace metal proxies. **Palaeogeography, Palaeoclimatology, Palaeoecology**, v. 280, n. 3–4, p. 489–498, 2009.
- BERNER, R. A. Sedimentary pyrite formation: An update. **Geochimica et Cosmochimica Acta**, v. 48, n. 4, p. 605–615, 1984.
- BESTWICK, J.; UNWIN, D. M.; BUTLER, R. J.; HENDERSON, D. M.; PURNELL, M. A. Pterosaur dietary hypotheses: a review of ideas and approaches. **Biological Reviews**, v. 93, n. 4, p. 2021–2048, 2018.
- BÉTARD, F.; PEULVAST, J. P.; MAGALHÃES, A. DE O.; CARVALHO NETA, M. DE L.; FREITAS, F. I. DE. Araripe Basin: A Major Geodiversity Hotspot in Brazil. **Geoheritage**, v. 10, n. 4, p. 543–558, 2018.
- BEURLEN, K. A geologia da Chapada do Araripe. **Anais da Academia Brasileira de Ciências**, v. 34, n. 3, p. 365–370, 1962.
- BEZERRA, F. I.; MENDES, M. A palaeoecological analysis of the Cretaceous (Aptian) insect fauna of the Crato Formation, Brazil. **Palaeogeography, Palaeoclimatology, Palaeoecology**, v. 641, p. 112134, 2024.
- BOBCO, F. E. R.; TROMBETTA, M. C.; FERREIRA, L. O.; SILVEIRA, L. F.; KROTH, M.; MENDONÇA, J. O.; MENDONÇA FILHO, J. G.; SEDORKO, D.; ARAUJO, B. C.; BORGHI, L. Alternations of open and closed lakes in the Lower Aptian Codó Formation (Parnaíba Basin, Brazil). **Sedimentary Geology**, v. 455, p. 106478, 2023.
- BODIN, S.; CHARPENTIER, M.; ULLMANN, C. V.; RUDRA, A.; SANEI, H. Carbon cycle during the late Aptian–early Albian OAE 1b: A focus on the Kilian–Paquier levels interval. **Global and Planetary Change**, v. 222, p. 104074, 2023.
- BOM, M. H. H.; KOCHHANN, K. G. D.; HEIMHOFER, U.; MOTA, M. A. L.; GUERRA, R. M. *et al.* Fossil-Bearing Concretions of the Araripe Basin Accumulated During Oceanic Anoxic Event 1b. **Paleoceanography and Paleoclimatology**, v. 38, n. 11, p. 1–17, 2023.

BOM, M. H. H.; CEOLIN, D.; KOCHHANN, K. G. D.; KRAHL, G.; FAUTH, G.; BERGUE, C. T.; SAVIAN, J. F.; STROHSCHOEN JUNIOR, O.; SIMÕES, M. G.; ASSINE, M. L. Paleoenvironmental evolution of the Aptian Romualdo Formation, Araripe Basin, Northeastern Brazil. **Global and Planetary Change**, v. 203, 2021.

BOND, D. P. G.; GRASBY, S. E. On the causes of mass extinctions. **Palaeogeography, Palaeoclimatology, Palaeoecology**, v. 478, p. 3–29, 2017.

BOS, R.; LINDSTRÖM, S.; KONIJNENBURG-VAN CITTERT, H. VAN; HILGEN, F.; HOLLAAR, T. P.; AALPOEL, H.; WEIJST, C. VAN DER; SANEI, H.; RUDRA, A.; SLUIJS, A.; SCHOOTBRUGGE, B. VAN DE. Triassic-Jurassic vegetation response to carbon cycle perturbations and climate change. **Global and Planetary Change**, v. 228, p. 104211, 2023.

BOTTINI, C.; ERBA, E. Mid-Cretaceous paleoenvironmental changes in the western Tethys. **Climate of the Past**, v. 14, n. 8, p. 1147–1163, 2018.

BOTTINI, C.; MUTTERLOSE, J. Integrated stratigraphy of early aptian black shales in the boreal realm: Calcareous nannofossil and stable isotope evidence for global and regional processes. **Newsletters on Stratigraphy**, v. 45, n. 2, p. 115–137, 2012.

BRAUN, O. Estratigrafia dos sedimentos da parte Inferior da Região Nordeste do Brasil (Bacias de Tucano- Jatobá, Mirandiba e Araripe). **Boletim de Divisão de Geologia e Mineralogia**, p. 69–71, 1966.

BREHM, U.; GASIEWICZ, A.; GERDES, G.; KRUMBEIN, W. Biolaminoid facies in a peritidal sabkha: Permian Platy Dolomite of northern Poland. **International Journal of Earth Sciences**, v. 91, n. 2, p. 260–271, 2002.

BRITO NEVES, B. B.; SANTOS, E. J.; SCHMUS, W. R. VAN. Tectonic history of the Borborema Province, Northeastern Brazil. In: **Tectonic Evolution of South America**. Rio de Janeiro: International Geological Congress, 2000. p. 151–182.

BRITO, P. M.; FERREIRA, P. L. N. The first hybodont shark, *Tribodus limae* ng, n. sp., from the Lower Cretaceous of Chapada do Araripe (North-East Brazil). **Anais da Academia Brasileira de Ciências**, v. 61, n. 1, p. 53–57, 1989.

BURGENER, L.; HYLAND, E.; REICH, B. J.; SCOTESE, C. Cretaceous climates: Mapping paleo-Köppen climatic zones using a Bayesian statistical analysis of lithologic, paleontologic, and geochemical proxies. **Palaeogeography, Palaeoclimatology, Palaeoecology**, v. 613, 2023.

CABRAL, F. A. A.; SILVEIRA, A. C.; RAMOS, G. M. S.; MIRANDA, T. S.; BARBOSA, J. A.; NEUMANN, V. H. M. L. Microfacies and diagenetic evolution of the limestones of the upper part of the Crato Formation, Araripe Basin, northeastern Brazil. **Brazilian Journal of Geology**, v. 49, n. 1, 2019.

CAI, S.; WEI, G.; LO, L.; HU, J.; SUN, Z.; ZENG, T.; WEI, Y.; ZHOU, Z.; XU, Y. G. Volcanism-driven lacustrine redox fluctuations were responsible for the formation of the Jehol Lagerstätte: Evidence from a high-resolution Aptian sedimentary core, Northeast China. **Palaeogeography, Palaeoclimatology, Palaeoecology**, v. 631, 2023.

CALVERT, S. E.; PEDERSEN, T. F. Geochemistry of recent oxic and anoxic marine sediments: implications for the geological record. **Marine geology**, v. 113, n. 1-2, p. 67-88, 1993.

CAO, H.; WANG, Z.; DONG, L.; XIAO, Y.; HU, L.; CHEN, F.; WEI, K.; CHEN, C.; SONG, Z.; WU, L. Influence of hydrothermal and upwelling events on organic matter accumulation in the gas-bearing lower Cambrian shales of the middle Yangtze Block, South China. **Marine and Petroleum Geology**, v. 155, p. 106373, 2023.

CAO, J.; WU, M.; CHEN, Y.; HU, K.; BIAN, L.; WANG, L.; ZHANG, Y. Trace, and rare earth element geochemistry of Jurassic mudstones in the northern Qaidam Basin, northwest China. **Chemie der Erde**, v. 72, n. 3, p. 245–252, 2012.

CARDIA, F. M. S.; SANTUCCI, R. M.; BERNARDI, J. V. E.; ANDRADE, M. B. DE; OLIVEIRA, C. E. M. DE. Mercury concentrations in terrestrial fossil vertebrates from the Bauru Group (Upper Cretaceous), Brazil and implications for vertebrate paleontology. **Journal of South American Earth Sciences**, v. 86, p. 15–22, 2018.

CARVALHO, M. A.; BENGTSON, P.; LANA, C. C.; SÁ, N. P.; SANTIAGO, G.; GIANNERINI, M. C. S. Late Aptian (Early Cretaceous) dry–wet cycles and their effects on vegetation in the South Atlantic: Palynological evidence. **Cretaceous Research**, v. 100, p. 172–183, 2019.

CASTRO, R.; SANTOS-SILVA, T.; FAMBRINI, G.; SOUZA-NETO, J. A.; PEREIRA, R. Caracterização geoquímica de folhelhos betuminosos da Formação Ipubi, bacia do Araripe, NE Brasil. **Geochimica Brasiliensis**, v. 31, n. 1, p. 11–27, 2017.

CATTO, B.; JAHNERT, R. J.; WARREN, L. V.; VAREJAO, F. G.; ASSINE, M. L. The microbial nature of laminated limestones: Lessons from the Upper Aptian, Araripe Basin, Brazil. **Sedimentary Geology**, v. 341, p. 304–315, 2016.

CHADWICK, M. A.; FEMINELLA, J. W.; HENRY; RAYMOND P. Salt and water balance in *Hexagenia limbata* (Ephemeroptera: Ephemeridae) when exposed to brackish water. **Florida Entomologist**, v. 85, n. 4, p. 650–651, 2002.

CHAGAS, D. B. **Análise faciológica frente ao controle paleoambiental baseado na palinologia do intervalo Aptiano- Albiano da Bacia do Araripe (Sub-Bacias Cariri e Feira Nova), NE do Brasil**. Fortaleza: Universidade Federal do Ceará, 2017.

CHARBONNIER, G.; FÖLLMI, K. B. Mercury enrichments in lower Aptian sediments support the link between Ontong Java large igneous province activity and oceanic anoxic episode 1a. **Geology**, v. 45, n. 1, p. 63–66, 2017.

CHEN, W.; KEMP, D. B.; HE, T.; NEWTON, R. J.; XIONG, Y.; JENKYNS, H. C.; IZUMI, K.; CHO, T.; HUANG, C.; POULTON, S. W. Shallow- and deep-ocean Fe cycling and redox evolution across the Pliensbachian–Toarcian boundary and Toarcian Oceanic Anoxic Event in Panthalassa. **Earth and Planetary Science Letters**, v. 602, 2023.

CHEN, W.; KEMP, D. B.; NEWTON, R. J.; HE, T.; HUANG, C.; CHO, T.; IZUMI, K. Major sulfur cycle perturbations in the Panthalassic Ocean across the Pliensbachian-

Toarcian boundary and the Toarcian Oceanic Anoxic Event. **Global and Planetary Change**, v. 215, p. 103884, 2022.

CHUMAKOV, N. M. et al. Climatic belts of the mid-Cretaceous time. **Stratigraphy and Geological Correlation**, v. 3, n. 3, p. 42-63, 1995.

CLAES, H.; MIRANDA, T.; FALCÃO, T. C.; SOETE, J.; MOHAMMADI, Z.; ZIEGER, L.; ERTHAL, M. M.; AGUILAR, J.; SCHMATZ, J.; BUSCH, A.; SWENNEN, R. Model for calcite spherulite formation in organic, clay-rich, lacustrine carbonate shales (Barbalha Formation, Aptian, Araripe Basin, NE Brazil). **Marine and Petroleum Geology**, v. 128, 2021.

COCCIONI, R.; SABATINO, N.; FRONTALINI, F.; GARDIN, S.; SIDERI, M.; SPROVIERI, M. The neglected history of Oceanic Anoxic Event 1b: insights and new data from the Poggio le Guaine section (Umbria–Marche Basin). **Stratigraphy**, v. 11, n. 3–4, p. 245–282, 2014.

COFFIN, M.; DUNCAN, R.; ELDHOLM, O.; FITTON, J. G.; FREY, F.; LARSEN, H. C.; MAHONEY, J.; SAUNDERS, A.; SCHLICH, R.; WALLACE, P. Large Igneous Provinces, and Scientific Ocean Drilling: Status Quo and A Look Ahead. **Oceanography**, v. 19, n. 4, p. 150–160, 2006.

COFFIN, M. F.; PRINGLE, M. S.; DUNCAN, R. A.; GLADCZENKO, T. P.; STOREY, M.; MÜLLER, R. D.; GAHAGAN, L. A. Kerguelen hotspot magma output since 130 Ma. **Journal of Petrology**, v. 43, n. 7, p. 1120–1140, 2002.

COIMBRA, J. C.; ARAI, M.; CARREÑO, L. A. Biostratigraphy of Lower Cretaceous microfossils from the Araripe basin, northeastern Brazil. **Geobios**, v. 35, n. 6, p. 687–698, 2002.

COUTINHO, D. L. C.; COUTINHO, J. C.; COUTINHO, C. C.; DUQUE, R.; ASAKURA, Y.; BRANDÃO, A. M.; BARBOSA, C. G. et al. A Coleção Paleontológica do Museu de Ciências Naturais e de História Barra do Jardim da Fundação Francisco de Lima Botelho, Jardim, Ceará, Brasil. **Anuário do Instituto de Geociências**, v. 44, n. 1, 2021.

CRESSEY, R.; PATTERSON, C. Fossil Parasitic Copepods from a Lower Cretaceous Fish. **Science**, v. 180, n. 4092, p. 1283–1285, 1973.

CUSTÓDIO, M. A.; QUAGLIO, F.; WARREN, L. V.; SIMÕES, M. G.; FÜRSICH, F. T.; PERINOTTO, J. A. J.; ASSINE, M. L. The transgressive-regressive cycle of the Romualdo Formation (Araripe Basin): Sedimentary archive of the Early Cretaceous marine ingressions in the interior of Northeast Brazil. **Sedimentary Geology**, v. 359, p. 1–15, 2017.

DAVIES, M. A.; SCHRÖDER-ADAMS, C. J.; HERRLE, J. O.; HÜLSE, P.; SCHNEIDER, S. Bottom water redox conditions and benthic foraminiferal morphogroup response in the Late Cretaceous Sverdrup Basin, Arctic Canada: Implications for Oceanic Anoxic Event 3. **Cretaceous Research**, v. 111, 2020.

DAVIS, S. P.; MARTILL, D. M. The gonorynchiform fish *Dastilbe* from the lower Cretaceous of Brazil. **Palaeontology**, v. 42, n. 4, p. 715–740, 1999.

DAVIS, W. J. Mass Extinctions and Their Relationship with Atmospheric Carbon Dioxide Concentration: Implications for Earth's Future. **Earth's Future**, v. 11, n. 6, jun. 2023.

DA SILVA, C. P. As viagens filosóficas de João da Silva Feijó (1760-1824) no Ceará. **História: Questão & Debates**, n. 47, 2007.

EIDE, M.; OLSEN, A.; NINNEMANN, U. S.; JOHANNESSEN, T. A global ocean climatology of preindustrial and modern ocean  $\delta^{13}\text{C}$ . **Global Biogeochemical Cycles**, v. 31, n. 3, p. 515–534, 2017.

ERBA, E.; DUNCAN, R. A.; BOTTINI, C.; TIRABOSCHI, D.; WEISSERT, H.; JENKYN, H. C.; MALINVERNO, A. Environmental consequences of Ontong Java Plateau and Kerguelen Plateau volcanism. **Special Paper of the Geological Society of America**, v. 511, p. 271–303, 2015.

ERICKSEN, J. A.; GUSTIN, M. S.; SCHORRAN, D. E.; JOHNSON, D. W.; LINDBERG, S. E.; COLEMAN, J. S. Accumulation of atmospheric mercury in forest foliage. **Atmospheric Environment**, v. 37, n. 12, p. 1613–1622, 2003.

EVANS, G.; AUGUSTINUS, P.; GADD, P.; ZAWADZKI, A.; DITCHFIELD, A.; HOPKINS, J. A multi-proxy paleoenvironmental interpretation spanning the last glacial cycle (ca.  $117 \pm 8.5$  ka BP) from a lake sediment stratigraphy from Lake Kai Iwi, Northland, New Zealand. **Journal of Paleolimnology**, v. 65, n. 1, p. 101–122, 2021.

FAMBRINI, G. L.; SILVESTRE, D. D. C.; MENEZES-FILHO, J. A. B.; COSTA, I. C.; NEUMANN, V. H. D. M. L. Architectural and facies characterization of the aptian fluvial Barbalha Formation, Araripe basin, NE Brazil. **Geological Society Special Publication**, v. 488, n. 1, p. 119–150, 2019.

FAMBRINI, G. L.; SILVESTRE, D. C.; BARRETO JUNIOR, A. M.; SILVA-FILHO, W. F. Estratigrafia da Bacia do Araripe: estado da arte, revisão crítica e resultados novos. **Geologia USP. Série Científica**, v. 20, n. 4, p. 169–212, 2020.

FAN, D.; SHAN, X.; MAKEEN, Y. M.; HE, W.; SU, S.; WANG, Y.; YI, J.; HAO, G.; ZHAO, Y. Response of a continental fault basin to the global OAE1a during the Aptian: Hongmiaozi Basin, Northeast China. **Scientific Reports**, v. 11, n. 1, p. 7229, 2021.

FAN, H.; OSTRANDER, C. M.; AURO, M.; WEN, H.; NIELSEN, S. G. Vanadium isotope evidence for expansive ocean euxinia during the appearance of early Ediacara biota. **Earth and Planetary Science Letters**, v. 567, 2021.

FANG, T.; LU, W.; LI, J.; ZHAO, X.; YANG, K. Levels and risk assessment of metals in sediment and fish from Chaohu Lake, Anhui Province, China. **Environmental Science and Pollution Research**, v. 24, p. 15390-15400, 2017.

FARA, E.; SARAIVA, A. Á. F.; ALMEIDA CAMPOS, D. DE; MOREIRA, J. K. R.; CARVALHO SIEBRA, D.; KELLNER, A. W. A. Controlled excavations in the Romualdo Member of the Santana Formation (Early Cretaceous, Araripe Basin, northeastern Brazil): stratigraphic, palaeoenvironmental and palaeoecological implications. **Palaeogeography, Palaeoclimatology, Palaeoecology**, v. 218, n. 1–2, p. 145–160, 2005.

- FAUTH, G.; KERN, H. P.; VILLEGAS- MARTÍN, J.; MOTA, M. A. L.; SANTOS, M. A. B. et al. Early Aptian marine incursions in the interior of northeastern Brazil following the Gondwana breakup. **Scientific Reports**, v. 13, n. 1, p. 6728, 2023.
- FONT, E.; ADATTE, T.; SIAL, A. N.; DE LACERDA, L.; KELLER, G.; PUNEKAR, J. Mercury anomaly, Deccan volcanism, and the end-Cretaceous mass extinction. **Geology**, v. 44, n. 2, p. 171–174, 2016.
- FONT, E.; BOND, D. P. G. **Volcanism and Mass Extinction**. Em: Encyclopedia of Geology, 2. ed. Elsevier Inc., 2021.
- FREITAS, L. C. B.; MOURA, G. J. B. DE; SARAIVA, A. A. F. First Occurrence and Paleo-Ecological Implications of Insects (Orthoptera: Ensifera Gryllidae) in the Romualdo Member of the Santana Formation, Eo-Cretaceous of the Araripe Basin. **Anais da Academia Brasileira de Ciências**, v. 88, n. 4, p. 2113–2120, 2016.
- FÜRSICH, F. T.; CUSTÓDIO, M. A.; MATOS, S. A.; HETHKE, M.; QUAGLIO, F.; WARREN, L. V.; ASSINE, M. L.; SIMÕES, M. G. Analysis of a Cretaceous (late Aptian) high-stress ecosystem: The Romualdo Formation of the Araripe Basin, northeastern Brazil. **Cretaceous Research**, v. 95, p. 268–296, 2019.
- GALARAGA, F.; REATEGUI, K.; MARTÍNEZ, A.; MARTÍNEZ, M.; LLAMAS, J. F.; MÁRQUEZ, G. V/Ni ratio as a parameter in paleoenvironmental characterization of nonmature medium-crude oils from several Latin American basins. **Journal of Petroleum Science and Engineering**, v. 61, n. 1, p. 9–14, 2008.
- GALLOWAY, J. M.; GRASBY, S. E.; WANG, F.; HADLARI, T.; DEWING, K.; BODIN, S.; SANEI, H. A mercury and trace element geochemical record across Oceanic Anoxic Event 1b in Arctic Canada. **Palaeogeography, Palaeoclimatology, Palaeoecology**, v. 617, p. 111490, 2023.
- GAMBACORTA, G.; CAVALHEIRO, L.; BRUMSACK, H. J.; DICKSON, A. J.; JENKYNS, H. C.; SCHNETGER, B.; WAGNER, T.; ERBA, E. Suboxic conditions prevailed during the Toarcian Oceanic Anoxic Event in the Alpine-Mediterranean Tethys: The Sogno Core pelagic record (Lombardy Basin, northern Italy). **Global and Planetary Change**, p. 104089, 2023.
- GAMBOA RUIZ, W. L.; TOMIYASU, T. Distribution of mercury in sediments from Kagoshima Bay, Japan, and its relationship with physical and chemical factors. **Environmental Earth Sciences**, v. 74, n. 2, p. 1175–1188, 2015.
- GHIGNONE, J. I. et al. Estratigrafia e estrutura das bacias do Araripe, Iguatu e Rio do Peixe. In: **Congresso Brasileiro de Geologia**. 1986. p. 271-285.
- GIANNERINI, M. C. S.; CARVALHO, M. A.; LANA, C. C.; SANTIAGO, G.; PAULA SÁ, N.; CORREIA, G. C. Late Aptian paleoclimate reconstruction of the Brazilian equatorial margin: inferences from palynology. **Climate of the Past**, v. 19, n. 8, p. 1715–1742, 2023.
- GLASSPOOL, I. J.; SCOTT, A. C.; WALTHAM, D.; PRONINA, N.; SHAO, L. The impact of fire on the Late Paleozoic Earth system. **Frontiers in Plant Science**, v. 6, p. 756, 2015.

GODOT SOUZA, J. F.; ISOZAKI, Y.; TSUTSUMI, Y.; SCHMITT, R. S.; MEDEIROS, S. R.; ALMEIDA, C. N.; ARAUJO, B. C.; RICHETTI, P.; SILVA, E. A.; RIOS NETTO, A. M. Provenance analysis of the Araripe intracontinental basin, northeast Brazil – Routes for proto-Atlantic marine incursions in northwest Gondwana. **Sedimentary Geology**, v. 440, 2022.

GOLDBERG, K.; PREMAOR, E.; BARDOLA, T.; SOUZA, P. A. Aptian marine ingressions in the Araripe Basin: Implications for paleogeographic reconstruction and evaporite accumulation. **Marine and Petroleum Geology**, v. 107, p. 214–221, 2019.

GRADSTEIN, F. M.; OGG, J. G.; SCHMITZ, M. D.; OGG, G. M. Oxygen Isotope Stratigraphy. *Em: Geological Time Scale*, 2° Ed. Elsevier, 279–308, 2020.

GRASBY, S. E.; BEAUCHAMP, B.; BOND, D. P. G.; WIGNALL, P.; TALAVERA, C.; GALLOWAY, J. M.; PIEPJAHN, K.; REINHARDT, L.; BLOOMEIER, D. Progressive environmental deterioration in northwestern Pangea leading to the latest Permian extinction. **Bulletin of the Geological Society of America**, v. 127, n. 9–10, p. 1331–1347, 2015.

GRASBY, S. E.; BOND, D. P. G. How Large Igneous Provinces Have Killed Most Life on Earth—Numerous Times. **Elements**, v. 19, n. 5, p. 276–281, 2023.

GRASBY, S. E.; THEM, T. R.; CHEN, Z.; YIN, R.; ARDAKANI, O. H. Mercury as a proxy for volcanic emissions in the geologic record. **Earth-Science Reviews**, v. 196, n. May, p. 102880, 2019.

GRATZER, R.; NEUMANN, V. H.; VORTISCH, W.; ROCHA, D. E. A.; BECHTEL, A. Stable isotopes of organics and inorganics, clay mineralogy and chemical environment of an Aptian lacustrine succession in northeastern Brazil. **Geological Society Special Publication**, v. 382, n. 1, p. 157–182, 2013.

GRAVEN, H.; KEELING, R. F.; ROGELJ, J. Changes to Carbon Isotopes in Atmospheric CO<sub>2</sub> Over the Industrial Era and Into the Future. **Global Biogeochemical Cycles**, v. 34, n. 11, 2020.

GREGORY, D. D.; LARGE, R. R.; HALPIN, J. A.; BATURINA, E. L.; LYONS, T. W. et al. Trace element content of sedimentary pyrite in black shales. **Economic Geology**, v. 110, n. 6, p. 1389–1410, 2015.

GRICE, K.; HOLMAN, A. I.; PLET, C.; TRIPP, M. Fossilized biomolecules and biomarkers in carbonate concretions from Konservat-Lagerstätten. **Minerals**, v. 9, n. 3, p. 158, 2019.

GUEGUEN, B.; ROUXEL, O.; FOUQUET, Y. Light Zn and Cu isotope compositions recorded in ferromanganese crusts during the Cenozoic as evidence for hydrothermal inputs in South Pacific deep seawater. **Geochimica et Cosmochimica Acta**, v. 333, p. 136–152, 2022.

GUERRA-SOMMER, M.; SIEGLOCH, A. M.; DEGANI-SCHMIDT, I.; SANTOS, Â. C. S. DOS; CARVALHO, I. DE S.; ANDRADE, J. A. F. G. DE; FREITAS, F. I. DE. Climate change during the deposition of the Aptian Santana Formation (Araripe Basin,

Brazil): Preliminary data based on wood signatures. **Journal of South American Earth Sciences**, v. 111, p. 103462, 2021.

GUO, Q.; SHIELDS, G. A.; LIU, C.; STRAUSS, H.; ZHU, M.; PI, D.; GOLDBERG, T.; YANG, X. Trace element chemostratigraphy of two Ediacaran-Cambrian successions in South China: Implications for organ sedimentary metal enrichment and silification in the Early Cambrian. **Palaeogeography, Palaeoclimatology, Palaeoecology**, v. 254, n. 1–2, p. 194–216, 2007.

GUSTAFSSON, J. P. Vanadium geochemistry in the biogeosphere–speciation, solid-solution interactions, and ecotoxicity. **Applied geochemistry**, v. 102, p. 1-25, 2019.

GUZMÁN, J.; PIOVESAN, E. K.; MELO, R. M.; ALMEIDA-LIMA, D.; JESUS SOUSA, A.; MIRANDA LOPES NEUMANN, V. H. Ostracoda and Foraminifera biostratigraphy and paleoenvironmental evolution of the Aptian Santana Group, post-rift of the Araripe Basin, Brazil. **Gondwana Research**, v. 124, p. 18 – 38, 2023.

HAMID, I. R. A.; LACERDA, L. D.; SARAIVA, A. Á. F.; SIAL, A. N.; BENIGNO, A. P. A.; AGUIAR, J. E. Aptian-Albian paleoenvironmental geochemistry: Araripe Basin, Northeastern Brazil. **Journal of South American Earth Sciences**, v. 137, p. 104856, 2024.

HASHEMPOUR, S. S.; MAGHFOURI, S.; RASTAD, E.; GONZÁLEZ, F. J. Mohammadabad Manganese deposit, southwest Sabzevar basin, Iran: Evidence of sea-floor exhalation and geochemical studies in the late Cretaceous volcano-sedimentary sequence. **Journal of Geochemical Exploration**, v. 245, p. 107 – 127, 2023.

HEIMHOFER, U.; ARIZTEGUI, D.; LENNIGER, M.; HESSELBO, S. P.; MARTILL, D. M.; RIOS-NETTO, A. M. Deciphering the depositional environment of the laminated Crato fossil beds (Early Cretaceous, Araripe Basin, Northeastern Brazil). **Sedimentology**, v. 57, n. 2, p. 677–694, 2010.

HEIMHOFER, U.; HESSELBO, S. P.; PANCAST, R. D.; MARTILL, D. M.; HOCHULI, P. A.; GUZZO, J. V. P. Evidence for photic zone euxinia in the Early Albian Santana Formation (Araripe Basin, NE Brazil). **Terra Nova**, v. 20, n. 5, p. 347–354, 2008.

HEIMHOFER, U.; HOCHULI, P. A. Early Cretaceous angiosperm pollen from a low-latitude succession (Araripe Basin, NE Brazil). **Review of Palaeobotany and Palynology**, v. 161, n. 3–4, p. 105–126, 2010.

HEIMHOFER, U.; MARTILL, D. M. The sedimentology and depositional environment of the Crato Formation. Edition: MARTIL, D. M.; BECHLY, G.; LOVERIDGE, R. F. *Em: The Crato Fossil Beds of Brazil*. Cambridge University Press, 2007. p. 44–62.

HEIMHOFER, U.; MEISTER, P.; BERNASCONI, S. M.; ARIZTEGUI, D.; MARTILL, D. M.; RIOS-NETTO, A. M.; SCHWARK, L. Isotope and elemental geochemistry of black shale-hosted fossiliferous concretions from the Cretaceous Santana Formation fossil Lagerstätte (Brazil). **Sedimentology**, v. 64, n. 1, p. 150–167, 2017.

HERNDON, E. M.; Havig, J. R.; SINGER, D. M.; MCCORMICK, M. L.; KUMP, L. R. Manganese and iron geochemistry in sediments underlying the redox-stratified Fayetteville Green Lake. **Geochimica et Cosmochimica Acta**, v. 231, p. 50–63, 2018.

HOEFS, J. Oxygen. *Em: JOCHEN HOEFS. Stable Isotope Geochemistry.* 6º ed. Berlin: Springer, p. 58–66, 2009.

HOUSE, B. M.; NORRIS, R. D. Unlocking the barite paleoproductivity proxy: A new high-throughput method for quantifying barite in marine sediments. **Chemical Geology**, v. 552, 2020.

HUANG, T.; MOOS, S. B.; BOYLE, E. A. Trivalent chromium isotopes in the eastern tropical North Pacific oxygen-deficient zone. **Proceedings of the National Academy of Sciences**, v. 118, n. 8, p. e1918605118, 2021.

HUBER, B. T.; LECKIE, R. M. PLANKTIC Foraminiferal species turnover across deep-sea Aptian/ Albian boundary sections. **The Journal of Foraminiferal Research**, v. 41, n. 1, p. 53–95, 2011.

JONES, B.; MANNING, D. A. C. Comparison of geochemical indices used for the interpretation of palaeoredox conditions in ancient mudstones. **Chemical geology**, v. 111, n. 1-4, p. 111-129, 1994.

JØRGENSEN, B. B. Mineralization of organic matter in the sea bed- the role of sulphate reduction. **Nature**, v. 296, n. 5858, p. 643–645, 1982.

KAUFMAN, A. J.; JACOBSEN, S. B.; KNOLL, A. H. The Vendian record of Sr and C isotopic variations in seawater: Implications for tectonics and paleoclimate. **Earth and Planetary Science Letters**, v. 120, n. 3–4, p. 409–430, 1993.

KAUFMAN, A.; KNOLL, A. Neoproterozoic variations in the C-isotopic composition of seawater: stratigraphic and biogeochemical implications. **Precambrian Research**, v. 73, n. 1–4, p. 27–49, 1995.

KELLER, G. Cretaceous climate, volcanism, impacts, and biotic effects. **Cretaceous Research**, v. 29, n. 5–6, p. 754–771, 2008.

KELLNER, A. W. A. Ocorrência de um novo crocodiliano no Cretáceo inferior da bacia do Araripe, Nordeste do Brasil: contribuição ao PICG—Projeto 242—Cretáceo da América Latina. **Anais da Academia Brasileira de Ciências**, v. 59, n. 3, p. 219–232, 1987.

KELLNER, A. W. A. Fossilized theropod soft tissue. **Nature**, v. 379, n. 6560, p. 32–32, 1996.

KELLNER, ALEXANDER W. A. Reinterpretation of a remarkably well-preserved pterosaur soft tissue from the Early Cretaceous of Brazil. **Journal of Vertebrate Paleontology**, v. 16, n. 4, p. 718–722, 1996.

KELLNER, A. W. A.; ALMEIDA CAMPOS, D. Sobre um novo pterossauro com crista sagital da Bacia do Araripe, Cretáceo Inferior do nordeste do Brasil. **Anais da Academia Brasileira de Ciências**, v. 60, n. 4, p. 459–469, 1988.

KELLNER, A. W. A.; ALMEIDA CAMPOS, D. A new species of *Tupuxuara* (Pterosauria, Tapejaridae) from the Early Cretaceous of Brazil. **Anais da Academia Brasileira de Ciências**, v. 66, n. 4, p. 467–474, 1994.

- KIFUMBI, C.; SCHERER, C. M. S.; ROS, L. F.; ROCHA, E. C.; SILVA, T. F.; ANGONESE, B. S.; MICHEL, R. D. L. A Pennsylvanian saline-alkaline lake in Gondwana mid-latitude: Evidence from the Piauí Formation chert deposits, Parnaíba Basin, Brazil. **Palaeogeography, Palaeoclimatology, Palaeoecology**, v. 603, p. 111192, 2022.
- KNIES, J.; GRASBY, S. E.; BEAUCHAMP, B.; SCHUBERT, C. J. Water mass denitrification during the latest Permian extinction in the Sverdrup Basin, Arctic Canada. **Geology**, v. 41, n. 2, p. 167–170, 2013.
- KONOVALOV, S.; SAMODUROV, A.; OGUZ, T.; IVANOV, L. Parameterization of iron and manganese cycling in the Black Sea suboxic and anoxic environment. **Deep-Sea Research Part I: Oceanographic Research Papers**, v. 51, n. 12, p. 2027–2045, 2004.
- KRUPP, R. Physicochemical aspects of mercury metallogenesis. **Chemical Geology**, v. 69, n. 3–4, p. 345–356, 1988.
- KUWAHARA, Y.; FUJINAGA, K.; NOZAKI, T.; OHTA, J.; YANO, M.; YASUKAWA, K.; NAKAMURA, K.; KATO, Y. Iron deposition during recovery from Late Devonian oceanic anoxia: Implications of the geochemistry of the Kawame ferromanganese deposit, Nedamo Belt, Northeast Japan. **Global and Planetary Change**, v. 216, p. 103920, 2022.
- KUYPERS, M. M. M.; BREUGEL, Y. VAN; SCHOUTEN, S.; ERBA, E.; DAMSTÉ, J. S. S. N<sub>2</sub>-fixing cyanobacteria supplied nutrient N for Cretaceous oceanic anoxic events. **Geology**, v. 32, n. 10, p. 853–856, 2004.
- LEANDRO, C. G.; SAVIAN, J. F.; KOCHHANN, M. V. L.; FRANCO, D. R.; COCCIONI, R.; GARDIN, S.; JOVANE, L.; FIGUEIREDO, M.; TEDESCHI, L. R.; JANIKIAN, L.; ALMEIDA, R. P.; TRINDADE, R. I. F. Astronomical tuning of the Aptian stage and its implications for age recalibrations and paleoclimatic events. **Nature Communications**, v. 13, n. 1, p. 2941, 2022.
- LECKIE, R. M.; BRALOWER, T. J.; CASHMAN, R. Oceanic anoxic events, and plankton evolution: Biotic response to tectonic forcing during the mid-Cretaceous. **Paleoceanography**, v. 17, n. 3, p. 13-1-13-29, 2002.
- LEWAN, M. D.; MAYNARD, J. B. Factors controlling enrichment of vanadium and nickel in the bitumen of organic sedimentary rocks. **Geochimica et Cosmochimica Acta**, v. 46, n. 12, p. 2547–2560, 1982.
- LI, L.; HE, W.; LIU, Z.; SONG, Y.; LI, Y.; BELOUSOVA, E.; LÖHR, S. C.; GEORGE, S. C. Volcanic activity drives lacustrine carbon sequestration after Oceanic Anoxic Event 1a. **Palaeogeography, Palaeoclimatology, Palaeoecology**, v. 621, 2023.
- LI, X.; JENKYNS, H. C.; ZHANG, C.; WANG, Y.; LIU, L.; CAO, K. Carbon isotope signatures of pedogenic carbonates from SE China: rapid atmospheric pCO<sub>2</sub> changes during middle–late Early Cretaceous time. **Geological Magazine**, v. 151, n. 5, p. 830–849, 2014.

LIGUORI, B. T. P.; ALMEIDA, M. G.; REZENDE, C. E. Barium and its importance as an indicator of (Paleo)productivity. *Anais da Academia Brasileira de Ciências*, v. 88, n. 4, p. 2093–2103, 2016.

LIMA BARROS, C.; SILVA, S. C.; MACHADO, L. L.; MORAES RIOS NETTO, A.; SAMES, B.; ALVES, T. D.; SILVA JÚNIOR, R. P. DA. Non-marine ostracods of the Codó Formation (upper Aptian, Lower Cretaceous), Parnaíba Basin, NE Brazil: new biostratigraphic and paleoecological insights. *Cretaceous Research*, v. 133, p. 105125, 2022.

LIMA, F. J.; PIRES, E. F.; JASPER, A.; UHL, D.; SARAIWA, A. Á. F.; SAYÃO, J. M. Fire in the paradise: evidence of repeated palaeo-wildfires from the Araripe Fossil Lagerstätte (Araripe Basin, Aptian-Albian), Northeast Brazil. *Palaeobiodiversity and Palaeoenvironments*, v. 99, n. 3, p. 367–378, 2019.

LIMA, M. R. *Palinologia da Formação Santana (Cretáceo do Nordeste do Brasil)*. 1978. Tese de Doutorado. Universidade de São Paulo.

LINDOSO, R. M.; MAISEY, J. G.; CARVALHO, I. S. Ichthyofauna from the Codó Formation, Lower Cretaceous (Aptian, Parnaíba Basin), Northeastern Brazil and their paleobiogeographical and paleoecological significance. *Palaeogeography, Palaeoclimatology, Palaeoecology*, v. 447, p. 53–64, 2016.

LIU, J.; CAO, J.; HU, G.; WANG, Y.; YANG, R.; LIAO, Z. Water-level and redox fluctuations in a Sichuan Basin lacustrine system coincident with the Toarcian OAE. *Palaeogeography, Palaeoclimatology, Palaeoecology*, v. 558, p. 109942, 2020.

LIU, J.; PELLERIN, A.; WANG, J.; RICKARD, D.; ANTHER, G.; ZHAO, J.; WANG, Z. JØRGENSEN, B. B.; ONO, S. Multiple sulfur isotopes discriminate organoclastic and methane-based sulfate reduction by sub-seafloor pyrite formation. *Geochimica et cosmochimica acta*, v. 316, p. 309-330, 2022.

LIU, Q.; LI, P.; JIANG, L.; JIN, Z.; LIANG, X.; ZHU, D.; PANG, Q.; ZHANG, R.; LIU, J. Distinctive volcanic ash-rich lacustrine shale deposition related to chemical weathering intensity during the Late Triassic: Evidence from lithium contents and isotopes. *Science Advances*, v. 10, n. 11, 2024.

LOPES, G. L. B.; BARRETO, A. M. F. Paleoecological and biomechanical inferences regarding the paleoichthyofauna of the Romualdo Formation, Aptian-Albian of the Araripe Basin, state of Pernambuco, northeastern Brazil. *Journal of South American Earth Sciences*, v. 111, p. 103444, 2021.

LU, M.; LU, Y.; IKEJIRI, T.; SUN, D.; CARROLL, R.; BLAIR, E. H.; ALGEO, T. J.; SUN, Y. Periodic oceanic euxinic and terrestrial fluxes linked to astronomical forcing during the Late Devonian Frasnian–Famennian mass extinction. *Earth and Planetary Science Letters*, v. 562, p. 116839, 2021.

LU, Y.; HAO, F.; YAN, D.; LU, YONGCHAO. Volcanism-induced late Boda warming in the Late Ordovician: Evidence from the Upper Yangtze Platform, South China. *Palaeogeography, Palaeoclimatology, Palaeoecology*, v. 578, 2021.

LÚCIO, T.; MOURA, W. A. L.; ALBUQUERQUE, G. C. S.; SOUZA NETO, J. A. Tracing marine conditions in the Ipubi Black Shales, Araripe Basin, NE Brazil: An approach by chemical elements contents. **Journal of South American Earth Sciences**, v. 116, n. June, p. 103880, 2022.

LUO, H.; CHENG, Q.; PAN, X. Photochemical behaviors of mercury (Hg) species in aquatic systems: a systematic review on reaction process, mechanism, and influencing factor. **Science of The Total Environment**, v. 720, p. 137540, 2020.

MACKEY, J. E.; STEWART, B. W. Evidence of SPICE-related anoxia on the Laurentian passive margin: Paired  $\delta^{13}\text{C}$  and trace element chemostratigraphy of the upper Conasauga Group, Central Appalachian Basin. **Palaeogeography, Palaeoclimatology, Palaeoecology**, v. 528, p. 160–174, 2019.

MADHAVARAJU, J.; SCOTT, R. W.; SELVARAJ, K.; LEE, Y. IL; LÖSER, H. Isotopic chemostratigraphy and biostratigraphy of Lower Cretaceous Alisitos Formation (Punta China section), Baja California, Mexico. **Geological Journal**, v. 56, n. 5, p. 2550–2570, 2021.

MAISEY, J. G. Santana fossils: an illustrated atlas. Tropical Fish Hobbyist Publications, New Jersey, USA, p; 459, 1991.

MAISEY, J. G. Predator-prey relationships and trophic level reconstruction in a fossil fish community. **Environmental Biology of Fishes**. v. 40, p. 1 -22, 1994.

MALDANIS, L.; CARVALHO, M.; ALMEIDA, M. R.; FREITAS, F. I.; ANDRADE, J. A. F. G.; NUNES, R. S.; ROCHITTE, C. E.; POPPI, R. J.; FREITAS, R. O. et al. Heart fossilization is possible and informs the evolution of cardiac outflow tract in vertebrates. **Elife**, v. 5, p. e14698, 2016.

MANFROI, J.; DUTRA, T. L.; GNAEDINGER, S.; UHL, D.; JASPER, A. The first report of a Campanian palaeo-wildfire in the West Antarctic Peninsula. **Palaeogeography, Palaeoclimatology, Palaeoecology**, v. 418, p. 12–18, 2015.

MARTILL, D. M. Preservation of fish in the Cretaceous Santana Formation of Brazil. **Paleontology Association**, v. 31, p. 1–18, 1988.

MARTILL, D. M.; BRITO, P. M.; WASHINGTON-EVANS, J. Mass mortality of fishes in the Santana Formation (Lower Cretaceous, Albian) of northeast Brazil. **Cretaceous Research**, v. 29, n. 4, p. 649–658, 2008.

MARTILL, D. M.; LOVERIDGE, R. F.; ANDRADE, J. A. F. G. DE; CARDOSO, A. H. An unusual occurrence of amber in laminated limestones: the Crato Formation Lagerstätte (Early Cretaceous) of Brazil. **Palaeontology**, v. 48, n. 6, p. 1399–1408, 2005.

MARTILL, D. M.; LOVERIDGE, R.; HEIMHOFER, U. Halite pseudomorphs in the Crato Formation (Early Cretaceous, Late Aptian-Early Albian), Araripe Basin, northeast Brazil: further evidence for hypersalinity. **Cretaceous Research**, v. 28, n. 4, p. 613–620, 2007.

MARTINE, A. M. Reconstituições de cenários paleoambientais cretáceos: Membro Crato (Formação Santana, Bacia do Araripe) e Formação Adamantina (Bacia Bauru). 2013. Tese de Doutorado.

MARTINS NETO, R. G. Sistemática dos Ensifera Insecta, (Orthopteroida) da Formação Santana (Cretáceo inferior do nordeste do Brasil). 1991. Tese de Doutorado. Universidade de São Paulo.

MARTINS-NETO, R. G. Insetos fósseis como bioindicadores em depósitos sedimentares: um estudo de caso para o Cretáceo da Bacia do Araripe (Brasil). **Revista Brasileira de Zoociências**, v. 8, n. 2, p. 155–183, 2006.

MASON, E.; WIESER, P. E.; LIU, E. J.; EDMONDS, M.; ILYINSKAYA, E.; WHITTY, R. C. W.; MATHER, T. A.; ELIAS, T.; NADEAU, P. A.; WILKES, T. C.; McGONIGLE, A. J. S.; PERING, T. D.; MIMS, F. M.; KERN, C.; SCHNEIDER, D. J.; OPPENHEIMER, C. Volatile metal emissions from volcanic degassing and lava–seawater interactions at Kīlauea Volcano, Hawai’i. **Communications Earth & Environment**, v. 2, n. 1, p. 79, 2021.

MCCORMACK, J.; KWIECIEN, O. Coeval primary and diagenetic carbonates in lacustrine sediments challenge palaeoclimate interpretations. **Scientific Reports**, v. 11, n. 1, p. 7935, 2021.

MEHAY, S.; KELLER, C. E.; BERNASCONI, S. M.; WEISSERT, H.; ERBA, E.; BOTTINI, C.; HOCHULI, P. A. A volcanic CO<sub>2</sub> pulse triggered the Cretaceous Oceanic Anoxic Event 1a and a biocalcification crisis. **Geology**, v. 37, n. 9, p. 819–822, 2009.

MELO, R. M.; GUZMÁN, J.; ALMEIDA-LIMA, D.; PIOVESAN, E. K.; NEUMANN, V. H. DE M. L.; SOUSA, A. DE J. E. New marine data, and age accuracy of the Romualdo Formation, Araripe Basin, Brazil. **Scientific Reports**, v. 10, n. 1, p. 1–15, 2020.

MENDES, M.; BEZERRA, F. I.; ADAMI, K. Ecosystem Structure and Trophic Network in the Late Early Cretaceous Crato Biome. Edition: IANNUZZI, R.; KUNZMANN, L., *Em: Brazilian Paleofloras*. Cham: Springer International Publishing, 2020. p. 1–19.

MENON, F.; MARTILL, D. M. Taphonomy and preservation of Crato Formation arthropods. Edition: MARTIL, D. M.; BECHLY, G.; LOVERIDGE, R. F. *Em: The Crato Fossil Beds of Brazil: Window into an Ancient World*. Cambridge University Press, 2007. p. 79–96.

MERLI, M.; BONADIMAN, C.; PAVESE, A. Aluminium distribution in an Earth’s non-primitive lower mantle. **Geochimica et Cosmochimica Acta**, v. 276, p. 70–91, 2020.

MILLER, J. N.; MILLER, J. C. Statics and chemometrics for analytical chemistry. **Harlow, England: PEARSON**, 2010.

MILLERO, F. J. The Marine Inorganic Carbon Cycle. **Chemical Reviews**, v. 107, n. 2, p. 308–341, 2007.

MILOT, J.; BLICHERT-TOFT, J.; SANZ, M. A.; FETTER, N.; TÉLOUK, P.; ALBARÈDE, F. The significance of galena Pb model ages and the formation of large Pb-Zn sedimentary deposits. **Chemical Geology**, v. 583, 2021.

MIN-NA A.; ZHANG, F. Q.; YANG, S. F.; CHEN, H. L.; BATT, G. E.; SUN, M. D.; MENG, Q. A.; ZHU, D. F.; CAO, R. C.; LI, J. S. Early Cretaceous provenance change in the southern Hailar Basin, northeastern China and its implication for basin evolution. **Cretaceous Research**, v. 40, p. 21–42, 2013.

MOCHIUTTI, N. F.; GUIMARÃES, G. B.; MOREIRA, J. C.; LIMA, F. F.; FREITAS, F. I. Os valores da geodiversidade: Geossítios do Geopark Araripe/CE. **Anuário do Instituto de Geociências**, v. 35, n. 1, p. 173–189, 2012.

MONTERO-SERRANO, J. C.; FÖLLMI, K. B.; ADATTE, T.; SPANGENBERG, J. E.; TRIBOVILLARD, N.; FANTASIA, A.; SUAN, G. Continental weathering and redox conditions during the early Toarcian Oceanic Anoxic Event in the northwestern Tethys: Insight from the Posidonia Shale section in the Swiss Jura Mountains. **Palaeogeography, Palaeoclimatology, Palaeoecology**, v. 429, p. 83–99, 2015.

MORSE, J. W.; LUTHER III, G. W. Chemical influences on trace metal-sulfide interactions in anoxic sediments. **Geochimica et Cosmochimica Acta**, v. 63, n. 19-20, p. 3373-3378, 1999.

MULDER, E. W. A. On the piscivorous behaviour of the Early Cretaceous amiiform neopterygian fish *Calamopleurus cylindricus* from the Santana Formation, northeast Brazil. **Netherlands Journal of Geosciences - Geologie en Mijnbouw**, v. 92, n. 2–3, p. 119–122, 2013.

MURRAY, M. S.; MCROY, C. P.; DUFFY, L. K.; HIRONS, A. C.; SCHAAF, J. M.; TROCINE, R. P.; TREFRY, J. Biogeochemical analysis of ancient Pacific Cod bone suggests Hg bioaccumulation was linked to paleo sea level rise and climate change. **Frontiers in Environmental Science**, v. 3, p. 8, 2015.

MUSCENTE, A. D.; MARTINDALE, R.; SCHIFFBAUER, J. D.; CREIGHTON, A. L.; BOGAN, B. A. Exceptionally preserved fossil assemblages through geologic time and space. **Gondwana Research**, v. 48, p. 164-188, 2017.

MUSCENTE, A. D.; MARTINDALE, R. C.; SCHIFFBAUER, J. D.; CREIGHTON, A. L.; BOGAN, B. A. Taphonomy of the lower Jurassic Konservat-Lagerstätten at Ya Ha Tinda (Alberta, Canada) and its significance for exceptional fossil preservation during oceanic anoxic events. **PALAIOS**, v. 34, n. 11, p. 515–541, 2019.

NAAFS, B. D. A.; CASTRO, J. M.; GEA, G. A. DE; QUIJANO, M. L.; SCHMIDT, D. N.; PANCAST, R. D. Gradual, and sustained carbon dioxide release during Aptian Oceanic Anoxic Event 1a. **Nature Geoscience**, v. 9, n. 2, p. 135–139, 2016.

NANA YOBO, L.; HOLMDEN, C.; BRANDON, A. D.; LAU, K. V.; ELDRETT, J. S.; BERGMAN, S. LIP volcanism (not anoxia) tracked by Cr isotopes during Ocean Anoxic Event 2 in the proto-North Atlantic region. **Geochimica et Cosmochimica Acta**, v. 332, p. 138–155, 2022.

NASCIMENTO, D. R. DO; SILVA FILHO, W. F. DA; ERTHAL, F. Crato Lake Deposits. Rocks to Preserve an Extraordinary Fossil Lagerstätten. Edition: IANNUZZI, R.; KUNZMANN, L. Em: **Brazilian Paleofloras**. Cham: Springer International Publishing, 2023. p. 1–53, 2023

NASEMANN, P.; JANSSEN, D. J.; RICKLI, J.; GRASSE, P.; FRANK, M.; JACCARD, S. L. Chromium reduction and associated stable isotope fractionation restricted to anoxic shelf waters in the Peruvian Oxygen Minimum Zone. **Geochimica et Cosmochimica Acta**, v. 285, p. 207–224, 2020.

NESBITT, H. W.; YOUNG, G. M. Early Proterozoic climates and plate motions inferred from major element chemistry of lutites. **Nature**, v. 299, n. 5885, p. 715–717, 1982.

NEUMANN, V. H.; BORREGO, A. G.; CABRERA, L.; DINO, R. Organic matter composition and distribution through the Aptian-Albian lacustrine sequences of the Araripe Basin, northeastern Brazil. **International Journal of Coal Geology**, v. 54, n. 1–2, p. 21–40, 2003.

NEUMANN, V. H. M. L. **Estratigrafía, sedimentología, geoquímica y diagénesis de los sistemas lacustres Aptiense-Albienses de la cuenca de Araripe (noroeste de Brasil)**. Publicacions Universitat de Barcelona, 1999.

NEVES, B. D. B.; SCHMUS, W. R. VAN; SANTOS, E. J. DOS; CAMPOS NETO, M. C.; KOZUCH, M. o evento Carirís Velhos na Província Borborema: Integração de dados, implicações e perspectivas. **Revista Brasileira de Geociências**, v. 25, n. 4, p. 279–296, 1995.

NÚÑEZ-USECHE, F.; BARRAGÁN, R.; TORRES-MARTÍNEZ, M. A.; LÓPEZ-ZÚÑIGA, P. A.; MORENO-BEDMAR, J. A.; CHÁVEZ-CABELLO, G.; CANET, C.; CHACON-BACA, E. Response of the western proto-North Atlantic margin to the early Aptian oceanic anoxic event (OAE) 1a: an example from the Cupido platform margin-Gulf of Mexico, NE Mexico. **Cretaceous Research**, v. 113, p. 104448, 2020.

OGG, J. G.; OGG, G. M.; GRADSTEIN, F. **A concise geologic time scale**. Elsevier, 2016.

O'LEARY, M. H. Carbon isotope fractionation in plants. **Phytochemistry**, v. 20, n. 4, p. 553–567, 1981.

OSÉS, G. L.; PETRI, S.; BECKER- KERBER, B.; ROMERO, G. R.; RIZZUTTO, M. A.; RODRIGUES, F.; GALANTE, D.; SILVA, T. F.; CURADO, J. F.; RANGEL, E. C.; RIBEIRO, R. P.; ALVES, M. L. Deciphering the preservation of fossil insects: a case study from the Crato Member, Early Cretaceous of Brazil. **PeerJ**, v. 4, n. 12, p. e2756, 2016.

OSÉS, G. L. *et al.* Deciphering pyritization-kerogenization gradient for fish soft-tissue preservation. **Scientific Reports**, v. 7, n. 1, p. 1468, 2017.

OSTRANDER, C. M.; OWENS, J. D.; NIELSEN, S. G. Constraining the rate of oceanic deoxygenation leading up to a Cretaceous Oceanic Anoxic Event (OAE-2: ~ 94 Ma). **Science advances**, v. 3, n. 8, p. e1701020, 2017.

PARRY, L. A.; SMITHWICK, F.; NORDÉN, K. K.; SAITTA, E. T.; LOZANO-FERNANDEZ, J.; TANNER, A. R.; CARON, J.; EDGECOMBE, G. D.; BRIGGS, D. E. G.; VINTHER, J. Soft-Bodied Fossils Are Not Simply Rotten Carcasses – Toward a Holistic Understanding of Exceptional Fossil Preservation. **BioEssays**, v. 40, n. 1, 2018.

PAULA FREITAS, A. B. L.; BORGHI, L. Estratigrafia de alta resolução do intervalo siliciclástico Aptiano da Bacia do Araripe. **Geociências**, v. 30, n. 4, p. 529-543, 2011.

PEARSON, P. N. Oxygen Isotopes in Foraminifera: Overview and Historical Review. **The Paleontological Society Papers**. Cambridge University Press (CUP), 2012. v. 18p. 1–38.

PÊGAS, R. V; COSTA, F. R.; KELLNER, A. W. A. Reconstruction of the adductor chamber and predicted bite force in pterodactyloids (Pterosauria). **Zoological Journal of the Linnean Society**, v. 193, n. 2, p. 602–635, 2021.

PERCIVAL, L. M. E.; WITT, M. L. I.; MATHER, T. A.; HERMOSO, M.; JENKYNS, H. C.; HESSELBO, S. P.; AL-SUWAIDI, A. H.; STORM, M. S.; XU, W.; RUHL, M. Globally enhanced mercury deposition during the end-Pliensbachian extinction and Toarcian OAE: A link to the Karoo–Ferrar Large Igneous Province. **Earth and Planetary Science Letters**, v. 428, p. 267–280, 2015.

PEROPADRE, C.; LIESA, C. L.; MELÉNDEZ, N. High-frequency, moderate to high-amplitude sea-level oscillations during the late Early Aptian: Insights into the Mid-Aptian event (Galve sub-basin, Spain). **Sedimentary Geology**, v. 294, p. 233–250, 2013.

PESSENCIA, L. C. R.; GOUVEIA, S. E. M.; FREITAS, H. A. DE; RIBEIRO, A. D. S.; ARAVENA, R.; BANDASSOLLI, J. A.; LEDRU, M.-P.; SIFEDDINE, A.; SCHEEL-YBERT, R. Isótopos do Carbono e suas aplicações em estudos Paleoambientais. **Quaternário do Brasil**. Ribeirão Preto (SP): Holos, 2005.

PETRIZZO, M. R.; HUBER, B. T.; GALE, A. S.; BARCHETTA, A.; JENKYNS, H. C. Abrupt planktic foraminiferal turnover across the niveau kilian at col de pré-guittard (Vocontian Basin, southeast France): New criteria for defining the Aptian/Albian boundary. **Newsletters on Stratigraphy**, v. 45, n. 1, p. 55–74, 2012.

PEULVAST, J.-P.; BÉTARD, F. A history of basin inversion, scarp retreat and shallow denudation: The Araripe basin as a keystone for understanding long-term landscape evolution in NE Brazil. **Geomorphology**, v. 233, p. 20–40, 2015.

PEYSER, C. E.; POULSEN, C. J. Controls on Permo-Carboniferous precipitation over tropical Pangaea: A GCM sensitivity study. **Palaeogeography, Palaeoclimatology, Palaeoecology**, v. 268, n. 3–4, p. 181–192, 2008.

PINEDO-GONZÁLEZ, P.; WEST, A. J.; TOVAR- SÁNCHEZ, A.; DUARTE, C. M.; MARAÑÓN, E.; CERMEÑO, P.; GONZÁLEZ, N.; SOBRINO, C.; HUETE- ORTEGA, M.; FERNÁNDEZ, A.; LÓPEZ- SANDOVAL, D. C.; VIDAL, M.; BLASCO, D.; ESTRADA, M.; SAÑUDO- WILHELMY, S. A. Surface distribution of dissolved trace metals in the oligotrophic ocean and their influence on phytoplankton biomass and productivity. **Global Biogeochemical Cycles**, v. 29, n. 10, p. 1763–1781, 2015.

PINTO, I. D.; PURPER, I. A new Blattoid from the Cretaceous of Brazil. **Pesquisas em Geociências**, v. 18, n. 18, p. 5, 1986.

PONTE, F. C.; PONTE- FILHO, F. C. **Estrutura geológica e evolução tectônica da Bacia do Araripe**. Recife: Departamento Nacional da Produção Mineral, p. 68, 1996.

PONTES, N. V.; CHAGAS, D. B.; SOUZA, A. C. B.; NASCIMENTO JUNIOR, D. R.; SILVA FILHO, W. F.; CAPILLA, R.; GARCIA, A. J. V.; ARAÚJO, J. N. N. Organic and isotopic geochemistry of evaporites and shales of the Santana group (Araripe basin, Brazil): Clues on the evolution of depositional systems and global correlation during the lower cretaceous. **Minerals**, v. 11, n. 8, 2021.

POROPAT, S. F.; COLIN, J.-P. Early Cretaceous ostracod biostratigraphy of eastern Brazil and western Africa: An overview. **Gondwana Research**, v. 22, n. 3–4, p. 772–798, 2012.

LINDOSO, R. M.; CARVALHO, I. S. The Cretaceous fishes of Brazil: a paleobiogeographic perspective. Edition: Pradel, A.; John, S. S.; Janvier, P. Em: **Ancient Fishes and their Living Relatives**. München: Germany, p. 233–235, 2021.

PRADO, L. A. C. DO; CALADO, T. C. DOS S.; BARRETO, A. M. F. New records of shrimps from the Lower Cretaceous Romualdo Formation, Araripe Basin, northeastern Brazil, with new taxa of Penaeoidea (Crustacea: Decapoda: Dendrobranchiata). **Cretaceous Research**, v. 99, p. 96–103, 2019.

PRADO, L. A. C. DO; FAMBRINI, G. L.; BARRETO, A. M. F. Tafonomy of macroinvertebrates and Albian marine ingressions as recorded by the Romualdo Formation (Cretaceous, Araripe Basin, Brazil). **Brazilian Journal of Geology**, v. 48, n. 3, p. 519–531, 2018.

PRICE, L. I. Sobre um crocodilídeo notossuquio do Cretáceo Brasileiro. **Boletim da Divisão de Geologia e Mineralogia**, p. 1–56, 1959.

PRICE, L. I. A presença de pterosauria no Cretáceo Inferior da chapada do Araripe, Brasil. **Anais da Academia brasileira de Ciências**, v. 43, n. Supplement, p. 452-461, 1971.

PRICE, L. I. Quelônio amphichelydia no Cretáceo inferior do nordeste do Brasil. **Revista Brasileira de Geociências**, v. 3, n. 2, p. 84-95, 1973.

PYLE, D. M.; MATHER, T. A. The importance of volcanic emissions for the global atmospheric mercury cycle. **Atmospheric Environment**, v. 37, n. 36, p. 5115–5124, 2003.

RACKI, Grzegorz. Big 5 mass extinctions. Em: Elias S. and Alderton, D. Edição: **2º Encyclopedia of geology**, Elsevier, Amsterdam, p. 603-616, 2021.

RAMÍREZ- PÉREZ, A. M.; BLAS, E. DE. Iron reactivity in anoxic sediments in the Ría de Vigo (NW Spain). **Chemosphere**, v. 174, p. 8 – 19, 2017.

RAND, H. M.; MANSO, V. A. V. Levantamento gravimétrico e magnetométrico da Bacia do Araripe. In: **Congresso Brasileiro de Geologia**. 1984. p. 2011-2016.

RAUP, D. M. Biological Extinction in Earth History. **Thought**, v. 231, p. 1528–1533, 1986.

RAUP, D. M.; SEPkoski, J. J. Mass Extinctions in the Marine Fossil Record. **Science**, v. 215, n. 4539, p. 1501–1503, 1982.

REINHARD, C. T.; PLANAVSKY, N. J.; WANG, X.; FISCHER, W. W.; JOHNSON, T. M.; LYONS, T. W. The isotopic composition of authigenic chromium in anoxic marine sediments: A case study from the Cariaco Basin. **Earth and Planetary Science Letters**, v. 407, p. 9–18, 2014.

RIBEIRO, A. C.; POYATO-ARIZA, F. J.; VAREJÃO, F. G.; BOCKMANN, F. A. The branchial skeleton in Aptian chanid fishes (Gonorynchiformes) from the Araripe Basin (Brazil): Autecology and paleoecological implications. **Cretaceous Research**, v. 112, p. 104454, 2020.

RIBEIRO, A. C.; RIBEIRO, G. C.; VAREJÃO, F. G.; BATTIROLA, L. D.; PESSOA, E. M.; SIMÕES, M. G.; WARREN, L. V.; RICCOMINI, C.; POYATO-ARIZA, F. J. Towards an actualistic view of the Crato Konservat-Lagerstätte paleoenvironment: A new hypothesis as an Early Cretaceous (Aptian) equatorial and semi-arid wetland. **Earth-Science Reviews**, v. 216, p. 103573, 2021.

RINKLEBE, J.; SHAHEEN, S. M. Redox chemistry of nickel in soils and sediments: A review. **Chemosphere**, v. 179, p. 265–278, 2017.

RIOS-NETTO, A. D. M.; REGALI, M. D. S. P.; CARVALHO, I. D. S.; FREITAS, F. I. DE. Palinoestratigrafia do intervalo Alagoas da Bacia do Araripe, Nordeste do Brasil. **Revista Brasileira de Geociências**, v. 42, n. 2, p. 331–342, 2012.

RIVERA, H. A.; ROUX, J. P. LE; SÁNCHEZ, L. K.; MARIÑO-MARTÍNEZ, J. E.; SALAZAR, C.; BARRAGÁN, J. C. Palaeoredox conditions and sequence stratigraphy of the Cretaceous storm-dominated, mixed siliciclastic-carbonate ramp in the Eastern Cordillera Basin (Colombia): Evidence from sedimentary geochemical proxies and facies analysis. **Sedimentary Geology**, v. 372, p. 1–24, 2018.

ROBBINS, L. J.; FAKHRAEE, M.; SMITH, A. J. B.; BISHOP, B. A.; SWANNER, E. D.; PEACOCK, C. L.; WANG, C.; PLANAVSKY, N. J.; REINHARD, C. T.; CROWE, S. A.; LYONS, T. W. Manganese oxides, Earth surface oxygenation, and the rise of oxygenic photosynthesis. **Earth-Science Reviews**, v. 239, p. 104368, 2023.

ROBIN, E.; RABOUILLE, C.; MARTINEZ, G.; LEFEVRE, I.; REYSS, J. L.; BEEK, P. VAN; JEANDEL, C. Direct barite determination using SEM/EDS-ACC system: implication for constraining barium carriers and barite preservation in marine sediments. **Marine Chemistry**, v. 82, n. 3–4, p. 289–306, 2003.

ROBOCK, A. Volcanic eruptions and climate. **Reviews of Geophysics**, v. 38, n. 2, p. 191–219, 2000.

RODEN, E. E.; LEONARDO, M. R.; FERRIS, F. G. Immobilization of strontium during iron biomineralization coupled to dissimilatory hydrous ferric oxide reduction. **Geochimica et Cosmochimica Acta**, v. 66, n. 16, p. 2823–2839, 2002.

RODRÍGUEZ-CUICAS, M. E.; MONTERO-SERRANO, J. C.; GARBÁN, G. Paleoenvironmental changes during the late Albian oceanic anoxic event 1d: An example from the Capacho Formation, southwestern Venezuela. **Palaeogeography, Palaeoclimatology, Palaeoecology**, v. 521, p. 10–29, 2019.

RUDDIMAN, W. F. Insolation Control of Ice Sheets. *Em: RUDDIMAN, W. Earth's Climate*, 2008. v. 2°Ed., p. 161–170.

SAAD, E. M.; WANG, X.; PLANAVSKY, N. J.; REINHARD, C. T.; TANG, Y. Redox-independent chromium isotope fractionation induced by ligand-promoted dissolution. **Nature Communications**, v. 8, n. 1, p. 1590, 2017.

SABATINO, N.; COCCIONI, R.; SALVAGIO MANTA, D.; BAUDIN, F.; VALLEFUOCO, M.; TRAINA, A.; SPROVIERI, M. High-resolution chemostratigraphy of the late Aptian-early Albian oceanic anoxic event (OAE 1b) from the Poggio le Guaine section (Umbria-Marche Basin, central Italy). **Palaeogeography, Palaeoclimatology, Palaeoecology**, v. 426, p. 319–333, 2015.

SABATINO, N.; FERRARO, S.; COCCIONI, R.; BONSIGNORE, M.; CORE, M. DEL; TANCREDI, V.; SPROVIERI, M. Mercury anomalies in upper Aptian-lower Albian sediments from the Tethys realm. **Palaeogeography, Palaeoclimatology, Palaeoecology**, v. 495, n. January, p. 163–170, 2018.

SALGADO, F. L. K.; CARVALHO, I. DE S. Cannibal predatory habits and their relationships with body shape and swimming pattern in the Cretaceous fish *Dastilbe crandalli* Jordan, 1910 from the Araripe Basin, Northeastern Brazil. **Cretaceous Research**, v. 152, p. 105685, 2023.

SALGADO-CAMPOS, V. M. J.; CARVALHO, I. DE S.; BERTOLINO, L. C.; DUARTE, T. A.; ARAÚJO, B. C.; BORGHI, L. Clay mineralogy and lithogeochemistry of lutites from the Lower Cretaceous Crato Member, Araripe Basin, NE Brazil: Implications for paleoenvironmental, paleoclimatic and provenance reconstructions. **Journal of South American Earth Sciences**, v. 110, p. 103329, 2021.

SALOMONS, W.; FORSTNER, U. Metals in the Hydrocycle. **Journal of Applied Ecology**, v. 22, n. 3, p. 1028, 1985.

SANEI, H.; GRASBY, S. E.; BEAUCHAMP, B. Latest permian mercury anomalies. **Geology**, v. 40, n. 1, p. 63–66, 2012.

SANTOS, Â. C. S. DOS; GUERRA-SOMMER, M.; DEGANI-SCHMIDT, I.; SIEGLOCH, A. M.; CARVALHO, I. S.; MENDONÇA FILHO, J. G.; MENDONÇA, J. DE O. Fungus–plant interactions in Aptian Tropical Equatorial Hot arid belt: White rot in araucarian wood from the Crato fossil Lagerstätte (Araripe Basin, Brazil). **Cretaceous Research**, v. 114, p. 104525, 2020.

SANTOS, Â. C. S.; SIEGLOCH, A. M.; GUERRA-SOMMER, M.; DEGANI-SCHMIDT, I.; CARVALHO, I. *Agathoxylon santanensis* sp. nov. from the Aptian Crato fossil Lagerstätte, Santana Formation, Araripe Basin, Brazil. **Journal of South American Earth Sciences**, v. 112, p. 103633, 2021.

SANTOS, F. H. DOS; SILVA AMARAL, W. DA; CHI-FRU, E.; SOUZA, A. C. B. DE; BOSCO-SANTOS, A. Paleoproterozoic manganese oxide precipitation in oxic seawater surface and reductive enrichment in anoxic seafloor. **Chemical Geology**, v. 588, 2022.

SILVA SANTOS, R. *Santanichthys*, Novo Epíteto Générico para *Leptolepis diasii* Silva Santos, 1958 (Pisces-Teleostei) da Formação Santana (Aptiano), Bacia do Araripe, NE do Brasil. **Anais da Academia brasileira de Ciências**, v. 67, n. 2, p. 249-258, 1995.

SAUCEDO-SAMANIEGO, J. C.; MADHAVARAJU, J.; SIAL, A. N.; MONREAL, R.; SCOTT, R. W.; PEREZ-ARVIZU, O. Upper Aptian-lower albian seawater composition and OAEs: Geochemistry of Agua Salada and Lampazos Formations, Sonora, Mexico. **Journal of South American Earth Sciences**, v. 109, p. 103193, 2021.

SAYÃO, J. M.; SARAIVA, A. A. F.; BRUM, A. S.; BANTIM, R. A. M.; ANDRADE, R. C. L. P. DE; CHENG, X.; LIMA, F. J. DE; PAULA SILVA, H. DE; KELLNER, A. W. A. The first theropod dinosaur (Coelurosauria, Theropoda) from the base of the Romualdo Formation (Albian), Araripe Basin, Northeast Brazil. **Scientific Reports**, v. 10, n. 1, p. 10892, 2020.

SCHERER, C. M. S.; GOLDBERG, K.; BARDOLA, T. Facies architecture and sequence stratigraphy of an early post-rift fluvial succession, Aptian Barbalha Formation, Araripe Basin, northeastern Brazil. **Sedimentary Geology**, v. 322, p. 43–62, 2015.

SCOTESE, C. R.; SONG, H.; MILLS, B. J. W.; MEER, D. G. V. Phanerozoic paleotemperatures: The earth's changing climate during the last 540 million years. **Earth-Science Reviews**, v. 215, p. 103503, 2021.

SHEN, J.; CHEN, J.; ALGEO, T. J.; YUAN, S.; FENG, Q.; YU, J.; ZHOU, L.; O'CONNELL, B.; PLANAVSKY, N. J. Evidence for a prolonged Permian–Triassic extinction interval from global marine mercury records. **Nature Communications**, v. 10, n. 1, p. 1563, 2019.

SHEN, J.; SCHOEPPER, S. D.; FENG, Q.; ZHOU, L.; YU, J.; SONG, H.; WEI, H.; ALGEO, T. J. Marine productivity changes during the end-Permian crisis and Early Triassic recovery. **Earth-Science Reviews**, v. 149, p. 136-162, 2015.

SHOOP, W.; TILSON, E. Plunge diving by Brown Pelicans resembles a Split-S Turn. **Journal of Field Ornithology**, v. 93, n. 1, 2022.

SIAL, A. N. CHEN, J.; LACERDA, L. D.; FREI, R.; TEWARI, V. C.; PANDIT, M. K.; GAUCHER, C.; FERREIRA, V. P.; CIRILLI, S.; PERALTA, S.; KORTE, C.; BARBOSA, J. A. PEIREIRA, N. S. Mercury enrichment and Hg isotopes in Cretaceous–Paleogene boundary successions: Links to volcanism and palaeoenvironmental impacts. **Cretaceous Research**, v. 66, p. 60–81, 2016.

SIAL, A. N. CHEN, J.; LACERDA, L. D.; FREI, R.; HIGGINS, J. A.; TEWARI, V. C.; GAUCHER, C.; FERREIRA, V. P.; CIRILLI, S.; KORTE, C.; BARBOSA, J. A.; PEREIRA, N. S.; RAMOS, D. S. Chemostratigraphy Across the Cretaceous-Paleogene (K-Pg) Boundary: Testing the Impact and Volcanism Hypotheses. **Chemostratigraphy Across Major Chronological Boundaries**, p. 223-257, 2018.

SIAL, A. N.; CHEN, J.; KORTE, C.; PANDIT, M. K.; SPANGENBERG, J. E.; SILVA-TAMAYO, J. C.; LACERDA, L. D.; FERREIRA, V. P.; BARBOSA, J. A.; GAUCHER, C.; PEREIRA, N. S.; RIEDEL, P. R. Hg Isotopes and Enhanced Hg Concentration in the

Meishan and Guryul Ravine Successions: Proxies for Volcanism Across the Permian-Triassic Boundary. **Frontiers in Earth Science**, v. 9, p. 651224, 2021.

SIAL, A. N.; GAUCHER, C.; FILHO, M. A. DA S.; FERREIRA, V. P.; PIMENTEL, M. M.; LACERDA, L. D.; FILHO, E. V. S.; CEZARIO, W. C., Sr-isotope and Hg chemostratigraphy of Neoproterozoic cap carbonates of the Sergipano Belt, Northeastern Brazil. **Precambrian Research**, v. 182, n. 4, p. 351–372, 2010.

SIAL, A. N.; LACERDA, L. D.; FERREIRA, V. P.; FREI, R.; MARQUILLAS, R. A.; BARBOSA, J. A.; GAUCHER, C.; WINDMÖLLER, C. C.; PEREIRA, N. S. Mercury as a proxy for volcanic activity during extreme environmental turnover: The Cretaceous–Paleogene transition. **Palaeogeography, Palaeoclimatology, Palaeoecology**, v. 387, p. 153–164, 2013.

SILVA, V. R. DA; VAREJÃO, F. G.; MATOS, S. A.; RODRIGUES, M. G.; FÜRSICH, F. T.; SKAWINA, A.; SCHNEIDER, S.; WARREN, L. V.; ASSINE, M. L.; SIMÕES, M. G. New freshwater mussels (Bivalvia, Unionida) with potential trigonoidid and hyriid affinities from the Early Cretaceous of Brazil. **Geobios**, v. 61, p. 41–54, 2020.

SILVEIRA, A. C.; VAREJÃO, F. G.; NEUMANN, V. H.; SIAL, A. N.; ASSINE, M. L.; FERREIRA, V. P.; FAMBRINI, G. L. Quimioestratigrafia de Carbono e Oxigênio dos Carbonatos Lacustres Aptianos da Serra do Toná, Sub-Bacia de Tucano Norte, NE do Brasil. **Estudos Geológicos**, v. 24, n. 2, p. 47–63, 2014.

SILVESTRE, D. D. C.; FAMBRINI, G. L.; COSTA, I. C. DA. Análise Faciológica, Sistemas Deposicionais e Estratigrafia de Sequências da Formação Barbalha (Aptiano Superior), Bacia do Araripe: Dados de Testemunhos de Sondagem. **Anuário do Instituto de Geociências**, v. 43, n. 4, p. 34–47, 2020.

SINHA, S.; MUSCENDE, A. D.; SCHIFFBAUER, J. D.; WILLIAMS, M.; SCHWEIGERT, G.; MARTINDALE, R. C. Global controls on phosphatization of fossils during the Toarcian Oceanic Anoxic Event. **Scientific Reports**, v. 11, n. 1, p. 24087, 2021.

SOUA, M.; ZAGHBIB-TURKI, D.; JEMIA, H. BEN; SMAOUI, J.; BOUKADI, A. Geochemical Record of the Cenomanian-Turonian Anoxic Event in Tunisia: Is it Correlative and Isochronous to the Biotic Signal? **Acta Geologica Sinica - English Edition**, v. 85, n. 6, p. 1310–1335, 2011.

SOUZA-LIMA, W.; SILVA, R. O. Aptian-Albian paleophytogeography and paleoclimatology from Northeastern Brazil sedimentary basins. **Review of palaeobotany and palynology**, v. 258, p. 163–189, 2018.

STEIN, M.; FÖLLMI, K. B.; WESTERMANN, S.; GODET, A.; ADATTE, T.; MATERA, V.; FLEITMANN, D.; BERNER, Z. Progressive palaeoenvironmental change during the Late Barremian-Early Aptian as prelude to Oceanic Anoxic Event 1a: Evidence from the Gorgo a Cerbara section (Umbria-Marche basin, central Italy). **Palaeogeography, Palaeoclimatology, Palaeoecology**, v. 302, n. 3–4, p. 396–406, 2011.

STEINER, Z.; LAZAR, B.; TORFSTEIN, A.; EREZ, J. Testing the utility of geochemical proxies for paleoproductivity in oxic sedimentary marine settings of the Gulf of Aqaba, Red Sea. **Chemical Geology**, v. 473, p. 40–49, 2017.

STORARI, A. P.; RODRIGUES, T.; BANTIM, R. A. M.; LIMA, F. J.; SARAIVA, A. A. F. Mass mortality events of autochthonous faunas in a Lower Cretaceous Gondwanan Lagerstätte. **Scientific Reports**, v. 11, n. 1, p. 6976, 2021.

SUN, Y. D.; WIGNALL, P. B.; JOACHIMSKI, M. M.; BOND, D. P. G.; GRASBY, S. E.; SUN, S.; YAN, C. B.; WANG, L. N.; CHEN, Y. L.; LAI, X. L. High amplitude redox changes in the late Early Triassic of South China and the Smithian-Spathian extinction. **Palaeogeography, Palaeoclimatology, Palaeoecology**, v. 427, p. 62–78, 2015.

SWART, P. K. The geochemistry of carbonate diagenesis: The past, present and future. **Sedimentology**, v. 62, n. 5, p. 1233–1304, 2015.

TANG, L.; SONG, Y.; JIANG, S.; JIANG, Z.; LI, Z.; YANG, Y.; LI, X.; XIAO, L. Organic matter accumulation of the Wufeng-Longmaxi shales in southern Sichuan Basin: Evidence and insight from volcanism. **Marine and Petroleum Geology**, v. 120, p. 104564, 2020.

TEDESCHI, L. R.; JENKYN, H. C.; ROBINSON, S. A.; LANA, C. C.; MENEZES SANTOS, M. R. F.; TOGNOLI, F. M. W. Aptian carbon-isotope record from the Sergipe-Alagoas Basin: New insights into oceanic anoxic event 1a and the timing of seawater entry into the South Atlantic. **Newsletters on Stratigraphy**, v. 53, n. 3, p. 333–364, 2020.

TEIXEIRA, M. C.; MENDONÇA FILHO, J. G.; OLIVEIRA, A. D. DE; ASSINE, M. L. Faciologia orgânica da Formação Romualdo (Grupo Santana, Cretáceo Inferior da Bacia do Araripe): caracterização da matéria orgânica sedimentar e interpretação paleoambiental. **Geologia USP. Série Científica**, v. 17, n. 4, p. 19, 2018.

THIBODEAU, A. M.; RITTERBUSH, K.; YAGER, J. A.; WEST, A. J.; IBARRA, Y.; BOTTJER, D. J.; BERELSON, W. M.; BERGQUIST, B. A.; CORSETTI, F. A. Mercury anomalies and the timing of biotic recovery following the end-Triassic mass extinction. **Nature Communications**, v. 7, p. 1–8, 2016.

TOUATI, Z.; HAJI, T. A. Redox, productivity and paleotectonic studies in the southern Tethyan margin of northern Tunisia. **Marine and Petroleum Geology**, v. 99, p. 310–322, 2019.

TRIBOVILLARD, N.; ALGEO, T. J.; LYONS, T.; RIBOULLEAU, A. Trace metals as paleoredox and paleoproductivity proxies: An update. **Chemical Geology**, v. 232, n. 1–2, p. 12–32, 2006.

TRIBOVILLARD, N. et al. Geochemical study of organic-matter rich cycles from the Kimmeridge Clay Formation of Yorkshire (UK): productivity versus anoxia. **Palaeogeography, Palaeoclimatology, Palaeoecology**, v. 108, n. 1-2, p. 165-181, 1994.

TUREKIAN, K. K.; WEDEPOHL, K. H. Distribution of the Elements in Some Major Units of the Earth's Crust. **Geological Society of America Bulletin**, v. 72, n. 2, p. 175–192, 1961.

TYSON, R. The nature of organic matter in sediments. **Sedimentary Organic Matter: Organic Facies and Palynofacies**, p. 7-28, 1995.

TYSON, R. V.; PEARSON, T. H. Modern, and ancient continental shelf anoxia: an overview. **Geological Society, London, Special Publications**, v. 58, n. 1, p. 1-24, 1991.

VALENÇA, L. M. M.; NEUMANN, V. H.; MABESOONE, J. M. An overview on Callovian-Cenomanian intracratonic basins of Northeast Brazil: Onshore stratigraphic record of the opening of the southern Atlantic. **Geologica Acta**, v. 1, n. 3, p. 261–275, 2003.

VALLEJO, J. D.; PIOVESAN, E. K.; ARAUJO CARVALHO, M. DE; GUZMÁN, J. Palynofacies analyses of Santana Group, upper Aptian of the Araripe Basin, northeast Brazil: Paleoenvironmental reconstruction. **Journal of South American Earth Sciences**, v. 121, p. 104154, 2023.

VAREJÃO, F. G.; FÜRSICH, F. T.; WARREN, L. V.; MATOS, S. A.; RODRIGUES, M. G.; ASSINE, M. L.; SALES, A. M. F.; SIMÕES, M. G. Microbialite fields developed in a protected rocky coastline: The shallow carbonate ramp of the Aptian Romualdo Formation (Araripe Basin, NE Brazil). **Sedimentary Geology**, v. 389, p. 103–120, 2019.

VAREJÃO, FILIPE GIOVANINI; SILVA, V. R.; ASSINE, M. L.; WARREN, L. V.; MATOS, S. A.; RODRIGUES, M. G.; FÜRSICH, F. T.; SIMÕES, M. G. Marine or freshwater? Accessing the paleoenvironmental parameters of the Caldas Bed, a key marker bed in the Crato Formation (Araripe Basin, NE Brazil). **Brazilian Journal of Geology**, v. 51, n. 1, p. e2020009, 2021.

VAREJÃO, F. G.; WARREN, L. V.; PERINOTTO, J. A. DE J.; NEUMANN, V. H.; FREITAS, B. T.; ALMEIDA, R. P. DE; ASSINE, M. L. Upper Aptian mixed carbonate-siliciclastic sequences from Tucano Basin, Northeastern Brazil: Implications for paleogeographic reconstructions following Gondwana break-up. **Cretaceous Research**, v. 67, p. 44–58, 2016.

VAREJÃO, FILIPE G.; WARREN, L. V.; SIMÕES, M. G.; BUATOIS, L. A.; MÁNGANO, M. G.; BAHNIUK RUMBELSPERGER, A. M.; ASSINE, M. L. Mixed siliciclastic–carbonate sedimentation in an evolving epicontinental sea: Aptian record of marginal marine settings in the interior basins of north-eastern Brazil. **Sedimentology**, v. 68, n. 5, p. 2125–2164, 2021.

VAREJÃO, FILIPE G.; WARREN, L. V.; SIMÕES, M. G.; FÜRSICH, F. T.; MATOS, S. A.; ASSINE, M. L. Exceptional preservation of soft tissues by microbial entombment: Insights into the taphonomy of the Crato Konservat-Lagerstätte. **Palaios**, v. 34, n. 7, p. 331–348, 2019.

WALKER-TRIVETT, C.; KENDER, S.; BOGUS, K.; LITTLER, K.; EDWARDSEN, T.; LENG BRITISH GEOLOGICAL SURVEY JACK LACEY BRITISH, M. Oceanic Anoxic Event 2 triggered by Kerguelen Plateau volcanism, v. 15, p. 5154, 2024.

WANG, Y.; BODIN, S.; BLUSZTAJN, J. S.; ULLMANN, C.; NIELSEN, S. G. Orbitally paced global oceanic deoxygenation decoupled from volcanic CO<sub>2</sub> emission during the middle Cretaceous Oceanic Anoxic Event 1b (Aptian-Albian transition). **Geology**, v. 50, n. 11, p. 1324–1328, 2022.

WARREN, L. V.; VAREJÃO, F. G.; QUAGLIO, F.; SIMÕES, M. G.; FÜRSICH, F. T.; POIRÉ, D. G.; CATTO, B.; ASSINE, M. L. Stromatolites from the Aptian Crato Formation, a hypersaline lake system in the Araripe Basin, northeastern Brazil. **Facies**, v. 63, n. 1, p. 1-19, 2017.

WEBER, T.; ALLARD, T.; BENEDETTI, M. F. Iron speciation in interaction with organic matter: Modelling and experimental approach. **Journal of Geochemical Exploration**, v. 88, n. 1-3 SPEC. ISS., p. 166–171, 2006.

WEDEPOHL, K. H. The composition of the continental crust. **Geochimica et Cosmochimica Acta**, v. 59, n. 7, p. 1217-1232, 1995.

WEI, W.; ALGEO, T. J. Elemental proxies for paleosalinity analysis of ancient shales and mudrocks. **Geochimica et Cosmochimica Acta**, v. 287, p. 341–366, 15 out. 2020.

WEISSERT, H.; ERBA, E. Volcanism, CO<sub>2</sub> and palaeoclimate: a Late Jurassic–Early Cretaceous carbon and oxygen isotope record. **Journal of the Geological Society**, v. 161, n. 4, p. 695–702, 2004.

WEISSERT, H.; LINI, A.; FÖLLMI, K. B.; KUHN, O. Correlation of Early Cretaceous carbon isotope stratigraphy and platform drowning events: a possible link? **Palaeogeography, Palaeoclimatology, Palaeoecology**, v. 137, n. 3–4, p. 189–203, 1998.

WILBY, P. R.; MARTILL, D. M. Fossil Fish Stomachs: A Microenvironment for Exceptional Preservation. **Historical Biology**, v. 6, n. 1, p. 25–36, 1992.

WILKIN, R. T.; BARNES, H. L.; BRANTLEY, S. L. The size distribution of frambooidal pyrite in modern sediments: An indicator of redox conditions. **Geochimica et Cosmochimica Acta**, v. 60, n. 20, p. 3897–3912, 1996.

WITTON, Mark P.; NAISH, Darren. Azhdarchid pterosaurs: water-trawling pelican mimics or “terrestrial stalkers”? **Acta Palaeontologica Polonica**, v. 60, n. 3, p. 651-660, 2013.

WU, F.; OWENS, J. D.; HUANG, T.; SARAFIAN, A.; HUANG, K.-F.; SEN, I. S.; HORNER, T. J.; MORTON, P.; NIELSEN, S. G. Vanadium isotope composition of seawater. **Geochimica et Cosmochimica Acta**, v. 244, p. 403-415, 2019.

WU, F.; OWENS, J. D.; SCHOLZ, F.; HUANG, L.; LI, S.; RIEDINGER, N.; PETERSON, L. C.; GERMAN, C. R.; NIELSEN, S. G. Sedimentary vanadium isotope signatures in low oxygen marine conditions. **Geochimica et Cosmochimica Acta**, v. 284, p. 134–155, 2020.

WU, X.; LUO, H.; ZHANG, J.; CHEN, Q.; FANG, X.; WANG, W.; LI, W.; SHI, Z.; ZHANG, Y. Volcanism-driven marine eutrophication in the end-Ordovician: Evidence from radiolarians and trace elements of black shale in South China. **Journal of Asian Earth Sciences**, v. 253, p. 105687, 2023.

XU, X.; SHAO, L.; ERIKSSON, K. A.; ZHOU, J.; WANG, D.; HOU, H.; HILTON, J.; WANG, S.; LU, J.; JONES, T. P. Widespread wildfires linked to early Albian Ocean Anoxic Event 1b: Evidence from the Fuxin lacustrine basin, NE China. **Global and Planetary Change**, v. 215, p. 103858, 2022.

XU, X. T.; SHAO, L. Y.; ERIKSSON, K. A.; PANG, B.; WANG, S.; YANG, C. X.; HOU, H. H. Terrestrial records of the early Albian Ocean Anoxic Event: Evidence from the Fuxin lacustrine basin, NE China. **Geoscience Frontiers**, v. 13, n. 1, p. 101275, 2022.

YEOMANS, J. C.; BREMNER, J. M. A rapid and precise method for routine determination of organic carbon in soil. **Communications in soil science and plant analysis**, v. 19, n. 13, p. 1467–1476, 1988.

ZHANG, P. *et al.* Middle Jurassic terrestrial environmental and floral changes linked to volcanism: Evidence from the Qinghai-Tibet Plateau, China. **Global and Planetary Change**, v. 223, p. 104094, 2023.

ZHOU, Y.; LI, Y.; ZHENG, W.; TANG, S.; PAN, S.; CHEN, J.; HE, X.-F.; SHEN, J.; ALGEO, T. J. The role of LIPs in Phanerozoic mass extinctions: An Hg perspective. **Earth-Science Reviews**, v. 249, p. 104667, 2024.

ZOU, C.; MAO, L.; SHAN, S.; ZHAOCHENG, S.; MO, D. Holocene Environmental Evolution Response to the Human Activities and East Asian Summer Monsoon Variation in the Liangzhu Ancient City Complex, Eastern China. **Frontiers in Marine Science**, v. 9, p. 910125, 2022.

## Material Suplementar- CAPÍTULO 1

Tabela 1. Valores dos indicadores geoquímicos de aportes detriticos, vulcanismo, paleosalinidade, estado redox e paleoprodutividade na Formação Barbalha.

Formação	Amostra	Hg (ng g <sup>-1</sup> )	TOC (%)	Al (%)	Hg/TOC	Sr/Ba	V/Cr	V/V+Ni	V/Ni	Pb <sup>EF</sup>	Mn <sup>EF</sup>	V <sup>EF</sup>	Cr <sup>EF</sup>	Fe <sup>EF</sup>	Cu <sup>EF</sup>	Ni <sup>EF</sup>	Zn <sup>EF</sup>	Ba <sup>EF</sup>
Barbalha (camada Batateira)	8.1A	12.4	1,9	6,9	6,5	0,05	6,4	0,82	4,6	0,62	0,27	2,1	0,25	1,1	2,3	0,79	0,91	0,32
	8.1B	3,9	1,6	5,3	2,5	0,05	5,7	0,82	4,7	0,42	0,37	1,9	0,26	1,2	1,7	0,71	1,0	0,29
	8.2A	10,4	2,4	7,1	4,3	0,06	5,2	0,79	3,9	2,0	0,58	2,0	0,29	1,1	3,4	0,88	1,5	0,26
	8.2B	11,0	2,1	6,2	5,4	0,08	6,5	0,81	4,1	1,7	0,37	2,3	0,28	1,2	3,6	0,99	1,3	0,19
	17B	16,6	1,7	8,9	9,6	0,06	5,5	0,80	3,9	0,87	0,43	1,3	0,18	0,68	2,1	0,56	0,79	0,16
	17A	43,6	3,3	0,72	13,3	1,4	8,2	0,75	3,0	59,9	34	5,5	0,52	2,9	44	3,2	59	1,2
	18	13,3	1,4	4,1	9,3	0,07	5,4	0,78	3,5	1,3	0,90	2,4	0,35	1,9	5,0	1,2	2,4	0,44
	19B	5,1	0,9	3,7	5,3	0,39	3,6	0,67	2,0	2,9	0,27	0,48	0,10	0,28	0,74	0,41	7,2	0,04
	19A	30,6	1,5	6,4	20,2	0,03	4,7	0,80	4,0	0,62	0,38	1,9	0,31	1,0	2,4	0,82	1,0	0,19
	20	3,5	0,4	4,2	8,1	0,04	2,2	0,67	2,0	0,65	0,49	1,3	0,44	2,2	1,6	1,08	1,4	0,35
	21B	3,9	0,3	2,5	12,2	0,50	2,9	0,83	4,7	0,69	3,1	2,1	0,54	0,92	0,91	0,75	1,1	0,12
	21A	2,7	0,4	5,5	6,4	0,09	5,5	0,75	2,9	0,33	0,34	1,6	0,23	1,6	1,4	0,94	1,2	0,17
	22	3,6	0,3	3,0	11,9	0,19	2,3	0,78	3,5	1,3	0,03	0,47	0,16	0,22	0,60	0,23	0,45	0,05

**Tabela 2.** Matriz de correlação de Spearman para os metais estudados na Formação Barbalha. Os valores em negrito são significativos ( $p < 0,05$ ;  $n=13$ ).

	Al	Fe	Mn	Cu	Zn	Ni	Pb	Cr	Sr	V	Ba	Hg	TOC	Hg/TOC	Sr/Ba
Al	1	<b>0,62</b>	<b>-0,58</b>	0,17	<b>-0,50</b>	<b>0,76</b>	<b>-0,42</b>	<b>0,81</b>	<b>-0,57</b>	<b>0,79</b>	<b>0,58</b>	-0,18	0,12	<b>-0,58</b>	<b>-0,74</b>
Fe		1	-0,35	0,29	-0,41	<b>0,91</b>	-0,35	<b>0,77</b>	-0,33	<b>0,75</b>	<b>0,82</b>	-0,18	<b>0,54</b>	<b>-0,46</b>	<b>-0,62</b>
Mn			1	<b>0,55</b>	<b>0,77</b>	-0,27	<b>0,87</b>	-0,39	<b>0,98</b>	-0,27	-0,13	<b>0,76</b>	<b>0,58</b>	0,24	<b>0,93</b>
Cu				1	0,47	<b>0,52</b>	<b>0,68</b>	0,26	<b>0,59</b>	<b>0,52</b>	<b>0,54</b>	<b>0,72</b>	<b>0,91</b>	-0,10	0,31
Zn					1	-0,30	0,9	<b>-0,57</b>	<b>0,83</b>	-0,35	-0,2	<b>0,63</b>	<b>0,65</b>	-0,04	<b>0,83</b>
Ni						1	-0,18	<b>0,83</b>	-0,26	<b>0,92</b>	<b>0,81</b>	0,03	<b>0,66</b>	-0,41	<b>-0,55</b>
Pb							1	<b>-0,41</b>	<b>0,93</b>	-0,19	-0,09	<b>0,75</b>	<b>0,76</b>	0,06	<b>0,85</b>
Cr								1	-0,46	<b>0,81</b>	<b>0,70</b>	-0,09	0,09	-0,19	<b>-0,65</b>
Sr									1	-0,26	-0,01	<b>0,76</b>	<b>0,64</b>	0,17	<b>0,92</b>
V										1	<b>0,79</b>	0,07	<b>0,72</b>	-0,35	<b>-0,52</b>
Ba											1	0,09	<b>0,70</b>	<b>-0,43</b>	-0,42
Hg												1	<b>0,72</b>	<b>0,47</b>	<b>0,62</b>
TOC													1	-0,19	0,42
Hg/TOC														1	0,26
Sr/Ba															1

**Tabela 3.** Valores dos indicadores geoquímicos de aportes detriticos, vulcanismo, paleosalinidade, estado redox e paleoprodutividade na Formação Barbalha.

FORMAÇÃO	Amostra	Hg (ng g <sup>-1</sup> )	TOC (%)	Hg/TOC	Al (%)	Sr/Ba	V/Cr	V/V+Ni	V/Ni	Pb <sup>EF</sup>	Mn <sup>EF</sup>	V <sup>EF</sup>	Cr <sup>EF</sup>	Fe <sup>EF</sup>	Cu <sup>EF</sup>	Ni <sup>EF</sup>	Zn <sup>EF</sup>	Ba <sup>EF</sup>
FORMAÇÃO CRATO	<b>12</b>	19,8	0,63	31,5	6,7	0,08	2,6	0,58	1,4	1,05	0,30	0,64	0,19	0,93	2,1	0,80	2,6	0,12
	<b>11E</b>	12,5	0,45	27,7	0,02	0,31	2,3	0,86	6,4	572	1,989	229	76,4	44,6	348	63,1	816	138
	<b>11D</b>	9,7	0,42	23,2	2,5	0,24	8,8	0,83	5,0	3,73	3,4	2,7	0,24	0,82	5,9	0,94	88,7	0,89
	<b>11C</b>	34,2	0,32	107	0,04	0,68	5,3	0,86	5,9	4,245	889	168	24,7	164	679	49,8	1,359	29,7
	<b>11B</b>	9,9	0,26	38,1	0,69	0,50	6,4	0,87	6,4	7,93	172	7,3	0,88	1,1	22,7	1,9	348	2,1
	<b>11A</b>	8,1	0,59	13,7	6,3	0,36	3,4	0,73	2,7	1,01	0,50	1,5	0,34	1,0	4,2	0,96	30,1	0,10
	<b>5A</b>	2,5	0,8	3,1	6,1	0,20	2,8	0,68	2,1	1,20	0,93	0,76	0,21	0,64	1,0	0,63	4,3	0,15
	<b>5B</b>	1,6	0,78	1,9	4,5	0,25	10,8	0,80	4,0	0,84	5,7	1,2	0,08	1,2	0,69	0,51	8,6	0,64
	<b>5C</b>	1,2	0,95	1,2	8,3	0,07	3,5	0,68	2,1	0,50	0,51	0,59	0,13	0,52	0,76	0,49	4,4	0,15
	<b>5D</b>	3,8	1,01	3,8	2,6	0,17	4,4	0,72	2,5	1,66	10,2	0,92	0,17	2,1	0,92	0,64	24,4	0,50
	<b>5E</b>	2,2	0,9	2,4	4,9	0,20	5,3	0,80	3,9	0,88	8,0	1,7	0,24	0,85	1,1	0,75	13,7	0,23
	<b>10D</b>	23	0,25	92	0,11	0,47	2,0	0,84	5,2	132	311	29,2	11,4	10,6	54,3	9,9	232,8	14,2
	<b>10C</b>	5,2	0,77	6,8	6,6	0,18	2,8	0,78	3,6	1,36	0,38	1,6	0,44	0,78	2,8	0,75	1,8	0,25
	<b>10B</b>	2,5	0,39	6,3	4,9	0,26	5,8	0,76	3,2	1,25	0,53	1,1	0,15	0,70	0,85	2,3	2,3	0,14
	<b>10A</b>	6,1	0,16	37,8	2,4	0,42	5,4	0,82	4,7	2,73	17,6	1,8	0,26	3,2	1,0	0,76	7,4	0,49
	<b>1B</b>	31	1,44	21,6	6,1	0,08	4,2	0,71	2,4	4,12	2,0	1,1	0,20	1,0	4,8	0,62	8,0	0,49
	<b>1C</b>	19	1,67	11,7	4,2	0,15	3,1	0,73	2,7	2,93	2,9	0,94	0,24	0,9	3,0	0,55	7,6	0,34
	<b>1D</b>	34	1,84	18,9	6,3	0,02	4,3	0,67	2,1	5,17	3,0	0,65	0,12	0,64	4,1	7,6	6,9	0,40
	<b>1E</b>	44	0,54	81,6	0,24	2,4	5,4	0,82	4,7	395	211	19,6	2,8	4,2	901	15,3	286	8,3
	<b>13</b>	21	1,16	17,7	0,02	3,5	4,2	0,91	10,1	568	1,939	87,9	16,4	170	130	15,3	98,9	75,3
	<b>14</b>	7,6	0,35	21,7	0,04	3,9	10,9	0,86	6,4	148	606	56,1	4,0	29,2	109	0,76	87,4	34,1

**Tabela 4.** Matriz de correlação de Spearman para os metais estudados na Formação Barbalha. Os valores em negrito são significativos ( $p < 0,05$ ;  $n=21$ ).

	Al	Fe	Mn	Cu	Zn	Ni	Pb	Cr	Sr	V	Ba	Hg	TOC	Hg/TOC	Sr/Ba
<b>Al</b>	1	0,33	<b>-0,59</b>	-0,11	-0,32	<b>0,90</b>	-0,31	<b>0,50</b>	<b>-0,56</b>	<b>0,52</b>	-0,04	-0,30	<b>0,47</b>	<b>-0,62</b>	<b>-0,59</b>
<b>Fe</b>		1	-0,30	-0,15	0,03	<b>0,50</b>	0,08	<b>0,67</b>	-0,30	<b>0,52</b>	-0,15	-0,07	-0,05	<b>0,77</b>	-0,33
<b>Mn</b>			1	-0,08	0,26	<b>-0,57</b>	0,01	-0,36	0,26	-0,25	0,10	0,03	-0,26	0,32	0,23
<b>Cu</b>				1	0,12	0,02	0,42	-0,04	-0,02	-0,05	-0,13	<b>0,72</b>	0,04	<b>0,72</b>	0,18
<b>Zn</b>					1	-0,08	<b>0,71</b>	0,02	-0,18	0,29	-0,05	0,21	-0,32	<b>0,49</b>	-0,16
<b>Ni</b>						1	-0,16	<b>0,71</b>	<b>-0,57</b>	<b>0,71</b>	-0,14	-0,19	0,30	<b>-0,42</b>	<b>-0,58</b>
<b>Pb</b>							1	-0,09	-0,02	0,01	-0,06	<b>0,66</b>	-0,04	<b>0,71</b>	0,06
<b>Cr</b>								1	-0,43	<b>0,75</b>	-0,12	-0,17	0,04	-0,14	<b>-0,45</b>
<b>Sr</b>									1	<b>-0,47</b>	0,05	0,11	-0,09	0,08	<b>0,97</b>
<b>V</b>										1	0,01	-0,30	-0,04	<b>0,43</b>	<b>-0,50</b>
<b>Ba</b>											1	0,14	0,38	-0,16	-0,08
<b>Hg</b>												1	0,25	<b>0,68</b>	0,21
<b>TOC</b>													1	<b>-0,44</b>	-0,15
<b>Hg/TOC</b>														1	0,19
<b>Sr/Ba</b>															1

**Tabela 5.** Valores dos indicadores geoquímicos de aportes detriticos, vulcanismo, paleosalinidade, estado redox e paleoprodutividade na Formação Barbalha.

FORMAÇÃO	Amostra	Hg (ng g <sup>-1</sup> )	TOC (%)	Hg/TOC	Al (%)	Sr/Ba	V/Cr	V/V+Ni	V/Ni	Pb <sup>EF</sup>	Mn <sup>EF</sup>	V <sup>EF</sup>	Cr <sup>EF</sup>	Fe <sup>EF</sup>	Cu <sup>EF</sup>	Ni <sup>EF</sup>	Zn <sup>EF</sup>	Ba <sup>EF</sup>
Formação Romualdo	23	2,5	0,6	4,5	1,05	0,65	4,2	0,8	4,7	2,3	9,8	1,8	0,3	1,0	2,1	2,1	1,2	1,2
	4.1	5,6	1,4	3,9	6,93	0,48	3,9	0,8	4,9	1,4	0,3	1,9	0,4	1,9	2,5	2,2	2,3	0,3
	4.1.1	5,1	1,4	3,6	6,72	0,37	4,1	0,8	3,0	1,6	1,1	2,2	0,4	1,5	3,4	4,0	4,3	0,1
	4.2.1	11,7	1,2	9,7	1,48	0,42	11,0	0,9	8,3	3,2	31,4	4,7	0,3	1,3	6,5	3,1	4,2	0,7
	15 D	1,5	0,8	1,8	5,72	0,21	3,4	0,7	2,6	0,7	0,7	1,4	0,3	2,1	1,5	2,9	2,7	0,1
	15C	2,0	0,6	3,2	2,07	0,64	1,6	0,8	4,8	2,5	3,7	0,6	0,3	0,4	0,4	0,7	0,4	0,3
	15B	2,3	0,7	3,1	6,58	0,76	1,6	0,6	1,6	0,6	0,4	0,8	0,4	1,8	0,7	2,7	2,3	0,0
	15A	6,9	1,0	6,9	3,85	0,23	1,3	0,8	3,2	1,2	0,6	1,2	0,7	3,2	1,7	2,1	2,4	0,1
	3A	1,1	0,5	2,2	2,18	0,41	12,8	0,9	12,7	4,6	2,8	2,0	0,1	0,4	0,4	0,9	0,5	0,3
	3B	26,3	0,7	39,3	3,70	0,06	1,4	0,6	1,5	9,0	0,9	1,4	0,7	2,2	6,7	5,1	4,7	0,9
	3C	6,8	0,8	8,1	1,97	0,58	6,5	0,8	3,5	2,7	11,6	2,0	0,2	2,1	3,6	3,2	0,3	0,5
	3D	2,8	0,7	4,1	1,86	0,72	12,8	0,9	6,8	1,8	10,8	1,3	0,1	0,2	1,9	1,1	1,4	0,6
	3E	2,0	0,5	4,1	5,06	0,18	1,5	0,7	1,9	2,5	0,3	0,4	0,2	1,0	0,7	1,1	0,8	0,3

**Tabela 6.** Matriz de correlação de Spearman para os metais estudados na Formação Barbalha. Os valores em negrito são significativos ( $p < 0,05$ ;  $n=13$ ).

	Al	Fe	Mn	Cu	Zn	Ni	Pb	Cr	Sr	V	Ba	Hg	TOC	Hg/TOC	Sr/Ba
Al	1	<b>0,87</b>	<b>-0,58</b>	<b>0,53</b>	<b>0,84</b>	<b>0,84</b>	0,3	<b>0,84</b>	-0,29	<b>0,68</b>	-0,08	-0,08	<b>0,46</b>	-0,11	<b>-0,53</b>
Fe		1	<b>-0,51</b>	<b>0,52</b>	<b>0,69</b>	<b>0,79</b>	0,17	<b>0,93</b>	-0,29	<b>0,64</b>	-0,12	0,07	<b>0,54</b>	0,00	-0,31
Mn			1	-0,08	-0,10	-0,36	-0,24	-0,55	0,37	-0,06	0,12	0,14	0,22	-0,01	0,31
Cu				1	<b>0,56</b>	<b>0,79</b>	<b>0,69</b>	<b>0,66</b>	-0,05	<b>0,76</b>	0,33	<b>0,63</b>	<b>0,70</b>	<b>0,52</b>	<b>-0,42</b>
Zn					1	<b>0,8</b>	0,1	<b>0,61</b>	0,04	<b>0,82</b>	-0,09	-0,17	<b>0,73</b>	-0,29	0,06
Ni						1	0,39	<b>0,84</b>	-0,31	<b>0,77</b>	-0,10	0,24	<b>0,57</b>	0,18	-0,27
Pb							1	0,35	0,09	0,46	<b>0,39</b>	<b>0,51</b>	0,3	<b>0,5</b>	-0,24
Cr								1	-0,40	0,63	-0,13	0,27	<b>0,55</b>	0,21	-0,37
Sr									1	0,08	<b>0,70</b>	-0,19	0,21	-0,24	<b>0,53</b>
V										1	0,16	0,05	<b>0,89</b>	-0,11	-0,15
Ba											1	0,29	<b>0,72</b>	0,26	-0,14
Hg												1	0,15	<b>0,97</b>	<b>-0,49</b>
TOC													1	-0,08	-0,04
Hg/TOC														1	<b>-0,49</b>
Sr/Ba															1

## Material Supplementar- CAPÍTULO 2

**Tabela 7.** Valores dos indicadores geoquímicos de aportes detriticos, vulcanismo, paleoprodutividade, paleoredox, paleosalinidade, paleoclima e paleosalinidade no *Konservat-Lagerstätte* do paleolago Crato.

Altura (cm)	Aportes detriticos		Vulcanismo			Fator de Enriquecimento com o Alumínio						Fator de Enriquecimento com o Ferro						Clima	Salin.	Nível Lago	
	Al	Fe	Hg	Hg/Al	Hg/Fe	Cu	Zn	Ni	Ba	Pb	Mn	Fe	Cu	Zn	Ni	Ba	Pb	Mn			
1,72	0,1	0,2	18	273	90	149	79	8	3	166	27	1	118	63	6	3	132	22	1	4	1
1,73	0,1	0,6	42	433	76	15	112	5	2	203	17	2	6	48	2	1	86	7	11	5	4
1,74	0,1	0,1	54	521	377	17	67	1	3	137	17	1	30	117	1	5	241	30	8	3	1
1,83	0,1	0,7	24	256	35	98	39	2	3	320	20	3	32	13	1	1	105	6	1	3	4
2,05	0,1	0,3	54	782	175	217	93	7	2	128	25	2	118	50	4	1	69	14	1	5	2
2,17	0,1	0,3	77	1.048	271	141	53	7	1	204	21	2	88	33	4	1	128	13	1	8	2
2,5	0,1	0,9	124	1.515	145	173	92	6	2	136	20	4	40	21	1	0,5	32	5	1	3	6
10	0,0	0,5	57	1.719	124	1399	197	19	12	412	45	6	245	34	3	2	72	8	1	5	3
11,2	0,0	0,4	57	1.753	130	1377	214	32	9	260	46	6	248	39	6	2	47	8	0,2	2	3
14	0,1	0,9	28	528	32	570	151	10	8	188	41	7	83	22	1	1	27	6	0,3	1	5
16	0,3	1,7	355	1.154	210	183	52	4	9	211	8	2	81	23	2	4	93	3	0,1	0,1	8
17	0,1	0,3	160	2.485	502	34	64	8	19	229	28	2	16	31	4	9	112	14	4	0,4	2
19,5	0,0	0,4	135	3.050	356	42	141	14	24	316	48	4	12	40	4	7	90	14	6	1	2
20	0,1	0,1	130	1.862	882	15	288	6	6	100	33	1	17	331	7	7	115	38	11	1	1
25,2	0,0	0,2	58	1.750	265	26	128	12	14	301	59	3	9	47	4	5	111	22	11	1	1
28	0,1	0,5	81	888	170	151	141	1	7	201	17	2	70	66	0,5	3	93	8	1	1	4
35	0,3	0,8	122	478	152	102	48	3	4	66	8	1	79	37	3	3	51	6	2	3	5
55	0,1	1,0	47	689	47	36	166	6	7	289	31	6	6	27	1	1	47	5	4	1	5
67,2	0,1	1,3	56	617	43	109	335	13	5	181	23	6	18	57	2	1	31	4	1	1	7
69,2	0,1	0,7	28	209	39	105	153	4	4	45	15	2	48	70	2	2	21	7	1	1	4
75	0,1	0,3	20	201	57	309	155	2	5	134	33	1	212	106	2	3	92	23	1	4	1

83,2	0,1	0,5	13	148	28	398	139	3	6	62	22	2	179	62	1	3	28	10	1	5	3
88,6	0,1	0,3	58	836	168	766	237	13	6	414	55	2	374	116	6	3	202	27	1	6	1
95,7	0,2	0,2	34	211	160	94	45	1	2	58	17	1	173	83	2	4	106	31	3	8	1
103	0,1	0,4	25	229	55	411	180	8	6	123	25	2	239	105	5	3	71	15	0,4	2	2
110	0,2	0,3	22	122	68	173	74	1	2	76	14	1	231	100	1	3	102	19	3	14	1
115	0,5	1,2	22	42	19	322	98	3	1	67	3	1	348	106	3	1	73	4	0,1	1	8
125	0,1	0,4	90	714	213	440	183	6	5	133	15	1	319	133	5	3	97	11	1	4	2
138	0,2	0,9	57	362	65	715	252	9	3	118	12	2	312	110	4	1	51	5	0,2	3	5
138,1	0,1	0,5	32	391	64	595	180	8	2	221	35	3	237	72	3	1	88	14	1	10	2
144,9	0,2	0,7	26	130	35	422	134	3	1	99	9	2	274	87	2	1	64	6	0,2	5	5
148,1	0,1	0,1	20	192	151	259	124	5	2	123	18	1	496	238	9	3	236	34	2	14	1
150	0,1	0,3	40	29	126	314	94	4	1	445	13	1	323	97	4	1	458	13	0,4	6	2
151,4	0,1	0,1	23	341	172	268	118	5	2	521	32	1	328	145	6	3	638	39	2	15	1
151,8	0,1	0,2	35	245	221	173	68	2	2	86	18	0,5	379	150	4	5	188	40	1	3	1
152,3	0,1	0,3	26	443	76	678	232	13	3	288	33	2	281	96	6	1	119	14	1	11	2
155,8	0,1	0,1	32	396	243	272	104	4	2	937	23	1	405	155	5	3	1393	34	2	14	1
156	0,1	0,1	28	232	211	192	97	1	3	129	17	0,5	424	215	2	7	286	38	3	8	1
158,1	0,1	0,3	30	305	98	379	355	2	5	145	19	1	296	278	1	4	114	15	2	8	2
158,6	0,1	0,7	31	281	44	1128	249	4	4	162	21	3	424	94	1	2	61	8	0,1	2	4
158,8	0,1	0,2	12	195	53	635	136	<LD	15	184	35	2	416	89	<LD	10	121	23	2	4	1
159	0,1	0,2	26	336	116	467	72	6	7	209	27	1	392	60	5	5	175	23	0,4	1	1
160	0,7	0,7	149	217	218	131	76	1	1	42	3	0,4	319	184	3	2	101	7	1	7	4
162,7	0,2	0,1	50	327	425	121	51	2	3	93	8	0,3	382	160	7	8	292	25	4	12	1
165,6	0,1	0,7	39	341	53	637	172	2	3	143	18	3	238	64	1	1	53	7	1	10	4
176,3	0,2	0,8	69	306	87	527	123	2	2	90	8	1	366	86	1	1	62	6	1	11	5
176,6	0,1	1,0	23	190	23	1107	264	6	3	156	17	3	325	78	2	1	46	5	0,1	2	6
179,1	0,3	0,8	52	167	68	275	61	2	2	94	5	1	271	60	2	2	93	5	1	5	5
179,2	0,1	0,4	21	211	57	476	111	2	3	141	19	2	313	73	2	2	93	12	0,2	2	2
180	0,1	1,9	58	618	31	2545	451	9	5	477	17	8	308	55	1	1	58	2	0,2	5	13
180,5	0,1	0,2	31	245	127	328	99	2	4	140	15	1	414	125	2	5	176	19	0,3	2	1
180,9	0,1	0,4	31	229	88	307	100	3	5	94	13	1	287	93	3	5	88	12	1	3	2
181,7	0,1	0,1	38	301	470	133	52	2	4	99	8	0	505	196	8	14	376	29	1	1	1

182	0,1	0,3	32	340	105	366	128	1	13	143	20	1	274	96	1	10	107	15	1	2	2
183,1	0,1	0,3	25	259	80	433	144	2	3	131	20	1	324	108	2	3	98	15	0,3	2	2
186,3	0,1	0,3	34	390	133	697	263	2	<LD	151	20	1	579	218	2	<LD	126	16	1	<LD	2
189,3	0,1	0,5	33	498	69	612	107	6	11	338	28	3	205	36	2	4	113	9	1	4	3
191	0,1	0,4	28	375	70	635	243	2	6	434	23	2	286	110	1	3	196	10	1	4	3
191,3	0,1	0,2	20	282	83	586	157	3	5	380	29	1	418	111	2	3	270	20	0,3	2	1
191,7	0,1	0,3	44	475	159	485	153	1	5	111	16	1	394	124	1	4	90	13	2	10	2
192	0,1	0,4	47	437	130	413	145	3	4	145	20	1	299	105	2	3	105	14	1	7	2
193	0,1	0,4	40	452	105	385	124	2	6	157	21	2	218	70	1	3	89	12	1	5	2
193,4	0,1	0,3	31	348	91	400	142	2	5	121	26	2	253	90	1	3	76	16	2	7	2
194	0,1	0,9	54	601	61	939	230	3	5	213	20	4	231	56	1	1	52	5	1	6	6
195	0,1	0,7	82	572	121	472	182	4	3	190	13	2	243	94	2	1	98	6	0,2	2	4
197	0,1	0,9	168	2.388	197	881	341	5	8	467	27	5	176	68	1	2	94	5	1	9	5
199	0,1	0,4	49	830	115	332	195	4	8	337	31	3	111	65	1	3	113	11	5	12	3
201	0,0	0,3	69	1.800	248	461	219	3	7	246	46	3	154	73	1	2	82	15	5	20	2
205	0,1	0,7	60	590	91	259	201	1	4	306	14	3	97	75	0,5	2	114	5	4	13	5
214	0,1	0,5	74	604	138	121	149	1	2	170	12	2	67	82	1	1	94	7	7	20	4
217	0,1	0,7	146	1.329	217	173	203	2	5	243	15	3	68	80	1	2	96	6	5	11	5
224	0,2	0,5	102	579	190	123	70	0,2	2	115	7	1	98	56	0,2	1	92	6	5	20	5
226	0,1	0,3	235	1.715	696	72	77	1	3	212	13	1	71	76	1	3	209	13	11	13	2
229,5	0,1	0,8	109	1.158	129	317	148	2	5	357	16	4	85	40	1	1	96	4	4	13	6
235	0,1	0,4	62	792	156	168	97	<LD	10	206	23	2	80	46	<LD	5	98	11	7	6	2
242	0,1	0,8	117	996	152	179	129	<LD	5	312	12	3	66	48	<LD	2	116	4	6	11	6
255	0,2	1,6	46	187	29	211	142	1	2	136	6	3	80	54	0,5	1	51	2	2	13	13
258	0,1	0,8	75	960	96	227	272	<LD	5	224	20	4	55	66	<LD	1	54	5	5	13	6
265	0,1	0,4	68	1.236	165	418	302	<LD	8	230	32	3	135	98	<LD	3	75	11	4	12	3
274,5	0,1	0,4	118	1272	301	219	124	<LD	5	78	17	2	126	71	<LD	3	45	10	4	10	3
284,5	0,0	0,5	88	1943	174	239	239	3	10	641	35	5	52	52	1	2	139	8	13	17	4
285	0,1	0,6	93	806	148	95	118	<LD	5	273	13	2	42	52	<LD	2	121	6	10	10	5
288	0,1	0,5	49	890	101	184	187	4	15	272	31	4	50	51	1	4	74	8	11	8	3
295	0,1	0,5	61	834	121	246	412	<LD	12	164	21	3	87	145	<LD	4	58	7	6	7	4

**Tabela 8.** Matriz de correlação de Spearman para os metais estudados no *Konservat-Lagerstätte* do paleolago Crato. Os valores em negrito são significativos ( $p < 0,05$ ;  $n=84$ ).

	Al	Fe	Mn	Cu	Pb	Zn	Ni	Hg	Ba	Sr/Cu	Sr/Ba	Hg/Al	Hg/Fe	Fe/Mn
<b>Al</b>	1	<b>0,34</b>	-0,02	<b>0,42</b>	<b>0,28</b>	<b>0,61</b>	<b>0,40</b>	<b>0,33</b>	0,20	<b>-0,32</b>	<b>-0,34</b>	<b>-0,33</b>	-0,08	<b>0,35</b>
<b>Fe</b>		1	-0,11	<b>0,55</b>	<b>0,39</b>	<b>0,61</b>	<b>0,48</b>	<b>0,34</b>	<b>0,32</b>	<b>-0,27</b>	-0,17	0,06	<b>-0,38</b>	<b>0,96</b>
<b>Mn</b>			1	0,05	-0,07	-0,04	0,25	0,03	0,08	-0,07	-0,09	-0,1	-0,12	<b>-0,31</b>
<b>Cu</b>				1	<b>0,27</b>	<b>0,71</b>	<b>0,39</b>	-0,1	0,03	<b>-0,46</b>	-0,07	<b>-0,30</b>	<b>-0,33</b>	<b>0,51</b>
<b>Pb</b>					1	<b>0,25</b>	0,20	<b>0,29</b>	<b>0,21</b>	-0,15	0,22	-0,05	-0,09	<b>0,38</b>
<b>Zn</b>						1	<b>0,43</b>	-0,03	0,13	<b>-0,31</b>	-0,02	<b>-0,30</b>	<b>-0,42</b>	<b>0,59</b>
<b>Ni</b>							1	<b>0,29</b>	0,25	-0,08	<b>-0,33</b>	0,04	-0,05	<b>0,35</b>
<b>Hg</b>								1	<b>0,56</b>	0,03	-0,13	<b>0,62</b>	<b>0,51</b>	<b>0,25</b>
<b>Ba</b>									1	0,03	<b>-0,39</b>	0,21	0,07	0,21
<b>Sr/Cu</b>										1	<b>0,47</b>	<b>0,37</b>	<b>0,42</b>	-0,1
<b>Sr/Ba</b>											1	-0,18	-0,05	-0,09
<b>Hg/Al</b>												1	<b>0,54</b>	<b>-0,31</b>
<b>Hg/Fe</b>													1	<b>-0,4</b>
<b>Fe/Mn</b>														1
<b>Mortality</b>														

**Tabela 9.** Matriz de correlação de Spearman para o Fator de Enriquecimento do Alumínio (Al) no *Konservat-Lagerstätte* do paleolago Crato. Os valores em negrito são significativos ( $p < 0,05$ ;  $n=84$ ).

	Cu <sup>EF</sup>	Zn <sup>EF</sup>	Ni <sup>EF</sup>	Ba <sup>EF</sup>	Pb <sup>EF</sup>	Mn <sup>EF</sup>	Fe <sup>EF</sup>	Hg	Hg/Al	Hg/Fe	Sr/Ba	Sr/Cu	Fe/Mn	Mortality
<b>Cu<sup>EF</sup></b>	1	<b>0.58</b>	0.19	0.02	0.27	0.24	<b>0.51</b>	-0,19	-0,03	<b>-0,34</b>	<b>-0,05</b>	<b>-0,45</b>	<b>0.32</b>	<b>0.33</b>
<b>Zn<sup>EF</sup></b>		1	0.23	0.21	<b>0.29</b>	0.25	<b>0.61</b>	-0,2	0.12	<b>-0,41</b>	0.03	-0,13	<b>0.34</b>	0.07
<b>Ni<sup>EF</sup></b>			1	<b>0.30</b>	0.19	<b>0.57</b>	<b>0.44</b>	0.11	<b>0.41</b>	0.10	<b>-0,25</b>	0.21	0.06	0.03
<b>Ba<sup>EF</sup></b>				1	<b>0.28</b>	<b>0.57</b>	<b>0.34</b>	0.22	<b>0.62</b>	0.17	<b>-0,38</b>	<b>0.30</b>	-0,1	0.18
<b>Pb<sup>EF</sup></b>					1	<b>0.41</b>	<b>0.36</b>	0.05	0.33	-0,04	<b>0.25</b>	0.10	0.04	0.18
<b>Mn<sup>EF</sup></b>						1	<b>0.40</b>	-0,14	<b>0.49</b>	0.11	-0,11	0.24	<b>-0,36</b>	0.14
<b>Fe<sup>EF</sup></b>							1	0.06	<b>0.41</b>	<b>-0,29</b>	-0,16	-0,02	<b>0.57</b>	-0,06
<b>Hg</b>								1	<b>0.62</b>	<b>0.51</b>	-0,06	0.23	<b>0.21</b>	-0,09
<b>Hg/Al</b>									1	<b>0.54</b>	-0,09	<b>0.44</b>	<b>-0,31</b>	0.11
<b>Hg/Fe</b>										1	-0,03	<b>0.54</b>	<b>-0,4</b>	0.13
<b>Sr/Ba</b>											1	<b>0.28</b>	-0,08	<b>-0,25</b>
<b>Sr/Cu</b>												1	-0,05	<b>-0,31</b>
<b>Fe/Mn</b>													1	<b>0.28</b>
<b>Mortality</b>														1

**Tabela 10.** Matriz de correlação de Spearman para o Fator de Enriquecimento com o Ferro (Fe) no *Konservat-Lagerstätte* do paleolago Crato. Os valores em negrito são significativos ( $p < 0,05$ ;  $n=84$ ).

	Cu <sup>EF</sup>	Zn <sup>EF</sup>	Ni <sup>EF</sup>	Ba <sup>EF</sup>	Pb <sup>EF</sup>	Mn <sup>EF</sup>	Hg	Hg/Al	Hg/Fe	Sr/Ba	Sr/Cu	Fe/Mn	Mortality
<b>Cu<sup>EF</sup></b>	1	<b>0,68</b>	0.18	0.23	<b>0,33</b>	<b>0,40</b>	<b>-0,43</b>	<b>-0,51</b>	-0,17	0.15	<b>-0,55</b>	<b>-0,30</b>	<b>0,49</b>
<b>Zn<sup>EF</sup></b>		1	0.33	<b>0,45</b>	<b>0,37</b>	<b>0,53</b>	<b>-0,3</b>	<b>-0,41</b>	0.07	0.29	-0,17	<b>-0,41</b>	0.29
<b>Ni<sup>EF</sup></b>			1	<b>0,36</b>	<b>0,38</b>	<b>0,64</b>	-0,1	-0,04	<b>0,43</b>	0.02	0.24	<b>-0,44</b>	0.06
<b>Ba<sup>EF</sup></b>				1	0.19	<b>0,55</b>	0.02	0.10	<b>0,51</b>	-0,24	0.20	<b>-0,49</b>	<b>0,27</b>
<b>Pb<sup>EF</sup></b>					1	<b>0,55</b>	-0,11	-0,04	0.22	0.37	0.12	<b>-0,33</b>	0.21
<b>Mn<sup>EF</sup></b>						1	-0,27	-0,13	<b>0,43</b>	0.18	0.17	<b>-0,73</b>	<b>0,26</b>
<b>Hg</b>							1	<b>0,64</b>	<b>0,51</b>	-0,06	0.23	<b>0,28</b>	-0,09
<b>Hg/Al</b>								1	<b>0,58</b>	-0,06	<b>0,44</b>	<b>-0,31</b>	-0,04
<b>Hg/Fe</b>									1	-0,04	<b>0,54</b>	<b>-0,4</b>	0.13
<b>Sr/Ba</b>										1	<b>0,28</b>	-0,08	<b>-0,25</b>
<b>Sr/Cu</b>											1	-0,1	<b>-0,31</b>
<b>Fe/Mn</b>												1	<b>0,28</b>
<b>Mortality</b>													1

## Material Suplementar- CAPÍTULO 3

Tabela 11. Concentração de mercúrio (ng g<sup>-1</sup>) em espécimes de vertebrados fósseis (Hgfossil), das concreções (Hgrocha), a razão de bioacumulação (Hgamostra) na Formação Romualdo, Bacia do Araripe, Nordeste do Brasil.

<b>Amostra</b>	<b>Táxon</b>	<b>Hg fóssil (ng g<sup>-1</sup>)</b>	<b>Hg rocha (ng g<sup>-1</sup>)</b>	<b>Hgrazão</b>
MPPCN P 5319	<i>Calamopleurus cylindrius</i>	20,73	13,53	1,53
MPPCN P 5320		26,95	17,74	1,52
MPPCN P 5354		202,16	9,59	21,08
<b>Média</b>				<b>8,04</b>
MPPCN P 2425	<i>Cladocyclus gardneri</i>	22,90	22,99	1,00
MPPCN P 2448		20,93	16,89	1,24
MPPCN P 2436		10,83	8,29	1,31
<b>Média táxon</b>				<b>1,18</b>
MCNHB 134	<i>Neoproscinetes panalvai</i>	34,29	29,59	1,16
MCNHB 364		31,22	28,89	1,08
<b>Média táxon</b>				<b>1,12</b>
MCNHB 353	<i>Baitodea</i>	45,31	41,83	1,08
MCNHB 043		41,13	42,93	0,96
<b>Média táxon</b>				<b>1,02</b>
MPPCN P 5311	<i>Vinctifer comptoni</i>	10,13	22,55	0,45
MPPCN P 5313		111,29	125,68	0,89
MPPCN P 5314		6,73	12,29	0,55
MPPCN P 5317		18,64	25,96	0,72
MPPCN P 5309		112,02	55,80	2,01
<b>Média táxon</b>				0,92
MPPCN P 5356	<i>Rhacolepis buccalis</i>	157,16	1,330	0,12
MPPCN P 5358		105,25	304,62	0,35
MPPCN P 5359		41,25	95,68	0,43
MPPCN P 5360		298,59	808,80	0,37
MPPCN P 5357		34,65	482,67	0,07
<b>Média táxon</b>				<b>0,43</b>
MCNHB 5038	Pterosauria ( <i>Thalassodrominae</i> )	10,72	4,19	2,56
MCNHB 1434	Pterosauria ( <i>Ornithocheiroidea ind.</i> )	10,91	4,14	2,64
MCNHB 105	Pterosauria ( <i>Ornithocheiriforme</i> )	1,46	4,45	0,33
MCNHB 345		3,85	17,92	0,21
<b>Média táxon</b>				<b>0,27</b>
TR1	<i>Tharrhias araripis</i>	17,72	20,11	0,88
TR2		8,28	9,72	0,85
<b>Média táxon</b>				<b>0,87</b>